

Júnia Cristina Avelar Batista

LEI DO DIREITO AUTORAL
Todos os direitos reservados e protegidos
pela Lei 9.810/1998.
Este arquivo não pode ser reproduzido ou
transmitido sejam quais forem os meios
empregados: eletrônicos, mecânicos,
fotográficos ou quaisquer outros.

“ Promising Duplex Coatings
for Tribological Applications at
Elevated Temperatures “

N.Cham 669 B333p 2001

Autor: Batista, Junia Cristina Avelar.

Título: Promising duplex coatings for tr



118140505

Ac. 343335

UNIVERSIDADE FEDERAL DE MINAS GERAIS
Post-Graduation Course in Metallurgical and Mining Engineering

LEI DO DIREITO AUTORAL
Todos os direitos reservados e protegidos
pela Lei 9.610/1998
Este arquivo não pode ser reproduzido ou
transmitido sejam quais forem os meios
empregados: eletrônicos, mecânicos,
fotográficos ou quaisquer outros.

Doctoral thesis

**"Promising duplex coatings
for tribological applications
at elevated temperatures"**

Author: Júnia Cristina Avelar Batista

Supervisors: Prof. Geralda Cristina Durães de Godoy - UFMG

Prof. Allan Matthews – University of Hull

March/2001

Avenida
34 33 35

UNIVERSIDADE FEDERAL DE MINAS GERAIS
Allan Matthews

UNIVERSIDADE FEDERAL DE MINAS GERAIS
Post-Graduation Course in Metallurgical and Mining Engineering

Júnia Cristina Avelar Batista

**PROMISING DUPLEX COATINGS
FOR TRIBOLOGICAL APPLICATIONS
AT ELEVATED TEMPERATURES**

**Being a doctoral thesis submitted to
the Post-Graduation Course in Metallurgical and Mining Engineering,
Universidade Federal de Minas Gerais**

Area: Materials Science and Engineering
Supervisors: Prof. Geralda Cristina Durães de Godoy - UFMG
Prof. Allan Matthews – University of Hull

Belo Horizonte
School of Engineering, UFMG

2001

DIREITO AUTORAL
Todos os direitos reservados e protegidos
pela Lei nº 9.610, de 1998.
Este arquivo não pode ser reproduzido ou
transmitido sejam quais forem os meios
empregados: eletrônicos, mecânicos,
fotográficos ou quaisquer outros.

669
B 333P
200L

ok 06

UFMG - Universidade Federal de Minas Gerais
Biblioteca Central

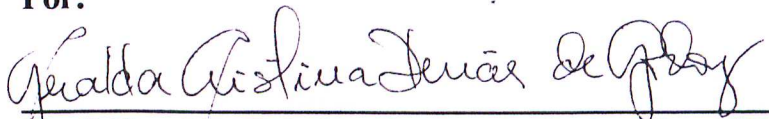
PROMISING DUPLEX COATINGS FOR
TRIBOLOGICAL APPLICATIONS AT ELEVATED
TEMPERATURES

Júnia Cristina Avelar Batista

Tese submetida à Comissão Examinadora designada pelo Colegiado do Curso de Pós-Graduação em Engenharia Metalúrgica e de Minas da Universidade Federal de Minas Gerais como requisito parcial para obtenção do grau de Doutor em Engenharia Metalúrgica e de Minas.

Aprovada em 09 de abril de 2001

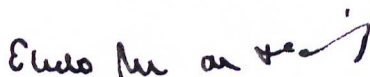
Por:



Profª GERALDA CRISTINA DURÃES DE GODOY, Dr. (UFMG)
Orientadora




Prof. ALLAN MATHEWS, Ph.D. (University of Hull)



Prof. EVANDO MIRRA DE PAULA E SILVA, Dr. Ing. (UFMG/CNPq)

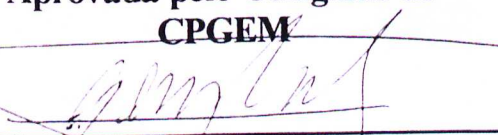


Prof. PAULO EMÍLIO MIRANDA, Dr. (UFRJ)



Prof. PAULO JOSÉ MODENESI, Ph.D. (UFMG)

Aprovada pelo Colegiado do
CPGEM



Prof. GEORGE EDUARDO SALES
Valadão

Versão final aprovada por



Professor/Orientador

*“The intuitive mind is a sacred gift and
the rational mind is a faithful servant.”*

(Albert Einstein)

LEI DO DIREITO AUTORAL
Todos os direitos reservados e protegidos
pela Lei 9.610/1998.
Este arquivo não pode ser reproduzido ou
transmitido sejam quais forem os meios
empregados: eletrônicos, mecânicos,
fotográficos ou quaisquer outros.

To my mum,

Rosângela das Neves Avelar

ACKNOWLEDGEMENTS

I would like to express my deepest gratitude to all past and present colleagues for providing such a nice and friendly atmosphere. In especial, I want to mention the following persons:

Prof. Geralda Cristina Durães de Godoy, for her friendship, constant assistance and patience, encouragement, constructive criticism and close supervision over all these years.

Prof. Allan Matthews, director of the Research Centre in Surface Engineering, University of Hull, for his constant support, supervision, expert advice and giving me the opportunity to work at the centre.

Dr Jonathan Housden, Tecvac Ltd., and Mr Marvin Joseph, Research Centre in Surface Engineering, University of Hull, for producing single-layered and duplex (Ti,Al)N, Cr-N coatings at Tecvac Ltd., Cambridge, England.

Mr Garry Robinson, School of Engineering, University of Hull, for his invaluable assistance at the SEM.

Dr Andrew Wilson and Mr Marvin Joseph, Research Centre in Surface Engineering, University of Hull, for being such nice friends and helping me to operate the instruments at the centre.

Ms Carole Forth and Ms Di Suddaby, Research Centre in Surface Engineering, University of Hull, for their affection and efficient help with all kinds of administrative details.

Mr John Robson, Mr Tony Pawson, Dr Steve Dowey, colleagues from the Research Centre in Surface Engineering, University of Hull, for their technical support.

Dr Mike Simmonds, Materials Research Institute, Sheffield Hallam University, for carrying out the GDOES analyses.

Centro Tecnológico de Minas Gerais (CETEC-MG), for the use of the Balzers-BAI 640R equipment.

Miss Ana Eugênia Marques, for her assistance in producing duplex TiN coatings at CETEC-MG.

Prof. Vicente Tadeu Lopes Buono, Department of Metallurgical Engineering and Materials, Universidade Federal de Minas Gerais, for useful discussions about the XRD analyses.

Mrs Marília Mendonça de Lima, Mr Elias Alves de Souza, Mr Renato Françoso de Ávila, Mr Rafael Drumond Mancosu and Mr Eustáquio Roberto Apolinário, colleagues from the Department of Metallurgical Engineering and Materials, Universidade Federal de Minas Gerais, for their friendship and fruitful suggestions throughout these years.

Mr Renato Françoso de Ávila, Department of Metallurgical Engineering and Materials, Universidade Federal de Minas Gerais, for his invaluable help with scheduling the heat treatment of AISI H13 steels at Brasimet S.A.

My housemate Elisa Costa Villaverde, for being such a good friend and making my stay in England quite enjoyable.

Mrs Patrícia Mara Trigueiro de Azevedo and Ms Viviane Mara de Souza, Department of Metallurgical Engineering and Materials, Universidade Federal de Minas Gerais, for carrying out the SEM and XRD analyses, respectively.

Mrs Sandra Cristina Estêvão Machado Texeira and Ms Rita de Cássia Buzato Mallafate, Department of Mining Engineering, Universidade Federal de Minas Gerais, for performing SEM and XRD analyses.

Mr Nelson Antônio de Azevedo, Ms Maria Aparecida Pacheco, Mr Vicente de Paulo Carvalho Alves and Miss Efigênia Neves de Araújo, Department of Metallurgical Engineering and Materials, Universidade Federal de Minas Gerais, for their incredible assistance over the years and invaluable help with practical every-day details.

Miss Núbia Silva Pinheiro, Department of Metallurgical Engineering and Materials, Universidade Federal de Minas Gerais, for the optical micrographs.

CNPq – Conselho Nacional de Desenvolvimento Científico e Tecnológico, FAPEMIG - Fundação de Amparo à Pesquisa do Estado de Minas Gerais and FINEP/RECOPE, for financially supporting this work.

Last, but not least, I deeply would like to thank my family for their love, patience and unconditional support during these years.

CONTENTS

CHAPTER 1: INTRODUCTION	1
CHAPTER 2: OBJECTIVES	5
CHAPTER 3: DUPLEX COATINGS	6
3.1. Background	6
3.1.1. One possible industrial application for duplex coatings	6
3.1.2. Plasma nitriding	8
3.1.3. The ion plating process	14
3.1.4. Generation of d.c. glow discharges: diode x triode layouts	17
3.1.5. Duplex coatings	20
3.1.6. The BAI 640R equipment	22
3.2. Experimental Procedure	25
3.2.1. Materials	25
3.2.2. Surface preparation	26
3.2.3. Plasma nitriding	26
3.2.4. Characterisation of plasma nitrided samples	27
3.2.5. Duplex treatment	28
3.2.6. Characterisation of the duplex TiN coating	28
3.3. Results and Discussion	31
3.3.1. Characterisation of the substrate	31
3.3.2. Characterisation of plasma nitrided samples	34
3.3.3. Characterisation of the duplex TiN coating	39
3.4. Conclusions	45
CHAPTER 4: EFFECTS OF AN INTERMEDIATE TREATMENT ON ADHESION AND IMPACT RESISTANCE OF DUPLEX TiN COATINGS ...	47
4.1. Background	47
4.2. Experimental Procedure	48
4.2.1. Materials and intermediate treatments	48
4.2.2. Structural characterisation	49
4.2.3. Scratch testing	49
4.2.4. Impact testing	50

LEI DO DIREITO AUTORAL
 Todos os direitos reservados e protegidos
 pela Lei 9.610/1998.
 Este arquivo não pode ser reproduzido ou
 transmitido sem a qualificação dos meios
 empregados: eletrônicos, mecânicos,
 fotográficos ou quaisquer outros.

4.3. Results and Discussion	50
4.3.1. Interfacial nitrided layer/coating structure	50
4.3.2. Adhesion	52
4.3.3. Impact resistance	55
4.4. Conclusions	61
CHAPTER 5: PROMISING DUPLEX COATINGS FOR TRIBOLOGICAL APPLICATIONS AT ELEVATED TEMPERATURES	62
5.1. Background	62
5.2. Experimental Procedure	64
5.2.1. Treatments	64
5.2.2. Analysis of the coatings	67
5.3. Results and Discussion	68
5.3.1. Surface roughness	68
5.3.2. Knoop hardness measurements	69
5.3.3. Cross-sectional structure of the coatings	71
5.3.4. Coating morphology	74
5.3.5. XRD analyses	76
5.3.6. GDOES analyses	78
5.3.7. Scratch testing	83
5.4. Conclusions	85
CHAPTER 6: MICRO-ABRASIVE WEAR TESTING	88
6.1. Background	88
6.2. Experimental Procedure	89
6.2.1. Materials	89
6.2.2. Treatments	89
6.2.3. Mechanical properties	90
6.2.4. Micro-abrasion resistance	90
6.3. Results and Discussion	94
6.3.1. Surface roughness and coating thickness	94
6.3.2. Coating microhardness	95
6.3.3. Coating adhesion	96
6.3.4. Micro-abrasive wear tests	97

6.4. Conclusions	111
CHAPTER 7: IMPACT TESTING	113
7.1. Background	113
7.2. Experimental Procedure	116
7.2.1. Sample preparation	116
7.2.2. Coating deposition and characterisation	116
7.2.3. Scratch testing	117
7.2.4. Impact testing	117
7.3. Results and Discussion	118
7.3.1. Coating characterisation	118
7.3.2. Scratch testing	119
7.3.3. Impact testing	119
7.3.3.1. Tests using a tungsten carbide ball (F = 900N)	119
7.3.3.2. Tests using a hardened AISI E52100 steel ball (F = 480N)	124
7.4. Conclusions	131
CHAPTER 8: GENERAL CONCLUSIONS	132
CHAPTER 9: RELEVANCE OF RESULTS AND MAJOR CONTRIBUTIONS	136
CHAPTER 10: RECOMMENDATIONS FOR FUTURE WORK	138
REFERENCES	140

FIGURE CAPTIONS

Figure 3.1	Continuous ingot casting process at Gerdau S.A	7
Figure 3.2	Superior shear knife which is used to cut the ingots	7
Figure 3.3	Voltage – current characteristics of different types of discharges in argon ⁽⁴⁵⁾	9
Figure 3.4	Typical gas composition and the resulting metallurgical configuration of the nitrided case ⁽³³⁾	10
Figure 3.5	Surface reactions during plasma nitriding according to Kölbel's model ⁽³³⁾	12
Figure 3.6	Schematic drawing of the BAI 640R equipment in the heating mode. The dashed line represents the path of the electron beam	23
Figure 3.7	Schematic drawing of the BAI 640R equipment in the etching mode. The dashed line represents the path of the electron beam	24
Figure 3.8	Schematic drawing of the BAI 640R equipment in the coating mode. The dashed lines represent the path of the electron beams	25
Figure 3.9	Microstructure of the AISI H13 steel substrate. Nital etchant (4%). SEM	32
Figure 3.10	X-ray diffractogram of the AISI H13 steel substrate	33
Figure 3.11	X-ray diffractograms of plasma nitrided AISI H13 substrates (a) for 2 hours and (b) for 3 hours	35
Figure 3.12	Polished cross-section of a 2h plasma nitrided sample. Nital etchant (4%). SEM	36
Figure 3.13	Polished cross-section of a 3h plasma nitrided sample. Nital etchant (4%). SEM	36
Figure 3.14	Influence of the treatment time on the Knoop hardness profile of plasma nitrided AISI H13 steels	37
Figure 3.15	X-ray diffractogram of the duplex TiN coating	40
Figure 3.16	SEM micrograph of the duplex TiN coating	40

- Figure 3.17 SEM micrograph of the duplex TiN coating at a higher magnification. Note that a $1\mu\text{m}$ thick, dense ϵ compound layer was formed during the duplex treatment 41
- Figure 3.18 Knoop hardness profile. Duplex TiN coating 42
- Figure 3.19 Tensile cracks (1) in the interior of the scratch channel. The arrow indicates the scratch direction 43
- Figure 3.20 At higher loads, external transverse cracks (2) start to form at the edge of the scratch channel. The arrow indicates the scratch direction 44
- Figure 3.21 End of the scratch channel, showing that the substrate has not been exposed. Tensile cracks (1), external transverse cracks (2) and coating chipping (3) can be distinguished at this stage. The normal load at the end of scratch was 188N. The arrow indicates the scratch direction 44
- Figure 4.1 Cross-sectional views of (a) sample 1, $T_{\text{heating}}=673\text{K}$, $t_{\text{etching}}=10\text{min}$; (b) sample 2, $T_{\text{heating}}=573\text{K}$, $t_{\text{etching}}=0\text{min}$; (c) sample 3, $T_{\text{heating}}=773\text{K}$, $t_{\text{etching}}=20\text{min}$ and (d) sample 4, $T_{\text{heating}}=573\text{K}$, $t_{\text{etching}}=20\text{min}$. Note that a compound layer, without any black layer, can be seen only in sample 2. SEM 51
- Figure 4.2 Results of the scratch test on (a-d) duplex TiN coatings and (e) single-layered TiN coating. The nitrided layer comprises only a diffusion zone in (a) sample 1, (c) sample 3 and (d) sample 4. Sample 2 (b) has a $\sim 1.0\text{-}1.2\mu\text{m}$ thick mono-phase $\epsilon\text{-Fe}_{2-3}\text{N}$ compound layer + diffusion zone. Arrows indicate the scratch direction 53
- Figure 4.3 Impact craters (10^3 , 10^4 and 5×10^4) produced in sample 1 (nitrided case comprising a diffusion zone) and sample 2 (nitrided case comprising a $1.0\text{-}1.2\mu\text{m}$ thick mono-phase ϵ compound layer + diffusion zone). SEM. The elliptical shape of some impact craters results from the tilt employed in the SEM imaging 57

Figure 4.4	Impact craters (10^3 , 10^4 and 5×10^4) produced in sample 3 (nitrided case comprising a diffusion zone) and sample 4 (nitrided case also comprising a diffusion zone). SEM. The elliptical shape of some impact craters results from the tilt employed in the SEM imaging	58
Figure 4.5	Impact craters (10^3 , 10^4 and 5×10^4) produced in a single-layered TiN coating. SEM. The elliptical shape of some impact craters results from the tilt employed in the SEM imaging	59
Figure 5.1	Knoop hardness data for the AISI H13 steel substrate, single-layered and duplex (Ti,Al)N, Cr-N coatings. Although the error bars are not shown in the plot, the standard deviation was not larger than 5%	70
Figure 5.2	Knoop hardness profiles of duplex (Ti,Al)N and Cr-N coatings	71
Figure 5.3	SEM fracture cross-sections of (a) Duplex (Ti,Al)N coating, (b) Duplex Cr-N coating, (c) Single-layered (Ti,Al)N coating and (d) Single-layered Cr-N coating. 5000X	72
Figure 5.4	Polished cross-sections of (a) Duplex (Ti,Al)N and (b) Duplex Cr-N. Nital etchant (4%). 5000X. SEM	73
Figure 5.5	LOM polished cross-sections of (a) duplex (Ti,Al)N coating and (b) duplex Cr-N coating. Nital etchant (4%). 400X	74
Figure 5.6	Coating surface morphology: (a) single-layered (Ti,Al)N, (b) duplex (Ti,Al)N, (c) single-layered Cr-N and (d) duplex Cr-N. SEM. 3000X	75
Figure 5.7	Diffraction patterns of duplex and single-layered (Ti,Al)N coatings on AISI H13 substrates	77
Figure 5.8	Diffraction patterns of duplex and single-layered Cr-N coatings on AISI H13 substrates	78
Figure 5.9	GDOES profiles of (a) single-layered (Ti,Al)N coating and (b) duplex (Ti,Al)N coating. Note the different scales used for erosion time	80

Figure 5.10	GDOES profiles of (a) single-layered Cr-N coating and (b) duplex Cr-N coating. Note the different scales used for erosion time	82
Figure 5.11	SEM photomicrographs of scratches in (a) single-layered (Ti,Al)N, (b) duplex (Ti,Al)N coating, (c) single-layered Cr-N coating and (d) duplex Cr-N coating. The arrows indicate the scratch direction. 200X	84
Figure 6.1	Schematic drawing illustrating the geometry of the micro-abrasive apparatus used in the present study	92
Figure 6.2	Outer (b) and inner (a) diameters of the wear crater	93
Figure 6.3	Knoop microhardness (0.25, 0.49, 0.98, 1.96, 4.90 and 9.81N) of uncoated AISI H13 steel, duplex and single-layered (Ti,Al)N, TiN, Cr-N coatings. Although the error bars are not shown in the plot, the standard deviation was not larger than 5%	96
Figure 6.4	Fitted line and its 95% confidence interval (CI) provided by the regression analysis. Duplex (Ti,Al)N coating	98
Figure 6.5	Fitted line and its 95% confidence interval (CI) provided by the regression analysis. Single-layered (Ti,Al)N coating	99
Figure 6.6	Fitted line and its 95% confidence interval (CI) provided by the regression analysis. Duplex TiN coating	99
Figure 6.7	Fitted line and its 95% confidence interval (CI) provided by the regression analysis. Single-layered TiN coating	100
Figure 6.8	Fitted line and its 95% confidence interval (CI) provided by the regression analysis. Duplex Cr-N coating	100
Figure 6.9	Fitted line and its 95% confidence interval (CI) provided by the regression analysis. Single-layered Cr-N coating	101
Figure 6.10	Fitted line and its 95% confidence interval (CI) provided by the regression analysis. Uncoated substrate (AISI H13)	101
Figure 6.11	Coating wear resistance of single-layered and duplex (Ti,Al)N, TiN and Cr-N coatings	103

Figure 6.12	Micrographs of the 1000 revolution wear crater: (a) uncoated substrate (AISI H13), (b) substrate of single-layered Cr-N coating, (c) substrate of duplex Cr-N coating, (d) substrate of single-layered TiN coating, (e) substrate of duplex TiN coating, (f) substrate of single-layered (Ti,Al)N coating and (g) substrate of duplex (Ti,Al)N coating. SEM. 500X	110
Figure 7.1	Schematic arrangement of the impact tester	114
Figure 7.2	Typical failure zones encountered after the impact test	115
Figure 7.3	Impact craters of single-layered and duplex (Ti,Al)N coatings after 10^3 , 10^4 and 5×10^4 impacts using a tungsten carbide ball, diameter, 6mm, $F = 900\text{N}$. SEM. The elliptical shape of some impact craters results from the tilt employed in the SEM imaging	121
Figure 7.4	Duplex (Ti,Al)N coating. Bottom of the 5×10^4 impact crater, showing the thin adhesive platelets transferred to the coating surface	122
Figure 7.5	EDX analyses of the impact crater shown in figure 7.4. Light area (a) and thin platelets (b)	122
Figure 7.6	Impact craters of single-layered and duplex Cr-N coatings after 10^3 , 10^4 and 5×10^4 impacts using a tungsten carbide ball, diameter, 6mm, $F = 900\text{N}$. SEM. The elliptical shape of some impact craters results from the tilt employed in the SEM imaging	123
Figure 7.7	Impact craters of single-layered (Ti,Al)N coatings after 10^3 , 10^4 and 5×10^4 impacts using a hardened AISI E52100 ball, diameter, 10mm, $F = 480\text{N}$	125
Figure 7.8	Impact craters of duplex (Ti,Al)N coatings after 10^3 , 10^4 and 5×10^4 impacts using a hardened AISI E52100 ball, diameter, 10mm, $F = 480\text{N}$	127
Figure 7.9	Impact craters of single-layered Cr-N coatings after 10^3 , 10^4 and 5×10^4 impacts using a hardened AISI E52100 ball, diameter, 10mm, $F = 480\text{N}$	128

Figure 7.10

Impact craters of duplex Cr-N coatings after 10^3 , 10^4 and 5×10^4 impacts using a hardened AISI E52100 ball, diameter 10mm, $F = 480\text{N}$

LEI DO DIREITO AUTORAL
Todos os direitos reservados, protegidos
pela Lei 9.610/1998.
Este arquivo não pode ser reproduzido ou
transmitido sejam quais forem os meios
empregados: eletrônicos, mecânicos,
fotográficos ou quaisquer outros.

TABLES

Table III.1	Nominal chemical composition of AISI H13 tool steels (100-102)	26
Table III.2	Plasma nitriding parameters of AISI H13 substrates	27
Table III.3	Deposition parameters of the duplex TiN coating	29
Table III.4	Surface roughness of AISI H13 discs	31
Table III.5	Vickers microhardness of the annealed AISI H13 substrate	32
Table III.6	EDS analyses at 3 different areas of the AISI H13 steel substrate	33
Table III.7	Spot EDS analyses at 10 and 40 μ m from the surface. The numbers 1 and 2 indicate two different analyses that were performed at a fixed probe position	38
Table III.8	Knoop hardness and its confidence interval (95%)	42
Table III.9	Critical load L_{C1} and its standard deviation	44
Table IV.1	Coating thickness of duplex coated samples which were subjected to an intermediate treatment	52
Table IV.2	Critical loads L_{C1} , L_{C2} and their confidence interval, C.I.(95%)	54
Table V.1	Sputter cleaning parameters used during the production of single-layered and duplex (Ti,Al)N, Cr-N coatings	65
Table V.2	Plasma heating parameters used during the production of single-layered and duplex (Ti,Al)N, Cr-N coatings	66
Table V.3	Deposition parameters of single-layered (Ti,Al)N and Cr-N coatings	66
Table V.4	Deposition parameters of duplex (Ti,Al)N and Cr-N coatings	67
Table V.5	Surface roughness of single-layered (Ti,Al)N, Cr-N and duplex (Ti,Al)N, Cr-N coatings	69
Table V.6	Coating thickness	72
Table V.7	Critical loads L_{C1} and L_{C2}	84
Table VI.1	Surface roughness of single-layered and duplex TiN, (Ti,Al)N and Cr-N coatings	95

Table VI.2	Thickness of single-layered and duplex TiN, (Ti,Al)N and Cr-N coatings	95
Table VI.3	Critical loads L_{C1} and L_{C2} recorded for duplex and single-layered (Ti,Al)N, TiN, Cr-N coatings	97
Table VI.4	Coating and substrate wear coefficients (k_c and k_s)	98
Table VI.5	Vickers hardness of single-layered and duplex (Ti,Al)N, TiN, Cr-N coatings, plasma nitrided and hardened AISI H13 steels	104
Table VII.1	Knoop microhardness and coating thickness of single-layered (Ti,Al)N, Cr-N and duplex (Ti,Al)N, Cr-N coatings. Nitrided case structure and thickness are also shown for the duplex coatings	119
Table VIII.1	Summary of the most relevant coating properties	132

SYMBOLS AND ABBREVIATIONS

SYMBOLS

λ	= Mean free path for charge exchange collision (m)
a	= Inner diameter of the wear crater (m)
b	= Outer diameter of the wear crater (m)
c	= Intercept of a straight line
C.I. (95%)	= Confidence interval (95%)
D	= Contact diameter in the impact test (m)
d	= Impact ball to sample distance (cm)
F	= Impact force (N)
f	= Impact frequency (Hz)
F_t	= Tangential friction force (N)
$HK_{0.01}$	= Knoop microhardness at a load of 10gf (kgf mm ⁻²)
$HK_{0.025}$	= Knoop microhardness at a load of 25gf (kgf mm ⁻²)
$HK_{0.05}$	= Knoop microhardness at a load of 50gf (kgf mm ⁻²)
$HV_{0.1}$	= Vickers microhardness at a load of 100gf (kgf mm ⁻²)
I_{Arc}	= Low voltage electron source (arc) current (A)
I_{ef}	= Ionisation efficiency
$I_{emission}$	= Emission current (A)
$I_{filament}$	= Filament current (A)
$I_{Substrate}$	= Substrate current (A)
k	= Wear coefficient for bulk materials (m ³ N ⁻¹ m ⁻¹)
k_c	= Coating wear coefficient (m ³ N ⁻¹ m ⁻¹)
k_s	= Substrate wear coefficient (m ³ N ⁻¹ m ⁻¹)
l	= Cathode sheath thickness (m)
L	= Normal force on the sample (N)
L_{C1}	= Critical load for cohesive failure (N)
L_{C2}	= Critical load for adhesive failure (N)

LEI DO DIREITO AUTORAL
 Todos os direitos reservados e protegidos
 pela Lei 9.610/1998.
 Este arquivo não pode ser reproduzido ou
 transmitido sejam quais forem os meios
 empregados: eletrônicos, mecânicos,
 fotográficos ou quaisquer outros.

M	=	Impact mass
m	=	Gradient of a straight line
N_i	=	Number of ions arriving at the sample per square centimetre per second
N_{np}	=	Total number of bombardments per square centimetre per second
P	=	Static air pressure
P_{Ar}	=	Argon partial pressure (Pa)
P_{N_2}	=	Nitrogen partial pressure (Pa)
P_{Total}	=	Total gas pressure (Pa)
P_{ult}	=	Ultimate pressure (Pa)
R	=	Radius of the ball (m)
R_a	=	Centre line average value for the roughness of the surface (μm)
S	=	Distance slid by the ball (m)
t	=	Coating thickness (μm)
$t_{etching}$	=	Etching time used in the intermediate treatment (min)
T_{final}	=	Final temperature (after nitriding or coating) (K)
$T_{heating}$	=	Heating temperature used in the intermediate treatment (K)
V	=	Wear volume (m^3)
V_{Arc}	=	Low arc voltage (V)
V_c	=	Coating volume in the wear crater (m^3)
$V_{Substrate}$	=	Substrate volume (m^3)
V_T	=	Total volume of the wear crater (m^3)

LEI DO DIREITO AUTORAL
 Todos os direitos reservados e protegidos
 Lei 9.610/1998.
 Este arquivo não pode ser reproduzido ou
 transmitido sem a permissão dos meios
 empregados eletrônicos, mecânicos,
 fotográficos ou quaisquer outros.

ABBREVIATIONS

AE	=	Acoustic emission
BAI 640R	=	Name of a Balzers triode ion plating system
CVD	=	Chemical vapour deposition
d.c.	=	Direct current
EDS	=	Energy dispersive spectroscopy
EDX	=	X-ray energy dispersive analyses
EHV	=	High voltage power supply for the e-gun (Balzers PAPVD equipment)
GDOES	=	Glow discharge optical emission spectroscopy
GL73	=	Constant current low voltage (Balzers PAPVD equipment)
IP35L	=	Name of a Tecvac triode ion plating system
IP70L	=	Name of a Tecvac triode ion plating system
LOM	=	Light optical microscopy
OES	=	Optical emission spectroscopy
PACVD	=	Plasma-assisted chemical vapour deposition
PAPVD	=	Plasma-assisted physical vapour deposition
PVD	=	Physical vapour deposition
r.f.	=	Radio frequency
SEM	=	Scanning electron microscopy
TCR	=	Constant voltage power supply (Balzers PAPVD equipment)
XRD	=	X-ray diffraction

LEI DO DIREITO AUTORAL
Todos os direitos reservados e protegidos
pela Lei 9.610/1998.
Este arquivo não pode ser reproduzido ou
transmitido sejam quais forem os meios
empregados: eletrônicos, mecânicos,
fotográficos ou quaisquer outros.

ABSTRACT

It has already been reported that duplex coatings, consisting of plasma nitriding of steel substrates and subsequent deposition of hard coatings by PAPVD (plasma-assisted physical vapour deposition), can improve both wear and contact fatigue resistance and also the load support capability of steel substrates. However, the adhesion at coating/substrate interface can be strongly affected by the presence of a compound layer, which can be produced during the plasma nitriding step. This compound layer can destabilise during coating deposition; its destabilisation would lead duplex coatings to exhibit poor adhesion. The aim of this thesis was to produce well adherent PAPVD duplex coatings on AISI H13 steel substrates for tribological applications at elevated temperatures. In the first stage of the project, duplex TiN coatings have been used to investigate the problem of compound layer destabilisation. An intermediate treatment consisting of cooling down the samples in vacuum and carrying out an Ar plasma-etching step has been developed. This treatment allows the production of duplex coatings with good adhesion strength by successfully avoiding compound layer destabilisation. It also elucidates a systematic approach to produce duplex coatings which are compound-layer-free, by removing this iron nitride layer through an Ar sputter mechanism. The same adhesion strength was measured for duplex TiN coatings with nitrated cases consisting of mono-phase ϵ compound layer + diffusion zone and for duplex TiN coatings with nitrated cases consisting of a diffusion zone only. Furthermore, a duplex TiN coating with a mono-phase ϵ compound layer + diffusion zone outperformed duplex TiN coatings with diffusion zones in impact tests, suggesting that hard, dense mono-phase compound layers are able to act as a proper interface between harder, more brittle PVD coatings and relatively softer, more ductile diffusion layers of plasma nitrated substrates. In the second stage, single-layered and duplex (Ti,Al)N, Cr-N coatings were prepared and characterised by XRD, GDOES, LOM, SEM, Knoop microhardness measurements and scratch testing. Their wear resistance (and also of single-layered and duplex TiN coatings) was evaluated by micro-abrasive wear tests. Impact tests were also carried out to investigate their resistance to dynamic loading. Results pointed out that the duplex treatment improved the performance of single-layered PAPVD coatings with respect to micro-abrasive wear and impact

impact resistance. This was mainly achieved by increasing the load support for the thin, hard PAPVD coatings and also preventing substrate elastic and plastic deformation. Therefore, duplex coatings are expected to be successfully used on tribological applications that require both wear and dynamic impact resistances. Duplex (Ti,Al)N coatings had the highest wear resistance to micro-abrasion, followed by single-layered (Ti,Al)N coatings whereas duplex (Ti,Al)N and duplex Cr-N coatings had the best performances in the impact tests. This work reveals that both duplex (Ti,Al)N and Cr-N coatings are promising duplex coatings for tribological applications at elevated temperatures. In particular, these coatings have a great potentiality to improve the lifetime of AISI H13 shear knives, which are used to cut steel ingots during a continuous ingot cast process. Nevertheless, further optimisations are still required in order to introduce these coatings on industrial field tests. For instance, film thickness needs to be optimised for the duplex Cr-N coatings in order to yield a satisfactory resistance to abrasive wear.

CHAPTER 1: INTRODUCTION

In today's industry, plasma surface engineering technologies, owing to a number of advantages over conventional surface engineering processes, are increasingly being used to improve the tribological surface quality of various steels. Plasma surface engineering processes can be divided into two main groups: i) plasma-activated treatment of the surface and ii) plasma-assisted deposition of hard coatings. Plasma immersion ion implantation, plasma nitriding and carburizing are typical processes which belong to the first group whereas Plasma-Assisted Physical Vapour Deposition (PAPVD), Plasma-Assisted Chemical Vapour Deposition (PACVD) and plasma spraying are technologies traditionally used for coating deposition.

The duplex surface engineering, also referred to as the second generation surface engineering, emerged in the late 1980's. It comprises the sequential application of two or more established surface technologies to produce a surface composite with combined properties which are unobtainable through any individual surface technology. Since the possible combinations of plasma surface technologies are virtually unlimited, many duplex treatments have been developed so far. One of these duplex treatments involves plasma nitriding followed by PAPVD deposition of hard coatings.

PAPVD thin hard coatings can provide a surface with dramatically improved properties in terms of low friction and high resistance to wear and corrosion, but catastrophic premature failure will occur if the substrate plastically deforms under a high applied load. On the other hand, a nitrided subsurface exhibits a high load bearing capacity and high fatigue strength, which in turn helps in preventing elastic and plastic deformation of the substrate.

It seems that a combined treatment of plasma nitriding and PAPVD coating was invented by Berghaus in the early 1930's⁽¹⁻³⁾. Since then many duplex coatings have been produced by means of a two-stage process: substrates are first plasma nitrided in a nitriding plant (conventional diode plasma nitriding) and subsequently coated in a PAPVD equipment. In the early 1980's, Korhonen and Sirvio⁽⁴⁾ showed for the first

time that it was possible to achieve a plasma-assisted nitriding treatment in a standard low pressure PAPVD equipment. In 1983, the first duplex coating consisting of plasma nitriding and ion-plated TiN coating was continuously produced in a PAPVD plant⁽⁵⁾.

Many attempts have been made in order to produce duplex coatings by means of a continuous process in PAPVD systems⁽⁶⁻¹⁹⁾. This approach has many advantages that compensate for the disadvantage of using an expensive PVD coater for a nitriding treatment, such as⁽²⁰⁻²²⁾: i) better control of adhesion because of an optimum transition between thermochemical treatment and coating; ii) improved kinetics of the low pressure triode process; iii) carbon-free ϵ compound layers that exhibit better corrosion resistance; iv) simpler logistics and better delivery time for the customer and v) lower gas flow rates.

Obtaining satisfactory adhesion strength between PAPVD hard coatings and nitrided layers is a key issue in duplex coating processing. The difficulties arise from compatibility problems between plasma nitriding and coating deposition. Incorrect process control will lead to the formation of a soft “black layer” below the coating by thermochemical decomposition of the compound layer (iron nitride layer), which deteriorates the load bearing capacity of the composite and, consequently, the adhesion between the hard coating and the nitrided subsurface. Therefore, good coating-subsurface adhesion can only be achieved if these two processes are properly combined and carefully controlled.

With exception of Anjing *et al.*⁽²⁷⁾ who considered the presence of a γ' -compound layer as a favourable factor for the adhesion of their duplex coatings, several authors reported poor adhesion if an iron nitride layer was formed during plasma nitriding^(6,11-15,23-26). The lack of consistency in several results is probably related to the varying nitriding and coating procedures applied on different surfaces. The transition from plasma nitriding to coating deposition seems to be particularly important.

The problem of the formation of a “black layer” has been addressed by avoiding compound layer formation during plasma nitriding (bright nitriding) or performing a

mechanical grinding of this layer before coating. The first procedure can be easily performed by adjusting process parameters (total gas pressure, partial gas pressures, temperature, bias voltage, etc). The latter, however, is not practical if plasma nitriding and coating deposition are carried out in a continuous process.

Glow discharges often used in plasma surface engineering processes can exhibit different characteristics/properties depending on how the discharge is generated. Up to now, a universal model for plasma nitriding has not been proposed yet. Typical plasma nitriding is usually carried out at high gas pressures (~0.1-1.0kPa) in a diode configuration whilst most of plasma based coatings are produced at comparatively lower pressures (0.1-1.0Pa) in a triode layout. Results indicate that the energy distribution of species in a d.c. diode discharge is quite different from that in a d.c. triode configuration^(6,28-30). Hence, it is expected that the mechanisms and process parameters leading to compound layer formation in a triode system will be distinct from the ones in a diode layout.

There are several reports concerning major improvements in the lifetime of cutting tools by applying hard thin coatings⁽³¹⁾. It has been claimed to be more difficult to achieve lifetime improvements for tools operating at hot working conditions^(31,32). Coating failure is often initiated by cracking which immediately leads to micro-pickup of work material along the cracks and formation of large strongly adherent welded regions.

In many industrial applications, tools are subjected to repeated mechanical and thermal loading which often lead to dimensional changes in the workpiece. Finally, damage to the stressed tool surface occurs. The damage appears as wear, plastic deformation, thermal or mechanical fatigue and wear in the form of adhesion or friction welding. At elevated temperatures, chemical stability as well as oxidation/corrosion resistance become important factors in preventing coating failure. Thus, in such harsh environments, the coating material should provide good abrasive wear resistance, low adhesion to the workpiece material but high adhesion to the tool material, high chemical stability, toughness and oxidation/corrosion resistance. Hence, duplex coatings have a great potentiality to be applied on tools which operate under such conditions. The

nitrided case will increase the fatigue resistance of the composite system; good wear and oxidation resistance can be achieved by selecting thin hard coatings to fulfil such requirements.

In the present thesis, tribological duplex coatings intended for high temperature applications were evaluated with respect to their fundamental mechanical and tribological properties. Special attention was given to a better understanding of duplex coating processing, especially to the development of an intermediate treatment that allows to produce duplex coatings with good adhesion even if a compound layer is formed during plasma nitriding. This intermediate treatment also provides a way to produce duplex coatings which are compound-layer-free.

CHAPTER 2: OBJECTIVES

This work aimed at producing PAPVD duplex coatings for tribological applications at elevated temperatures. Plasma nitriding and coating deposition were carried out in a PAPVD equipment by means of a continuous process. Three hard PVD coatings were used for producing duplex coatings on plasma nitrided AISI H13 steel substrates: TiN, (Ti,Al)N and Cr-N. Single-layered TiN, (Ti,Al)N and Cr-N coatings on AISI H13 substrates (i.e., without plasma nitriding) were also produced for comparison. The choice of such coatings was based on their promising application onto AISI H13 shear knives that are used to cut steel ingots during a continuous ingot casting process at Gerdau S.A.

An intermediate treatment was performed in order to investigate the compound layer destabilisation during coating deposition. In this first stage, duplex TiN coatings were employed. After ensuring that well-adherent coatings would be obtained, duplex and single-layered (Ti,Al)N and Cr-N coatings were produced. These coatings were characterised by microhardness and surface roughness measurements, XRD, SEM, GDOES and scratch tests. Tribological tests were also carried out to evaluate their micro-abrasive wear and impact resistance.

CHAPTER 3: DUPLEX COATINGS

3.1. Background

In this chapter, a brief summary of plasma nitriding and ion plating techniques is presented and the most important issues concerning duplex coating development are discussed. The possibilities of carrying out a duplex treatment in a PAPVD ion plating equipment is highlighted and the first results from a duplex treatment consisting of plasma nitriding + TiN coating are presented.

3.1.1. One possible industrial application for duplex coatings

During continuous ingot casting at Gerdau S.A. (figures 3.1 and 3.2), two shear knives are used to cut hot steel ingots. The shear knives are hardened and tempered AISI H13 steel (55HRC). A load equal to 200 tons is applied to the superior shear knife during cutting operation. The temperature of the ingots, when cutting is performed, is around 973-1063K. This superior shear knife is subjected to cyclical loading and its temperature varies from 653-693K (during cutting operation) to 503K. Such harsh oxidant environment leads to a severe damage in these tools. The damage appears as wear, probably initiated by cracks in the tool surface. Fatigue is also likely to occur due to cyclical loading and temperature cycles. The lifetime of such shear knife is estimated to be 6000-10000 cutting operations. By the end of its lifetime, some extent of plastic deformation can be seen at the cross-sectional surface of the ingots. The frequent stops to replace the shear knives have a detrimental effect on the productivity of the continuous ingot cast process.

LEI DO DIREITO AUTORAL
Todos os direitos reservados e protegidos
pela Lei 9.610/1998.
Este arquivo não pode ser reproduzido ou
transmitido sejam quais forem os meios
empregados: eletrônicos, mecânicos,
fotográficos ou quaisquer outros.

LEI DO DIREITO AUTORAL
Todos os direitos reservados e protegidos
n.º 610/1998.
reproduzido ou
mecânicos,
er outros.

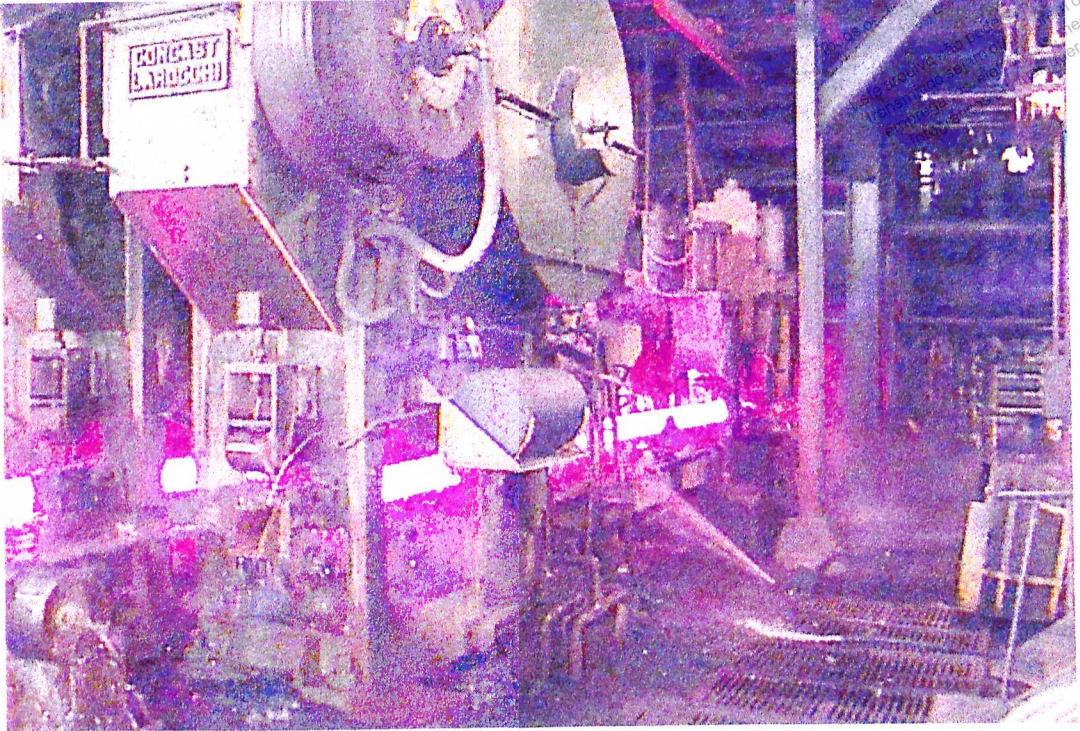


Figure 3.1 – Continuous ingot cast process at Gerdau S.A.

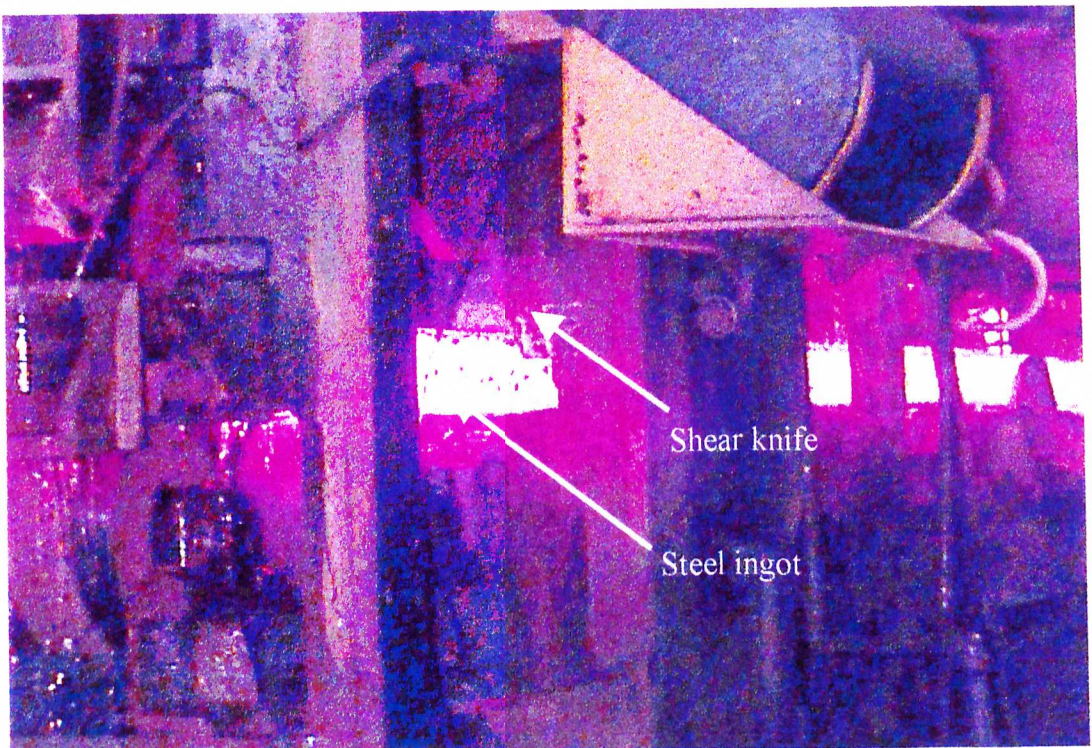


Figure 3.2 – Superior shear knife which is used to cut the steel ingots.

3.1.2. Plasma nitriding

Plasma nitriding (or ion nitriding) is a method of surface hardening using glow discharge technology to introduce nitrogen to the surface of a metal part for subsequent diffusion into its bulk. In a vacuum, high-voltage electrical energy is used to form a plasma, through which nitrogen ions are accelerated to impinge on the workpiece. The ion bombardment heats the workpiece, cleans the surface and provides active nitrogen. Plasma nitriding provides better control of case chemistry and uniformity and has other advantages, such as lower part distortion than conventional (gas) nitriding. The major difference between plasma and gas nitriding is the mechanism used to generate active nitrogen at the surface of the workpiece.

The plasma nitriding process has reached a high level of maturity and perfection, holding an important position in industry today. In the literature there are several reports about improving wear, corrosion and fatigue resistance through plasma nitriding⁽³³⁻⁴¹⁾.

The glow discharge used as a processing plasma for surface modification can be established and sustained in various ways: d.c. diode discharges, r.f. discharges, microwave discharges, electron emission configurations and magnetically enhanced discharges. In plasma nitriding the d.c. diode discharge is most widely used. Under these discharge conditions, pressures in the range of 133.3 to 1333.3Pa (1 to 10 Torr) and voltages of 500 to 1000V are normally employed.

Glow discharges are non-equilibrium plasmas which are characterised by a relatively low gas density. Because of their low gas density, the number of collisions between electrons and atoms/molecules is reduced when compared to equilibrium plasmas. Therefore, the temperature of the electrons is much higher than the temperature of the ions and neutrals. Electrons usually have temperatures of several tens of thousands of degrees Kelvin whilst the ions and neutrals have temperatures of a few hundred degrees Kelvin only⁽⁴²⁻⁴⁴⁾. Hence, electrons can promote excitation and ionisation of neutrals, resulting in more active chemical reactions. The degree of ionisation in glow discharges is rather low, typically 10^{-4} , and the gas consists mostly of neutrals^(42,44).

Several types of glow discharges exist, depending on the relationship between voltage and current, as shown in figure 3.3 for an argon discharge. Nearly all plasma thermochemical processes are performed in the abnormal glow in which the current increases with the voltage. In this region the glow covers the specimen (the cathode of the discharge) uniformly and therefore, uniform treatments can be expected^(33,34,45). The possibility that the abnormal, unstable glow discharge may turn into the stable arc discharge was a serious obstacle to large-scale application of plasma nitriding in industry many years ago. With the advancement of modern electronics, new plasma power generators have been developed to prevent the formation of arcs, so that the glow discharge can be safely maintained at high current densities in the abnormal glow.

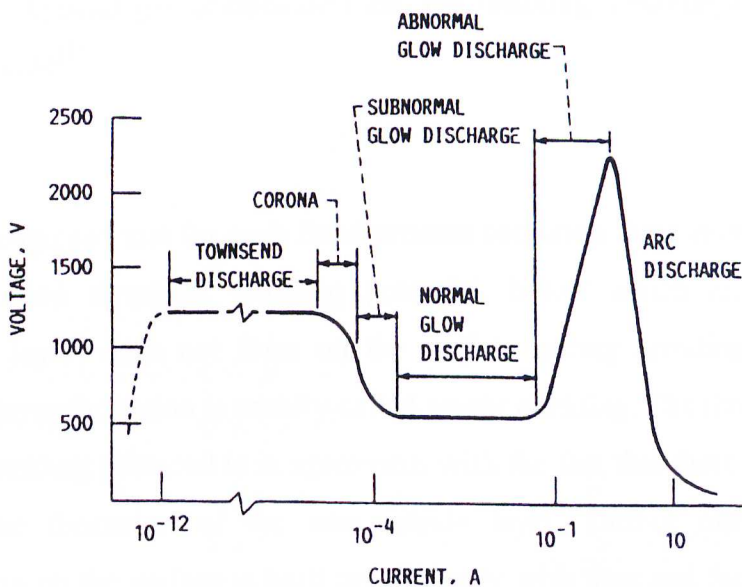


Figure 3.3 – Voltage – current characteristics of different types of discharges in argon⁽⁴⁵⁾.

During plasma nitriding, nitrogen is adsorbed on the surface of the steel, diffuses inward at temperatures around 773K and hardening is accomplished by precipitation of very fine nitride particles in the diffusion zone. Depending on nitrogen concentration, iron nitride layers (also known as compound layers) of face-centred cubic γ' Fe_4N or close-packed hexagonal ϵ Fe_{2-3}N may form. The structure of the nitrided case (compound layer + diffusion zone) can be carefully controlled by adjusting treatment parameters

such as temperature, gas composition, gas pressure, time and current density. The gas composition has a strong influence on the metallurgical structures of the nitrided case, as illustrated in figure 3.4.

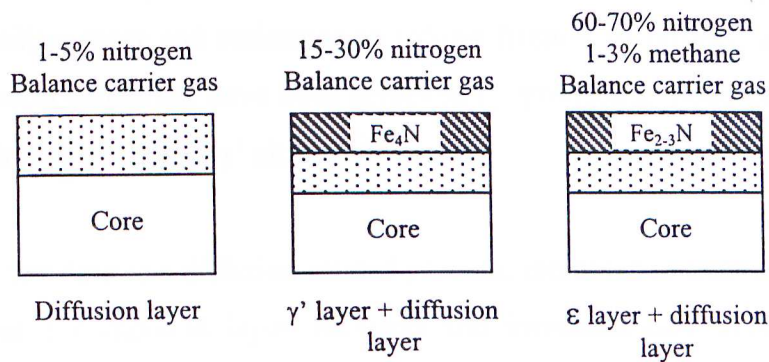


Figure 3.4 – Typical gas composition and the resulting metallurgical configuration of the nitrided case⁽³³⁾.

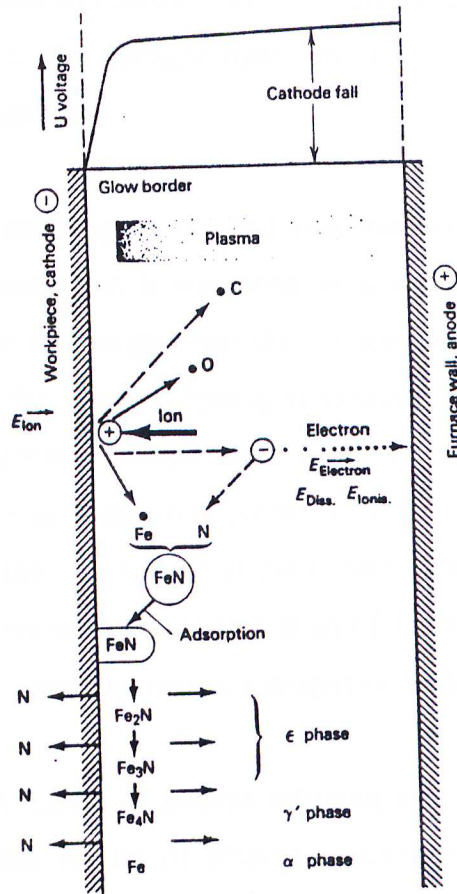
It is well recognised that for each fixed process condition there exists a critical nitrogen potential, called threshold nitriding potential, below which an iron nitride layer (compound layer) does not form on the surface during nitriding. Nitriding without compound layer formation is usually called *bright nitriding*. The time dependence of the threshold nitriding potential is in agreement with the fact that there exists an incubation time for the formation of the iron nitride layer. During nitriding, the nitrogen concentration on the surface is built up gradually with time and the incubation time for the formation of the iron nitride layer is the time necessary for the build up of the critical nitrogen concentration on the surface. The threshold nitriding potential is also temperature dependent⁽²³⁾. When the nitriding potential (i.e. the nitrogen/balance carrier gas) is above the threshold value, a compound layer consisting of γ' Fe_4N and/or ϵ $\text{Fe}_{2.3}\text{N}$ will form on the surface of a steel component. A mono-phase γ' Fe_4N compound layer is often produced on the surface when the nitriding temperature is very high or the nitriding potential is sufficiently low. With decreasing nitriding temperature and time or increasing nitriding potential the mono-phase ϵ $\text{Fe}_{2.3}\text{N}$ compound layer is usually formed. Plasma nitriding provides much more dense compound layers than

conventional (gas) nitriding. Iron nitride layers produced by the latter process have a high level of porosity in the outer region of the layer. Dual-phase layers consisting of γ' Fe_4N and ϵ Fe_{2-3}N are susceptible to fracture because of two factors: weak bonding at the interface between phases and different thermal expansion coefficients in the two phases^(33,46). The homogeneity of the compound layer structure and its thickness influence ductility, wear and resistance to rolling friction of nitrided steel substrates. Better mechanical properties have been achieved by producing mono-phase compound layers consisting of either ϵ or γ' nitrides⁽⁴⁶⁾.

Since plasma nitriding is a diffusion-related process, increases in treatment temperature lead to increased compound layer thickness and increased case depths for a given treatment time, but an overall decrease in peak hardness values is achieved. As with age-hardening steels, where a maximum in hardness is achieved at a particular aging temperature and time, the maximum hardness achieved by plasma nitriding is based on optimum precipitate density and size; these can be lost at higher temperatures and longer times due to precipitate growth and further tempering of the matrix⁽⁴⁷⁾.

Presently there is no universal model which explains the plasma nitriding process. Nevertheless numerous mechanisms have been suggested to explain this concept. The model which was proposed by Kölbel^(33-35,39) is by far the most used to describe the mechanisms that are supposed to take place during plasma nitriding of steel. This model is based on sputtering of Fe atoms from the workpiece and subsequent condensation of FeN on surface (see figure 3.5). The major mechanisms are:

1. production of ionised and neutral nitrogen atoms by energetic electrons;
2. sputtering of Fe and contaminants from the work surface by these ionised atoms;
3. formation of FeN iron nitrides by sputtered iron atoms and neutral nitrogen atoms;
4. condensation of the FeN nitride on uncooled cathodic workpiece surfaces;
5. decomposition of FeN into the lower nitrides Fe_2N , Fe_3N and Fe_4N ; the nitrogen which is liberated in this process will diffuse into the workpiece and, in part, back to the plasma.



LEI DO DIREITO AUTORAL
 Todos os direitos reservados e protegidos
 pela Lei 9.610/1998.
 Este arquivo não pode ser reproduzido ou
 transmitido sejam quais forem os meios
 empregados: eletrônicos, mecânicos,
 fotográficos ou quaisquer outros.

Figure 3.5 – Surface reactions during plasma nitriding according to Kölbel's model⁽³³⁾.

In 1973 Hudis⁽⁴⁸⁾ conducted a study of ion nitriding in N_2-H_2 , $Ar-N_2$ and $Ar-N_2-H_2$ gas mixtures. The aim of his work was to identify the active plasma ingredients which cause nitriding. Two possible mechanisms could explain plasma nitriding: gas absorption and ionic bombardment. The nitrogen partial pressure was kept constant in all gas mixtures and a mass-energy analyser was used. It was concluded that plasma nitriding does not take place by gas absorption, since an electrically floating 773K sample immersed in an r.f. plasma would not nitride. Plasma nitriding apparently required current and was caused by ionic bombardment of the cathode. The majority of ionic species in $Ar-N_2$ plasmas were N^+ and N_2^+ ; when hydrogen was added, H^+ and NH_3^+ became the dominant species and a large reduction of N^+ and N_2^+ was observed. When argon was completely replaced by hydrogen (N_2-H_2), the reduction of the ionic species N^+ and N_2^+ was even more dramatic. In such discharges, nitrogen was carried to the cathode by the

Formation of these nitrides at the very early stages of plasma nitriding suggested that these nitrides were produced by sputtering of iron atoms from the cathode surface, forming nitrides in the cathode sheath and condensing at the cathode surface as previously pointed out by Kölbl. In contrast to N_2-H_2 discharges, a N_2 discharge did not exhibit ξ phase formation. This was attributed either to the lower activation energy required to form this phase with the active ingredients of a N_2-H_2 discharge or to the reduced stability of the Fe_2N under pure nitrogen discharge that led to an immediate decomposition. The growth of the iron nitride layers was not parabolic with time at the initial stages of plasma nitriding as opposed to observations in gas nitriding. It seemed that the rate-limiting step is the nitrogen diffusion in the iron nitride layer which controls the total flux of nitrogen to diffuse into the bulk. The ion bombardment effect at the surface could produce faster diffusion in the iron nitride layer, therefore increasing the kinetics of nitriding in iron.

In 1982 Korhonen and Sirvio⁽⁴⁾ demonstrated, for the first time, that it was possible to achieve plasma nitriding of steel substrates in low pressure plasmas, using an ion plating equipment in triode configuration. Since then, several reports about achieving plasma nitriding in low pressure triode layouts have been produced^(5-11,52-56). The major differences between d.c. glow discharges in diode and triode configurations will be briefly discussed in section 3.1.4 and their impact on plasma nitriding will be highlighted.

3.1.3. The ion plating process

PVD (Physical vapour deposition) is a generic terminology used to designate deposition technologies which involve the atomisation or vaporisation of material from a solid source and its deposition on the substrate to form a coating. Evaporation, sputtering and ion plating are examples of PVD technologies^(31,43,44,57).

Although the most basic PVD process (the non-reactive evaporation technique) had been reported by Faraday in 1857, plasma-assisted PVD processes became available only in the 1930's⁽⁴³⁾. Thus the term "Plasma-assisted physical vapour deposition"

(PAPVD) refers to PVD processes which utilise a glow discharge to enhance the properties of the coating produced.

Ion plating is a generic term applied to atomistic coating deposition processes in which the substrate and/or the depositing coating is subjected to a flux of high energy particles sufficient to cause changes in the interfacial region or coating properties compared to the non-bombarded deposition. Such changes may be in the coating adhesion, coating morphology, coating density and coating stress. In 1964, the ion plating technique was first reported in the literature by Mattox^(43,44).

Bombardment of the substrate surface by energetic particles prior to the deposition of the coating material allows *in situ* cleaning of the surface. This bombardment for cleaning purposes is usually carried out in an inert gas discharge. The energetic species used to bombard the growing film can be either ions or neutrals, although charged ions are the majority species. The use of a partial pressure of reactive gas (i.e. nitrogen, oxygen, acetylene, hydrocarbon) allows the deposition of compounds in *reactive ion plating*.

Continuous ion bombardment during coating deposition will cause sputtering of the substrate surface. Therefore, for a coating to form, it is necessary for the deposition rate to exceed the sputtering rate. From the standpoint of adhesion, the major benefits obtained from the ion plating process are its ability to⁽⁴⁴⁾:

- modify the substrate surface in a manner conducive to good adhesion and maintain this condition until the coating begins to form;
- provide a high energy flux to the substrate, giving a high surface temperature, thus enhancing diffusion and chemical reactions without necessitating bulk heating;
- alter the surface and interfacial structure by introducing high defect concentrations, physically mixing the coating and substrate material, and influencing the nucleation and growth of the depositing coating.

Energetic bombardment prior to and during the initial stages of coating formation can enhance adhesion by^(44,57):

- removing contaminant layers;
- changing the surface chemistry;
- generating a microscopically rough surface;
- increasing the nucleation density by forming nucleation sites such as defects, implanted species and recoil implanted species;
- increasing the surface mobility of adatoms;
- decreasing the formation of interfacial voids;
- introducing thermal energy and defects directly into the near-surface region, thereby promoting reaction and diffusion.

Another advantage of the ion plating technique is its ability to promote a uniform coverage of surfaces when compared to vacuum evaporation processes. This ability results from gas scattering, entrainment and redeposition from the sputtered coating surface. This allows coatings to be formed in recesses and areas remote from the source-substrate line of sight, thus giving more complete surface coverage.

Energetic bombardment during coating growth can modify a number of coating properties, including density, bulk morphology, surface morphology, grain size, porosity, crystallographic orientation and electrical resistivity. Ion-plated coatings usually have relatively high compressive residual stresses due to energetic particle bombardment.

In ion plating processing, the discharge can be formed using a number of configurations. A d.c. diode configuration with an electrically conductive substrate serving as the cathode is often used. D.c. triode configurations have become quite popular over the years. This configuration is achieved by using a third positive electrode or a thermionic emitter (i.e. a biased tungsten filament) to enhance the degree of ionisation in the plasma^(55,58,59). Hence, much lower pressures are required to sustain the discharge. R.f. and microwave discharges are also commonly employed in ion plating processes.

It is important that bombardment of the substrate during surface preparation stage be continued into the deposition stage, where adatoms (atoms adsorbed on a surface so they will migrate over the surface) are continually being added to the surface. This prevents the surface from being re-contaminated. Bombardment also enhances the formation of a diffusion or compound-type interface on the “clean” surface if the materials are mutually soluble, or it enhances the formation of a pseudodiffusion-type of interface, due to energetic bombardment, if the materials are insoluble⁽⁵⁷⁾. Forward sputtering, sputtering and re-deposition, increased nucleation density and increased surface mobilities of adatoms on the surface under bombardment conditions can be important in disrupting the columnar structure of the coatings and thereby increasing coating density. The bombardment, which also improves surface coverage, reduces the pinhole porosity in a deposited coating. Better surface coverage and increased density are reflected in coatings properties such as:

- better corrosion resistance;
- lower chemical etch rate;
- higher hardness;
- lowered electrical resistivity of metal coatings;
- lowered gaseous and water vapour permeation through the coating;
- increased index of refraction of dielectric coatings.

However, a high level of gas incorporation, defect concentration, residual stress and formation of voids in ion-plated coatings have been observed if the bombarding species is too energetic and the substrate temperature is very low. At low temperatures (particularly advantageous when the substrate is thermally sensitive) the bombarding energy should be kept low (less than 300eV) in order to minimise gas incorporation effects⁽⁵⁷⁾.

3.1.4. Generation of d.c. glow discharges: diode x triode layouts

Although the use of plasma diagnostic techniques have increased throughout the years⁽⁶⁰⁻⁷⁰⁾, especially as a tool for controlling coating deposition and plasma nitriding, there are still little data available on the energy distribution of ions and neutrals reaching

the cathode. Undoubtedly higher ionisation rates can be achieved under triode conditions, whereby a third positive electrode or a thermionic electron source (i.e. a biased tungsten filament) will increase ionisation in the plasma^(55,58,59). Because of that, much lower pressures are required to sustain such discharges than in a diode layout. D.c. diode glow discharges are usually run at pressures of 100-1000Pa whilst d.c. triode glow discharges are operated at 0.1-1.0Pa. Besides, the cathode voltage is kept at 500-1000V in the former, oppositely to 100-500V of typical d.c. triode discharges. At lower pressures, fewer collisions are expected to occur within the cathode sheath and, therefore, most of the ions reaching the cathode are expected to have energies corresponding to the cathode fall voltage. Contrarily, under diode conditions, collisions are expected to occur within the sheath and the ions reaching the cathode will have much lower energies than the cathode fall voltage. Clearly the energy distribution of ions and neutrals reaching the cathode will greatly differ in diode and triode conditions, thus leading to differences in coating morphology and plasma nitriding performance.

Although plasma diagnostics is a topic outside the scope of this work, some results of the literature will be discussed in order to show how feasible plasma nitriding can be at low pressure triode layouts and, hence, possible to be performed in an ion plating equipment.

The factors which govern the distribution of energies for ions and neutrals arriving at the cathode are the mean free path for charge exchange collision (λ) and the cathode sheath thickness l (also known as the cathode fall length or the dark space distance)^(71,72). The ratio l/λ critically influences the distribution. Reducing l/λ produces an energy spectrum in which a larger proportion of the ions have energies nearer the maximum. Therefore, if there is a need for more ions to exceed some critical minimum energy, this can be achieved by decreasing l/λ .

Another relevant parameter is the degree of ionisation (ionisation efficiency, I_{ef}), defined as⁽²⁸⁾

$$I_{ef} = \frac{N_i \times 100\%_i}{N_{np}} \quad (3.1)$$

where N_i is the number of ions arriving at the sample per square centimetre per second and N_{np} is the total number of bombardments per square centimetre per second.

The degree of ionisation considers the effects of both pressure and current density. The cathode current density gives an indication of ions arriving at the cathode, but this on its own does not take account of the total number of bombarding particles, most of which are non-ionised in such discharge conditions. Although a proportion of these particles will be high energy neutrals (ions that have undergone charge exchange) the majority are thermal neutrals and their population tend to increase with pressure. Therefore, two discharge systems may have similar energy spectra and current density values, but if one requires a higher pressure than the other to obtain these characteristics, it may in practice be inferior, as the greater number of thermal neutrals will tend to dilute any beneficial effects from the more energetic species.

In argon d.c. diode discharges, the ratio l/λ is typically 10-15 whereas the d.c. triode discharge exhibit l/λ values less than unity⁽²⁸⁾. So, under triode conditions, a virtually collisionless cathode sheath regime will operate. An advantage of triode discharge systems is that the substrate current density (and thus discharge power) can be controlled via an electron emission source whilst total gas pressure and cathode voltage are independently adjusted. Therefore, lower pressures and voltages than those normally required can be employed, offering reductions in l/λ when compared to diode layouts. The ionisation efficiency (I_{ef}) is around 4% in triode discharges and only 0.01% in diode systems⁽²⁸⁾. Thus, in triode layouts, greater proportion of the total energy is supplied to the substrate by ionic species rather than by high energy neutrals. Thermionic support yields lower l/λ and higher I_{ef} values than a positively biased third electrode⁽²⁸⁾.

Under d.c. diode conditions, the majority of the ions incident at the substrate will be N^+ , although the primary ionic species in the cathode sheath are N_2^+ . In such systems, there is a large amount of dissociation of N_2^+ into N^+ via dissociative charge exchange

collisions in the sheath⁽²⁸⁻³⁰⁾. The same trend is not observed in triode discharges, where most of the ionic species reaching the cathode are N_2^+ ⁽²⁸⁻³⁰⁾.

There is evidence to suggest that there exists a threshold energy above which nitriding is effective. This threshold energy seems to be 100-150eV^(6,52). Under d.c. diode conditions, plasma nitriding starts to become effective when the cathode voltage is higher than 500V; at about 500V, only 10% of the incident species have sufficient energy to exceed the threshold. At cathode voltages as low as 200V, 0.001% of the incident species will exceed 150eV and nitriding becomes ineffective⁽⁶⁾. In triode layouts, plasma nitriding is feasible at voltages as low as 200V^(6,52), oppositely to diode layouts. At such voltages, a large amount of the incident species will have sufficient energy to exceed the threshold. An improvement of case hardness was observed with increasing voltages up to 500V in triode systems. However, the total case depth remained constant at around 60-70 μ m with a given power density⁽⁵²⁾. Nitriding at very low cathode voltages (< 200V) is possible under triode conditions and seems to be advantageous for the treatment of complex shaped components, where a thin sheath is desirable for optimum hole and recess penetration⁽⁶⁾.

3.1.5. Duplex coatings

In 1983, Korhonen and Sirvio⁽⁵⁾ showed for the first time that a plasma-assisted nitriding treatment was feasible in a standard low pressure ion plating equipment. Several “*duplex coatings*” consisting of plasma nitriding and subsequent PVD hard coatings have been produced since then^(6-27,73-99).

Duplex coatings have been proven to increase the load support capacity of substrates^(7,14,23,27,95). Improvements on wear^(7,9,11,16-18,23,92,93), corrosion^(16,19,21,82,89) and fatigue resistance^(7,16,90,92) of steel substrates have also been reported. However, there are little data available on their performance at elevated temperatures⁽¹⁸⁾. Some duplex coatings have been successfully used in industrial applications^(11,22,95,98), including tools for hot working⁽⁹⁴⁾.

collisions in the sheath⁽²⁸⁻³⁰⁾. The same trend is not observed in triode discharges, where most of the ionic species reaching the cathode are N_2^+ ⁽²⁸⁻³⁰⁾.

There is evidence to suggest that there exists a threshold energy above which nitriding is effective. This threshold energy seems to be 100-150eV^(6,52). Under d.c. diode conditions, plasma nitriding starts to become effective when the cathode voltage is higher than 500V; at about 500V, only 10% of the incident species have sufficient energy to exceed the threshold. At cathode voltages as low as 200V, 0.001% of the incident species will exceed 150eV and nitriding becomes ineffective⁽⁶⁾. In triode layouts, plasma nitriding is feasible at voltages as low as 200V^(6,52), oppositely to diode layouts. At such voltages, a large amount of the incident species will have sufficient energy to exceed the threshold. An improvement of case hardness was observed with increasing voltages up to 500V in triode systems. However, the total case depth remained constant at around 60-70 μ m with a given power density⁽⁵²⁾. Nitriding at very low cathode voltages (< 200V) is possible under triode conditions and seems to be advantageous for the treatment of complex shaped components, where a thin sheath is desirable for optimum hole and recess penetration⁽⁶⁾.

3.1.5. Duplex coatings

In 1983, Korhonen and Sirvio⁽⁵⁾ showed for the first time that a plasma-assisted nitriding treatment was feasible in a standard low pressure ion plating equipment. Several “*duplex coatings*” consisting of plasma nitriding and subsequent PVD hard coatings have been produced since then^(6-27,73-99).

Duplex coatings have been proven to increase the load support capacity of substrates^(7,14,23,27,95). Improvements on wear^(7,9,11,16-18,23,92,93), corrosion^(16,19,21,82,89) and fatigue resistance^(7,16,90,92) of steel substrates have also been reported. However, there are little data available on their performance at elevated temperatures⁽¹⁸⁾. Some duplex coatings have been successfully used in industrial applications^(11,22,95,98), including tools for hot working⁽⁹⁴⁾.

A critical issue in duplex coatings processing is the adhesion of the hard PVD coating to the nitrided case of steel. Bad adhesion has been observed in many duplex-treated systems. Sun and Bell^(23,24) showed that the lack of adhesion was due to a soft “black layer” between the hard coating and the compound layer. This layer was named “black layer” due to its etching behaviour in Nital. If the compound layer was removed by grinding or the specimen was bright nitrided prior to coating, no black layer could be observed in the composite. X-ray diffraction results indicated that the soft layer was mainly α -Fe, suggesting that the black layer was the product of the decomposition of the outer part of the compound layer during the ion plating process. Obviously this soft layer below the coating deteriorates the load-bearing capability of the composite through reduced bonding strength between the nitrided surface and the outermost hard coating. Since the iron nitrides ϵ -Fe_{2.3}N and γ' -Fe₄N are unstable at temperatures around 773K, compound layer destabilisation (i.e., formation of the black layer) is greatly dependent on PVD process temperature. As a matter of fact, when the temperature had been held below 723K in a H₂ plasma, decomposition of the compound layer did not occur^(23,24).

In a companion study, Dingremont *et al.*⁽¹³⁾ showed that not only the PVD process temperature could promote black layer formation, but also the ion bombardment during the etching step of the coating process would lead to compound layer destabilisation. Compound layer destabilisation occurred in a pure argon plasma when the temperature exceeded 623K. They attributed this destabilisation to a breakthrough of a thin oxide layer by the ion etch process. It was assumed that a thin oxide layer had probably been formed on the surface of the substrate during the nitriding treatment or in the coating phase during the final degassing of the reactors wall during heating. This film is supposed to act as a diffusion barrier between the compound layer and the plasma; if this diffusion barrier is destroyed, superficial destabilisation of the nitrided layer will be induced by nitrogen retrodiffusion from the solid phase to the plasma because of the chemical gap which characterises this interface. The presence of titanium ions in the ion etching process can also promote the decomposition of compound layers^(25,26,85).

Because of this apparent incompatibility between the two treatments (plasma nitriding and PVD coating), the problem of the formation of undesirable black layer has been addressed by either carrying out a bright nitriding (avoiding formation of compound layers) or grinding off the compound layer prior to coating. The latter proposition is quite feasible when plasma nitriding and PVD coating are performed in a two-way process, that is, nitriding is carried out in a nitriding plant and then the nitrided sample is coated in a PVD equipment. However, if a continuous processing is desired, this approach is not practical. A continuous processing is cost effective, since very low gas flow rates are usually employed and shorter cycles times are required due to the higher kinetics offered by a triode layout^(20,58).

It seems to be possible to improve the adhesion of duplex coatings by carrying out intermediate treatments between plasma nitriding and coating deposition^(11,12). If these two processes are properly combined and carefully controlled, in a way to avoid compound layer destabilisation, good adhesion strength can be achieved, since the hard compound layer + diffusion zone will improve the load support capability of the substrates. A duplex coating with a dense compound layer would be particularly useful in corrosive environments, since the iron nitride layer could block the localised attack which takes place throughout the PVD hard coating^(16,82).

3.1.6. The BAI 640R equipment

The BAI 640R is a triode ion plating system commercially manufactured by BALZERS. It is a 0.640m³ stainless vacuum vessel equipped with a high vacuum pumping system. A rotary vane vacuum pump and a roots pump are connected to the chamber to create a pre-vacuum of 10⁻² mbar. An oil diffusion pump is used to obtain the working pressure. A constant voltage power supply (TCR) can be connected to a rotating table to bias the substrates (diameter of 0.6m, rotation period of 10s). A constant current low voltage thermionic electron source (GL73) with a tungsten filament is used for enhancing the ionisation of the plasma (ionisation chamber). The metal is evaporated by means of a high voltage thermionic e-gun (EHV) that has a maximum power of 11KW. The electrons are emitted by a tungsten filament and are bent over 270° to the copper

crucible. The copper crucible has a diameter of 0.070m and rotation period of 40s. The chamber pressure is measured by a capacitance gauge, the Baratron of MKS Instruments. Gases are admitted into the chamber by mass flow-controllers from MKS Instruments. The temperature is measured with a K-type thermocouple attached to the sample/substrate holder surfaces. There are two cooling systems: the first operates with cold water ($< 285\text{K}$) to cool down the diffusion pump and the second operates with warm water ($318\text{-}323\text{K}$) which circulates into the copper crucible, auxiliary anode, ionisation chamber and chamber door. The BAI 640R operates at different configurations during coating production: heating mode, etching mode and coating mode.

Heating Mode

In the heating mode (see figure 3.6), the substrate holder or rotating table (anode) is connected to the positive terminal of the LV electron source (GL73) to attract the electrons. The substrates can be heated up to 773K . Normally, the argon pressure is $2.5 \times 10^{-3} \text{ mbar}$ (0.25Pa) and the heating time is around 15 minutes. The samples are also degassed during this mode.

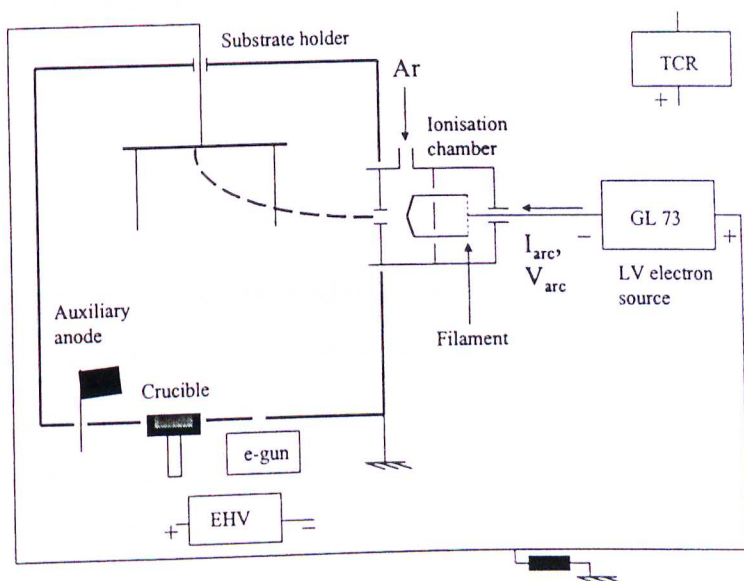


Figure 3.6 – Schematic drawing of the BAI 640R equipment in the heating mode. The dashed line represents the path of the electron beam.

Etching Mode

The substrate holder is connected to the negative terminal of the TCR power supply to attract the ions, while the electrons are attracted to an auxiliary anode that is connected to the positive terminal of the LV electron source (GL73), see figure 3.7. In this mode, possible contamination on the substrates is sputtered by an argon plasma.

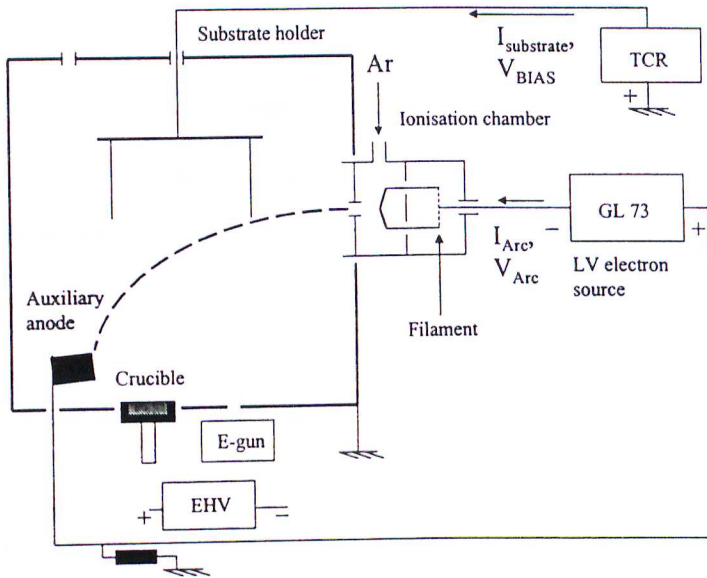


Figure 3.7 – Schematic drawing of the BAI 640R equipment in the etching mode. The dashed line represents the path of the electron beam.

Coating Mode

In the coating mode the substrate holder is connected to the negative terminal of the TCR power supply (see figure 3.8) to attract the ions, while the electrons are attracted to the evaporation crucible which is connected to the positive terminal of the LV electron source (GL73). At the evaporation crucible, the metal is melted by means of the HV electron gun (EHV). In this configuration, the so-called ion plating mode, ion bombardment of the substrate is continued, whilst coating material is simultaneously deposited.

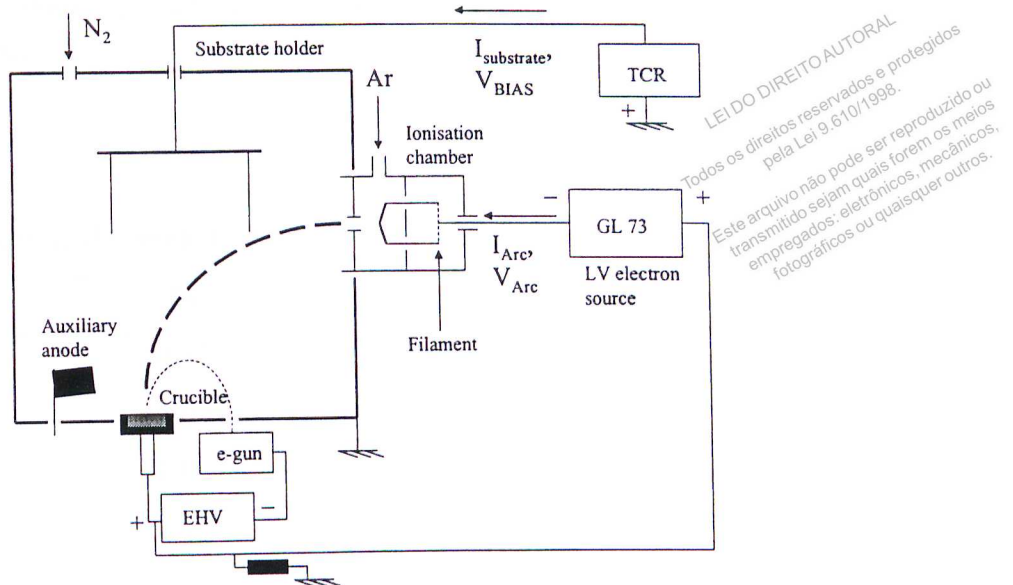


Figure 3.8 – Schematic drawing of the BAI 640R equipment in the coating mode. The dashed lines represent the path of the electron beams.

3.2. Experimental Procedure

3.2.1. Materials

An AISI H13 tool steel was chosen to be the substrate of this work. This choice was based on a promising application of duplex coatings onto AISI H13 shear knives which are used to cut steel ingots during a continuous ingot casting process. At this first stage, 32.5mm x 6.0mm discs were machined to be plasma nitrided and subsequently coated with TiN in the BAI 640R equipment. No heat treatment was carried out in the discs, that is, the steel was used in an annealed (spheroidised) condition. At this first stage, the aim was to successfully perform plasma nitriding and duplex treatments in the ion plating equipment. In the procedures described in the next chapters, however, the substrates will be hardened and tempered AISI H13 steel.

The nominal chemical composition of the AISI H13 tool steel is shown in table III.1⁽¹⁰⁰⁻¹⁰²⁾.

Table III.1 – Nominal chemical composition of AISI H13 tool steels⁽¹⁰⁰⁻¹⁰²⁾

Element	%
C	0.35
Cr	5.00
V	1.00
Mo	1.50
Fe	92.15

3.2.2. Surface preparation

Disc specimens were ground by 100, 240, 320 and 400 mesh SiC papers before plasma nitriding and TiN coating. The surface roughness (R_a value) was assessed using a Taylor-Hobson SURTRONIC 3+ portable roughness analyser. Six measurements were taken parallel to the grinding direction and six measurements were taken perpendicular to it.

3.2.3. Plasma Nitriding

In order to optimise the hardness and thickness of the nitrided layer before producing a duplex TiN coating, two steel discs were plasma nitrided in the BAI 640R equipment, using a triode configuration. The specimens named “disc 1” and “disc 2” were plasma nitrided for 2 and 3 hours, respectively. Plasma nitriding was performed in the etching mode, using a 60%Ar – 40% N₂ plasma. The process parameters were kept constant in both runs, except that the treatment time was increased from 2 to 3 hours. Nitriding treatment was carried out in sequential steps: 1. pumping down the chamber until an ultimate pressure of 2×10^{-5} mbar (2×10^{-3} Pa) was reached; 2. heating the samples in an argon plasma; 3. sputter cleaning in an argon plasma; 4. plasma nitriding in an argon-

nitrogen plasma; 5. cooling (nitrogen gas). The process parameters related to these steps are given in table III.2.

Table III.2 – Plasma nitriding parameters of AISI H13 substrates

1. Pumping	2. Heating (heating mode)	3. Sputter cleaning (etching mode)	4. Plasma nitriding (etching mode)	5. Cooling
$P_{ult} = 2 \times 10^{-3} \text{Pa}$ ($2 \times 10^{-5} \text{mbar}$)	$P_{Total} = P_{Ar} = 2.5 \times 10^{-1} \text{Pa}$ ($2.5 \times 10^{-3} \text{mbar}$) $I_{filament} = 200 \text{A}$ $I_{Arc} = 180 \text{A}$ $V_{Arc} = 41 \text{V}$ Ar flow = 120sccm Time = 15 minutes T = 683K (410°C)	$P_{Total} = P_{Ar} = 2.4 \times 10^{-1} \text{Pa}$ ($2.4 \times 10^{-3} \text{mbar}$) $I_{filament} = 200 \text{A}$ $I_{Arc} = 150 \text{A}$ $V_{Arc} = 43 \text{V}$ Ar flow = 105sccm $V_{BIAS} = -200 \text{V}$ $I_{Substrate} = -2.1 \text{A}$ Time = 5 minutes T = 661K (388°C)	$P_{Total} = 4.0 \times 10^{-1} \text{Pa}$ ($4.0 \times 10^{-3} \text{mbar}$) $P_{Ar} = 2.4 \times 10^{-1} \text{Pa}$ ($2.4 \times 10^{-3} \text{mbar}$) $P_{N_2} = 1.6 \times 10^{-1} \text{Pa}$ ($1.6 \times 10^{-3} \text{mbar}$) $I_{filament} = 200 \text{A}$ $I_{Arc} = 150 \text{A}$ $V_{Arc} = 45 \text{V}$ Ar flow = 105sccm N_2 flow = 70sccm $V_{BIAS} = -250 \text{V}$ $I_{Substrate} = -2.0 \text{A}$ Time = 120 /180 minutes T = 683-693K (410-420°C)	$P_{N_2} = 1.0 \times 10^4 \text{Pa}$ ($1.0 \times 10^2 \text{mbar}$) Time = 10 minutes

Note: The gas flow reading is in standard (0°C and 1 atm) cubic centimetres per minute (sccm). The SI unit is in $\text{Pa m}^3 \text{s}^{-1}$. The conversion to the SI unit ($\text{Pa m}^3 \text{s}^{-1}$) is done by $1 \text{sccm} = 1 \text{atm cm}^3 \text{min}^{-1} = 1/600 \text{Pa m}^3 \text{s}^{-1} = 1/79 \text{Torr l s}^{-1}$.

3.2.4. Characterisation of plasma nitrided samples

X-ray diffraction (XRD) was performed using a Philips PW1710 diffractometer to identify the phases which had been formed during the plasma nitriding treatment. This technique is particularly useful in determining whether or not a compound layer was formed on the nitrided steel surface. The radiation used was $\text{Cu-K}\alpha$ ($\lambda = 0.154056 \text{nm}$) and the diffractograms were recorded by scanning the samples at a 2θ step of 0.02° per second from 0 to 100° .

SEM (Scanning Electron microscopy) investigations and EDS (Energy Dispersive Spectroscopy) analyses were carried out on polished cross-sections of plasma nitrided samples, using a JEOL JSM-35C scanning electron microscope and a VOYAGER 3050 scanning electron microprobe. Polished cross-sections were prepared according to metallographic procedures described in the literature⁽¹⁰³⁾. Specimens were cut with SiC abrasive discs, mounted in an acrylic resin (Epofix from STRUERS) and thin steel plates were used for edge retention. Grinding was accomplished by using 240, 400, 600 and 1000 mesh SiC papers and polishing was performed with 9, 3 and 1 μ m diamond pastes. Polished samples were chemically etched with Nital (4%) before SEM observation. A FUTURE TECH FM-1 microhardness tester was used to evaluate the Knoop hardness of the nitrided surfaces. A load equal to 9.81×10^{-2} N (10gf) was employed. Knoop hardness measurements as a function of the depth from the surface were also performed under a load of 9.81×10^{-2} N (10gf). Therefore, the hardness profile of the nitrided layer as well as its thickness could be determined for the different treatment times (2 and 3 hours).

3.2.5. Duplex treatment

AISI H13 discs were nitrided for 2 hours in a 60%Ar – 40% N₂ plasma and coated with a TiN coating in the Balzers industrial-size triode ion plating equipment. As previously carried out for nitriding, the chamber was pumped down to 2×10^{-3} Pa (2×10^{-5} mbar) and the samples were heated in an Ar plasma, followed by a sputter cleaning step, plasma nitriding, coating deposition and cooling. The process parameters of the duplex treatment are given in table III.3. A Ti interlayer was deposited for 1 minute, just before starting TiN deposition. Coating deposition was initiated immediately after plasma nitriding, that is, no cooling in vacuum or plasma etching was performed between plasma nitriding and coating.

3.2.6. Characterisation of the duplex TiN coating

Duplex-coated samples were characterised by XRD, SEM, EDS and Knoop microhardness measurements, as previously described for the nitrided samples. XRD

measurements were performed with a Cu-K α radiation ($\lambda=0.154056\text{nm}$). The samples were scanned stepwise (2θ) at intervals of 0.02° per second from 0 to 100°

LEI DO DIREITO AUTORAL
 Todos os direitos reservados e protegidos
 pela Lei 9.610/1998.
 Este arquivo não pode ser reproduzido ou
 transmitido sejam quais forem os meios
 empregados: eletrônicos, mecânicos,
 fotográficos ou quaisquer outros.

Table III.3 – Deposition parameters of the duplex TiN coating

Heating (<i>heating mode</i>)	Sputter cleaning (<i>etching mode</i>)	Plasma nitriding (<i>etching mode</i>)	Coating Deposition (<i>coating mode</i>)	5. Cooling
$P_{\text{Total}} = P_{\text{Ar}} = 2.5 \times 10^{-1} \text{Pa}$ ($2.5 \times 10^{-3} \text{mbar}$)	$P_{\text{Total}} = P_{\text{Ar}} = 2.4 \times 10^{-1} \text{Pa}$ ($2.4 \times 10^{-3} \text{mbar}$)	$P_{\text{Total}} = 4.0 \times 10^{-1} \text{Pa}$ ($4.0 \times 10^{-3} \text{mbar}$)	<i>Ti interlayer*</i> $P_{\text{Ar}} = 1.2 \times 10^{-1} \text{Pa}$ ($1.2 \times 10^{-3} \text{mbar}$)	$P_{\text{N}_2} = 1.0 \times 10^4 \text{Pa}$ ($1.0 \times 10^2 \text{mbar}$)
$I_{\text{filament}} = 200 \text{A}$	$I_{\text{filament}} = 200 \text{A}$	$P_{\text{Ar}} = 2.4 \times 10^{-1} \text{Pa}$ ($2.4 \times 10^{-3} \text{mbar}$)	$I_{\text{filament}} = 200 \text{A}$	Time = 10 minutes
$I_{\text{Arc}} = 180 \text{A}$	$I_{\text{Arc}} = 150 \text{A}$	$P_{\text{N}_2} = 1.6 \times 10^{-1} \text{Pa}$ ($1.6 \times 10^{-3} \text{mbar}$)	$I_{\text{Arc}} = 100 \text{A}$	
$V_{\text{Arc}} = 41 \text{V}$	$V_{\text{Arc}} = 43 \text{V}$		$V_{\text{Arc}} = 48 \text{V}$	
Ar flow = 120 sccm	Ar flow = 105 sccm	$I_{\text{filament}} = 200 \text{A}$	$V_{\text{BIAS}} = -110 \text{V}$	
Time = 15 minutes	$V_{\text{BIAS}} = -200 \text{V}$	$I_{\text{Arc}} = 150 \text{A}$	$I_{\text{Substrate}} = -2.0 \text{A}$	
$T = 685 \text{K}$ (412°C)	$I_{\text{Substrate}} = -2.1 \text{A}$	$V_{\text{Arc}} = 47 \text{V}$	$I_{\text{emission}} = 0.40 \text{A}$	
	Time = 5 minutes	Ar flow = 105 sccm	Time = 1 minute	
	$T = 665 \text{K}$ (392°C)	N_2 flow = 70 sccm	<i>TiN coating</i>	
		$V_{\text{BIAS}} = -250 \text{V}$	$P_{\text{Total}} = 1.7 \times 10^{-1} \text{Pa}$ ($1.7 \times 10^{-3} \text{mbar}$)	
		$I_{\text{Substrate}} = -2.0 \text{A}$	Ar flow = 48 sccm	
		Time = 120 minutes	N_2 flow = 140 sccm	
		$T = 683\text{-}693 \text{K}$ ($410\text{-}420^\circ \text{C}$)	$I_{\text{filament}} = 200 \text{A}$	
			$I_{\text{Arc}} = 100 \text{A}$	
			$U_{\text{Arc}} = 47 \text{V}$	
			$V_{\text{BIAS}} = -110 \text{V}$	
			$I_{\text{Substrate}} = -2.0 \text{A}$	
			$I_{\text{emission}} = 0.40 \text{A}$	
			Time = 60 minutes	
			$T = 669\text{-}683 \text{K}$ ($396\text{-}410^\circ \text{C}$)	

* Usually a $0.1\text{-}0.2 \mu\text{m}$ thick Ti interlayer is produced under these conditions.

Knoop microhardness measurements were taken under a load of $9.81 \times 10^{-2} \text{N}$ (10gf) in order to determine the thickness of the nitrided layer. A load of $4.90 \times 10^{-1} \text{N}$ (50gf) was

employed to characterise the surface hardness. Polished cross-sections were observed in the SEM. Duplex-coated samples were cut with a diamond disc and mounted in an acrylic resin (Epofix from STRUERS). The mounted sample was cut again with a diamond disc to remove the resin from the cross-sectional surface, which gave a sufficiently smooth finishing. Previous metallographic preparations had failed, since nearly all the coating had been removed from the steel surface. It is strongly recommended to avoid large grit sizes when preparing thin, hard PVD coatings⁽¹⁰⁴⁾. Therefore, grinding was carried out by using 600 and 1000 mesh SiC papers only. Specimens were polished with 9, 3 and 1 μ m diamond pastes and then chemically etched with Nital (4%).

A CSEM Revetest scratch tester was used to evaluate coating adhesion. The scratch test has been extensively used for adhesion assessment^(31,105-111). In this test, a diamond (Rockwell C) stylus traverses the coated surface. The applied normal force is increased continuously or stepwise until the coating is detached. The normal force at which coating failure occurs is known as *the critical load*, L_c . Two critical loads are usually recorded: the first one, L_{C1} corresponding to cohesive failure (i.e., failure within the coating) and the second, L_{C2} , corresponding to coating detachment (adhesive failure). Coating failure can be detected by a sudden increase in acoustic emission (AE) or tangential friction force (F_t) readings, or by a post-test examination using SEM or light optical microscopy (LOM).

Scratch testing was performed using a 200 μ m Rockwell C stylus, a continuously increasing normal load (load rate, 100N/min) and a scratching speed of 10mm/min. Acoustic emission (AE) and tangential friction force (F_t) were recorded versus the normal load. All results are the average values of three measurements and the samples were observed, after each scratch, by scanning electron microscopy in order to determine the critical loads L_{C1} and L_{C2} . The critical load L_{C2} was taken as the load at which first exposure of the substrate occurred.

employed to characterise the surface hardness. Polished cross-sections were observed in the SEM. Duplex-coated samples were cut with a diamond disc and mounted in an acrylic resin (Epofix from STRUERS). The mounted sample was cut again with a diamond disc to remove the resin from the cross-sectional surface, which gave a sufficiently smooth finishing. Previous metallographic preparations had failed, since nearly all the coating had been removed from the steel surface. It is strongly recommended to avoid large grit sizes when preparing thin, hard PVD coatings⁽¹⁰⁴⁾. Therefore, grinding was carried out by using 600 and 1000 mesh SiC papers only. Specimens were polished with 9, 3 and 1 μ m diamond pastes and then chemically etched with Nital (4%).

A CSEM Revetest scratch tester was used to evaluate coating adhesion. The scratch test has been extensively used for adhesion assessment^(31,105-111). In this test, a diamond (Rockwell C) stylus traverses the coated surface. The applied normal force is increased continuously or stepwise until the coating is detached. The normal force at which coating failure occurs is known as *the critical load*, L_c . Two critical loads are usually recorded: the first one, L_{C1} corresponding to cohesive failure (i.e., failure within the coating) and the second, L_{C2} , corresponding to coating detachment (adhesive failure). Coating failure can be detected by a sudden increase in acoustic emission (AE) or tangential friction force (F_t) readings, or by a post-test examination using SEM or light optical microscopy (LOM).

Scratch testing was performed using a 200 μ m Rockwell C stylus, a continuously increasing normal load (load rate, 100N/min) and a scratching speed of 10mm/min. Acoustic emission (AE) and tangential friction force (F_t) were recorded versus the normal load. All results are the average values of three measurements and the samples were observed, after each scratch, by scanning electron microscopy in order to determine the critical loads L_{C1} and L_{C2} . The critical load L_{C2} was taken as the load at which first exposure of the substrate occurred.

3.3. Results and Discussion

3.3.1. Characterisation of the substrate

The surface roughness (R_a value) of AISI H13 disc substrates is shown in table III.4. The surface preparation (grinding) was quite uniform in all samples, since their R_a values are statistically similar. The substrate hardness (see table III.5) is particularly low, as expected for an annealed tool steel.

The microstructure of the steel substrate, which is shown in figure 3.9, consists of uniformly dispersed spheroidised carbides in a matrix of Widmanstätten's ferrite. This microstructure surely comes from an annealing treatment. XRD analysis (see figure 3.10) indicated the presence of α -Fe and Cr_7C_3 phases. Therefore, the carbides which can be seen in figure 3.9 are likely to be Cr_7C_3 carbides. If there are carbides of different alloying elements, their concentration is below the minimum that can be detected by the XRD analysis. This finding agrees with results from vertical sections of Fe-Cr-C alloys containing 5% chromium (i.e. AISI H13 steels)⁽¹⁰⁰⁾. The equilibrium structure at ambient temperature is expected to be M_7C_3 carbides in a matrix of ferrite, where M designates a transition metal. The M_7C_3 carbides are likely to occur with transition metals such as chromium and manganese⁽¹⁰⁰⁾. Since the AISI H13 steel does not contain Mn, it is quite reasonable to assume that the only carbides present in the steel are Cr_7C_3 .

Table III.4 – Surface roughness of AISI H13 discs

Specimen	R_a (μm)	C.I. (95%)
Disc 1	0.078	[0.067, 0.089]
Disc 2	0.075	[0.065, 0.085]
Disc 3	0.075	[0.063, 0.087]
Disc 4	0.076	[0.065, 0.087]

Table III.5 – Vickers microhardness of the annealed AISI H13 substrate

HV _{0.1}	C.I.(95%)
288	[278, 298]

LEI DO DIREITO AUTORAL
 Todos os direitos reservados e protegidos
 pela Lei 9.610/1998.
 Este arquivo não pode ser reproduzido ou
 transmitido sejam quais forem os meios
 empregados: eletrônicos, mecânicos,
 fotográficos ou quaisquer outros.

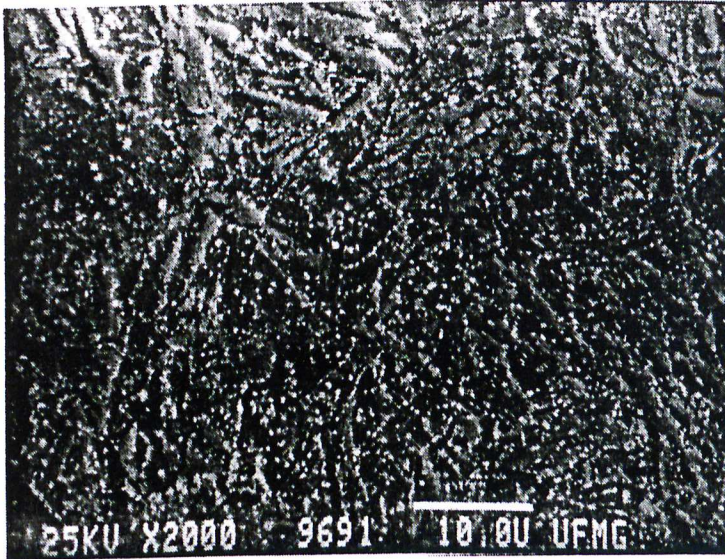


Figure 3.9 – Microstructure of the AISI H13 steel substrate.
 Nital etchant (4%). SEM.

EDS analyses, which were carried out at 3 different areas of the AISI H13 steel, are shown in table III.6. Results indicate the presence of Cr, V, Mo and Fe at compositions expected for the AISI H13 tool steel (see table III.1). The EDS analyses also detected Si. According to the nominal chemical composition given by the UNS, this element can be present at percentages from 0.80 to 1.20%⁽¹⁰¹⁾.

Table III.6 – EDS analyses at 3 different areas of the AISI H13 steel substrate.

Area 1		Area 2		Area 3	
Element	%	Element	%	Element	%
Cr	5.69	Cr	5.53	Cr	6.09
V	1.07	V	0.86	V	0.95
Mo	1.13	Mo	1.73	Mo	1.18
Fe	91.23	Fe	91.06	Fe	91.08
Si	0.88	Si	0.82	Si	0.70

Note: C could not be detected by the EDS analyses.

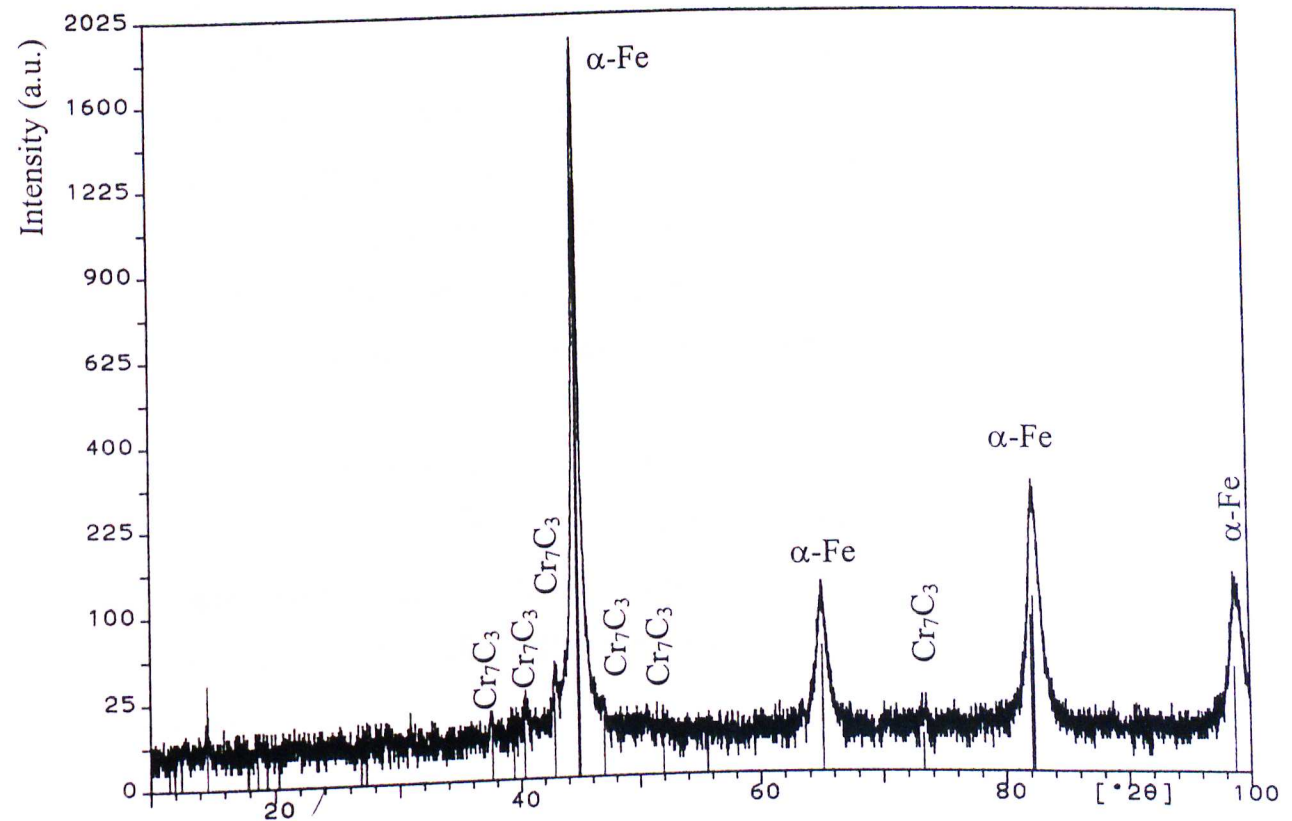


Figure 3.10 – X-ray diffractogram of the AISI H13 steel substrate.

3.3.2. Characterisation of plasma nitrided samples

X-ray diffractograms of plasma nitrided steels for 2 and 3 hours are shown in figure 3.11. The diffractogram of the 2h plasma nitrided sample is very similar to the diffractogram of the untreated AISI H13 steel (figure 3.11), apart from some few peaks corresponding to the ϵ -Fe₂₋₃N and CrN phases. There is an extensive line broadening of major ferritic peaks (designated as α -Fe) and Cr carbides seem to be converted to chromium nitrides. It was not possible to detect the γ' iron nitride, Fe₄N, by XRD. This result indicates that a plasma nitriding treatment for 2 hours yielded a thin mono-phase ϵ compound layer. The presence of ϵ -Fe₂₋₃N and CrN can also be observed in the diffractogram of the 3h plasma nitrided sample. However, there are more ϵ -Fe₂₋₃N and CrN peaks in this diffractogram and some peaks corresponding to α -Fe are not present anymore, indicating that the mono-phase ϵ -Fe₂₋₃N compound layer is probably thicker in this sample than the one which was formed for a treatment time of 2 hours. The 3h plasma nitrided sample shows the presence of an iron oxide, Fe₂O₃ (maghemite-Q). The XRD analyses indicate that it is feasible to carry out a plasma nitriding treatment in the Balzers triode ion plating equipment. The plasma nitriding parameters that had been set led to the formation of a mono-phase ϵ -Fe₂₋₃N compound layer. This compound layer could be identified on both 2h and 3h plasma nitrided samples.

SEM photomicrographs on metallographic cross-sections are shown in figures 3.12 and 3.13. For a 2h-treatment time, the thin ϵ compound layer is clearly seen (figure 3.12). Its thickness is around 1.0-1.2 μ m. Unfortunately the ϵ compound layer cannot be identified in figure 3.13, due to edge effects. However, XRD results indicated its presence for a 3h-treatment time.

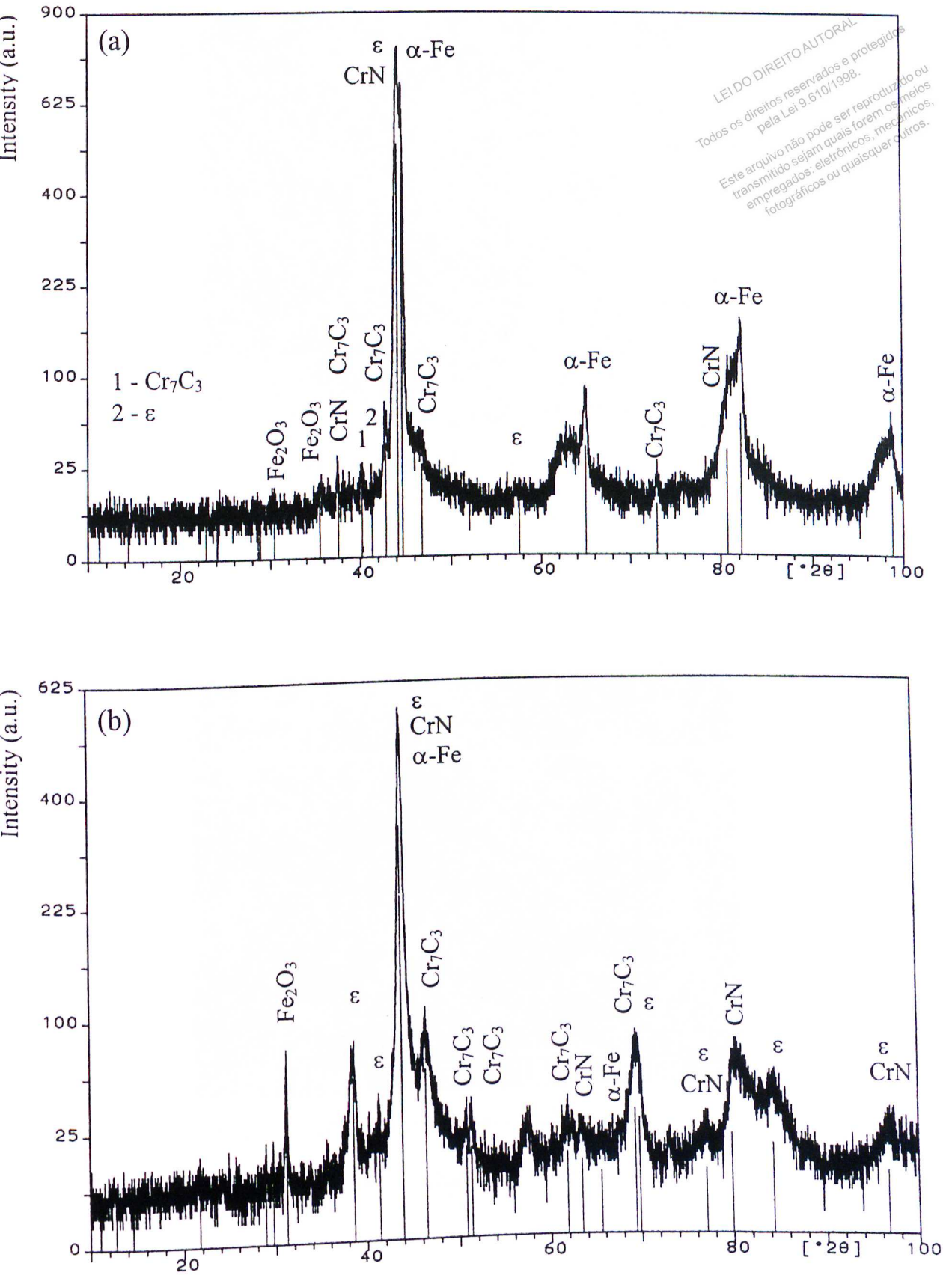


Figure 3.11 – X-ray diffractograms of plasma nitrided AISI H13 substrates (a) for 2 hours and (b) for 3 hours.

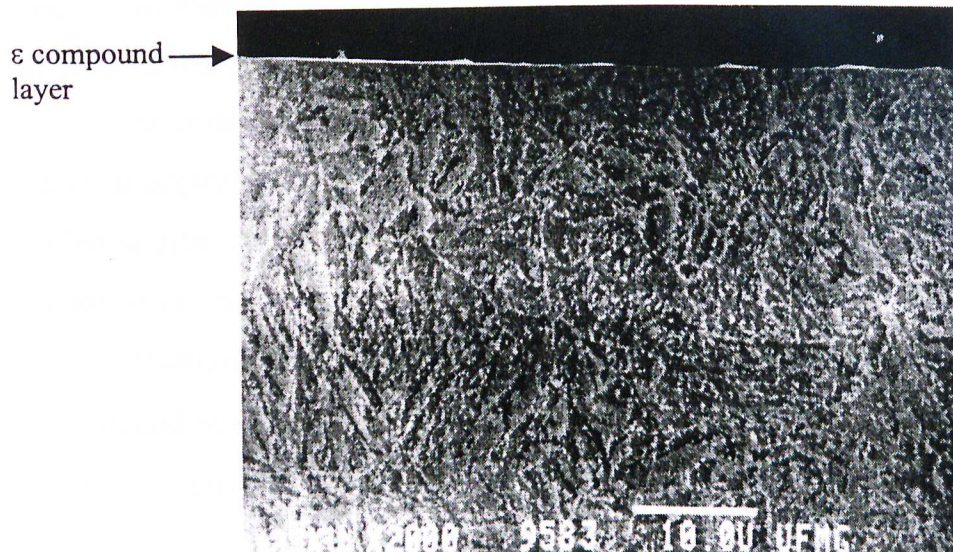


Figure 3.12 – Polished cross-section of a 2h plasma nitrided sample.

Nital etchant (4%). SEM.

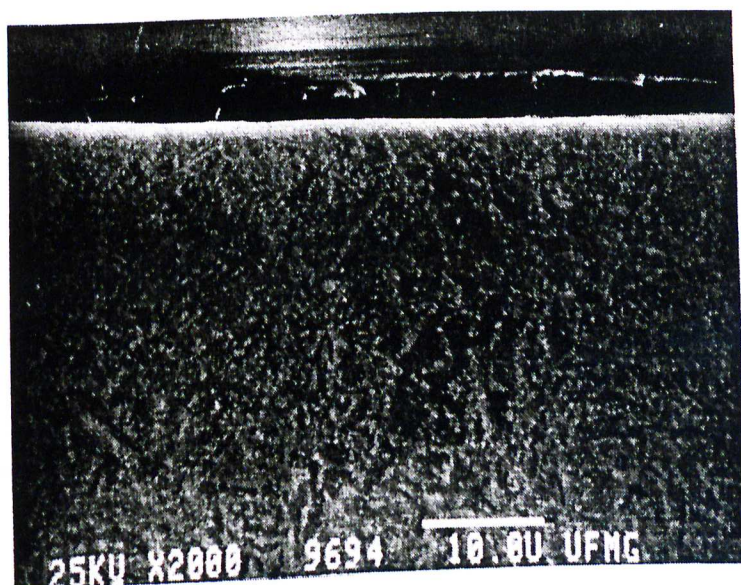


Figure 3.13 – Polished cross-section of a 3h plasma nitrided sample.

Nital etchant (4%). SEM.

Figure 3.14 shows the dependence of hardness on the treatment time. The maximum hardness values are obtained for a 2h-treatment time. After a 3h-treatment time there is a considerable decrease in the hardness of the diffusion zone, which is probably due to coarser precipitates being produced for longer treatment times. Both treatment times yielded similar surface hardness values, which can probably be attributed to the ϵ compound layers that were formed on both nitrided steel surfaces. Both treatment times yielded 35-40 μm thick nitrided cases. For cutting and forming tool steels, the nitrided depth should not exceed 50 μm in order to minimise embrittlement of the outer case resulting from nitriding, especially at sharp edges^(16,18).

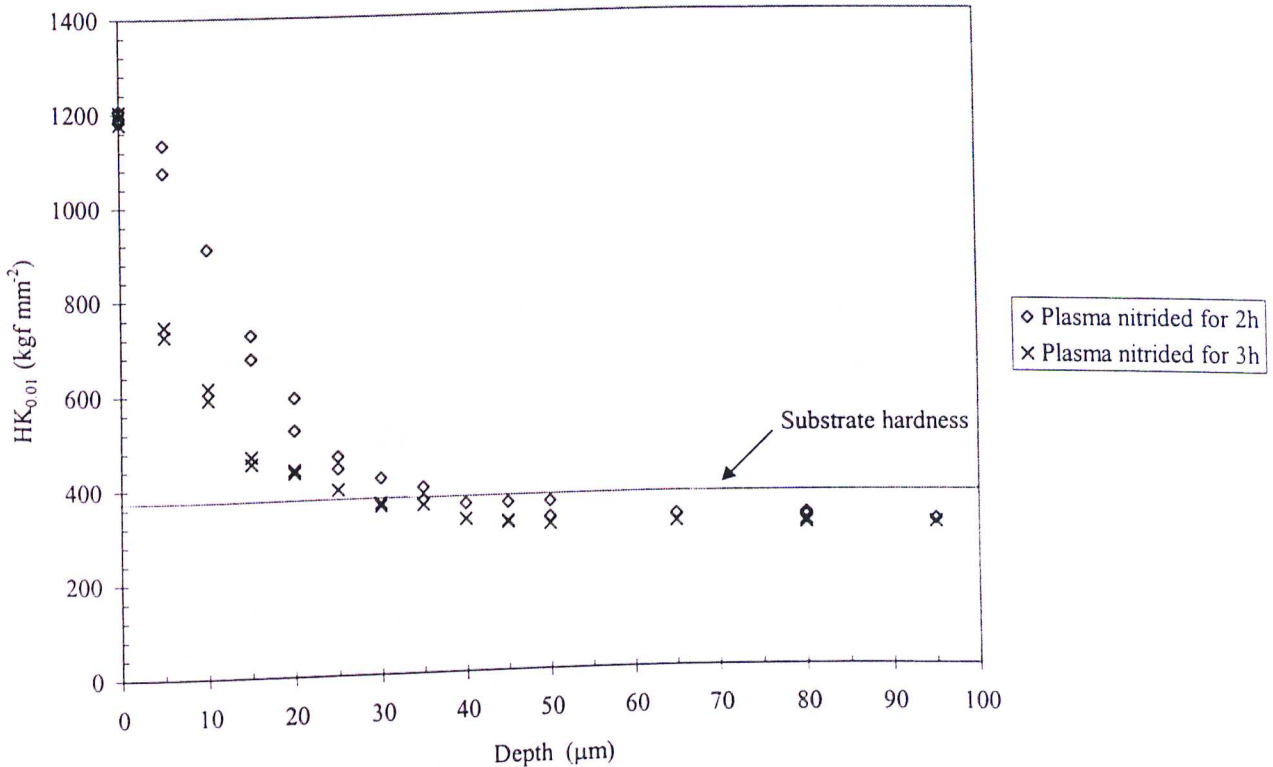


Figure 3.14 – Influence of the treatment time on the Knoop hardness profile of plasma nitrided AISI H13 steels.

EDS analyses were performed on metallographic cross-sections of plasma nitrided specimens. These analyses, which were carried out at 10 and 40 μm from the surface, are shown in table III.7. Two spots were analysed per each microprobe position.

Specimens nitrided for 2 and 3 hours show a slight increase in chromium concentration at 10 μm from the surface; such increase may be related to the formation of CrN precipitates in the diffusion zone. The difference in chromium content, recorded for both probe positions, is rather small (around 1%). EDS accuracy is thought to be 0.5-1.0%. Hence, the recorded increase in chromium concentration might not be significant.

Table III.7 – Spot EDS analyses at 10 and 40 μm from the surface. The numbers 1 and 2 indicate two different analyses that were performed at a fixed probe position.

Plasma nitrided for 2 hours				Plasma nitrided for 3 hours			
10 μm from the surface		40 μm from the surface		10 μm from the surface		40 μm from the surface	
1		1		1		1	
Element	%	Element	%	Element	%	Element	%
Si	1.15	Si	1.03	Si	1.16	Si	1.10
V	1.11	V	1.12	V	1.05	V	1.07
Cr	6.06	Cr	5.28	Cr	6.13	Cr	5.03
Fe	90.06	Fe	90.90	Fe	89.82	Fe	91.89
Mo	1.35	Mo	1.18	Mo	1.39	Mo	0.91
S	0.26	S	0.49	S	0.45	S	0.00
2		2		2		2	
Element	%	Element	%	Element	%	Element	%
Si	1.10	Si	1.19	Si	1.04	Si	1.07
V	1.16	V	1.24	V	1.15	V	0.90
Cr	6.30	Cr	4.98	Cr	6.41	Cr	5.33
Fe	89.86	Fe	90.39	Fe	89.87	Fe	90.83
Mo	1.28	Mo	1.40	Mo	1.53	Mo	1.10
S	0.30	S	0.80	S	0.00	S	0.77

In duplex coating processing, the main task of the nitride case is to increase the load bearing capacity of steel substrates. Since a 2h nitriding treatment yielded a harder nitrided layer and the same case thickness that was obtained for a 3h treatment time, it was decided to plasma nitride AISI H13 substrates for 2 hours before depositing a TiN coating.

3.3.3. Characterisation of the duplex TiN coating

Figure 3.15 shows the X-ray diffractogram of the duplex TiN coating. Diffraction peaks belonging to TiN, Ti, Fe, Cr_7C_3 and Fe_{2-3}N (ϵ) are present. Again, plasma nitriding yielded a mono-phase ϵ compound layer. This compound layer is probably thin, since small peaks corresponding to the ferritic substrate and carbides are observed. In addition to the dominant peaks corresponding to stoichiometric TiN, some small Ti peaks are present. The latter peaks probably correspond to the 0.1-0.2 μm titanium interlayer that was deposited. The TiN coating has a (1 1 1) preferred growth orientation, although (2 0 0), (2 2 0), (3 1 1), (2 2 2) and (4 0 0) TiN diffraction peaks can also be observed.

Polished cross-sections of the duplex TiN coating are shown in figures 3.16 and 3.17. In both micrographs, a 1 μm thick compound layer can be seen beneath the 3 μm thick TiN coating. No black layer is observed at the TiN/nitrided layer interface, which means that the ϵ compound layer was not destabilised during the duplex treatment. Since the TiN deposition temperature was held below 723K (see table III.3) and no plasma etching was performed between plasma nitriding and coating deposition, compound layer destabilisation would be very unlikely to occur under such conditions.

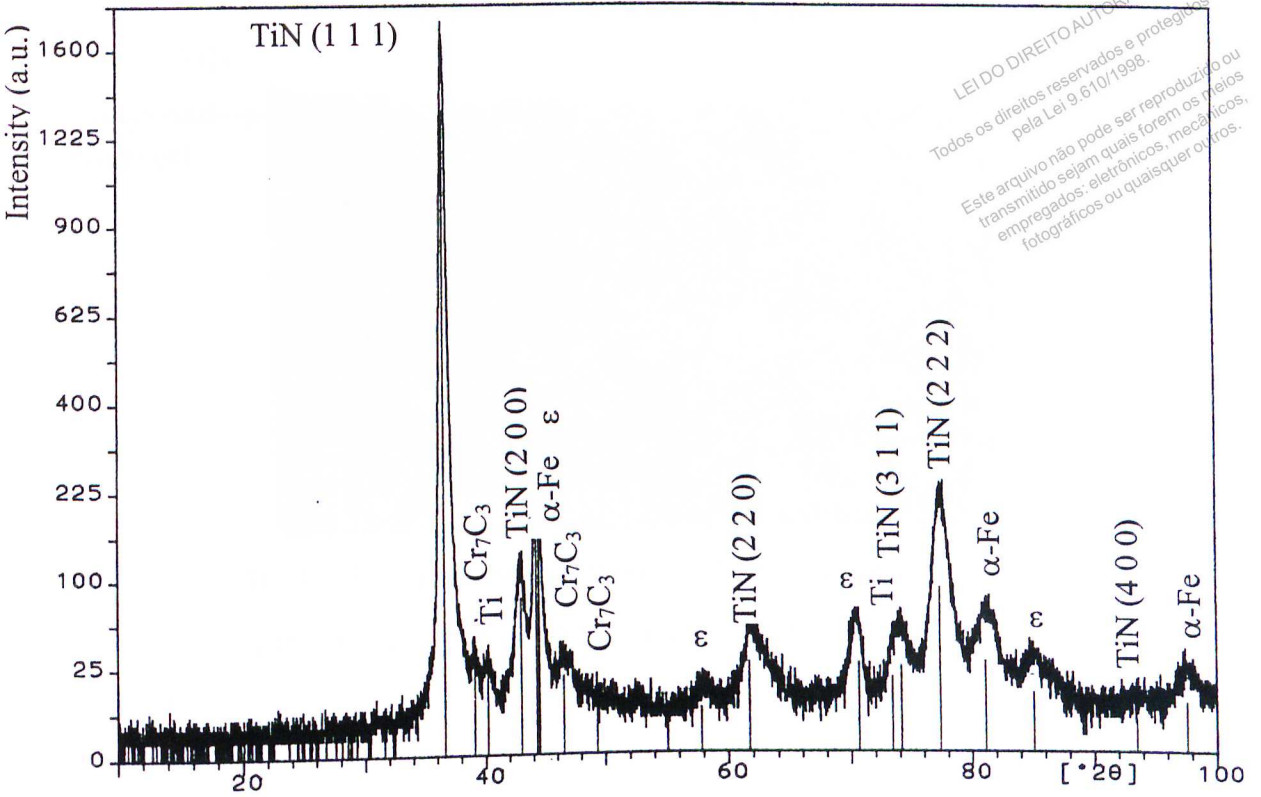


Figure 3.15 – X-ray diffractogram of the duplex TiN coating.

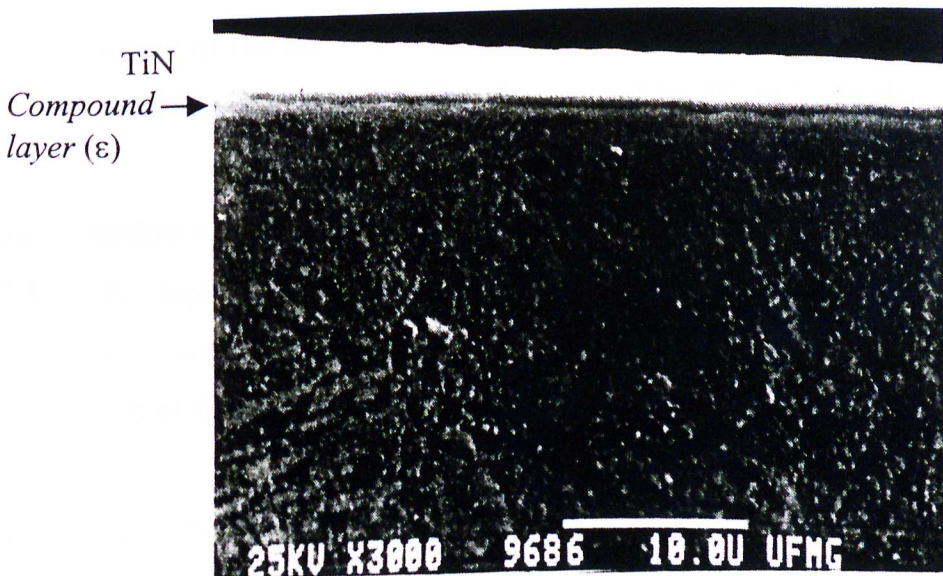


Figure 3.16 – SEM micrograph of the duplex TiN coating.

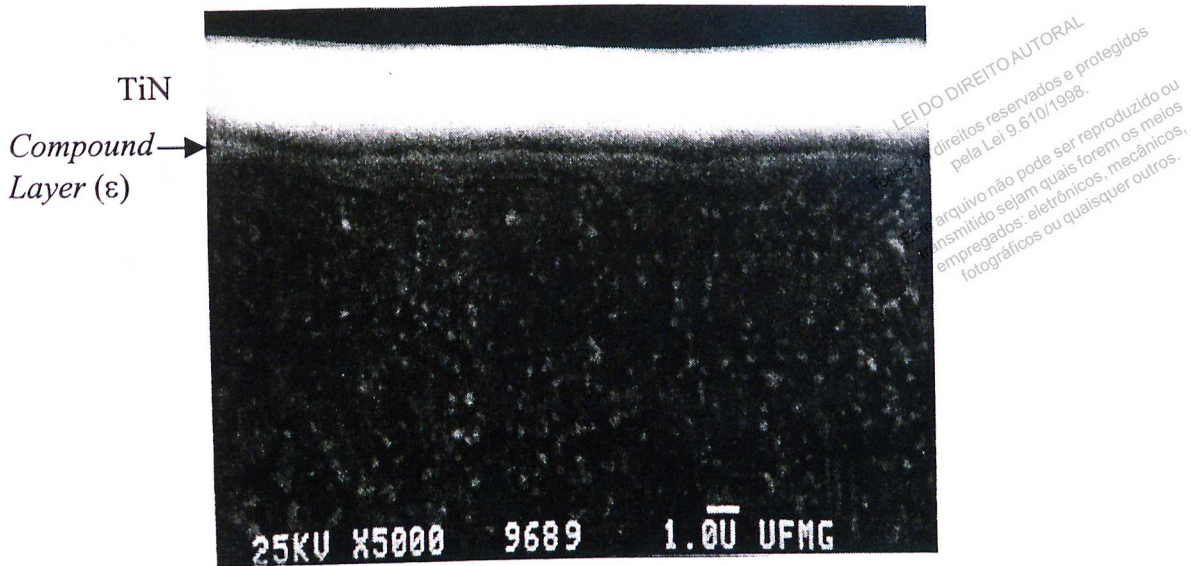


Figure 3.17– SEM micrograph of the duplex TiN coating at a higher magnification. Note that a $1\mu\text{m}$ thick, dense ϵ compound layer was formed during the duplex treatment.

Figure 3.18 shows the Knoop hardness profile that was obtained for the duplex TiN coating. This profile is quite similar to that of the 2h plasma nitrided substrate (see figure 3.14). The duplex treated AISI H13 also exhibits a $35\text{-}40\mu\text{m}$ nitrided layer consisting of diffusion zone and mono-phase ϵ compound layer. This indicates a good reproducibility of the BAI 640R triode ion plating equipment. The surface hardness is around 2500HK whilst a 900HK value is recorded for $10\mu\text{m}$ below the surface.

Knoop hardness measurements under a load of $4.90 \times 10^{-1}\text{N}$ (50gf) are shown in table III.8 for the duplex TiN coating, 2h plasma nitrided and untreated (annealed) AISI H13 steel. Under such load, the TiN coating hardness can be measured without a large contribution of the substrate.

Results show that the duplex treatment promoted a 6-fold increase in surface hardness of an annealed AISI H13 substrate. By carrying out plasma nitriding, the substrate hardness of an annealed AISI H13 steel was increased by a factor 3. Such improvement in hardness can be very interesting from a tribological point of view.

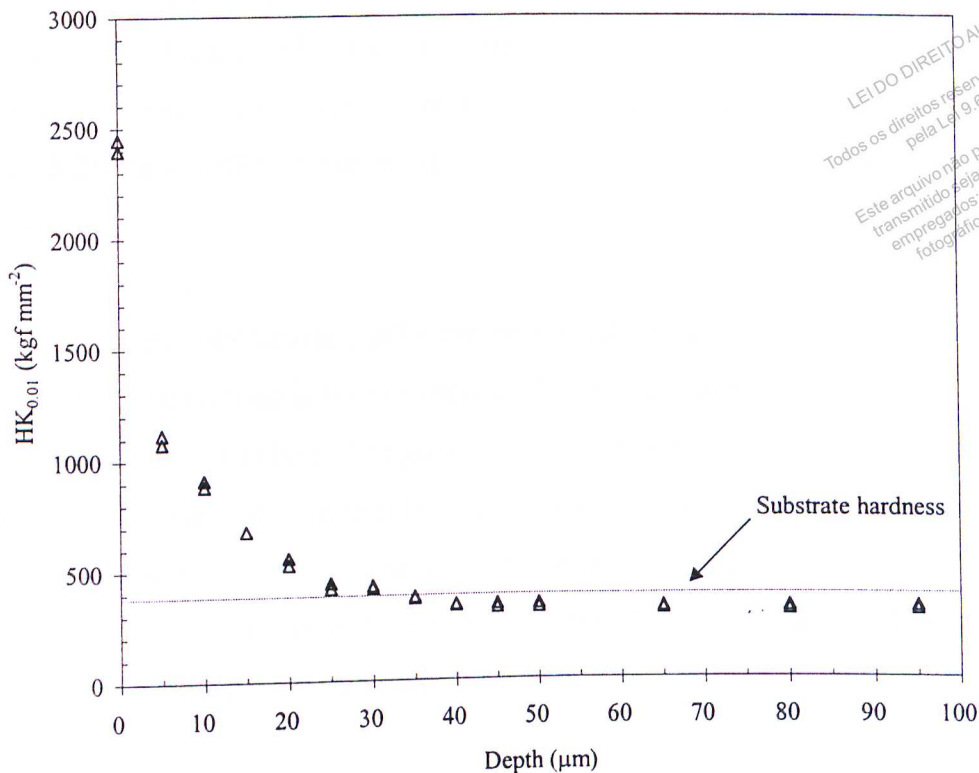


Figure 3.18 – Knoop hardness profile. Duplex TiN coating.

Table III.8 – Knoop hardness and its confidence interval (95%)

Material	HK _{0.05}	C.I. (95%)
Duplex TiN coating	2433	[2328, 2538]
2h plasma-nitrided AISI H13 steel	1193	[1154, 1232]
Annealed (spheroidised) AISI H13 steel	370	[365, 375]

In the scratch test, the duplex TiN coating did not show any adhesive failures under loads up to 188N (maximum load achieved during the test), indicating that the nitrided layer (mono-phase ϵ compound layer + diffusion zone) was quite effective in improving the load bearing capacity of a soft (annealed) substrate. The duplex coating exhibited semi-circular cracks in the interior of the scratch channel (tensile cracks). In this mode, semicircular crack traces are parallel to the trailing edge of the indenter. These cracks form as a result of the tensile stress present behind the trailing edge of the stylus; these

stresses balance the compressive frictional stresses ahead. Tensile cracking is a failure mode that characterises well-adherent coatings⁽¹¹¹⁾. The critical load L_{C1} was determined as the normal load at which tensile cracks started to form on the coating surface. Figures 3.19 to 3.21 show different stages of a scratch that had been performed on the duplex TiN coating.

At the first stage, only tensile cracks can be identified inside the scratch channel (figure 3.19). As the normal load is further increased, external transverse cracks start to form at the edge of the scratch channel (figure 3.20). At the end of the scratch, chipping of the coating is also observed with tensile and external transverse cracks (figure 3.21). Since the substrate had not been exposed up to a normal load of 188N (this was chosen as the failure criterion), it was not possible to determine L_{C2} for the duplex TiN coating. L_{C1} and its standard deviation are shown in table III.9.

The duplex TiN coating has very good adhesion strength, as demonstrated by the scratch test. The nitrided layer (ϵ compound layer + diffusion zone) prevented deformation of the substrate, increasing the load support for the $3\mu\text{m}$ thick TiN coating. This duplex coating is expected to have a superior performance when compared to an ordinary hard TiN coating, especially in applications where components are subjected to severe loading.

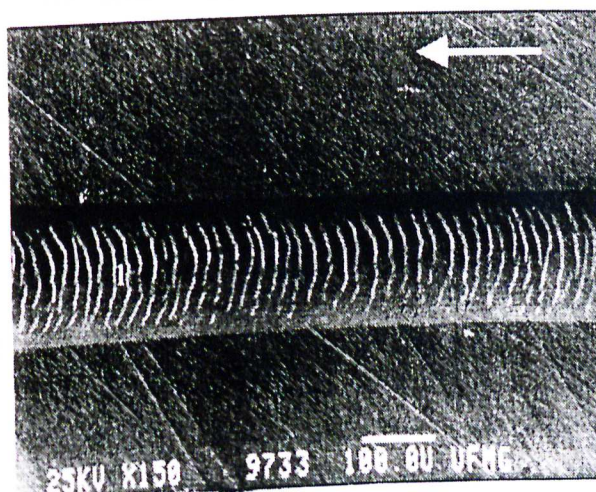
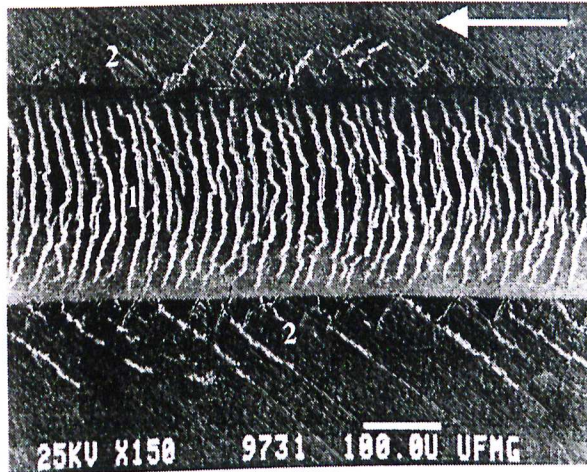


Figure 3.19 – Tensile cracks (1) in the interior of the scratch channel. The arrow indicates the scratch direction.



LEI DO DIREITO AUTORAL
 Todos os direitos reservados e protegidos
 pela Lei 9.610/1998.
 Este arquivo não pode ser reproduzido ou
 transmitido sejam quais forem os meios
 empregados: eletrônicos, mecânicos,
 fotográficos ou quaisquer outros.

Figure 3.20 – At higher loads, external transverse cracks (2) start to form at the edge of the scratch channel. The arrow indicates the scratch direction.

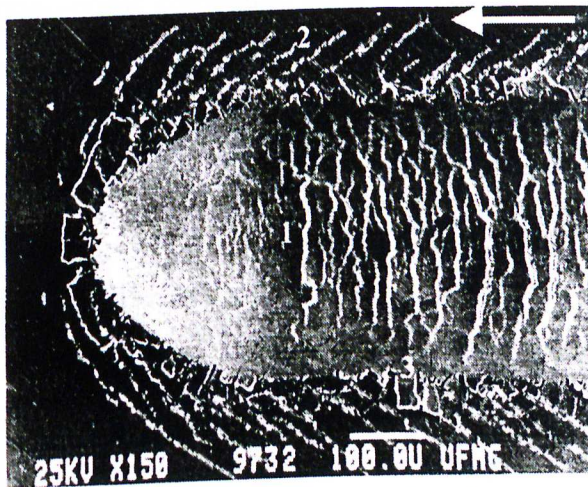


Figure 3.21 – End of the scratch channel, showing that the substrate has not been exposed. Tensile cracks (1), external transverse cracks (2) and coating chipping (3) can be distinguished at this stage. The normal load at the end of scratch was 188N. The arrow indicates the scratch direction.

Table III.9 – Critical load L_{C1} and its standard deviation

L_{C1} (N)	Standard deviation
48	± 2

The compound layer did not have any detrimental effect on duplex coating adhesion. According to the published literature, the presence of a soft black layer would surely reduce the adhesion of duplex coatings⁽²³⁻²⁴⁾. The first results presented here indicate that it is possible to produce well-adherent duplex coatings by avoiding compound layer destabilisation. It seems that the compound layer structure plays a key role on adhesion behaviour. It is well known that dual-phase ($\epsilon+\gamma'$) compound layers are susceptible to fracture at the interface between phases⁽³³⁾. Therefore, plasma nitriding treatments which lead to the formation of mono-phase compound layers can be quite attractive for duplex coating processing. A good adhesion reported here for duplex TiN coatings can be attributed to the presence of a hard, dense, mono-phase ϵ compound layer.

It would be interesting to compare the adhesion strength of duplex coatings consisting of a TiN coating + mono-phase compound layer + diffusion zone and a TiN coating + diffusion zone. Hence, a better understanding of the influence of compound layers on adhesion behaviour of duplex coatings could be established. In chapter 4, the influence of an intermediate treatment between plasma nitriding and coating deposition on adhesion is reported. Duplex TiN coatings with different configurations (TiN + mono-phase ϵ compound layer + diffusion zone and TiN + diffusion zone) were produced in order to characterise the influence of a compound layer on duplex coating adhesion. The intermediate treatment also elucidates a systematic approach to avoid compound layer destabilisation or produce duplex coatings which are compound-layer-free.

3.4. Conclusions

1. A low pressure plasma nitriding treatment in a 60%Ar-40%N₂ glow discharge yielded a 1 μ m thick mono-phase ϵ (Fe_{2.3}N) compound layer and a 35-40 μ m thick nitrided case for treatment times equal to 2 and 3 hours.
2. For a 2h-treatment time, the hardness of the nitrided case was superior to that achieved by a 3h-treatment time. However, the nitrided case thickness was similar

for both treatment times. A 2h nitriding treatment improved the hardness of an annealed AISI H13 by a factor 3.

3. A duplex treatment consisting of plasma nitriding for 2 hours and deposition of a $3\mu\text{m}$ TiN coating exhibited a high composite hardness ($2433\text{HK}_{0.05}$). The duplex treatment also yielded a nitrided layer consisting of a $1\mu\text{m}$ thick, dense mono-phase ϵ (Fe_{2-3}N) compound layer and a $35\text{-}40\mu\text{m}$ thick diffusion zone. By carrying out this duplex treatment on annealed AISI H13 steel substrates, the surface hardness was increased by a factor 6.
4. The nitrided case improved the load bearing capacity of annealed AISI H13 substrates. The duplex coating did not show any adhesive failures under loads up to 188N , indicating that the nitrided case (compound layer + diffusion zone) increased the load support for the TiN coating by preventing deformation of the substrate. This also indicates that it is possible to produce well-adherent duplex coatings even if a mono-phase compound layer is formed during plasma nitriding.
5. It seems that the presence of a compound layer is not detrimental for achieving good adhesion strength on duplex coatings. If compound layer destabilisation is avoided, well-adherent duplex coatings can be produced.
6. A mono-phase compound layer may have contributed for the good adhesion observed. Dual phase ($\epsilon+\gamma'$) compound layers are notably susceptible to fracture because of weak bonding at the interface between phases.

CHAPTER 4: EFFECTS OF AN INTERMEDIATE TREATMENT ON ADHESION AND IMPACT RESISTANCE OF DUPLEX TiN COATINGS

4.1. Background

Good adhesion between coatings and tool surfaces is essential for achieving a good performance. For duplex coatings consisting of a plasma nitrided layer and a hard PAPVD coating, this functional property can be very strongly influenced by the presence of a compound layer. Leyland *et al.*⁽⁶⁾ have shown that compound-layer-free nitrided cases can be produced on ASP 23 tool steels, using a low pressure triode plasma. However, if process parameters are carefully controlled in order to avoid the destabilisation of compound layers, it may be possible to produce well-adherent duplex coatings. Duplex coatings with compound layers seem to be particularly helpful in improving corrosion resistance^(16,82).

It has been proven that two process parameters play a key role in destabilising the compound layer: temperature and plasma etching^(13,23-26,85). Therefore, it is interesting to investigate the effects of both parameters on compound layer destabilisation. Such investigation was carried out by performing an intermediate treatment between plasma nitriding and coating deposition. The intermediate treatment consisted of cooling the samples in vacuum down to 393K, subsequent plasma heating to a certain temperature and sputter etching for different periods of time. The effect of this treatment on adhesion and impact resistance of duplex TiN coatings was evaluated.

4.2. Experimental Procedure

4.2.1. Materials and intermediate treatments

AISI H13 coupons (25mm x 25mm x 6mm) were quenched and tempered to (55±2)HRC. Samples were mechanically ground and polished to $R_a=(0.005\pm0.001)\mu\text{m}$. Plasma nitriding and coating deposition were performed in a Balzers BAI 640R equipment by means of a continuous process. After heating and cleaning, specimens were plasma nitrided in a 60% Ar - 40% N₂ plasma for 2 hours. The process parameters used here were the same ones given in table III.2. Afterwards, an intermediate treatment consisting of cooling *in vacuo*, subsequent heating and plasma etching, both in Ar plasmas, was carried out. Then a 0.1-0.2 μm thick Ti interlayer was deposited onto pre-nitrided substrates followed by TiN coating for 1 hour. The coating process parameters are shown in table III.3.

The intermediate treatment consisted of:

1. cooling the samples in vacuum down to 393K after plasma nitriding;
2. heating the samples in Ar plasma until the desired temperature was reached;
3. plasma etching in Ar plasma, using a bias voltage of -200V.

The heating temperature and etching time were varied from 553 to 773K and 0 to 20 minutes, respectively. Four samples were produced, as follows:

- sample 1: heating temperature = 673K, etching time = 10 minutes;
- sample 2: heating temperature = 573K, etching time = 0 (i.e., no etching step was performed and coating deposition started straightaway);
- sample 3: heating temperature = 773K, etching time = 20 minutes;
- sample 4: heating temperature = 573K, etching time = 20 minutes.

During the etching step and subsequent coating deposition, the temperature was kept constant by adjusting the emission current from an ionisation-enhancing filament housed in a separate chamber on the side of the deposition chamber. This has the effect of increasing the degree of ionisation occurring and therefore the ion current to the

substrate (which, together with the substrate bias, determines the plasma power which heats the substrate).

A single-layered TiN coating (i.e., without plasma nitriding) was also produced for comparison. Hardened and tempered AISI H13 coupons (25mm x 25mm x 6mm, 55±2 HRC, $R_a=(0.005\pm0.001)\mu\text{m}$) were plasma heated, sputter cleaned and then coated with a 0.1-0.2 μm Ti interlayer followed by TiN. The coating parameters were the standard ones used in chapter 3 (see table III.3). The TiN coating was also subjected to scratch and impact tests.

4.2.2. Structural characterisation

The layer structure of the TiN-coated nitrided steels (samples 1-4) was investigated by scanning electron microscopy (Cambridge S200 scanning electron microscope) in a cross-sectional view. The samples were mounted in a resin which allowed edge retention (Durofix from STRUERS) and ground with 45 μm and 14 μm diamond suspensions. Diamond pastes of 6, 3 and 1 μm were used during polishing. The specimens were chemically etched with Nital (4%).

4.2.3. Scratch testing

The scratch resistance was assessed using a commercial scratch adhesion tester (VTT scratch tester). Tests were carried out using a 200 μm Rockwell C stylus and a continuously increasing normal force (10Nmm⁻¹). Both L_{C1} and L_{C2} (loads for cohesive and adhesive failures respectively) were determined from a set of 3 scratches on each sample. L_{C2} was taken as the load in which the first exposure of the substrate could be identified. Scanning electron microscopy (SEM), acoustic emission (AE) and tangential force (F_t) measurements were used to determine L_{C1} and L_{C2} .

4.2.4. Impact testing

Impact resistance was investigated using a relatively new impact test⁽¹⁶⁸⁻¹⁷³⁾. In this test, the surface of a solid body is stressed periodically at a defined point by impacts of a hard sphere. Impact force, impact frequency and number of impacts are imposed via a control system (for details, see chapter 7). A tungsten carbide ball (grade 25 from SPHERIC) 6mm in diameter was used as the impacting body. The normal impact force and frequency were set, respectively, to 900N and 8Hz while the number of impacts was varied. Each sample was subjected to 3 tests with 10^3 , 10^4 and 5×10^4 impacts in unlubricated conditions. The tungsten carbide ball was always changed after carrying out a defined number of impacts and its surface, as well as the coating surface, was cleaned with acetone. After the test, samples were observed on the scanning electron microscope (Cambridge S200) in order to investigate coating failure. Energy Dispersive X-Ray Analyses (EDX) were performed on the impact craters by a Link Analytical QX2000 X-Ray Analyser.

4.3. Results and Discussion

4.3.1. Interfacial nitrided layer/coating structure

SEM photomicrographs of samples 1, 2, 3 and 4 are shown in figure 4.1. All samples, apart from sample 2 (etching time = 0), are compound-layer-free. The compound layer is 1.0-1.2 μ m thick (sample 2), as previously reported in chapter 3 for this set of parameters during plasma nitriding, using the Balzers triode ion plating equipment. This suggests that good reproducibility can be achieved through a proper control of process parameters.

Although the etching/coating temperature was relatively high for sample 3, the sputter/etch step removed the thin compound layer that was produced on the surface. Ar plasma etching at a substrate voltage of 200V was able to remove the compound layer in all samples that were subjected to such treatment, for both etching times of 10 and 20

minutes. Sample 2 does not exhibit any black layer, indicating that the compound layer was not destabilised during coating deposition. Although XRD analyses have not been carried out on these samples, a mono-phase ϵ compound layer was probably produced on sample 2. In the same way, a diffusion zone of 35-40 μm is expected for sample 2, since plasma nitriding parameters were similar to the ones used in chapter 3. The other samples (1, 3 and 4) are expected to have thinner diffusion zones due to the sputter/etch step that was carried out during the intermediate treatment. Probably samples 3 and 4, which were etched for 20 minutes, have relatively thinner nitrided cases than sample 1 (etched for 10 minutes).

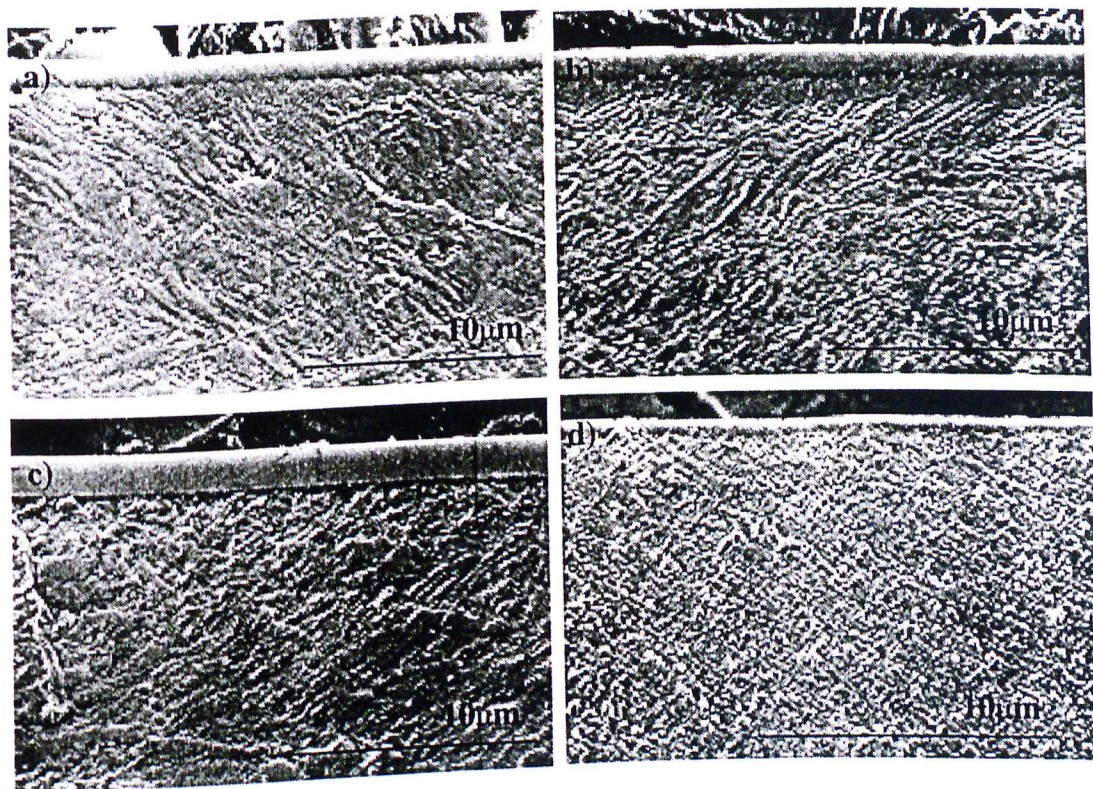


Figure 4.1 – Cross-sectional views of (a) sample 1, $T_{\text{heating}}=673\text{K}$, $t_{\text{etching}}=10\text{min}$; (b) sample 2, $T_{\text{heating}}=573\text{K}$, $t_{\text{etching}}=0\text{min}$; (c) sample 3, $T_{\text{heating}}=773\text{K}$, $t_{\text{etching}}=20\text{min}$ and (d) sample 4, $T_{\text{heating}}=573\text{K}$, $t_{\text{etching}}=20\text{min}$. Note that a compound layer, without any black layer, can be seen only in sample 2. SEM.

Destabilisation was mainly avoided by keeping the temperature below 723K. Obviously this temperature depends on the steel grade; temperatures around 723-743K have been reported as the temperature range at which a black layer could be produced in low alloy steels^(13,23,24). Coating thicknesses, determined by SEM, are given in table IV.1. Samples 1, 2 and 3 have similar coating thicknesses whilst sample 4 has a coating thickness around 0.5 μm thinner than the other samples. Although coating time was kept constant in all runs (1 hour), the difference can be attributed to a different positioning of the samples inside the PAPVD chamber. Sample 4 was positioned 0.2m further away from the vapour source than the others.

Table IV.1 – Coating thickness of duplex coated samples which were subjected to an intermediate treatment

Sample	Thickness (μm)	C.I. (95%)
1	1.68	[1.64, 1.72]
2	1.76	[1.66, 1.85]
3	1.74	[1.68, 1.80]
4	1.13	[1.03, 1.23]

4.3.2. Adhesion

Results of the scratch tests are shown in figure 4.2 and table IV.2. All duplex coatings exhibited a similar scratch behaviour, independent of having a nitrided layer consisting of a diffusion zone only or a mono-phase ϵ compound layer + diffusion zone. Coating failure mode was characterised by tensile cracking, a failure mode commonly found in well-adherent coatings⁽¹¹¹⁾. At high loads (i.e., >100N), substrate exposure occurred in all samples. This load was used as the critical load L_{C2} , while L_{C1} was the critical load at which tensile cracks started to form.

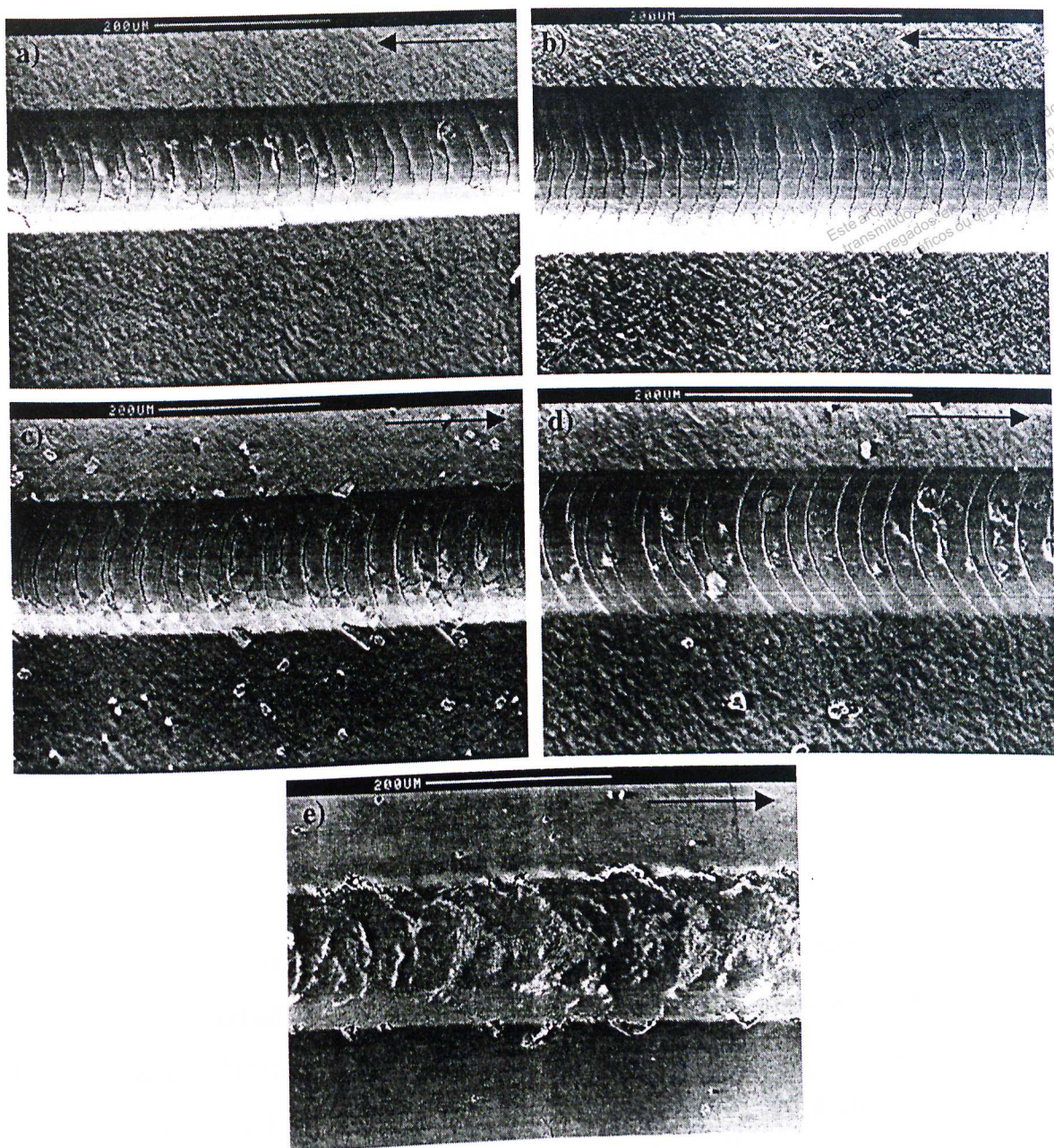


Figure 4.2 – Results of the scratch test on (a-d) duplex TiN coatings and (e) single-layered TiN coating. The nitrided layer comprises only a diffusion zone in (a) sample 1, (c) sample 3 and (d) sample 4. Sample 2 (b) has a $\sim 1.0\text{-}1.2\mu\text{m}$ thick mono-phase $\epsilon\text{-Fe}_{2-3}\text{N}$ compound layer + diffusion zone. Arrows indicate the scratch direction.

The critical loads L_{C1} and L_{C2} are quite similar for all duplex-coated samples. Sample 4 exhibits L_{C1} and L_{C2} values slightly lower than the other systems; however, such difference is not statistically significant. The critical load L_{C2} is lower than that of the

duplex TiN coating ($3\mu\text{m}$ thick) which was firstly produced in chapter 3. The substrate of that sample was not exposed up to 188N. Extrinsic parameters such as substrate hardness, coating thickness, residual stress, coating and substrate roughness can influence the scratch test results^(31,107). An increase of critical loads with thickness is observed⁽¹⁰⁷⁾ and this can explain a relatively higher L_{C2} value for a $3.0\mu\text{m}$ thick TiN coating in contrast to samples 1, 2 and 3 (coated with a $1.7\mu\text{m}$ thick TiN).

Table IV.2 – Critical loads L_{C1} , L_{C2} and their confidence interval, C.I.(95%)

Specimen	L_{C1} (N)	C.I. (95%)	L_{C2} (N)	C.I. (95%)
Sample 1	36.3	[31.8, 40.7]	152.1	[143.6, 160.6]
Sample 2	37.7	[34.3, 41.0]	152.8	[143.5, 162.1]
Sample 3	37.5	[33.1, 40.7]	150.5	[143.4, 157.6]
Sample 4	35.4	[30.6, 40.3]	147.5	[141.4, 153.6]
TiN	25.7	[22.5, 29.0]	52.3	[49.4, 55.2]

The presence of a mono-phase compound layer did not have any detrimental effect on adhesion. Very good adhesion was observed on sample 2, indicating that it is possible to produce a well-adherent duplex coating with a compound layer if process parameters are controlled in order to avoid its destabilisation. Since dual-phase compound layers are susceptible to fracture at the interface between phases^(33,46), a dense mono-phase compound layer may have helped in achieving an adhesion strength close to that which was obtained with nitrided layers consisting of a diffusion zone only. A hard thin compound layer + diffusion zone can prevent deformation of the substrate, as might otherwise be the case for a diffusion zone only. The hardness of the compound layer, being higher than that of the diffusion zone, should provide an additional resistance to substrate deformation and, hence, higher critical loads should be recorded. This was not observed in the scratch test, since the adhesion strength is the same for nitrided layer configurations with compound layer + diffusion zone and diffusion zone only.

In contrast to the duplex-coated samples, the single-layered TiN coating exhibits much lower L_{C1} and L_{C2} values. The coating failure mode was not by tensile cracking. Instead, the TiN coating showed flaking inside and along the edge of the scar. The scratch test results indicate that a plasma nitriding treatment before coating is quite effective in increasing the load-bearing capacity of steel substrates. This was effectively demonstrated by higher critical load values that were recorded for all duplex TiN coatings.

4.3.3. Impact resistance

Impact craters of all tested samples are illustrated in figure 4.3-4.5. Plastic deformation of the sample surface occurred in all tests. In all coating systems, an increase of both diameter and depth of the craters with increasing number of impacts was observed.

All TiN duplex coatings incorporating a diffusion layer (samples 1, 3 and 4), showed circular cracks (a cohesive failure mode) even after 10^3 impacts (figures 4.3 and 4.4). That was the main failure mechanism for those samples; coating delamination could not be detected up to 5×10^4 impacts. For hard brittle coatings, a high tensile stress in the immediate vicinity of the impact causes the development of a large number of cracks in the peripheral region of the impact crater. Cracks will arise when the hard coating is not ductile and/or tough enough to accommodate the stress of deformation under the indenter.

Sample 2, comprising a mono-phase ϵ compound layer + diffusion zone, did not show any circular cracks up to 5×10^4 impacts (figure 4.3). Besides, neither coating delamination nor cohesive failure inside the impact crater could be identified in this sample. Material transfer from the impact ball to the surface can be clearly seen in the impact craters corresponding to 10^4 and 5×10^4 impacts. EDX analyses indicated the presence of W in the bottom of these craters, confirming that material transfer from the ball to the impact crater took place.

A small area with coating delamination can be seen, in sample 3, after 10^3 impacts, at the intermediate zone (figure 4.4). However, only circular cracks can be seen after 10^4 and 5×10^4 impacts. The cohesive and adhesive failures at the intermediate zone should increase with increasing number of impacts. This was not observed, indicating that this small delamination after 10^3 impacts is probably related to a local area of the coating with insufficient cohesive/adhesive strength, since no coating delamination occurred after 10^4 and 5×10^4 impacts.

Single-layered TiN coating does not show any failure up to 10^3 impacts (figure 4.5). The main failure of this coating occurred in the central zone with coating delamination (exposure of the substrate material). Between 10^3 and 10^4 impacts, coating material starts to delaminate in the central zone of the impact crater. After 5×10^4 impacts, coating delamination is more intense in the bottom of the crater. This coating did not show any radial cracks, oppositely to the impact behaviour that was identified in the duplex coatings with a diffusion zone.

It seems that the diffusion zone, produced during plasma nitriding, helped in preventing substrate deformation under the impact body (tungsten carbide ball). No failure at the intermediate zone was observed in samples 1, 3 and 4. This zone corresponds to the cohesive-adhesive failure of the coating under the build-up of shear stresses that arise from plastic strain of the substrate during the ball indentation.

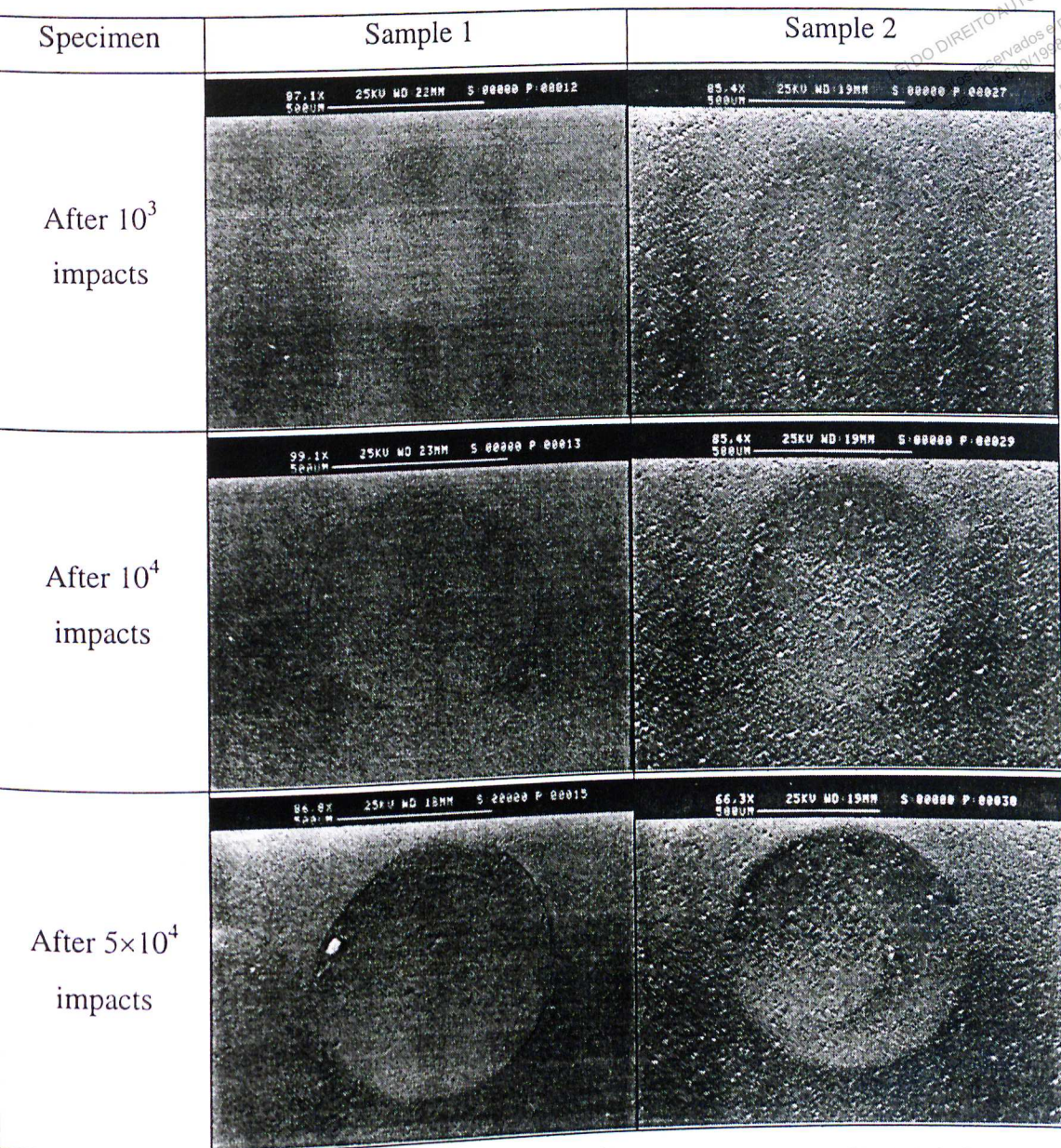


Figure 4.3 – Impact craters (10^3 , 10^4 and 5×10^4) produced in sample 1 (nitrided case comprising a diffusion zone) and sample 2 (nitrided case comprising a 1.0-1.2 μm thick mono-phase ϵ compound layer + diffusion zone). SEM. The elliptical shape of some impact craters results from the tilt employed in the SEM imaging.

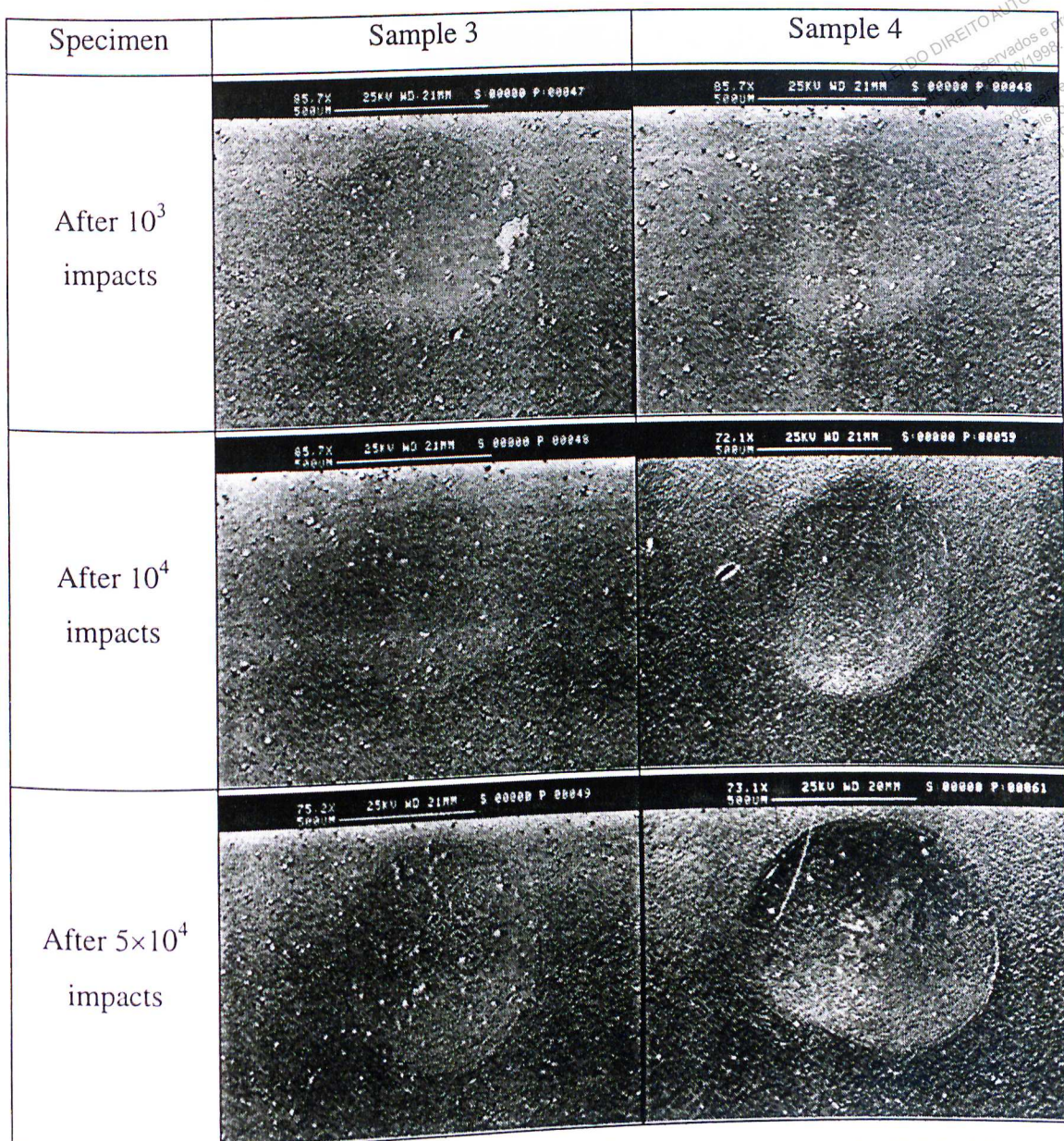
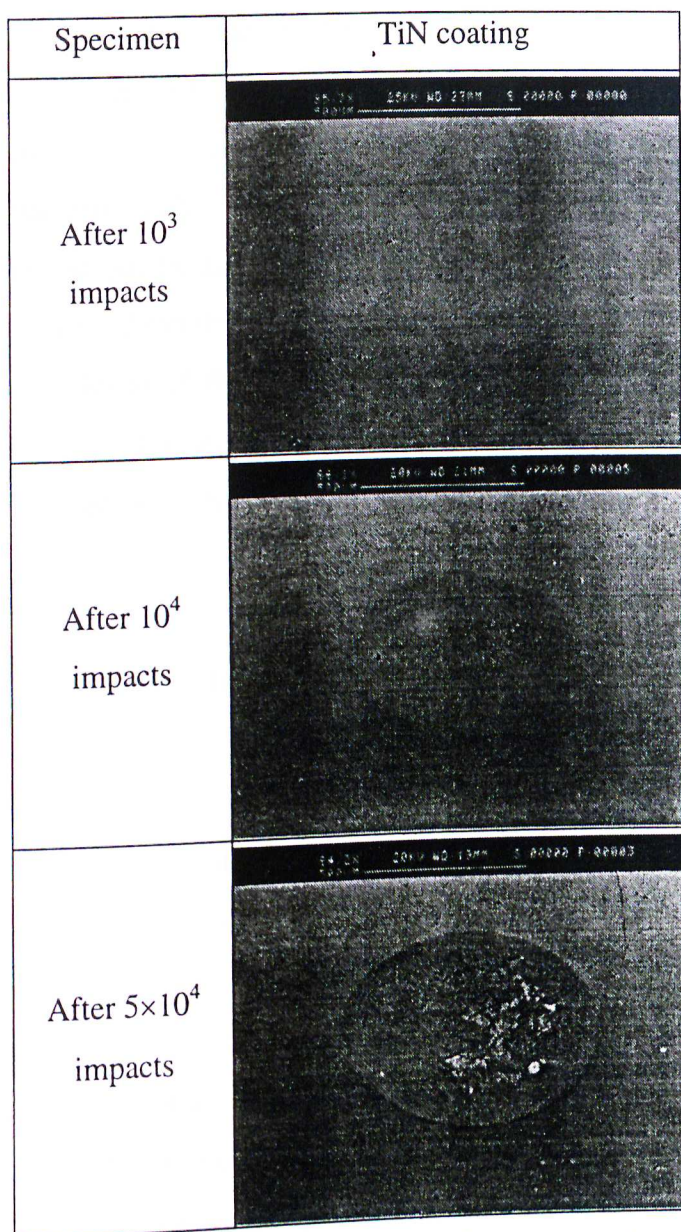


Figure 4.4 – Impact craters (10^3 , 10^4 and 5×10^4) produced in sample 3 (nitrided case comprising a diffusion zone) and sample 4 (nitrided case also comprising a diffusion zone). SEM. The elliptical shape of some impact craters results from the tilt employed in the SEM imaging.



LEI DO DIREITO AUTORAL
 Todos os direitos reservados e protegidos
 pela Lei 9.610/1998.
 Este arquivo não pode ser reproduzido ou
 transmitido sejam quais forem os meios
 empregados: eletrônicos, mecânicos,
 fotográficos ou quaisquer outros.

Figure 4.5 – Impact craters (10^3 , 10^4 and 5×10^4) produced in a single-layered TiN coating. SEM. The elliptical shape of some impact craters results from the tilt employed in the SEM imaging.

The hard ϵ compound layer provided a more “efficient” load support to the TiN coating than did the diffusion zone; this is probably due to the higher hardness of the former when compared to the latter. Sample 2 (mono-phase ϵ compound layer + diffusion zone) did not show any circular cracks in the peripheral zone or cohesive and adhesive failures at the intermediate and central zones. Therefore, the compound layer did not have a detrimental effect on the impact resistance of duplex coatings. On the contrary,

its presence seemed to improve the resistance of TiN coatings to dynamic impact. Such improvement can be achieved by producing hard, dense and mono-phase compound layers that are able to act as a proper interface between harder, more brittle PVD coatings and relatively softer, more ductile diffusion layers of plasma nitrided substrates. As pointed out by Edenhofer⁽⁴⁶⁾, the usefulness of the compound layer of normal structural steels depends on two factors: the homogeneity of the nitride layer structure and the thickness of the layer. In dual-phase compound layers, containing a heterogeneous mixture of ϵ and γ' phases, there are high inherent stresses in the transitional region between the different lattice structures (hexagonal and f.c.c., respectively) which may give rise to micro-cracks if even a slight external stress is superimposed. The brittleness of the compound layer produced by gas nitriding (always dual-phase $\epsilon + \gamma'$) and the less brittle compound layer of bath nitrided workpieces (exclusively ϵ nitride) confirm the influence of layer homogeneity⁽⁴⁶⁾. As far as the thickness of the nitride structure is concerned, it is well known that the ductility of the iron nitride layer decreases with increasing layer thickness⁽⁴⁶⁾. Based on these two factors, it is obvious that the optimum properties will be produced when the compound layer is mono-phased and of the minimum thickness necessary to meet specific properties such as wear and corrosion resistance. It seems that a 1.0-1.2 μm thick mono-phase ϵ compound layer had a positive influence on increasing the impact resistance of TiN coatings. It has already been reported, however, that nitrided cases (compound layer + diffusion zone) thicker than 50 μm have shown a substantial decrease of the wear resistance in consequence of the increasing embrittlement^(10,16,18).

Scratch and impact test results show that the presence of a mono-phase compound layer is not detrimental to either adhesion or impact behaviour. In fact, a thin, hard, dense mono-phase ϵ compound layer seems to improve the impact resistance of duplex TiN coatings. No differences in the adhesion strength of duplex coatings with different configurations (TiN + mono-phase ϵ compound layer + diffusion zone and TiN + diffusion zone) could be detected.

4.4. Conclusions

1. An intermediate treatment between plasma nitriding and coating deposition, consisting of cooling the samples in vacuum, subsequent plasma heating to predefined temperatures and sputter etching for different periods of time, was effective in removing a mono-phase ϵ (Fe_{2-3}N) compound layer, either for etching times equal to 10 or 20 minutes. If an Ar plasma etching was not performed and coating temperature was held below 673K, the compound layer was not destabilised and no black layer was formed. Therefore, the intermediate treatment elucidates a systematic approach to avoid compound layer destabilisation and/or produce duplex coatings which are compound-layer-free.
2. Scratch and impact test results indicate that a stable, mono-phase compound layer does not have any detrimental effects on adhesion and impact resistance. Although the critical loads determined for duplex coatings consisting of TiN + diffusion zones were statistically similar to those obtained for a duplex coating consisting of TiN + ϵ compound layer + diffusion zone, it was found that the duplex TiN coating with a hard, dense, mono-phase ϵ compound layer + diffusion zone can outperform a duplex coating with TiN + diffusion zone in impact tests.
3. The duplex coatings formed by TiN + diffusion zone presented circular cracks, whilst the one with an ϵ compound layer did not show any coating failure up to 5×10^4 impacts. If process parameters are carefully controlled in order to produce a hard, dense, mono-phase compound layer, and destabilisation is successfully avoided, then it is possible to obtain duplex coatings with adhesion strength comparable to PVD hard coatings on plasma nitrided steels with a diffusion zone only.
4. Finally, it was confirmed that a duplex treatment, consisting of plasma nitriding and subsequent TiN coating, yielded a great improvement in impact resistance and scratch test critical loads L_{C1} and L_{C2} over a single-layered TiN coating.

CHAPTER 5: PROMISING DUPLEX COATINGS FOR TRIBOLOGICAL APPLICATIONS AT ELEVATED TEMPERATURES

5.1. Background

PVD hard titanium aluminium nitride ((Ti,Al)N) and chromium nitride (Cr-N) coatings have become extremely important technological materials for several industrial applications. These coatings are successful alternatives to TiN in working processes at elevated temperatures, since the latter starts to oxidise at about 773K^(31,114).

The thermodynamically metastable, ternary-phase (Ti,Al)N shows high microhardness, high oxidation stability, low thermal conductivity and relatively low friction coefficient against steel^(31,112-121). Because of these remarkable advantages, (Ti,Al)N coatings are currently used for metal cutting operations such as drilling, milling and turning at high speeds^(112,114,122-123). These coatings can also improve the corrosion resistance of steel substrates⁽¹²⁴⁻¹²⁶⁾. Because of its high oxidation resistance and good thermal barrier properties, (Ti,Al)N often has better wear resistance than TiN at elevated temperatures. However, (Ti,Al)N coatings may be outperformed by TiN coatings in low sliding speeds or in interrupted cutting processes, because of their brittleness and higher friction coefficient.

(Ti,Al)N forms, in an oxidising environment and above 973K, a dense, highly adhesive, protective Al₂O₃ film at its surface, preventing diffusion of oxygen to the coating material, inhibiting further oxidation and reducing diffusion wear during high temperature machining^(120,122). At elevated temperatures, the hot hardness of (Ti,Al)N is higher than that of TiN and is also dependent on the aluminium content. Coatings with a higher aluminium content seem to have superior hot hardness⁽¹²⁷⁾. The oxidation behaviour and mechanical properties of (Ti,Al)N coatings are also influenced by the aluminium content. During oxidation, (Ti,Al)N coatings seem to generate a two-layer structure, with an outer Al-rich layer (Al₂O₃) and an inner Ti-rich layer (TiO₂)⁽¹²⁰⁾. The total thickness of the oxide layer decreases with increasing aluminium content⁽¹²⁰⁾. Best

mechanical properties have been reported for coatings with a composition close to $Ti_{0.50}Al_{0.50}N^{(117,120)}$.

Chromium nitride (Cr-N) has been used as a hard coating material on steel substrates. Industrial applications of Cr-N coatings include cutting and cold forming of Ni, Ti and alloys (monel, inconels, etc), pressure die-casting of aluminium, corrosion and wear protection of moulds, tools and components in the plastic industry⁽¹²⁸⁻¹³¹⁾, and for wood machining⁽¹³²⁾. In general, Cr-N coatings are characterised by their fine-grained and low stress structure, which allows deposition at much larger thickness (up to 10-25 μ m) than conventional PVD coatings of a few μ m⁽¹²⁸⁾. For instance, Cr-N is used on tools made of relatively soft substrates such as stainless steel, copper and aluminium alloys which cannot provide enough support for the more brittle coatings^(128,129). Cr-N has been reported to possess a lower friction coefficient than TiN under reciprocating sliding tests against steel⁽¹⁴⁹⁾. Its hardness, however, seems to be lower than that of TiN⁽¹⁴⁹⁾.

This nitride possesses two different crystalline phases: β -Cr₂N (hexagonal structure) and CrN (f.c.c. structure). Cr-N coatings can be prepared with a structure of a single phase (CrN or Cr₂N), or with a mixed structure of Cr + Cr₂N or Cr₂N + CrN⁽¹³³⁻¹³⁶⁾. The nitrogen partial pressure substantially affects phase formation and composition of Cr-N coatings⁽¹³³⁻¹³⁷⁾. The appearance of different phases, depending on the location of the substrates in the plasma, was also detected⁽¹³⁴⁾. The structure and morphology of Cr-N coatings also depend on the deposition process and deposition temperature⁽¹³⁷⁾. The highest hardness values were found for Cr₂N⁽¹³⁴⁻¹⁴⁰⁾ and the highest internal compressive stresses were detected for Cr₂N and CrN phases containing additional nitrogen⁽¹³⁴⁾.

Cr-N coatings are reported to provide resistance to oxidation up to 973-1073K^(114,136,141-143). At 723K⁽¹⁴³⁾ a protective Cr₂O₃ layer is formed on the top of the coating and further oxidation proceeds by progressive replacement of nitrogen by oxygen. At temperatures higher than 1073K, cracks appear at the surface⁽¹⁴³⁾. It was found that the oxidation resistance of coatings with the CrN phase is better than that for Cr or Cr₂N⁽¹³⁶⁾. These coatings are also well known for enhancing corrosion resistance of steel

mechanical properties have been reported for coatings with a composition close to $Ti_{0.50}Al_{0.50}N^{(117,120)}$.

Chromium nitride (Cr-N) has been used as a hard coating material on steel substrates. Industrial applications of Cr-N coatings include cutting and cold forming of Ni, Ti and alloys (monel, inconels, etc), pressure die-casting of aluminium, corrosion and wear protection of moulds, tools and components in the plastic industry⁽¹²⁸⁻¹³¹⁾, and for wood machining⁽¹³²⁾. In general, Cr-N coatings are characterised by their fine-grained and low stress structure, which allows deposition at much larger thickness (up to 10-25 μ m) than conventional PVD coatings of a few μ m⁽¹²⁸⁾. For instance, Cr-N is used on tools made of relatively soft substrates such as stainless steel, copper and aluminium alloys which cannot provide enough support for the more brittle coatings^(128,129). Cr-N has been reported to possess a lower friction coefficient than TiN under reciprocating sliding tests against steel⁽¹⁴⁹⁾. Its hardness, however, seems to be lower than that of TiN⁽¹⁴⁹⁾.

This nitride possesses two different crystalline phases: β -Cr₂N (hexagonal structure) and CrN (f.c.c. structure). Cr-N coatings can be prepared with a structure of a single phase (CrN or Cr₂N), or with a mixed structure of Cr + Cr₂N or Cr₂N + CrN⁽¹³³⁻¹³⁶⁾. The nitrogen partial pressure substantially affects phase formation and composition of Cr-N coatings⁽¹³³⁻¹³⁷⁾. The appearance of different phases, depending on the location of the substrates in the plasma, was also detected⁽¹³⁴⁾. The structure and morphology of Cr-N coatings also depend on the deposition process and deposition temperature⁽¹³⁷⁾. The highest hardness values were found for Cr₂N⁽¹³⁴⁻¹⁴⁰⁾ and the highest internal compressive stresses were detected for Cr₂N and CrN phases containing additional nitrogen⁽¹³⁴⁾.

Cr-N coatings are reported to provide resistance to oxidation up to 973-1073K^(114,136,141-143). At 723K⁽¹⁴³⁾ a protective Cr₂O₃ layer is formed on the top of the coating and further oxidation proceeds by progressive replacement of nitrogen by oxygen. At temperatures higher than 1073K, cracks appear at the surface⁽¹⁴³⁾. It was found that the oxidation resistance of coatings with the CrN phase is better than that for Cr or Cr₂N⁽¹³⁶⁾. These coatings are also well known for enhancing corrosion resistance of steel

substrates^(140,144-146). Deposition of a metallic Cr interlayer⁽¹⁴⁵⁾, electroless Ni⁽¹⁴⁶⁾ or ENiP (Electroless Nickel-Phosphorus)⁽¹⁴⁷⁾ interlayers seem to give further improvements on corrosion resistance of Cr-N coatings.

Cr-N coatings have proven to be more wear resistant than TiN coatings under reciprocating sliding⁽¹⁴⁸⁻¹⁵¹⁾ and in pin-on-disc tests^(140,152). The wear resistance is strongly affected by coating composition. It was observed that Cr-N coatings with a Cr content higher than stoichiometric CrN have relatively poor wear resistance⁽¹⁵³⁾. N-rich Cr-N coatings have enhanced wear resistance due to their low friction coefficient⁽¹⁵³⁾. Hence, CrN coatings usually have higher wear resistance than Cr₂N⁽¹⁴⁰⁾.

This chapter is focused on structural and mechanical characterisation of single-layered and duplex (Ti,Al)N, Cr-N coatings. Several analytical methods such as glow discharge optical emission spectroscopy (GDOES), Knoop hardness measurements, scratch tests, scanning electron microscopy (SEM) on fractured and polished cross-sections have been used to evaluate coating properties.

5.2. Experimental Procedure

5.2.1. Treatments

AISI H13 quenched and tempered steel discs (55HRC, 25mm x 7.5mm, $R_a=0.005\pm 0.001\mu\text{m}$) were plasma nitrided and coated with Cr-N and (Ti,Al)N in one single operation. Single-layered Cr-N and (Ti,Al)N coatings (i.e., without plasma nitriding) were also prepared for comparison. All coatings were produced by electron beam evaporation and plasma nitriding was performed in a 60%Ar-40%N₂ glow discharge for 2 hours. Single-layered (Ti,Al)N, duplex (Ti,Al)N and duplex Cr-N coatings were produced in a Tecvac IP35L equipment whereas single-layered Cr-N coatings were prepared in a Tecvac IP70L equipment. The main process parameters during nitriding (total gas pressure, partial gas pressure, substrate bias) were the same ones that had been used to produce duplex TiN coatings in the Balzers BAI 640R

equipment. However, due to geometrical differences in the PVD systems produced by Balzers and Tecvac, it was impossible to keep all process parameters (especially those related to the generation of the glow discharge) similar to the ones that were used for producing duplex TiN coatings. For instance, the Balzers triode ion plating equipment utilises an ionisation chamber to generate the plasma and a triode configuration is achieved by means of a third electrode (the auxiliary anode, see figure 3.7). Both Tecvac systems have a biased tungsten filament to enhance ionisation in the plasma.

All coatings were subjected to a sputter cleaning step followed by plasma heating in argon before initiating coating deposition. These parameters are shown in tables V.1 and V.2.

Table V.1 – Sputter cleaning parameters used during the production of single-layered and duplex (Ti,Al)N, Cr-N coatings

Coating	(Ti,Al)N	Cr-N	Duplex (Ti,Al)N	Duplex Cr-N
Ar pressure (Pa)	2.0	6.6×10^{-1}	2.0	2.0
Substrate bias (V)	1000	1000	1000	1000
Substrate current (A)	0.045	0.180	0.069	0.034
Temperature (K)	683	641	683	651

Note: The substrate current is higher for the Cr-N coating because these samples were put in with other tools in the production run.

A 0.1-0.2 μ m titanium interlayer was deposited in all (Ti,Al)N coatings. During the deposition of these coatings, OES (optical emission spectroscopy) was used for setting a Ti/Al ratio equal to 1. All duplex samples were cooled in vacuum down to 473K after plasma nitriding, in order to avoid deposition temperatures higher than 723K. This intermediate treatment was carried out to ensure that the compound layer, if formed during nitriding, would not be destabilised (see chapter 4). As the nitriding temperature was around 703-743K, it was necessary to cool down the samples to avoid deposition

temperatures higher than 723K. The deposition parameters of single-layered and duplex coatings are given in table V.3 and V.4, respectively.

Table V.2 – Plasma heating parameters used during the production of single-layered and duplex (Ti,Al)N, Cr-N coatings

Coating	(Ti,Al)N	Cr-N	Duplex (Ti,Al)N	Duplex Cr-N
Ar pressure (Pa)	3.0×10^{-1}	4.0×10^{-1}	6.5×10^{-1}	6.4×10^{-1}
Filament current (A)	58	49	58	58
Substrate bias (V)	1000	1000	1000	1000
Substrate current (A)	0.22	0.35	0.25	0.30
Ar flow (ml min ⁻¹)	22	50	32	32
Temperature (K)	720	663	720	752

Note: The substrate current is higher for the Cr-N coating because these samples were put in with other tools in the production run.

Table V.3 – Deposition parameters of single-layered (Ti,Al)N and Cr-N coatings

Coating	(Ti,Al)N	Cr-N
Total Pressure (Pa)	$4.0-4.3 \times 10^{-1}$	5.0×10^{-1}
Filament current (A)	74-66	72
Substrate bias (V)	50	50
Substrate current (A)	0.20-0.25	4.0-5.2
Ar flow (ml min ⁻¹)	9	27
N ₂ flow (ml min ⁻¹)	60	75
Temperature (K)	723-753	723-773
Deposition time (min)	100	60

Note: The substrate current is higher for the Cr-N coating because these samples were put in with other tools in the production run.

Table V.4 – Deposition parameters of duplex (Ti,Al)N and Cr-N coatings

	Duplex (Ti,Al)N		Duplex CrN	
	Plasma nitriding	Coating deposition	Plasma nitriding	Coating deposition
Total Pressure (Pa)	4.0-4.4×10 ⁻¹	4.1-4.3×10 ⁻¹	4.0-5.0×10 ⁻¹	3.9-4.2×10 ⁻¹
Filament current (A)	80-75	65-60	85-80	80-78
Substrate bias (V)	250	50	250	50
Substrate current (A)	1.04-1.06	0.20	1.70-1.80	1.20-1.30
Ar flow (ml min ⁻¹)	8	9	11	22
N ₂ flow (ml min ⁻¹)	5	60	7	49
Temperature (K)	723-743	573-698	703-723	663-715
Time (min)	120	100	120	60

5.2.2. Analysis of the coatings

Single-layered and duplex coatings had their surface roughness (R_a value) evaluated using a Veeco DEKTAK³ST profilometer. The coating phase composition was investigated by means of XRD using a Philips PW1710 diffractometer with a Cu-K α radiation ($\lambda=0.154056\text{nm}$). The diffractograms were recorded with a 2θ step of 0.02° from 30 to 100° . Scanning electron microscopy (SEM) was used to study the morphology and the cross-sectional structure of the coatings in a Cambridge S200 scanning electron microscope. Light optical microscopy (LOM) was also used to investigate the nitrided layers.

In order to determine the thickness of the nitrided layers, Knoop hardness measurements were made at a load of 0.23N (25gf) using a Mitutoyo MVK-G1 hardness tester. To characterise the surface hardness resulting from the combined treatment of plasma nitriding and PVD deposition, Knoop hardness measurements were made at various loads.

GDOES (Glow Discharge Optical Emission Spectroscopy) is a versatile technique for the simultaneous depth profiling of up to 30 elements (including hydrogen) in surface layers with thicknesses of $0.1\text{-}80\mu\text{m}$. The sample is used as a cathode to produce a glow

discharge in a small chamber. A cylindrical anode is located in front of the sample to constrict an argon plasma from which positive ions are accelerated towards the sample surface, resulting in removal of atoms by sputtering. The sputtered atoms are excited by electrons in the glow discharge and will emit optical radiation during the subsequent de-excitation process. By analysing the emitted light with an optical spectrometer and recording the intensity variations of individual spectral lines with time, an elemental depth profile is generated. Since the sputtering rate is known, semi-quantitative measurement of sample composition as a function of depth can be obtained by the GDOES technique. In the present experiments, a Leco GDS-750QDP glow discharge spectrometer was used for analysing the composition of single-layered and duplex (Ti,Al)N, Cr-N coatings. The sputtering parameters were 700V, 25mA.

The coating adhesion was assessed by means of the scratch test method (see chapter 3). The radius of the diamond indenter in the scratch test was 0.2mm and the measurements were carried out at a load increase rate of 100N min^{-1} and a table speed of 10mm min^{-1} . A set of three scratches was performed on each composite. Acoustic emission (AE), tangential friction force readings (F_t) were recorded and used for determining the critical loads. The scratches were also examined by means of SEM.

5.3. Results and Discussion

5.3.1. Surface roughness

The surface roughness (R_a value) of single-layered and duplex (Ti,Al)N and Cr-N coatings is shown in table V.5. It was found that the duplex treatment resulted in a considerably increased surface roughness. This increase in the R_a value can be attributed to sputter etching by argon/nitrogen ions on the substrate surface during plasma nitriding.

Table V.5 – Surface roughness of single-layered (Ti,Al)N, Cr-N and duplex (Ti,Al)N, Cr-N coatings

Specimen	R_a (μm)
Single-layered (Ti,Al)N coating	(0.018 \pm 0.005)
Duplex (Ti,Al)N coating	(0.043 \pm 0.005)
Single-layered Cr-N coating	(0.016 \pm 0.004)
Duplex Cr-N coating	(0.039 \pm 0.006)

LEI DO DIREITO AUTORAL
 Todos os direitos reservados e protegidos
 pela Lei 9.610/1998.
 Este arquivo não pode ser reproduzido ou
 transmitido sejam quais forem os meios
 empregados: eletrônicos, mecânicos,
 fotográficos ou quaisquer outros.

5.3.2. Knoop hardness measurements

It can be seen from figure 5.1 that the hardness of the investigated coatings varies between 2600 and 3600HK_{0.025} and increases in the order single-layered Cr-N < duplex Cr-N < single-layered (Ti,Al)N < duplex (Ti,Al)N. As the load increases, the increase in load-bearing capacity of duplex coatings can be seen. The plasma nitrided layer improves the mechanical support for the single-layered PVD coatings so that higher hardness values for the duplex-treated coating/substrate systems are measured. At lower loads (0.23N), the measured surface hardness is probably more influenced by the PVD coating rather than by the hardness of the substrate so that both duplex and single-layered (Ti,Al)N have the highest hardness values.

Knoop hardness profiles of duplex (Ti,Al)N and Cr-N coatings are shown in figure 5.2. The duplex (Ti,Al)N has a 55-60 μm thick nitrided case whereas the duplex Cr-N possesses a 35-40 μm thick nitrided layer. The nitrided case thickness obtained for the duplex Cr-N coating is quite similar to that of duplex TiN coatings that were produced in the Balzers triode ion plating equipment (see chapter 3). The duplex Cr-N exhibits a harder nitrided case in comparison with the duplex TiN coating. In chapter 3, an annealed AISI H13 steel (370HK_{0.025}) was used as the substrate for a TiN coating whilst a hardened and tempered AISI H13 steel (830HK_{0.025}) has been used as substrate for a duplex Cr-N and (Ti,Al)N. Therefore, such differences in nitrided case hardnesses are expected.

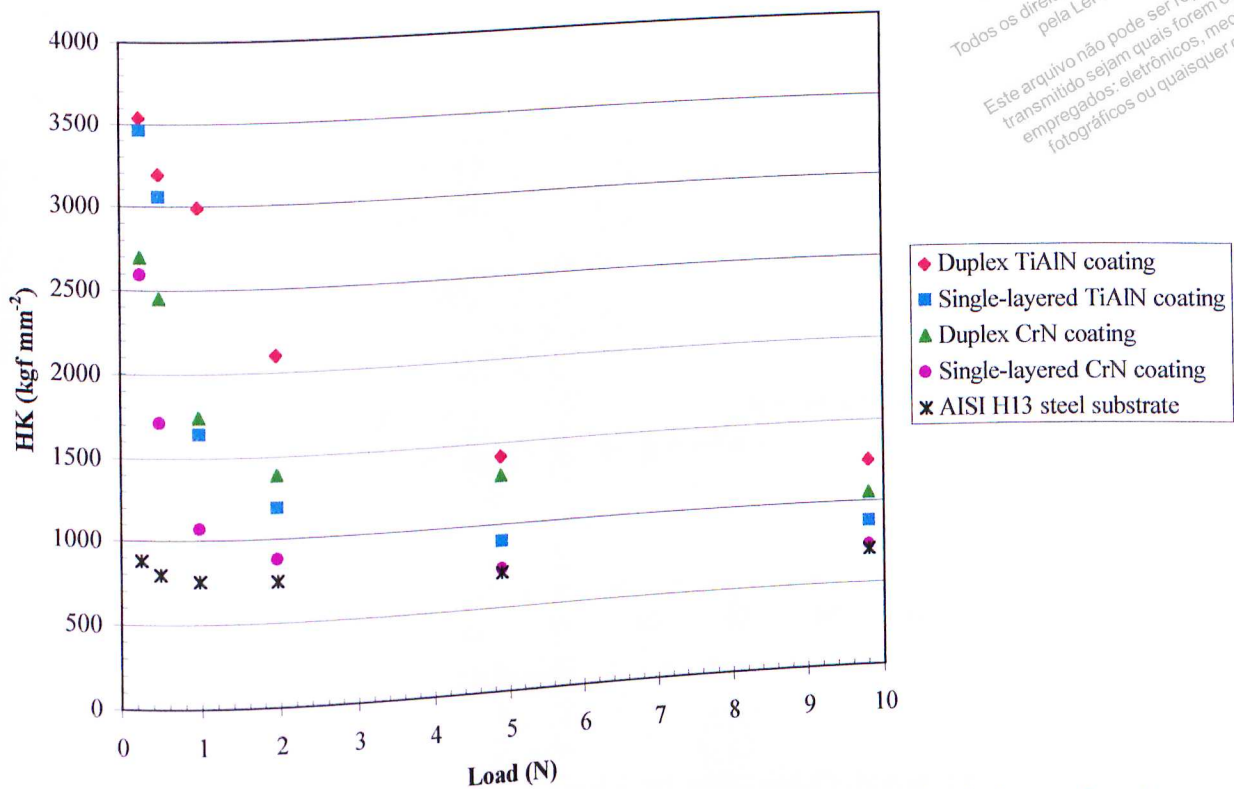


Figure 5.1 – Knoop hardness data for the AISI H13 steel substrate, single-layered and duplex (Ti,Al)N, Cr-N coatings. Although the error bars are not shown in the plot, the standard deviation was not larger than 5%.

It is interesting to note that the nitriding parameters were nearly the same for both duplex Cr-N and (Ti,Al)N coatings, except nitriding temperature, which was slightly higher for the latter (see table V.4). This might have led to a thicker and comparatively harder nitrided case for the same treatment time (2h). The nitrogen partial pressure and degree of ionisation in the plasma are believed to influence the nitriding performance. However, process parameters have been set for producing a 60%Ar-40%N₂ plasma in both runs. Hence, it is very unlikely that the differences in hardness and thickness of the nitrided case are due to variations in the nitrogen partial pressure. Although the current density values for both runs have not been recorded, variations in such parameter could also have led to the differences observed in both hardness and thickness of the nitrided layer.

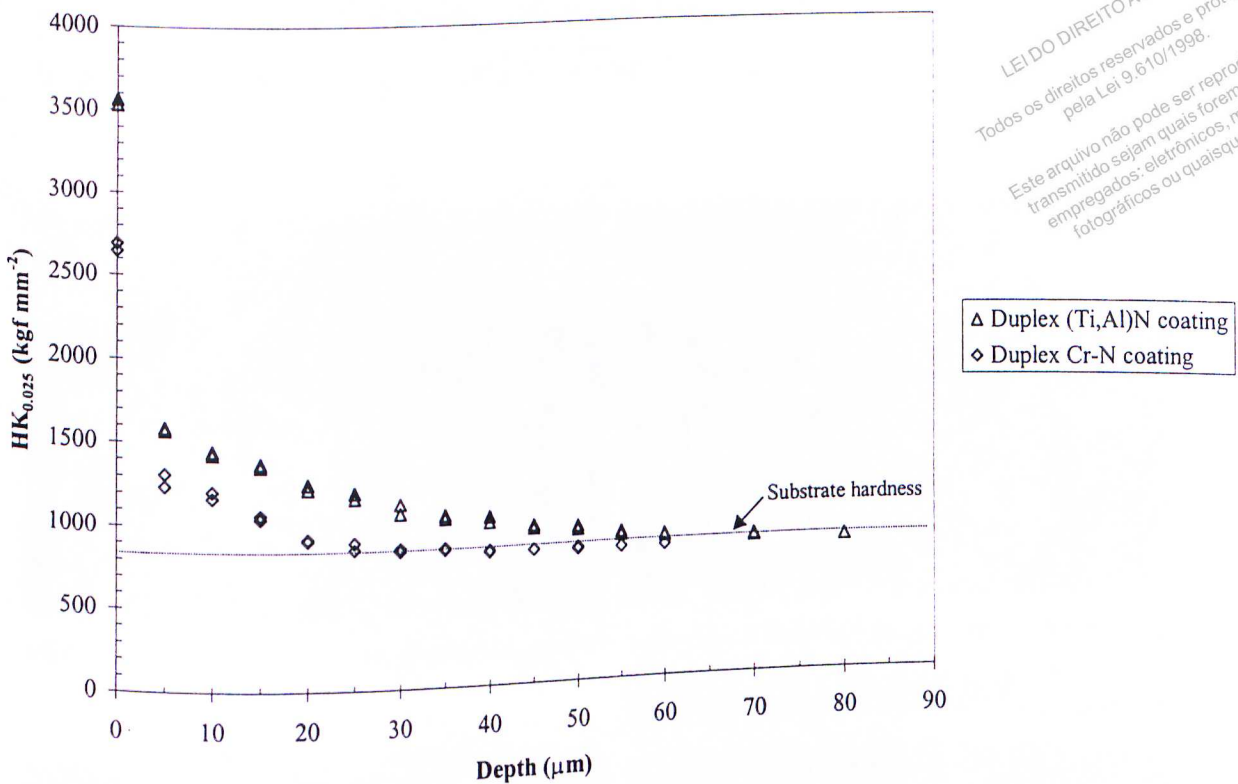


Figure 5.2 – Knoop hardness profiles of duplex (Ti,Al)N and Cr-N coatings.

5.3.3. Cross-sectional structure of the coatings

Figure 5.3 shows the SEM fracture cross-sections of the coatings. All coatings have a very dense columnar morphology, as expected for PVD coatings produced by the ion plating technique. The structure of single-layered coatings is more fine-grained than that exhibited by duplex coatings. The single-layered Cr-N coating possesses the finest grained structure among all coatings.

Note the different fracture behaviours showed by plasma nitrided (figure 5.3 (a) and (b)) and hardened and tempered (figure 5.3 (c) and (d)) AISI H13 steel substrates. The former exhibits a more brittle behaviour whilst the latter has a more ductile behaviour, confirming that quenched and tempered steels often suffer an additional loss in ductility due to nitriding⁽⁴⁶⁾.

Coating thicknesses were estimated from direct measurements on SEM fracture cross-sections. The coating thicknesses, which were obtained, are comparable (table V.6). The only exception is the duplex Cr-N coating, which is slightly thinner.

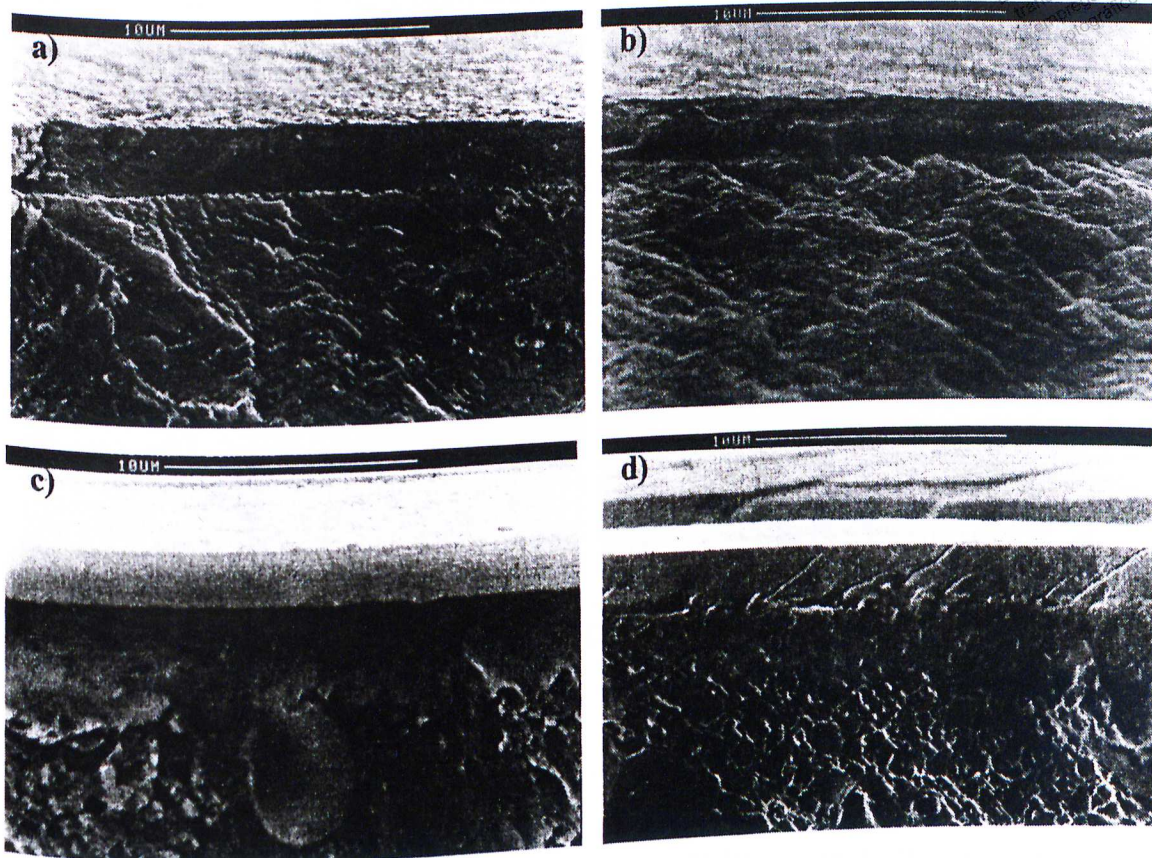


Figure 5.3 – SEM fracture cross-sections of (a) Duplex (Ti,Al)N coating, (b) Duplex Cr-N coating, (c) Single-layered (Ti,Al)N coating and (d) Single-layered Cr-N coating. 5000X.

Table V.6 – Coating thickness

Specimen	Coating thickness, t (μm)
Single-layered (Ti,Al)N coating	2.3-2.4
Duplex (Ti,Al)N coating	2.6-2.7
Single-layered Cr-N coating	2.5-2.6
Duplex Cr-N coating	2.0-2.1

Polished cross-sections of the duplex coatings (figure 5.4) revealed the absence of compound layers. Plasma nitriding in both Tecvac systems (IP35L and IP70L) did not yield any compound layers when using a 60%Ar-40%N₂ plasma. Such glow discharge composition yielded a mono-phase ϵ compound layer when plasma nitriding was carried out in the Balzers ion plating equipment.

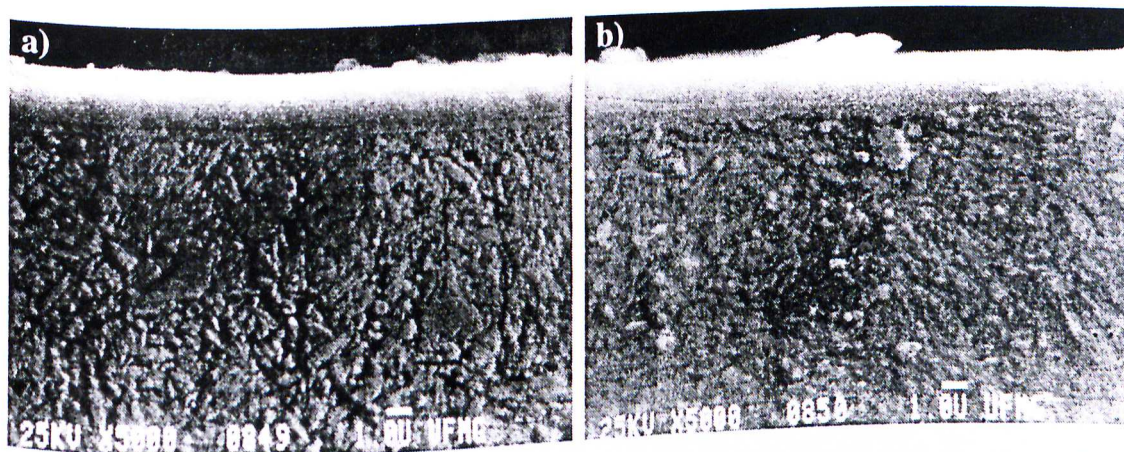


Figure 5.4 – Polished cross-sections of (a) Duplex (Ti,Al)N and (b) Duplex Cr-N. Nital etchant (4%). 5000X. SEM.

Glow discharge composition and bias voltage (250V) were kept the same for all nitriding runs. It seems that the nitriding potential (the critical nitrogen potential below which a compound layer does not form on the surface) was not above the threshold value when plasma nitriding was performed in the Tecvac IP35L equipment. Thus, no compound layer was formed on substrate surfaces. Although the current density values for all nitriding runs (in both Balzers and Tecvac systems) have not been recorded, variations in such parameter could have led to the differences observed in the structure of the nitrided layer. Conversely, if we assume that similar current density values were obtained when performing nitriding treatments in both Balzers and Tecvac ion plating systems, then such differences could be related to distinct ways of enhancing plasma ionisation in these systems. Since thermionic support yields lower I/λ and higher I_{ef} values than a positively biased third electrode, this may explain why a compound layer was not formed in the Tecvac system where a biased tungsten filament is used for

enhancing plasma ionisation. An increase of I_{ef} values and a reduction of the l/λ ratio imply an increase of high energy species reaching the cathode compared with a positively biased third electrode (Balzers equipment). Therefore, the likelihood of these high energy species being implanted into the near-surface is greater than being absorbed. Hence, the build-up of high nitrogen concentrations at the substrate surface is greatly reduced. Nitriding treatments that were carried out in a 75%N₂-25%H₂ glow discharge, using thermionic emitters to enhance plasma ionisation, yielded nitrided layers which were compound-layer-free⁽⁶⁾.

LOM observations of polished cross-sections also indicate that a 50-60 μ m thick diffusion zone was formed on the duplex (Ti,Al)N coating (figure 5.5 (a)). A 30-40 μ m thick diffusion zone can be seen on the duplex Cr-N coating (figure 5.5 (b)).

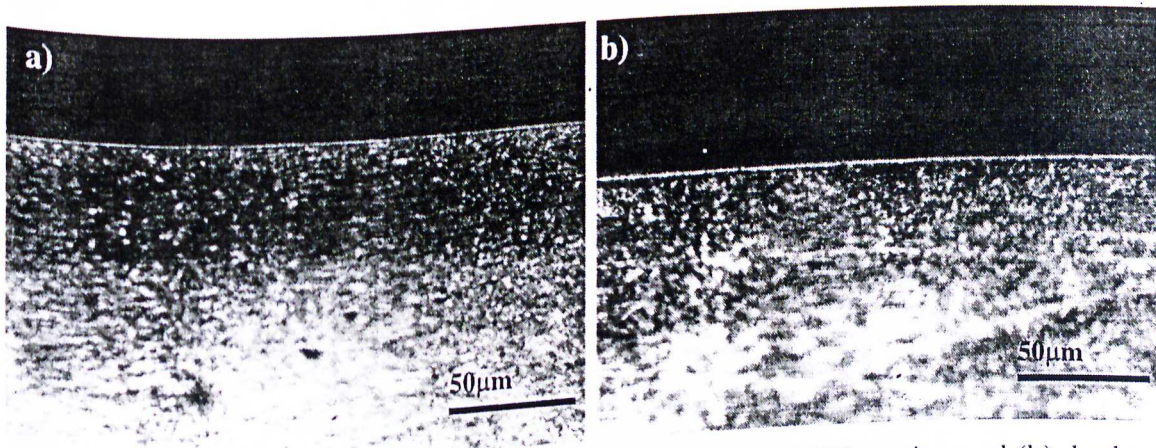


Figure 5.5 – LOM polished cross-sections of (a) duplex (Ti,Al)N coating and (b) duplex Cr-N coating. Nital etchant (4%). 400X.

5.3.4. Coating morphology

Single-layered (Ti,Al)N and Cr-N coatings displayed a fairly smooth surface with localised protuberances of 4-6 μ m in diameter (figure 5.6 (a) and (c)). The duplex (Ti,Al)N coating also showed protuberances on its surface (figure 5.6 (b)). Compared with the single-layered (Ti,Al)N, the duplex (Ti,Al)N has a larger number of protuberances per area. A variation in protuberance size could also be observed (smaller

protuberances of 1-2 μm in diameter and larger ones of 4 μm in diameter). The duplex Cr-N coating displayed relatively shallow depressions all over its surface. Some white protuberances were found to grow inside of more pronounced depressions (figure 5.6 (d)). EDS analyses that had been carried out indicated that the white protuberances are less rich in Cr than the rest of the coating. None of the coatings exhibited deep holes and/or pores.

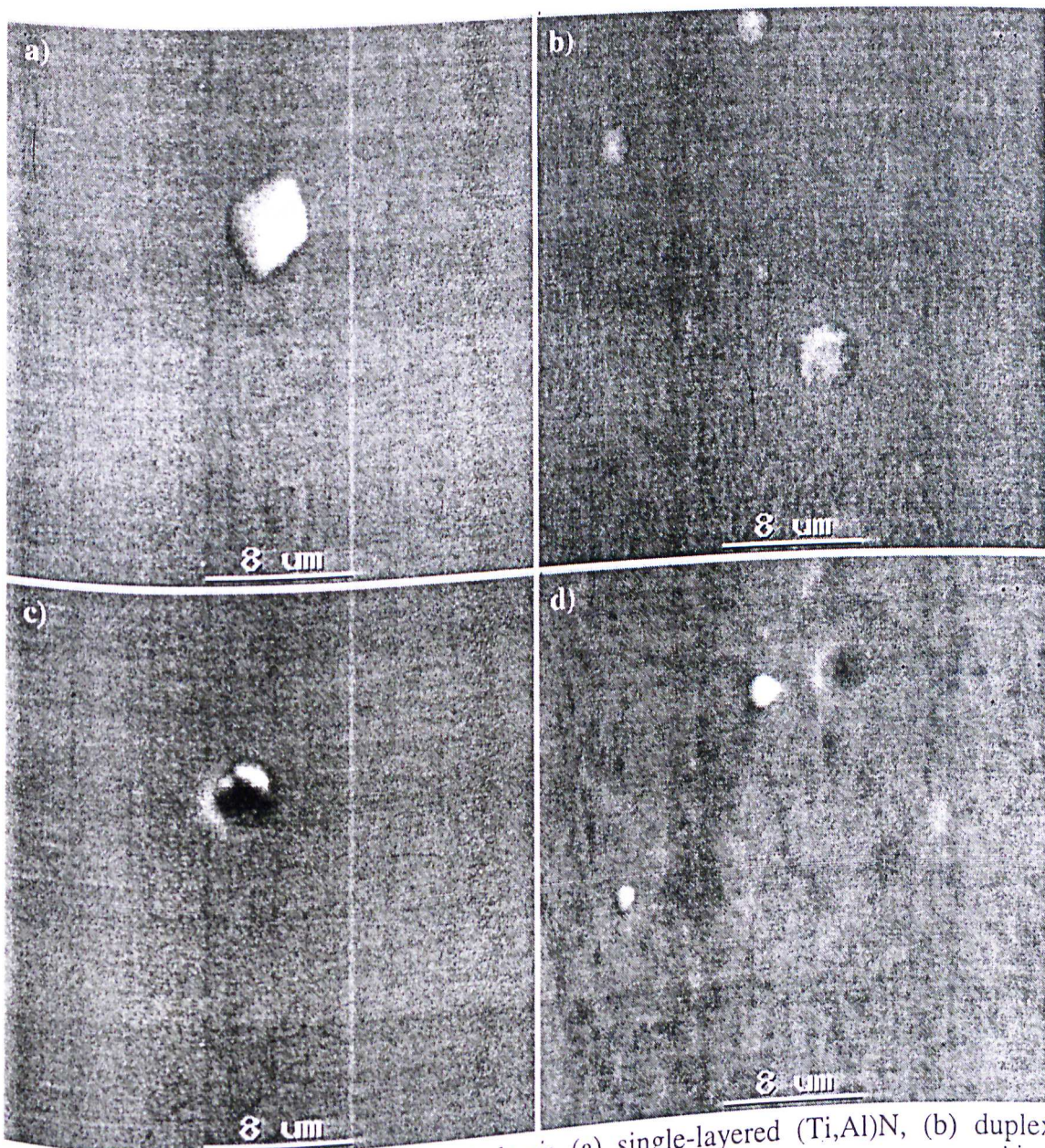


Figure 5.6 – Coating surface morphology: (a) single-layered (Ti,Al)N, (b) duplex (Ti,Al)N, (c) single-layered Cr-N and (d) duplex Cr-N. SEM. 3000X.

5.3.5. XRD analyses

From the XRD analysis, it was found that (Ti,Al)N coatings crystallised into three phases: $Ti_3Al_2N_2$ (hexagonal), Ti_2AlN (hexagonal) and TiN (f.c.c.). $Ti_3Al_2N_2$ and TiN phases have been reported for (Ti,Al)N coatings prepared by other deposition techniques⁽¹⁵⁴⁻¹⁵⁶⁾. Fe peaks corresponding to the martensitic substrate can be observed in the diffractograms (figure 5.7). The dominant phase in the single-layered (Ti,Al)N coating is $Ti_3Al_2N_2$ with a (1 0 7) preferred growth orientation. Small amounts of TiN and Ti_2AlN could also be detected. The duplex (Ti,Al)N coating has a large amount of TiN and Ti_2AlN phases and a comparatively small amount of $Ti_3Al_2N_2$. The most intense peaks are TiN with a (2 0 0) preferred growth orientation and Ti_2AlN with a (1 0 4) preferred growth orientation. Compared with the single-layered (Ti,Al)N, the duplex (Ti,Al)N coating has a large amount of amorphous material in its structure. The lower deposition temperature that was used for producing duplex (Ti,Al)N (see tables V.3 and V.4) probably influenced the relative amount of amorphous and crystalline phases formed.

Diffractograms of single-layered and duplex Cr-N are given in figure 5.8. It can be seen that the duplex Cr-N coating crystallised into Cr_2N and Cr phases. Fe diffraction peaks of the substrate are also present. The amount of Cr seems to be very small compared with the Cr_2N phase, and the Cr_2N phase has a (1 1 1) preferred growth orientation. The single-layered Cr-N coating contains CrN and Cr_2N with possible evidence of Cr. Fe peaks corresponding to the substrate can be seen; however, these peaks are smaller than those of the duplex Cr-N coating, indicating a slightly thicker coating (see table V.6). The Cr_2N phase has a (1 1 1) preferred growth orientation whilst the CrN phase has a (2 0 0) preferred growth orientation. It is expected that the amount of Cr phase is rather small in the single-layered Cr-N coating. A mixture of Cr + Cr_2N phases is expected to be formed when a lower nitrogen partial pressure is used. Higher nitrogen partial pressures allow the formation of Cr_2N + CrN phases.

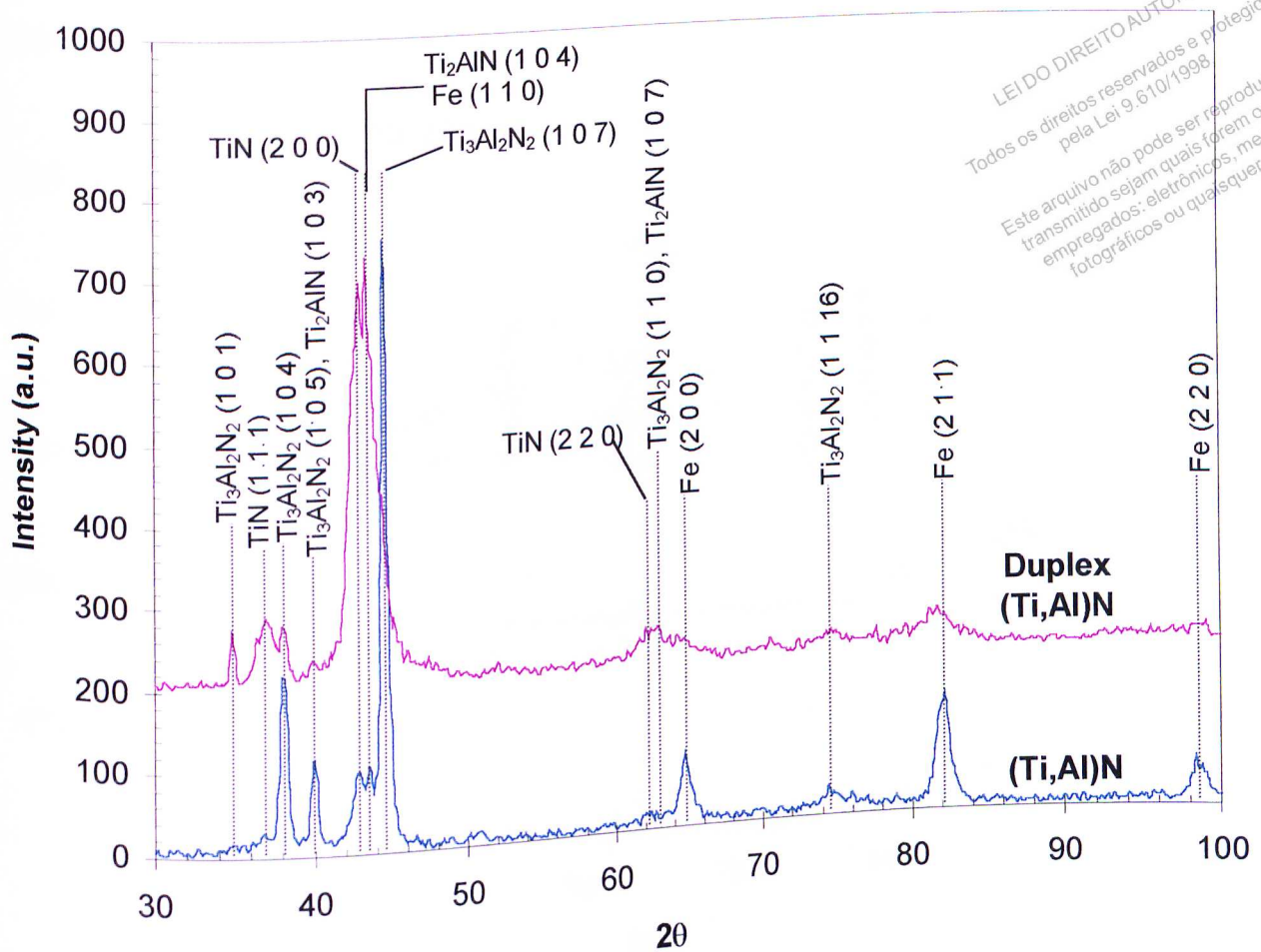


Figure 5.7 – Diffractograms of duplex and single-layered (Ti,Al)N coatings on AISI H13 substrates.

Since the Fe peaks are very close to those of Cr, the single-layered Cr-N coating probably does not contain any Cr phase and this film is basically a mixture of CrN and Cr_2N . During the deposition process of single-layered and duplex Cr-N coatings, the N_2 flow/Ar flow ratio was 2.8 for the former and 2.2 for the latter. This variation in the nitrogen partial pressure might have led the coatings to possess different phases, with the duplex Cr-N coating consisting of a mixture of Cr + Cr_2N and the single-layered Cr-N consisting of a mixture of Cr_2N + CrN. Variations in the amount of Cr evaporated could also lead both coatings to exhibit different phase structures.

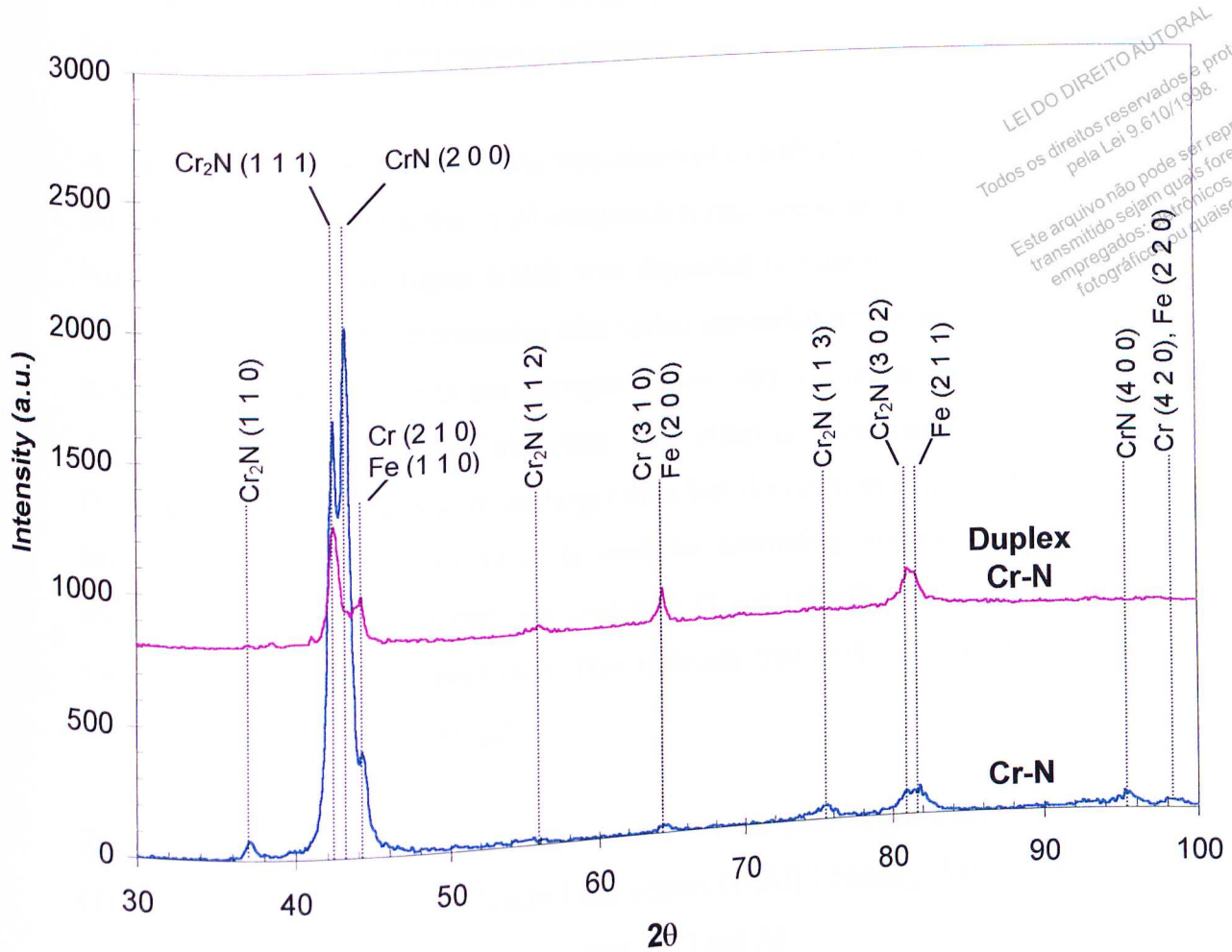


Figure 5.8 – Diffractograms of duplex and single-layered Cr-N coatings on AISI H13 substrates.

XRD analyses did not indicate the presence of ϵ (Fe_{2-3}N) and γ' (Fe_4N) phases, confirming that both duplex coatings are compound-layer-free.

5.3.6. GDOES analyses

The GDOES results presented here should be regarded as qualitative, since the apparatus was set up for TiN coatings. A quantitative analysis, indicating the atomic percentage of elements and the absolute thickness of coatings and nitrided layers was not possible to be carried out. The data is presented in terms of concentration (in

arbitrary units) and erosion time (in seconds). Nevertheless, relative concentrations can be obtained for the different coatings produced.

A cyclic variation on the Ti/Al ratio was observed in both (Ti,Al)N coatings (figure 5.9 (a) and (b)). Nevertheless, the Ti/Al composition ratio seems to be very close to unity in both films. The Ti interlayer which was deposited is clearly seen in both (Ti,Al)N coatings. The nitrogen concentration also varied somewhat within these coatings. Close to the surface, an increase in the nitrogen content with a simultaneous reduction in Ti and Al concentrations can be observed. This effect is more marked for the duplex (Ti,Al)N coating. For erosion times larger than 50s, the nitrogen concentration seems to become more stable. If this value is used for estimating coating composition, the titanium (or aluminium) to nitrogen ratio is 0.53 and 0.56 for the single-layered and duplex (Ti,Al)N films, respectively. This indicates that both (Ti,Al)N coatings have compositions close to $Ti_{0.50}Al_{0.50}N$.

The coating thickness does not differ very much for both single-layered and duplex (Ti,Al)N. Nevertheless, single-layered and duplex (Ti,Al)N coatings have an outer layer comparatively richer in nitrogen and poorer in Ti and Al.

The duplex (Ti,Al)N shows a high nitrogen concentration after a long erosion time, corresponding to the nitrided layer (diffusion zone). It is interesting to note that there is a reduction of C concentration in the substrate near its surface. This reduction is probably associated with carbide dissolution/nitride formation during plasma nitriding. The GDOES results seem to corroborate the formation of nitrides in the diffusion zone, as previously detected by XRD analyses of plasma nitrided AISI H13 steel substrates (figure 3.11).

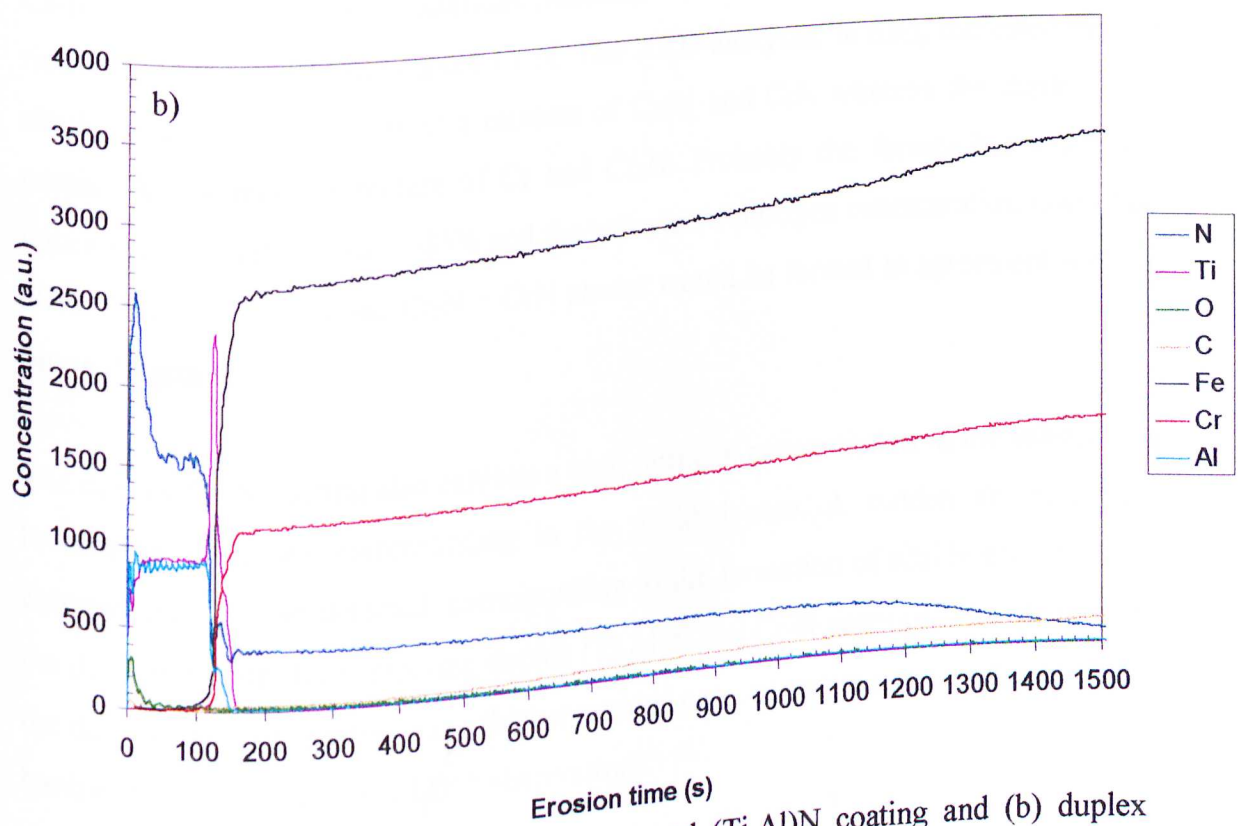
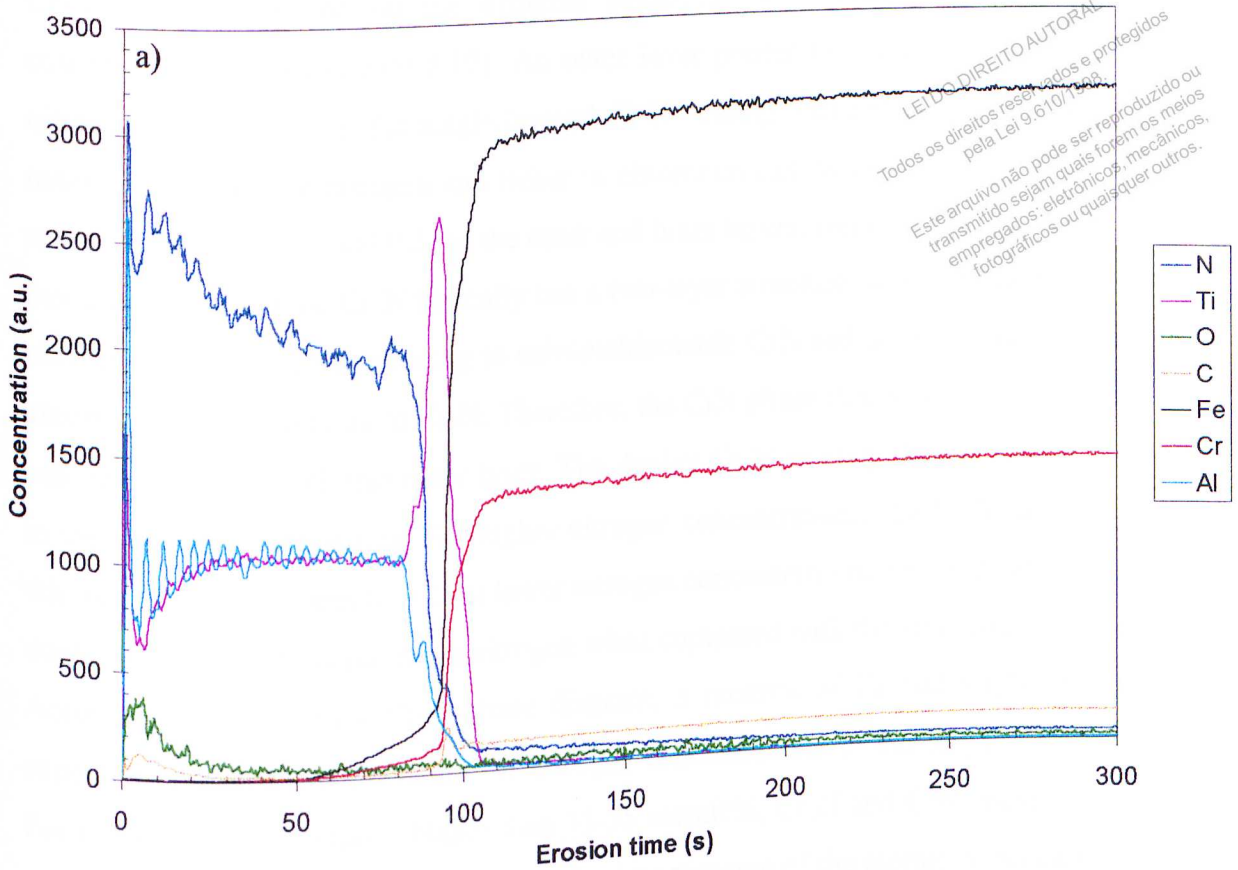


Figure 5.9 - GDOES profiles of (a) single-layered (Ti,Al)N coating and (b) duplex (Ti,Al)N coating. Note the different scales used for erosion time.

Cr-N coatings formed on the different substrates were found to have different composition profiles (figure 5.10). An outer layer poorer in chromium and richer in nitrogen can be seen in the single-layered Cr-N coating. Beneath this outer layer, an inner layer poorer in nitrogen and richer in chromium can be distinguished. The N/Cr ratios are around 0.86 and 0.5 for the outer and inner layers, respectively. This indicates that the single-layered Cr-N basically has a two-layer structure: an outer layer richer in nitrogen, probably corresponding to substoichiometric CrN and an inner layer richer in chromium, corresponding to Cr₂N. Therefore, the CrN phase that was detected by XRD can be associated with this outer layer. The duplex Cr-N coating also shows variations in the nitrogen composition. For higher nitrogen concentrations, the N/Cr ratio is 0.38 whilst this value reduces to 0.25 at lower nitrogen concentrations. This indicates that the duplex Cr-N coating is poorer in nitrogen when compared with the single-layered Cr-N. According to the binary Cr-N phase diagram, a mixture of Cr and Cr₂N phases is expected at ambient temperature for nitrogen concentrations in the range 17-30%⁽¹⁵⁷⁾. For nitrogen concentrations higher than 33-35 atomic%, Cr₂N and CrN phases coexist. Although it was not possible to have an absolute measure of the atomic nitrogen in both Cr-N coatings, the GDOES analyses indicated that the single-layered Cr-N coating is richer in nitrogen than the duplex Cr-N. The XRD analyses, in turn, indicated that the single-layered Cr-N coating is a mixture of Cr₂N and CrN whereas the duplex Cr-N coating has a mixed structure of Cr and Cr₂N. Probably the former has a nitrogen concentration higher than 33-35% and the latter has a nitrogen concentration lower than 30%. Thus, Cr + Cr₂N and Cr₂N + CrN phases would be formed in agreement with the phase diagram.

The duplex Cr-N coating also exhibits a high nitrogen concentration in the substrate up to erosion durations corresponding to the nitrided case. A sudden decrease in C concentration is also detected, corresponding to the formation of nitride precipitates in the diffusion zone. By comparing duplex (Ti,Al)N and Cr-N coatings, it is obvious that the duplex (Ti,Al)N coating has a thicker nitrided case, as previously detected by Knoop hardness measurements and LOM observations.

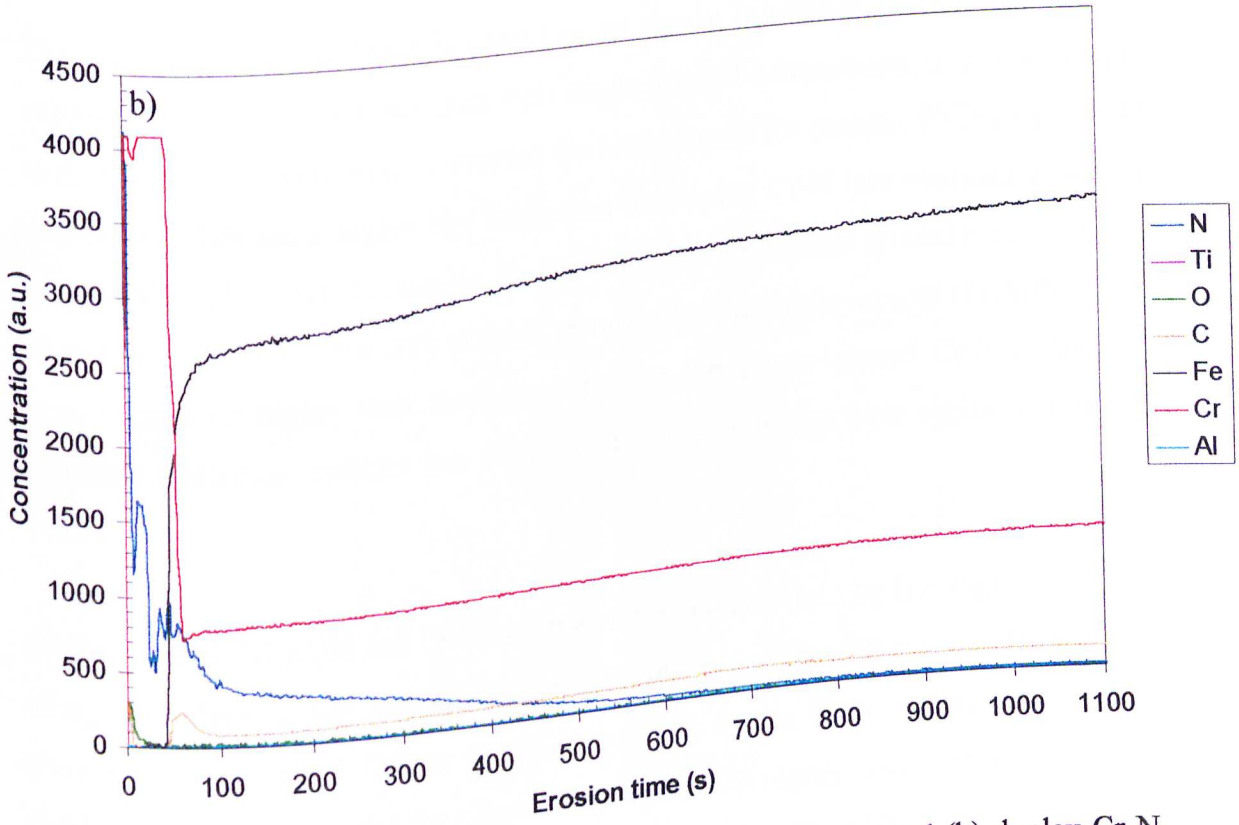
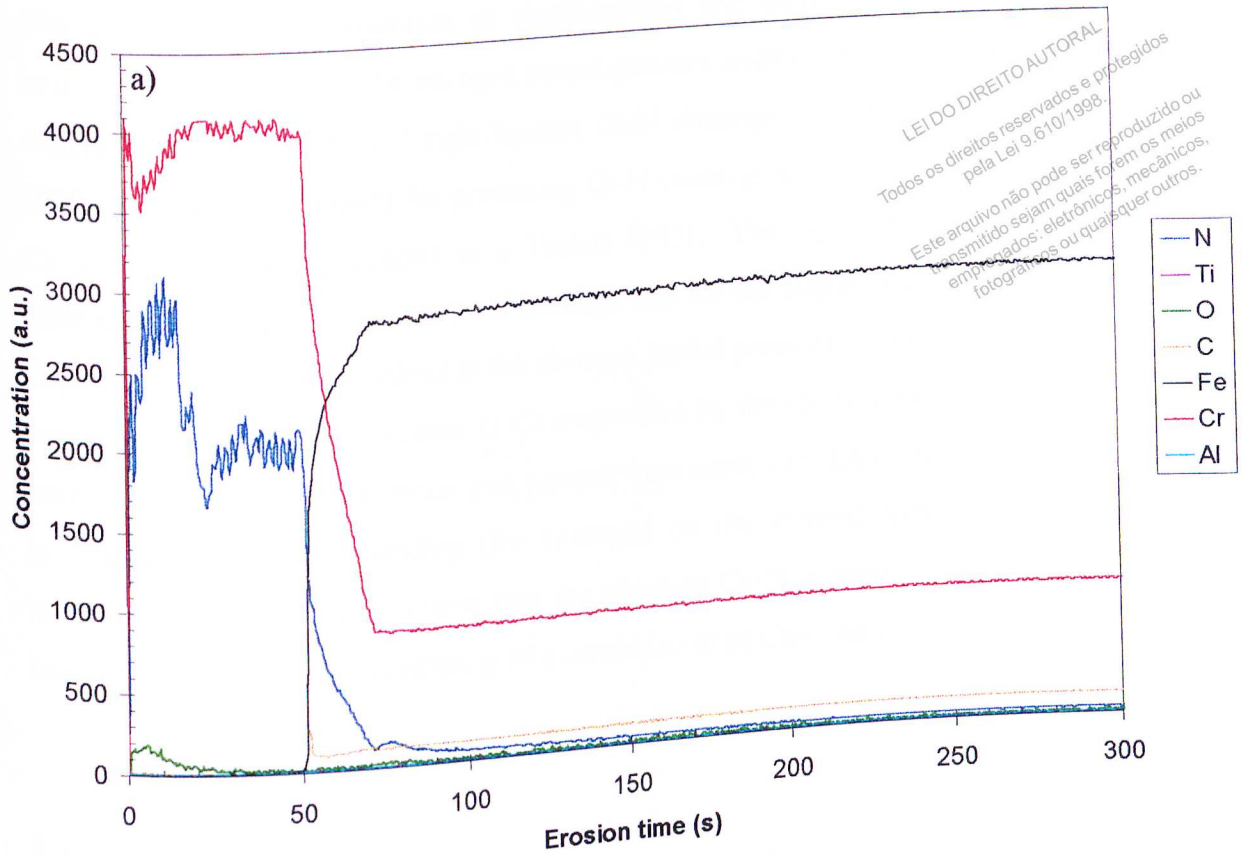


Figure 5.10 – GDOES profiles of (a) single-layered Cr-N coating and (b) duplex Cr-N coating. Note the different scales used for erosion time.

The differences in composition of single-layered and duplex Cr-N coatings can be attributed to variations in the nitrogen partial pressure and/or chromium evaporation rate during coating deposition. Single-layered Cr-N coatings were prepared in a Tecvac IP70L (standard equipment for producing Cr-N coatings at Tecvac Ltd.), whilst duplex Cr-N coatings were produced in a Tecvac IP35L. The N_2 flow/Ar flow ratio was different when depositing both Cr-N coatings (2.8 for the single-layered and 2.2 for the duplex). Not only the variations in the nitrogen partial pressure could have changed film composition but also the amount of Cr evaporated by the electron beam gun. Although nominally similar electron beam gun powers were used, variations could have occurred in evaporation rates, depending (for example) on the thermal contact of the source material to the crucible. It seems that the standard Cr-N process at Tecvac is set for producing Cr-N coatings consisting of a combination of CrN and Cr_2N .

5.3.7. Scratch testing

The scratch test critical loads L_{C1} and L_{C2} are shown in table V.7. All duplex coatings exhibited higher critical loads than their single-layered counterparts, indicating that the nitrided case (diffusion zone) increased the load support for ceramic PVD coatings. The duplex (Ti,Al)N has a higher L_{C2} value than the duplex Cr-N (see confidence intervals in table V.7). However, the duplex Cr-N coating has the highest critical load L_{C1} among all coatings. Although the critical loads recorded for the single-layered (Ti,Al)N coating were somewhat higher than those recorded for the single-layered Cr-N coating, the confidence intervals indicate that both single-layered coatings have similar L_{C1} and L_{C2} values.

Single-layered (Ti,Al)N and Cr-N coatings were characterised by flaking of the coating along the edges of the scratch (figure 5.11 (a) and (c)), with the (Ti,Al)N coating showing a more severe flaking on the ridges. The duplex Cr-N coating also exhibited flaking of the coating along the edges of the scratch. At higher loads, external transverse cracks started to form (figure 5.11 (d)). For the duplex (Ti,Al)N coating, a markedly different scratch behaviour was observed. In this coating the failure mode was by tensile

cracking, as previously observed in duplex TiN coatings (see chapters 3 and 4). The critical load at which tensile cracks started to form was used as the critical load for cohesive failure (L_{C1}). No external transverse cracks were formed until the substrate became exposed (figure 5.11 (b)).

Table V.7 – Critical loads L_{C1} and L_{C2}

Specimen	L_{C1} (N)	C.I. (95%) (N)	L_{C2} (N)	C.I. (95%) (N)
Single-layered (Ti,Al)N coating	31.8	[30.4, 33.2]	53.3	[51.9, 54.7]
Duplex (Ti,Al)N coating	44.0	[40.6, 47.4]	157.3	[154.5, 160.1]
Single-layered Cr-N coating	29.2	[26.1, 32.4]	55.3	[52.7, 57.8]
Duplex Cr-N coating	54.0	[50.2, 57.8]	117.2	[113.3, 121.2]

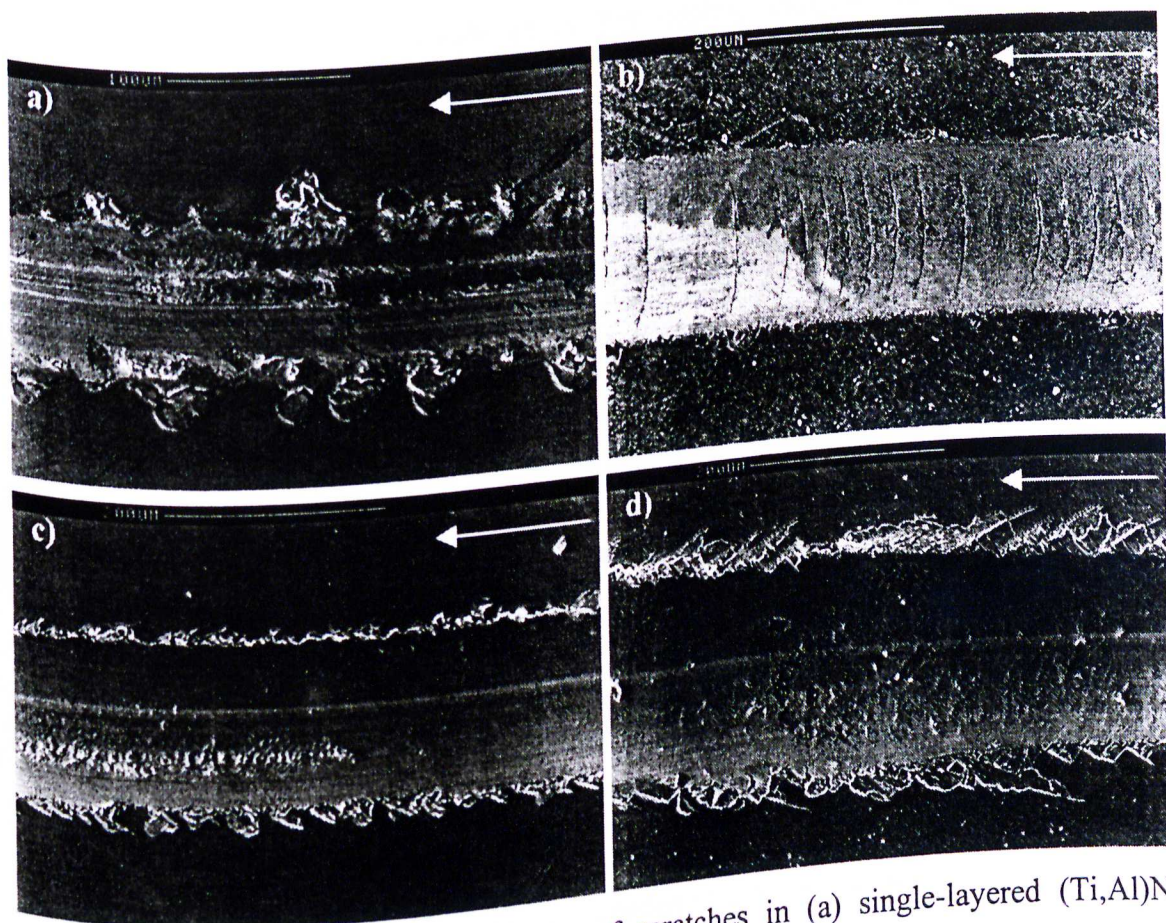


Figure 5.11 – SEM photomicrographs of scratches in (a) single-layered (Ti,Al)N, (b) duplex (Ti,Al)N coating, (c) single-layered Cr-N coating and (d) duplex Cr-N coating. The arrows indicate the scratch direction. 200X.

5.4. Conclusions

In this chapter, duplex and single-layered (Ti,Al)N and Cr-N coatings were characterised by SEM, LOM, XRD, GDOES, Knoop hardness measurements and their adhesion was evaluated by scratch testing. Based on the experimental results, the following main conclusions can be drawn:

1. After the duplex treatment, an increase in surface roughness of hard PVD coatings could be detected. The increase in surface roughness was probably due to sputtering etching by argon/nitrogen ions on substrate surface during the plasma nitriding step.
2. Duplex and single-layered (Ti,Al)N and Cr-N showed a very dense columnar morphology, with the single-layered Cr-N coating having the finest grained structure. Single-layered (Ti,Al)N and Cr-N coatings displayed a fairly smooth surface with localised protuberances. The duplex (Ti,Al)N coating also displayed protuberances on its surface, but in significantly higher quantity than the single-layered (Ti,Al)N coating. The duplex Cr-N coating exhibited shallow depressions and some Cr-poorer protuberances all over its surface. None of the coatings exhibited deep holes and/or pores.
3. Plasma nitriding treatments that were carried out in a Tecvac IP35L for 2 hours, using a 60%Ar-40%N₂ plasma, yielded nitrided cases which were compound-layer-free. This treatment provided a mono-phase ϵ compound layer when performed in a Balzers BAI 640R equipment. The mechanism of compound layer formation was attributed to different build-ups of the nitrogen concentration on the substrate surfaces. Although the current density values for all nitriding runs (in both Balzers and Tecvac systems) have not been recorded, variations in such parameter could have led to different build-ups of the nitrogen concentration and thus to different nitrided layer structures. The means of enhancing the ion current density can also influence the build-up of nitrogen concentration on the substrate surface. The Balzers system is expected to have a larger build-up of nitrogen on substrate surfaces due to a reduction of the high energy species reaching the cathode in

comparison with the Tecvac system. Hence, in the Balzers equipment, nitrogen absorption is expected to occur in a larger proportion than nitrogen implantation. Consequently a higher nitrogen content is generated at the substrate surface with subsequent formation of a thin compound layer.

4. Knoop hardness measurements indicated that the duplex (Ti,Al)N coating possessed a 55-60 μ m thick diffusion zone whereas the duplex Cr-N coating had a 35-40 μ m thick diffusion zone. This was also confirmed by LOM observations on polished cross-sections. The former coating also exhibited a relatively harder nitrided case.
5. The hardness of the investigated coatings varied between 2600 and 3600HK_{0.025} and increased in the following order: single-layered Cr-N < duplex Cr-N < single-layered (Ti,Al)N < duplex (Ti,Al)N coating.
6. XRD analyses indicated that single-layered and duplex coatings crystallised into different phases, probably due to the lower deposition temperatures that were used for producing duplex (Ti,Al)N and Cr-N coatings in comparison to those used for producing the single-layered coatings. The dominant phase in the single-layered (Ti,Al)N coating was Ti₃Al₂N₂ with a (1 0 7) preferred growth orientation whereas the duplex (Ti,Al)N coating had large amounts of TiN and Ti₂AlN with (2 0 0) and (1 0 4) preferred growth orientations, respectively. The duplex (Ti,Al)N coating also had a large amount of amorphous material in its structure in comparison with the single-layered (Ti,Al)N coating. The single-layered Cr-N coating was found to have a mixed structure of Cr₂N and CrN whilst the duplex Cr-N coating displayed a mixture of Cr and Cr₂N phases. In the single-layered Cr-N coating, the Cr₂N phase had a (1 1 1) preferred growth orientation whilst the CrN phase displayed a (2 0 0) preferred growth orientation. The (1 1 1) preferred growth orientation was observed for the Cr₂N phase in the duplex Cr-N coating.
7. GDOES analyses pointed out that the single-layered and duplex (Ti,Al)N coatings have compositions close to Ti_{0.50}Al_{0.50}N. Nevertheless, a cyclic variation on the Ti/Al ratio was observed in both (Ti,Al)N coatings and the nitrogen concentration

was found to vary somewhat within these coatings. The single-layered Cr-N coating displayed a two-layer structure, with an outer layer richer in nitrogen, probably corresponding to substoichiometric CrN and an inner layer richer in chromium, corresponding to Cr₂N. The duplex Cr-N coating also displayed variations in the nitrogen composition. This coating was comparatively poorer in nitrogen than the single-layered Cr-N coating and its composition seemed to be closer to that of the Cr₂N phase.

8. Scratch test results indicated that the duplex coatings exhibited higher critical loads than their single-layered counterparts. The highest critical loads were recorded for the duplex (Ti,Al)N coating.

CHAPTER 6: MICRO-ABRASIVE WEAR TESTING

6.1. Background

PVD hard coatings are well known for providing surfaces with enhanced tribological properties in terms of low friction and high wear resistance. However, their tribological performance is often limited by elastic and plastic deformation of the substrate, which can result in eventual coating failure⁽⁸¹⁻⁸³⁾. Duplex treatments consisting of plasma nitriding and hard PVD coating have been proven to be successful in improving wear, fatigue and corrosion resistance and the load carrying capability of steel substrates^(7,10-11,14,17-19,23,82,90,93). By increasing the hardness of substrates, the nitrided case often provides a suitable load support for PVD coatings so that superior mechanical and tribological performance can be achieved.

It has been well documented in the literature that TiN and (Ti,Al)N PVD coatings can reduce friction in tribological contacts and increase the abrasive wear resistance^(113,158). High performance in tool applications, e.g. drilling and turning, have been reported for both coatings⁽¹¹²⁾. In addition to enhanced abrasion resistance, (Ti,Al)N coatings can also provide wear and oxidation resistance, especially at high temperatures^(116,122).

Cr-N coatings have also been reported to have high hardness^(134-135,152-153), enhanced wear^(115,130,148-150) and corrosion resistance^(140,144-146), excellent diffusion barrier properties and good oxidation resistance up to 1073K^(136,141-143). The wear resistance of Cr-N coatings seems to be strongly affected by coating composition^(140,153). CrN coatings exhibit better wear resistance than Cr₂N coatings and a lower friction coefficient against steel⁽¹⁴⁰⁾. Thick Cr-N coatings have been proven to reduce the abrasive wear of tools in plastics and ceramics industries⁽¹²⁸⁾.

A new micro-abrasive wear test was proposed by Rutherford and Hutchings in the late 1990's⁽¹⁵⁹⁻¹⁶⁰⁾. The micro-abrasion test offers some advantages when compared to other tribological tests: it requires a small test area and the intrinsic wear coefficients of both substrate and coating can be evaluated simultaneously from their combined wear data.

Since there are little data available about the performance of PVD coatings in small-scale abrasion tests, the present chapter was intended to evaluate the micro-abrasive wear resistance of three duplex and single-layered coatings on hardened AISI H13 substrates: TiN, (Ti,Al)N and Cr-N. Coating and substrate wear coefficients are compared for all coatings under investigation and the effect of plasma nitriding prior to coating is also discussed.

6.2. Experimental Procedure

6.2.1. Materials

Single-layered and duplex (Ti,Al)N, TiN, Cr-N coatings (plasma nitriding + PVD coating) were deposited onto AISI H13 steel substrates. These substrates were quenched and tempered to (55 ± 2) HRC. Prior to plasma nitriding and/or coating deposition, the specimens were ground and polished to a surface finish of $R_a = (0.005 \pm 0.001) \mu\text{m}$.

6.2.2. Treatments

All PVD coatings under investigation were prepared by electron beam evaporation, as previously reported in chapters 3, 4 and 5. Single-layered and duplex TiN coatings were produced in a BALZERS BAI640R equipment whereas single-layered (Ti,Al)N, duplex (Ti,Al)N and duplex Cr-N were produced in a Tecvac IP35L equipment. A Tecvac IP70L system was used for preparing single-layered Cr-N coatings (see chapters 3 and 5 for more details about process parameters). The duplex samples were plasma nitrided and PVD-coated in a continuous process. For all coating systems under investigation, plasma nitriding was carried out in a 60%Ar + 40%N₂ plasma for 2 hours. The nitriding temperature varied somewhat depending on the specific duplex treatment. For the process conditions used, 35-40 μm and 55-60 μm thick diffusion zones were obtained, respectively, in duplex Cr-N and duplex (Ti,Al)N coatings. The duplex TiN also had a 35-40 μm diffusion zone and a 1 μm thick mono-phase ϵ (Fe₂₋₃N) compound layer.

Coating deposition temperatures were in the range 669-715K. For the duplex-treated specimens, coating deposition was initiated without carrying out any plasma etching between plasma nitriding and coating deposition. Coating temperature was held below 723K to ensure that compound layers, if formed, would not be destabilised. For the duplex (Ti,Al)N and Cr-N coatings, a cooling step in vacuum was performed between plasma nitriding and coating deposition. TiN and (Ti,Al)N coatings (both single-layered and duplex) had a 0.1-0.2 μm titanium interlayer.

6.2.3. Mechanical properties

Single-layered and duplex-treated specimens had their surface roughness (R_a value) assessed using a Veeco DEKTAK³ST profilometer. Knoop microhardness measurements were also taken on the uncoated substrate, single-layered and duplex coatings using a Mitutoyo MVK-G1 hardness tester. The load was increased from 0.23N up to 9.81N. The scratch resistance was evaluated using a commercial scratch adhesion tester (VTT Tech, Finland). Tests were carried out using a Rockwell C diamond indenter (tip radius = 200 μm) and a continuously increasing normal force (10Nmm⁻¹). Both L_{C1} and L_{C2} (loads for cohesive and adhesive failures respectively) were determined from a set of 3 scratches on each sample. L_{C2} was taken as the load at which first exposure of the substrate could be identified whilst L_{C1} was taken as the load at which failures within the coating started to occur.

6.2.4. Micro-abrasion resistance

A Plint TE66 micro-scale abrasion tester was used to evaluate the coating abrasive wear resistance. During the test, a directly driven ball is rotated against the specimen, which is mounted on a dead-weight load lever, in the presence of a slurry of SiC abrasive particles. The slurry is drip fed onto the contact between the specimen and the ball (figure 6.1) and the wear scar produced is assumed to reproduce the spherical geometry of the ball⁽¹⁵⁹⁾. By making a series of these craters and measuring the size of the scar dimensions, both coating and substrate wear coefficients (k_c and k_s) can be simultaneously determined from the test⁽¹⁵⁹⁻¹⁶⁰⁾.

For bulk materials, the equation which is assumed to describe the abrasive wear is⁽¹⁵⁹⁻¹⁶²⁾

$$SL = \frac{V}{k} \approx \frac{1}{k} \left(\frac{\pi b^4}{64R} \right) \quad \text{for } b \ll R \quad (6.1)$$

where S is the distance slid by the ball, V is the wear volume, L is the normal force on the sample, b is the diameter of the crater, R is the radius of the ball and k is the wear coefficient.

Equation (6.1) was extended to a model which combines the wear in the coating and substrate, providing both coating and substrate wear coefficients⁽¹⁵⁹⁻¹⁶⁰⁾

$$\frac{SL}{b^4} = \left(\frac{k_s - k_c}{k_s k_c} \right) \left(\frac{\pi t}{4b^2} - \frac{\pi R t^2}{b^4} \right) + \left(\frac{1}{k_s} \right) \left(\frac{\pi}{64R} \right) \quad (6.2)$$

where S is the distance slid by the ball, L is the normal force on the sample, t is the coating thickness, b is the outer diameter of the wear crater, k_c and k_s are, respectively, the coating and substrate wear coefficients and R is the radius of the ball. Both substrate and coating wear coefficients can be obtained from a linear plot of SL/b^4 versus $(\pi/4b^2 - \pi R t^2/b^4)$; the substrate wear coefficient, k_s , is obtained from the intercept of the linear plot and the coating wear coefficient, k_c , is calculated from the gradient of the plot. If m is the gradient and c is the intercept, then:

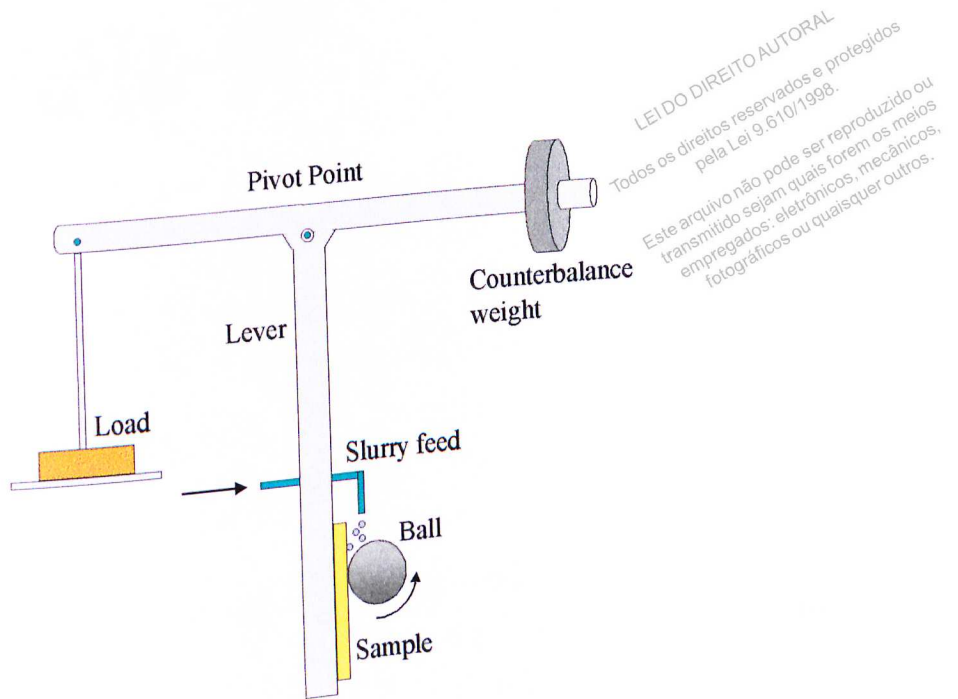
(6.3)

$$k_s = \left(\frac{\pi}{64Rc} \right)$$

and

(6.4)

$$k_c = \left(\frac{k_s}{1 + k_s m} \right)$$



LEI DO DIREITO AUTORAL
 Todos os direitos reservados e protegidos
 pela Lei 9.610/1998.
 Este arquivo não pode ser reproduzido ou
 transmitido sejam quais forem os meios
 empregados: eletrônicos, mecânicos,
 fotográficos ou quaisquer outros.

Figure 6.1 - Schematic drawing illustrating the geometry of the micro-abrasive apparatus used in the present study.

The coating thickness t can also be determined from the test by measuring the outer and inner diameters of the wear crater (figure 6.2).

The wear constants k_c and k_s are essentially a measure of the abrasive wear rate; the lower the wear constant, the better the resistance to abrasive wear. Problems may arise from this analysis when the wear coefficients of the coating and substrate are similar or when the coating wear coefficient is larger than that of the substrate. In the latter case, a linear plot of SL/b^4 versus $(\pi t/4b^2 - \pi R t^2/b^4)$ will provide a negative slope, since $k_c > k_s$. Allsopp⁽¹⁶³⁾ showed by error analysis that equation (6.2), is preferable when the ratio between the coating volume (V_c) and the total volume (V_T) is less than 0.5. If V_c/V_T is larger than 0.5, then equation (6.5) should be used:

$$\frac{SL}{b^4} = \left(\frac{1}{k_s} \right) \left(\frac{\pi}{64R} \right) - \left(\frac{k_c - k_s}{k_s k_c} \right) \left(\frac{\pi t}{4b^2} - \frac{\pi R t^2}{b^4} \right) \quad (6.5)$$

LEI DO DIREITO AUT. (6.5)
 Todos os direitos reservados e protegidos
 pela Lei 9.610/1998.
 Este arquivo não pode ser reproduzido ou
 transmitido sejam quais forem os meios
 empregados: eletrônicos, mecânicos,
 fotográficos ou quaisquer outros.

In this case:

$$k_s = \left(\frac{\pi}{64Rc} \right) \quad (6.6)$$

and

$$k_c = \left(\frac{k_s}{1 - k_s m} \right) \quad (6.7)$$

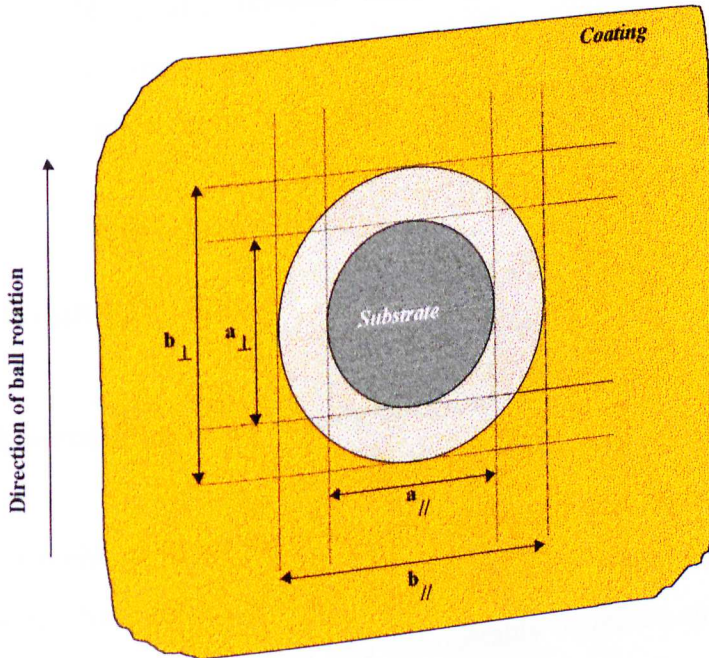


Figure 6.2 - Outer (b) and inner (a) diameters of the wear crater.

Before starting the micro-abrasion tests, the specimens were ultrasonically cleaned for 15 minutes, then rinsed in clean acetone and dried in a furnace at 110°C for 10 minutes.

A set of 6 wear craters was carried out for each sample, corresponding to 6 different numbers of ball revolutions - 100, 200, 300, 500, 700 and 1000. The sliding distance was increased from 7.85m (100 revolutions) up to 78.5m (1000 revolutions). The ball was a micro-blasted 25mm hardened steel sphere (AISI 52100, $R_a=(2.5 \pm 0.3)\mu\text{m}$) and the abrasive slurry was a suspension of SiC particles (Grade F1200-C6) in distilled water (proportion 35.44g to 100ml distilled water). The mean size of the SiC particles was 4-5 μm (mean size provided by the manufacturer, Washington and Mills Abrasives, Manchester, UK). The ball rotational speed and the applied normal load were set at 80rpm and 0.25N, respectively, in all tests.

After measuring the inner and outer diameters of the wear craters, regression analyses, according to eqs. (6.1), (6.2) and (6.5), were carried out in order to determine both k_s and k_c for each sample. The MINITAB for Windows software, release 10.2, was used to perform the regression analyses. The model adequacy was evaluated by the R^2 coefficient value, the percentage of explained variance, a test of p-value for each estimated parameter, and residual analysis⁽¹⁶⁴⁾. The coating thickness was also calculated from the micro abrasion test and the worn specimens were examined in the scanning electron microscope to investigate the wear mechanisms.

6.3. Results and Discussion

6.3.1. Surface roughness and coating thickness

The surface roughness of single-layered and duplex coatings is shown in table VI.1. The duplex coatings have higher surface roughness than the single-layered ones, indicating that the duplex treatment resulted in a considerably increased surface roughness. This increase in the R_a value can be attributed to sputter etching by argon/nitrogen ions on the substrate surface during plasma nitriding. The mean coating thickness coating thickness (table VI.2) was calculated from 6 wear crater measurements for all single-layered and duplex coatings. The coating thicknesses are comparable, with the duplex Cr-N and single-layered TiN coatings being the thinnest ones.

Table VI.1 - Surface roughness of single-layered and duplex TiN, (Ti,Al)N and Cr-N coatings

Specimen	R_a (μm)
Single-layered (Ti,Al)N coating	(0.018 \pm 0.005)
Duplex (Ti,Al)N coating	(0.043 \pm 0.005)
Single-layered TiN coating	(0.020 \pm 0.005)
Duplex TiN coating	(0.049 \pm 0.002)
Single-layered Cr-N coating	(0.016 \pm 0.004)
Duplex Cr-N coating	(0.039 \pm 0.006)

LEI DO DIREITO AUTORAL
 Todos os direitos reservados e protegidos
 pela Lei 9.610/1998.
 Este arquivo não pode ser reproduzido ou
 transmitido sejam quais forem os meios
 empregados: eletrônicos, mecânicos,
 fotográficos ou quaisquer outros.

Table VI.2 - Thickness of single-layered and duplex TiN, (Ti,Al)N and Cr-N coatings

Specimen	Coating thickness, t (μm)	C.I. (95%) (μm)
Single-layered (Ti,Al)N coating	2.4	[2.2, 2.6]
Duplex (Ti,Al)N coating	2.5	[2.3, 2.7]
Single-layered TiN coating	2.2	[2.0, 2.4]
Duplex TiN coating	2.3	[2.2, 2.4]
Single-layered Cr-N coating	2.5	[2.2, 2.8]
Duplex Cr-N coating	2.2	[2.0, 2.4]

6.3.2. Coating microhardness

The HK microhardness of the uncoated substrate, single-layered and duplex coatings is shown in figure 6.3. The plasma nitrided layer improves the mechanical support for the single-layered coatings so that higher hardness values for the duplex-treated coating/substrate systems are measured at higher loads. Both duplex and single-layered (Ti,Al)N have the highest hardness values, followed by duplex TiN, single-layered TiN,

duplex Cr-N and single-layered Cr-N. However, when the load is increased, higher hardness values are recorded for duplex (Ti,Al)N, TiN and Cr-N coatings.

LEI DO DIREITO AUTORAL
 Todos os direitos reservados e protegidos
 pela Lei 9.610/1998.
 Este arquivo não pode ser reproduzido ou
 transmitido sejam quais forem os meios
 empregados: eletrônicos, mecânicos,
 fotográficos ou quaisquer outros.

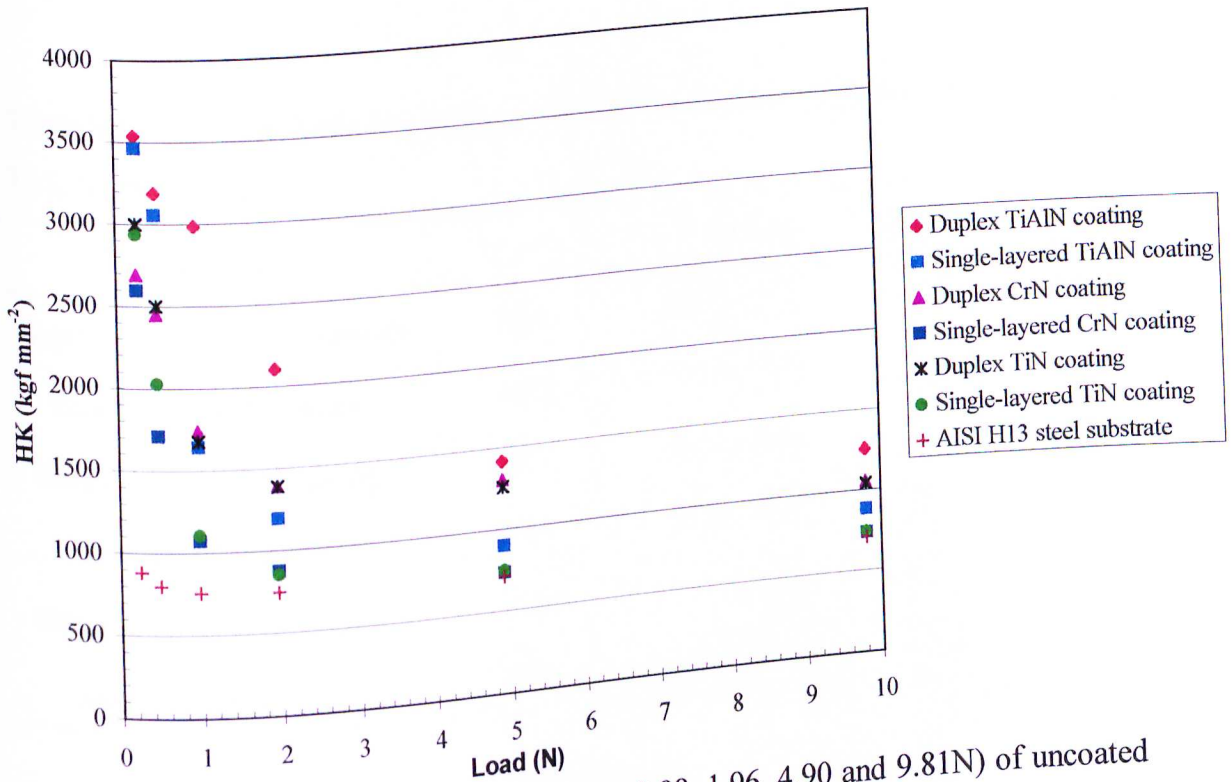


Figure 6.3 - Knoop microhardness (0.25, 0.49, 0.98, 1.96, 4.90 and 9.81N) of uncoated AISI H13 steel, duplex and single-layered (Ti,Al)N, TiN, Cr-N coatings. Although the error bars are not shown in the plot, the standard deviation was not larger than 5%.

6.3.3. Coating adhesion

The critical loads L_{C1} and L_{C2} are illustrated in table VI.3. Both L_{C1} and L_{C2} were lowest for the single-layered TiN and highest for the duplex (Ti,Al)N. All the duplex-treated specimens show higher cohesive and adhesive critical loads than the single-layered coatings. The improvement in L_{C2} (adhesive failure) is quite significant.

Moreover, the duplex-treated samples (apart from the duplex Cr-N) showed different failure mechanisms in comparison to the single-layered ones. Duplex (Ti,Al)N and TiN exhibited semicircular cracks (tensile cracks) along the scratch without any flaking whilst the scratches in single-layered (Ti,Al)N, TiN, Cr-N and duplex Cr-N coatings were characterised by flaking of the coating inside and along the edge of the scar.

Table VI.3 - Critical loads L_{C1} and L_{C2} recorded for duplex and single-layered (Ti,Al)N, TiN, Cr-N coatings

Specimen	L_{C1} (N)	C.I. (95%) (N)	L_{C2} (N)	C.I. (95%) (N)
Single-layered (Ti,Al)N coating	31.8	[30.4, 33.2]	53.3	[51.9, 54.7]
Duplex (Ti,Al)N coating	44.0	[40.6, 47.4]	157.3	[154.5, 160.1]
Single-layered TiN coating	25.7	[22.5, 29.0]	52.3	[49.4, 55.2]
Duplex TiN coating	37.5	[34.6, 40.4]	152.1	[146.3, 157.9]
Single-layered Cr-N coating	29.2	[26.1, 32.4]	55.3	[52.7, 57.8]
Duplex Cr-N coating	54.0	[50.2, 57.8]	117.2	[113.3, 121.2]

6.3.4. Micro-abrasive wear tests

The k_c and k_s wear coefficients are shown in table VI.4. These coefficients were obtained from the fitted lines in figures 6.4 to 6.10. The normal probability plots of residuals and the residuals versus predicted values plots, which were obtained for the regression in all samples, indicated that the residuals had a normal distribution and their variance was constant. The regression also indicated high values of R^2 and adequacy of fit in all composite systems, confirming that the proposed models, eqs.(6.1), (6.2) and (6.5), were successful in describing the experimental data.

Table VI.4 – Coating and substrate wear coefficients (k_c and k_s)

Specimen	Model	k_c ($\times 10^{-13} \text{ m}^3 \text{ N}^{-1} \text{ m}^{-1}$)	C.I. (95%) ($\times 10^{-13} \text{ m}^3 \text{ N}^{-1} \text{ m}^{-1}$)	k_s ($\times 10^{-13} \text{ m}^3 \text{ N}^{-1} \text{ m}^{-1}$)	C.I. (95%) ($\times 10^{-13} \text{ m}^3 \text{ N}^{-1} \text{ m}^{-1}$)
Single-layered (Ti,Al)N	Eq.(6.2)	2.36	[2.20, 2.55]	9.62	[8.22, 11.61]
Duplex (Ti,Al)N	Eq.(6.2)	1.44	[1.34, 1.54]	8.84	[8.63, 9.07]
Single-layered TiN	Eq.(6.2)	7.27	[7.15, 7.39]	9.65	[9.54, 9.76]
Duplex TiN	Eq.(6.2)	3.86	[3.81, 3.90]	8.75	[8.46, 9.05]
Single-layered Cr-N	Eq.(6.5)	27.79	[22.13, 38.09]	9.84	[9.58, 10.12]
Duplex Cr-N	Eq.(6.5)	18.11	[16.63, 19.86]	9.53	[9.39, 9.68]
Uncoated substrate	Eq.(6.1)			9.40	[9.00, 9.82]

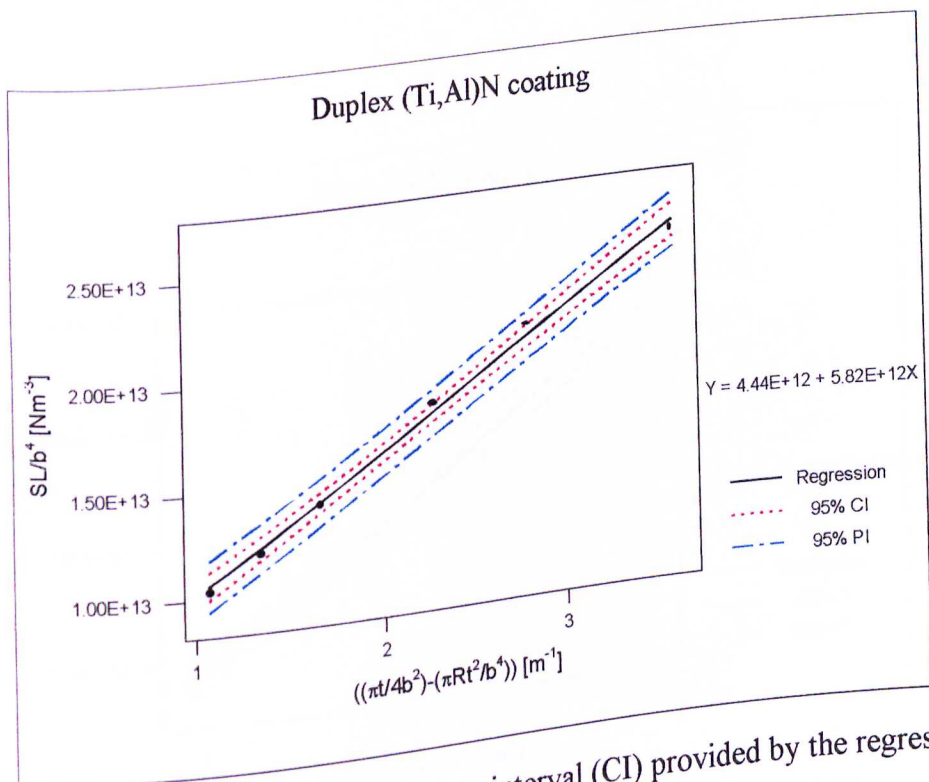


Figure 6.4 - Fitted line and its 95% confidence interval (CI) provided by the regression analysis. Duplex (Ti,Al)N coating.

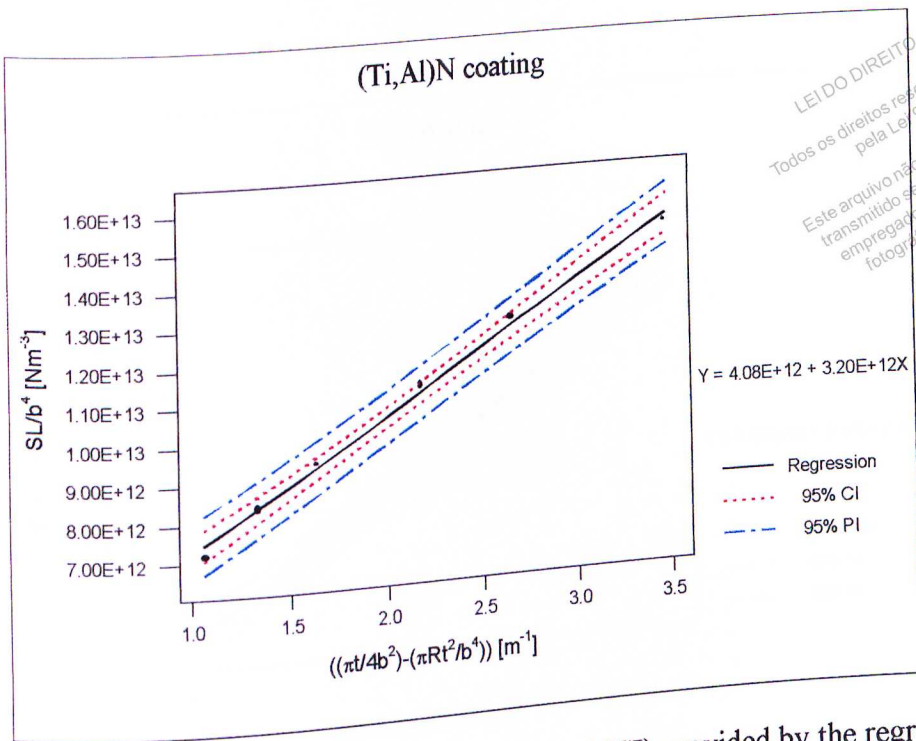


Figure 6.5 - Fitted line and its 95% confidence interval (CI) provided by the regression analysis. Single-layered (Ti,Al)N coating.

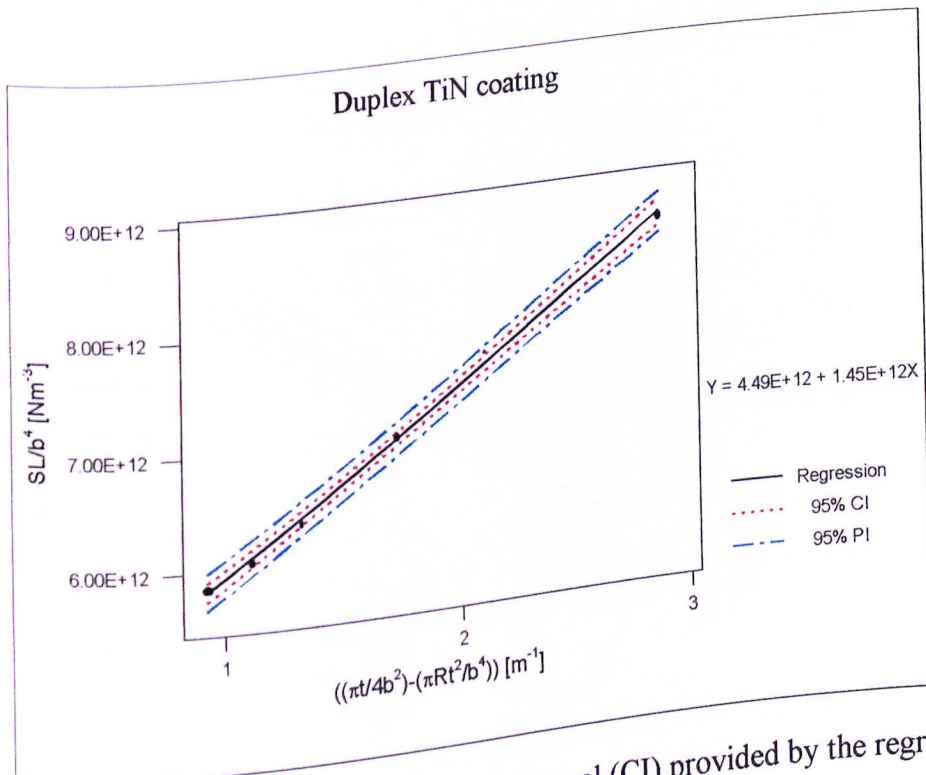
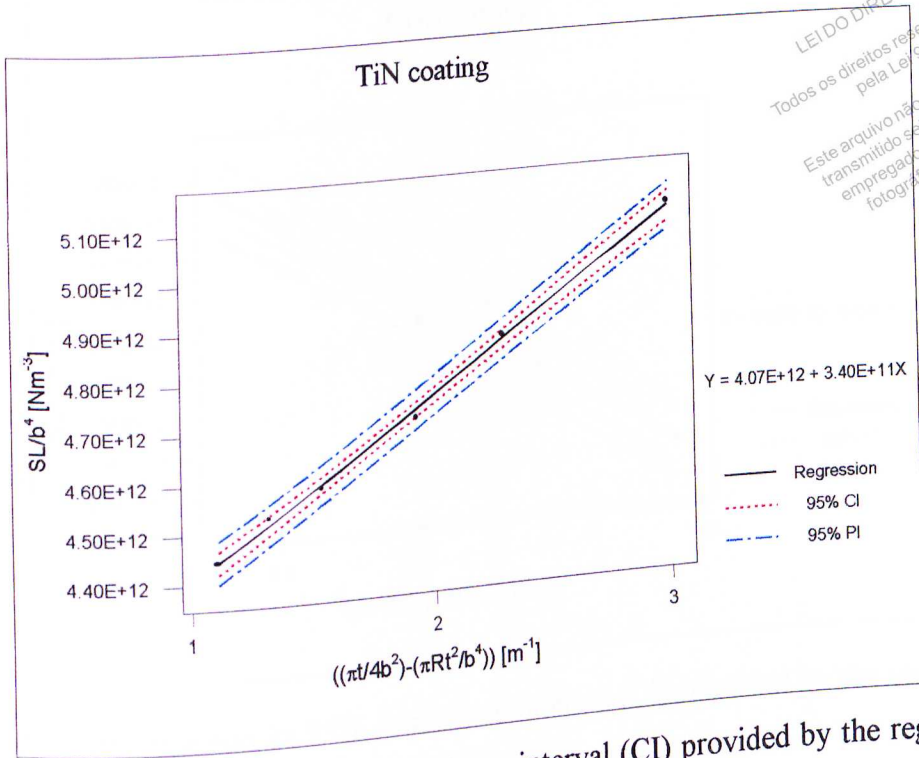


Figure 6.6 - Fitted line and its 95% confidence interval (CI) provided by the regression analysis. Duplex TiN coating.



LEI DO DIREITO AUTORAL
 Todos os direitos reservados e protegidos pela Lei nº 9.610/1998.
 Este arquivo não pode ser reproduzido ou transmitido sem quais forem os meios empregados: eletrônicos, mecânicos, fotográficos ou quaisquer outros.

Figure 6.7 - Fitted line and its 95% confidence interval (CI) provided by the regression analysis. Single-layered TiN coating.

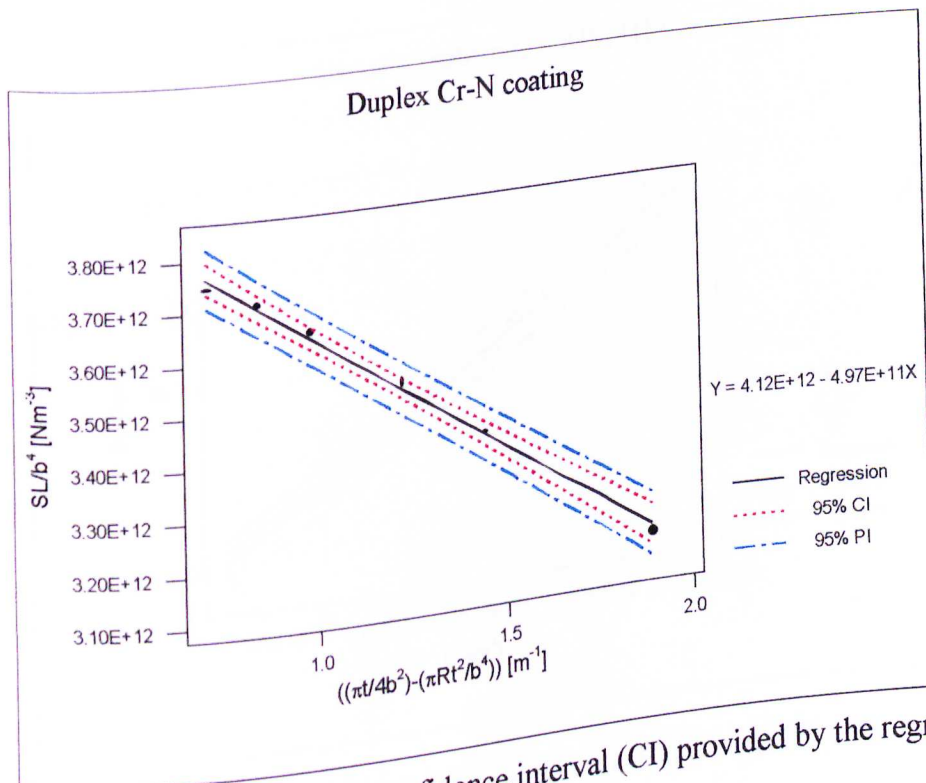


Figure 6.8 - Fitted line and its 95% confidence interval (CI) provided by the regression analysis. Duplex Cr-N coating.

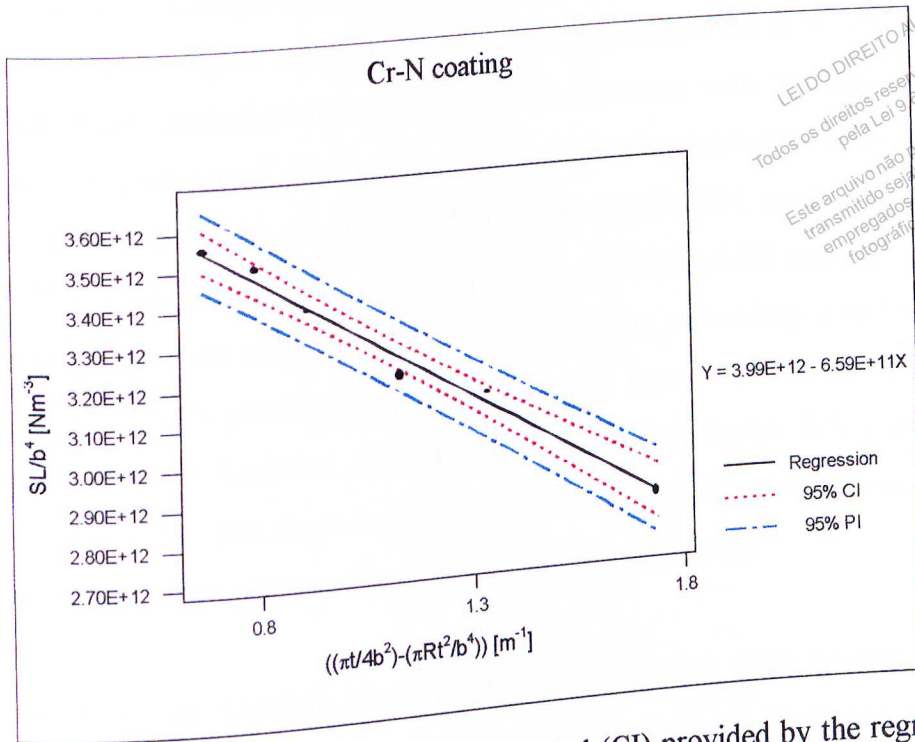


Figure 6.9 - Fitted line and its 95% confidence interval (CI) provided by the regression analysis. Single-layered Cr-N coating.

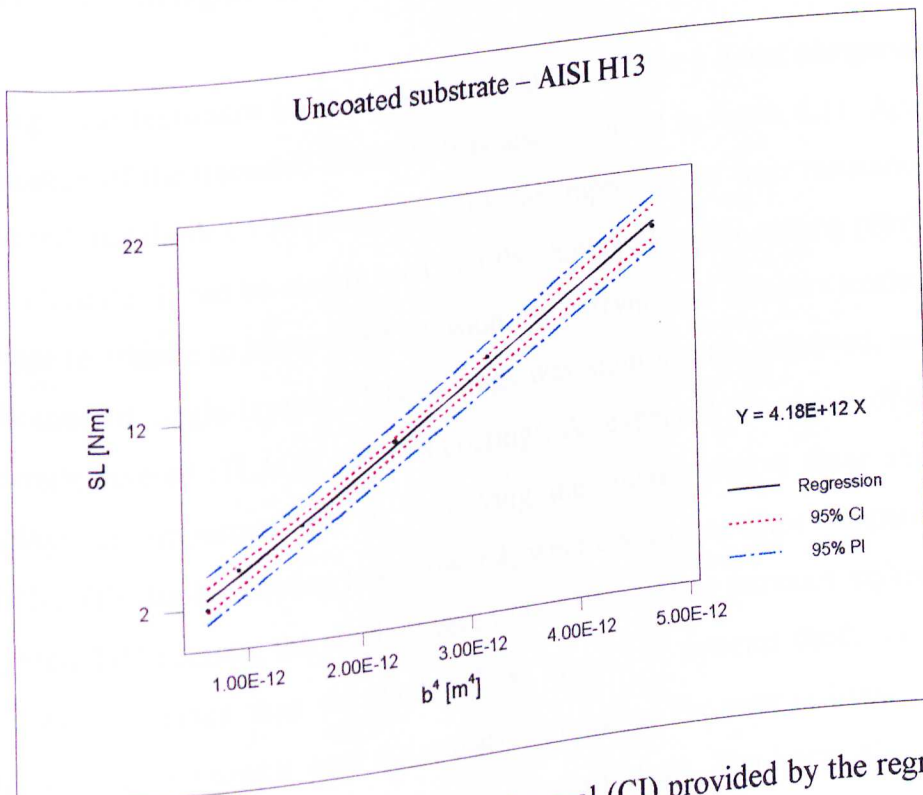


Figure 6.10 - Fitted line and its 95% confidence interval (CI) provided by the regression analysis. Uncoated substrate (AISI H13).

Despite of duplex and single-layered Cr-N coatings, all the other coating systems under investigation showed higher micro-abrasive wear resistance than the uncoated substrate. The coating wear coefficients (k_c) were found to decrease with increasing coating hardness for the same sort of abrasive. The duplex (Ti,Al)N exhibited the lowest k_c wear coefficient, followed by the single-layered (Ti,Al)N, duplex TiN, single-layered TiN, duplex Cr-N and single-layered Cr-N. By applying a duplex (Ti,Al)N coating onto AISI H13 steel substrates, the resistance to micro-abrasion was reduced by a factor 6. The single-layered (Ti,Al)N provided an improvement of a factor 4 in the micro-abrasive wear resistance of the hardened AISI H13 steel whilst the duplex TiN reduced the former by a factor 2.5. The single-layered TiN provided the lowest improvement in the k_c wear coefficient when compared to the uncoated substrate (23%).

The duplex treatment certainly improves the micro-abrasive wear resistance when compared to its single-layered counterpart. Such improvement can be mainly attributed to the load support provided by the nitrided layer. The k_c wear coefficient of single-layered (Ti,Al)N can be reduced by 38% when compared to the duplex (Ti,Al)N. The improvement is even higher for the TiN system (47%).

The coating wear resistance (k_c^{-1}) is shown in figure 6.11 for a direct comparison. The wear resistance of the uncoated substrate was also included in figure 6.11. Apart from single-layered and duplex Cr-N coatings, all films improved the wear resistance of the uncoated substrate. It can be clearly seen that the duplex (Ti,Al)N coating provided the highest wear resistance to micro-scale abrasion. By carrying out a duplex treatment, the wear resistance of single-layered PVD coatings was significantly improved, especially for both single-layered (Ti,Al)N and TiN coatings. As expected, the choice of the PVD coating plays an important role in improving the micro-abrasive wear resistance. Although the TiN duplex coating has a lower k_c wear coefficient when compared to the single-layered TiN coating, the single-layered (Ti,Al)N coating provides higher micro-abrasive wear resistance than the duplex TiN. The Cr-N systems (both duplex and single-layered) had the lowest wear resistances to abrasion. The wear resistance of these coatings was even lower than that of the uncoated substrate. The linear plot of SL/b^4 versus $(\pi/4b^2 - \pi Rl^2/b^4)$ had a negative slope for these coatings (figures 6.8 and 6.9),

confirming that both duplex and single-layered Cr-N coatings wore out at a higher rate than their substrates. Nevertheless, the duplex treatment still provided an improvement of 35% when compared to the single-layered Cr-N coating.

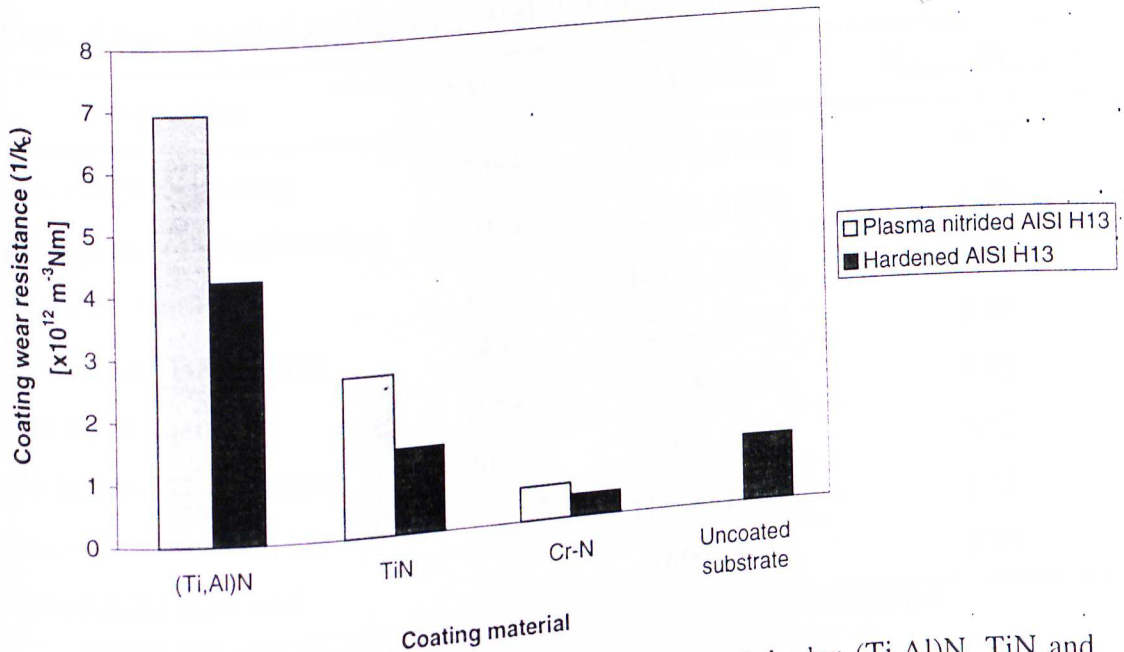


Figure 6.11 – Coating wear resistance of single-layered and duplex (Ti,Al)N, TiN and Cr-N coatings.

The Cr-N coatings are relatively softer than (Ti,Al)N and TiN coatings. In the micro-abrasive wear tests SiC particles, with a mean size of 4-5 μ m, were used as abrasives. Their size is larger than the thickness of all tested coatings. The indentation depths of abrasive particles on surfaces depend on the applied load, surface hardness and abrasive hardness⁽¹⁶⁵⁾. The measured Vickers hardness for the coatings is given in table VI.5. The SiC hardness is expected to be 2100-2600HV⁽¹⁶⁶⁾. Therefore, it can be seen that (Ti,Al)N coatings are harder than the SiC particles whereas the Cr-N coatings are softer. The TiN coatings have a comparable hardness value to that of the SiC abrasive particles. A well known parameter in abrasive wear testing is the ratio between the hardness of the abrasive particles (H_a) and the hardness of the surface (H_s). "Hard" abrasion typically occurs when the ratio H_a/H_s is higher than 1.2. In this situation, the

abrasion will lead to much greater wear rates⁽¹⁶⁶⁾. This ratio is shown in table VI.5 for all tested coatings.

Table VI.5 – Vickers hardness of single-layered and duplex (Ti,Al)N, TiN, Cr-N coatings, plasma nitrided and hardened AISI H13 steels.

Specimen	HV _{0.025}	C.I. (95%)	H _{abrasive} /H _{surface} *
Duplex (Ti,Al)N coating	3069	[2971, 3166]	0.78
Single-layered (Ti,Al)N coating	3023	[2925, 3121]	0.79
Duplex TiN coating	2509	[2422, 2595]	0.96
Single-layered TiN coating	2498	[2452, 2544]	0.96
Duplex Cr-N coating	2084	[1958, 2210]	1.15
Single-layered Cr-N coating	2053	[1907, 2199]	1.17
Plasma nitrided AISI H13 steel	1387	[1348, 1426]	1.73
Hardened AISI H13 steel	719	[699, 739]	3.34

* H_{abrasive} was taken as 2400HV, which is an average value of the hardness range presented in the text.

A dependence between the k_c values and the ratio H_a/H_s can be observed for all coated systems; the lower the ratio H_a/H_s , the higher is the micro-abrasive wear resistance (k_c^{-1} , see figure 6.11). However, such dependence was not observed for the Cr-N systems (duplex and single-layered) and uncoated substrate, since the latter had a higher H_a/H_s ratio than the former and displayed better micro-abrasive wear resistance. Although the hardness of the Cr-N were higher than that of the uncoated substrate, its relatively lower hardness (in comparison to that of the other coatings and to the SiC particles) in combination with a 2.0-2.5 μ m film thickness, could not provide an adequate improvement in terms of abrasive wear.

If the SiC particles deeply penetrated through the Cr-N coating because of its relatively low hardness, then the Cr-N coatings may have become partly delaminated or removed through a severe ploughing/cutting mechanism during the first stages of the test. This would explain the high wear rates recorded for these coatings. Tools for plastic

extrusion that were coated with (Ti,Al)N did not perform well due to the presence in the plastic of hard abrasives, larger than the coating thickness, ploughing through the relatively thin (Ti,Al)N coating to which the stainless steel substrate did not give sufficient support⁽¹¹⁵⁾. The Cr-N coatings probably behaved in a similar way and this might explain why these coatings had higher wear rates than the uncoated substrate, leading to a non-favourable abrasion resistance in these samples. Rutherford *et al.*⁽¹⁶⁷⁾ also recorded higher wear rates for Cr-N coatings than those of the uncoated substrate (AISI M2 steel) in similar micro-abrasion tests.

Although substrate deformation plays an important role in preventing abrasive wear, it seems that the wear mechanism in Cr-N coatings was probably more influenced by abrasive penetration rather than by substrate deformation. The load support provided by the nitrided case could not inhibit the occurrence of a severe ploughing/cutting through the coating and its subsequent delamination, since the duplex-coated sample also had a higher wear rate than that of the uncoated substrate. Nevertheless, it should be pointed out that the nitrided case provided an improvement in the micro-abrasive wear resistance of single-layered Cr-N coatings (see table VI.4 and figure 6.11). Perhaps the deposition of thicker Cr-N coatings (5-10 μ m) could yield an improvement in the abrasive wear resistance of these films. At such coating thickness, the SiC particles would not be able to penetrate a great extent into the Cr-N film and coating delamination would probably be inhibited. Thick Cr-N coatings have been reported to increase the abrasive wear resistance of tools used in plastic processing⁽¹²⁸⁾. Also, the surface hardness of intrinsically softer coatings can be improved by increasing their thickness⁽¹⁵⁰⁾. A 10 μ m thick CrN coating displayed a 3000 Vickers hardness value, close to that of a 7 μ m TiCN coating⁽¹⁵⁰⁾. It is rather interesting to note that the k_s values recorded for the duplex and single-layered Cr-N coated specimens were quite close to that of the uncoated substrate. This also supports the idea of the Cr-N coating being removed at a higher wear rate than the substrate, which led to the higher k_c values recorded for these samples. As a final remark, it should be noticed that the poorer wear resistance observed in Cr-N coatings do not seem to be related to an unsatisfactory adhesion. The critical loads measured for the single-layered Cr-N coatings were quite similar to those of the single-layered TiN coating (table VI.3).

It is sometimes reported in the literature that a reduction in abrasive wear resistance occurs with increasing surface roughness. This effect was not observed in this work since duplex (Ti,Al)N, TiN and Cr-N coatings exhibited higher resistance to micro-abrasion than their single-layered counterpart. This is probably due to an increased resistance to abrasive wear offered by the nitrided layer, more important than the supposed negative effect of the increased surface roughness. The nitrided layer improves the load support for the hard PVD coatings, preventing elastic and plastic deformation of the substrate.

The micro-abrasive wear test also discriminated between the different coatings whilst giving similar k_s wear coefficients for hardened steel substrates. The measured wear coefficient of the uncoated substrate was the same when tested in both coated (with single-layered coatings) and uncoated condition (see confidence intervals in table VI.4). The plasma nitrided substrates also showed comparable k_s wear coefficients to those recorded for the uncoated substrate and single-layer-coated samples. Although plasma nitrided substrates displayed slightly lower k_s wear coefficients, there was no statistical difference between the k_s values recorded for plasma-nitrided and hardened AISI H13 steel substrates. It seems that the improvements of the duplex treatment can be mainly identified in the k_c values rather than in the k_s ones. One of the claimed features of the micro-scale abrasion test is its ability to measure the wear resistance of the coating independently of the substrate properties⁽¹⁵⁹⁻¹⁶⁰⁾. In these experiments, all duplex coatings displayed different k_c values than those obtained for their single-layered counterparts. Considering the above feature of the micro-abrasive wear test, similar k_c values should have been recorded for duplex and single-layered coatings having the same top coating (e.g. (Ti,Al)N, TiN, Cr-N). However, if the nitrided layer were considered as part of the coating, then such differences in the k_c values would be expected to occur, especially bearing in mind that the recorded k_s values for both plasma nitrided and hardened AISI H13 were quite close. Indeed, the micro-scale abrasive wear test utilises sufficiently low loads and, therefore, the load support promoted by the nitrided substrate should not account for the different results recorded for k_c . Conversely, if the nitrided layer were regarded as part of the substrate, then the results obtained for k_c would reveal its dependence on substrate properties. This dependence

would be a different result from those which have been reported in the literature so far^(159,167).

A transition from grooving to rolling wear has been reported to occur in tool steels during the micro-abrasive wear test, depending on the load per particle, slurry concentration and type of abrasive used⁽¹⁶⁵⁾. Different transition points are expected for different abrasive particle sizes and shapes. The hardness of the surfaces being worn is also believed to influence the transition from grooving to rolling wear. However, the effects of particle size and surface hardness have not yet been fully investigated. A two-body grooving wear mechanism was found to be dominant at high loads and/or low slurry concentrations whilst the dominant mechanism at low loads and/or high slurry concentrations was a three-body rolling wear. Grooving occurs in the micro-abrasive wear test when a significant proportion of the particles embed in the surface of the ball bearing and act as fixed indenters, producing a series of fine parallel grooves in the sample surface. In the rolling wear process the abrasive particles do not embed but roll between the two surfaces producing a heavily deformed, multiply indented wear surface with no evident surface directionality.

SEM micrographs of the worn craters (substrate region only) corresponding to 1000 ball revolutions are shown in figure 6.12. The surface morphology indicated a wear mechanism involving plastic deformation, with only the scale of deformation being influenced by the hardness of the surface being worn. Ploughing and cutting on a scale comparable to the abrasive particle size could be identified. Although the wear pattern observed in the coating region of the wear crater is not shown here, the wear pattern in such region was exactly the same of that seen in the substrate region. Since similar wear patterns were observed for the coating and substrate regions, the remarks which will be made about the wear mechanisms hold equally to both regions of the wear crater.

A wear pattern consisting of parallel straight lines, i.e., grooves, is clearly seen in the uncoated substrate (figure 6.12 (a)). The same wear pattern is still observed in the substrates of the single-layered Cr-N (figure 6.12 (b)), duplex Cr-N coating (figure 6.12 (c)) and single-layered TiN coating (figure 6.12 (d)) but the separation between adjacent

grooves is smaller than that observed in the uncoated substrate. The grooving pattern observed suggests that the SiC abrasive particles probably got embedded in the surface of the ball, acting as fixed indenters and scratching the specimen surfaces. However, the wear pattern consisting of parallel grooves is less defined in the substrates shown in figures 6.12 (e), 6.12 (f) and 6.12 (g). From the wear patterns observed, it seems that the ability of the SiC abrasive particles to "scratch" the composite surface decreases in the order: single-layered Cr-N \cong single-layered TiN \cong duplex Cr-N > duplex TiN > single-layered (Ti,Al)N > duplex (Ti,Al)N. In the duplex (Ti,Al)N coating, grooves (resulting from scratching by the SiC particles) cannot be seen at all. The observation that a certain minimum ratio of hardness is needed for one material to be able to scratch another provided the physical basis for the scale of hardness devised by Mohs in 1824. This effect seems to have occurred during the micro-abrasive wear tests. The substrate of the hardest coating - the duplex (Ti,Al)N coating - does not show any scratches on its surface at all. In the substrate of the single-layered (Ti,Al)N coating, some very shallow grooves can be distinguished, probably owing to the absence of the hard nitrated case that is present in the duplex (Ti,Al)N coating. Single-layered and duplex (Ti,Al)N composites are harder than the SiC abrasive particles. The wear pattern observed in these samples suggests the occurrence of a mechanism basically involving rolling wear.

The substrate of the duplex TiN coating has comparatively more and slightly deeper grooves than the substrates of both duplex and single-layered (Ti,Al)N coatings (figure 6.12 (e)). In this sample, the wear pattern suggests the occurrence of a mixed mechanism involving grooving and rolling wear. The presence of a hard nitrated case, however, diminishes the scratching action of the SiC abrasive particles in comparison to the single-layered TiN system. The Cr-N coatings, being softer than the SiC particles, are not able to offer a significant resistance to the scratching action of the abrasive particles. As previously discussed, the SiC particles seemed to penetrate deeply in these coatings; as a result, larger amounts of coating material became removed through a scratching mechanism with subsequent coating delamination. The nitrated case of the duplex Cr-N coating probably minimised the scratching action of the abrasive coatings so that its wear rate was slightly lower than that obtained for a single-layered Cr-N coating.

The wear patterns seem to corroborate the results obtained from the linear regression analyses. After a certain number of ball revolutions, the coating material gets worn through, exposing the substrate material. After this point, the micro-abrasive wear resistance can be further increased by increasing the subsurface hardness. Although increased hardness does not necessarily result in better abrasive wear resistance (i.e. abrasive wear by brittle fracture), the present results indicate a strong influence of surface (and subsurface) hardness on the micro-scale abrasive wear performance, which suggests a mechanism of abrasive wear by plastic deformation⁽¹⁶⁶⁾.

The presence of a hard nitrided layer diminishes the scratching action of the SiC abrasive particles, since the H_a/H_s ratio is lower for a nitrided steel in comparison with a hardened one. Therefore, for a given sort of abrasive particles, the micro-abrasive wear resistance can be improved by increasing the surface hardness (i.e., by depositing a harder coating) and also by increasing the subsurface hardness (i.e., through a plasma nitriding treatment).

Another particularly useful parameter is the H/E ratio, which has been proposed as a ranking parameter to improve the wear resistance of materials⁽¹⁶⁸⁾. This ratio, which basically describes the elastic strain to failure of materials, has found great applicability in coated systems⁽¹⁶⁸⁾. Since similar elastic modulus values have been recorded for nitrided and bulk ferrous alloys⁽¹⁶⁹⁾, it is quite reasonable to assume that the elastic modulus of a plasma nitrided AISI H13 substrate is similar to that of a hardened AISI H13 substrate. Nevertheless, the former is harder than the latter (see table VI.5). Therefore, a plasma nitrided AISI H13 substrate has a longer strain to failure ratio (translated by a higher H/E ratio) in comparison to a hardened AISI H13 steel substrate. This might account for a decreased risk of plastic deformation in the nitrided layer so that any asperities on the nitrided substrate would be less likely to detach, reducing the probability of coating failure. Thus, duplex PVD coatings would be expected to have a superior wear behaviour than their single-layered counterparts due to a longer elastic strain to failure of the nitrided layer.

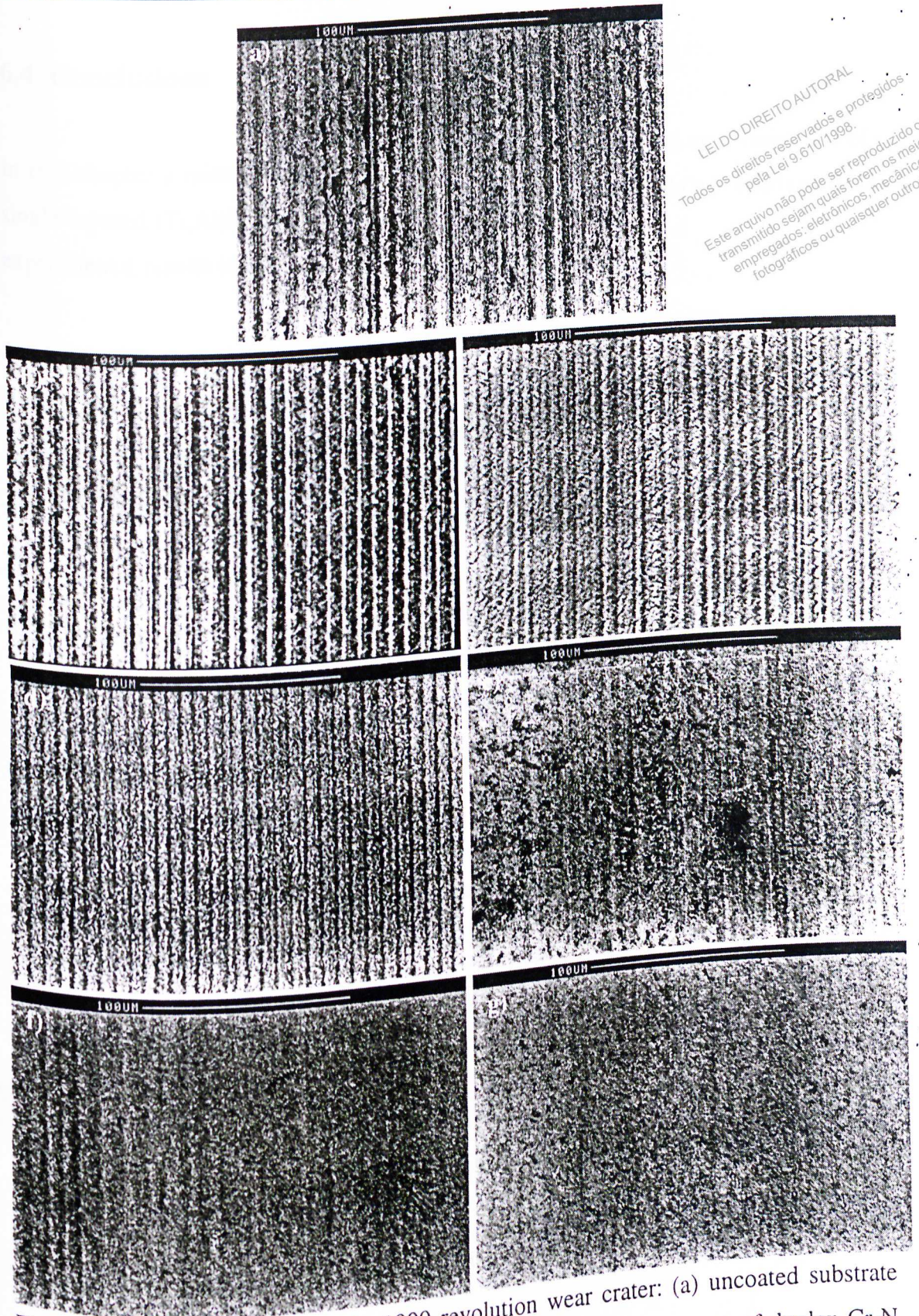


Figure 6.12 - Micrographs of the 1000 revolution wear crater: (a) uncoated substrate (AISI H13), (b) substrate of single-layered Cr-N coating, (c) substrate of duplex Cr-N coating, (d) substrate of single-layered TiN coating, (e) substrate of duplex TiN coating, (f) substrate of single-layered (Ti,Al)N coating and (g) substrate of duplex (Ti,Al)N coating. SEM. 500X.

6.4. Conclusions

In this chapter a micro-abrasive wear test was used to evaluate the wear resistance of single-layered (Ti,Al)N and Cr-N coatings and duplex (Ti,Al)N and Cr-N coatings. The experimental results indicated that:

1. All duplex coatings showed higher micro-abrasive wear resistance than their single-layered counterparts. The nitrided layer increased the load support beneath the surface, increasing the composite hardness and, consequently, the resistance to micro-abrasion. The best improvement was achieved by the duplex (Ti,Al)N coating.
2. Although the duplex treatment certainly improves the micro-abrasive wear resistance of its single-layered counterpart, single-layered (Ti,Al)N coatings exhibited a lower k_c wear coefficient than both duplex TiN and Cr-N, showing that the choice of the PVD coating plays an important role in reducing the micro-abrasive wear resistance.
3. The micro-abrasive wear test discriminated between the different coatings whilst giving similar wear coefficients k_s for hardened steel substrates. Furthermore, the same k_s values were measured for substrates in both coated (with single-layered coatings) and uncoated condition.
4. The measured k_s wear coefficients of hardened AISI H13 substrates were statistically similar to those determined for plasma nitrided AISI H13 steels. The improvements of the duplex treatment could mainly be identified in the k_c values rather than in the k_s ones, which might suggest a dependence of k_c on substrate properties.
5. The uncoated substrate and the substrates of single-layered Cr-N, duplex Cr-N and single-layered TiN coatings exhibited different wear patterns than those obtained for the substrates of duplex TiN coatings, single-layered (Ti,Al)N and duplex (Ti,Al)N.

The wear pattern was found to change from surfaces characterised by grooves to surfaces which exhibited multiply indented surfaces, indicating a transition between wear mechanisms. This transition was found to be dependent on the ratio between the hardness of the SiC abrasive particles and surface (coating) or subsurface hardness. By decreasing this ratio, the ability of the SiC abrasive particles to scratch the composite surface was reduced. After a certain number of ball revolutions, the coating material gets worn through, exposing the substrate material. After this point, the presence of a hard nitrided case diminished the scratching action of the SiC abrasive particles. A good correlation between the examination of the wear patterns and the results obtained from the determination of the k_c wear coefficients could be established, with the duplex (Ti,Al)N coating having the lowest wear rate, followed by a single-layered (Ti,Al)N coating. Nevertheless, further investigations are necessary in order to clarify the effect of both coating and subsurface hardness on the micro-scale abrasive wear test.

6. Single-layered and duplex Cr-N coatings were not effective in reducing the micro-abrasive wear resistance of the substrate, since their wear coefficients k_c were higher than the substrate wear coefficients (k_s). The hardness of the Cr-N coatings was found to be much lower than the hardness of the SiC abrasive particles. As a consequence, these coatings seem to have partly delaminated during the test due to the presence of harder SiC abrasives, larger than the coating thickness, which caused tearing of the coating with subsequent delamination. The deposition of thicker Cr-N coatings (5-10 μ m) may be expected to yield an improvement in the abrasive wear resistance, since the SiC particles would not be able to penetrate a great extent into the Cr-N film and coating delamination would be inhibited.

CHAPTER 7: IMPACT TESTING

7.1. Background

The impact test has been proposed by Knotek *et al.* in the early 1990's⁽¹⁷⁰⁾. The test represents a novel approach in evaluating the local fatigue strength of coating/substrate composites. During the impact test the specimen is cyclically loaded by a hard ball that repetitively impacts on the specimen surface. Hence, the impact test allows the investigation of coating properties under dynamic loading, simulating a wide range of tribological systems. The loading geometry is a ball-plane system and the stress distribution that arises from this contact is typically Hertzian⁽¹⁷⁰⁻¹⁷³⁾. Basically, a hydrostatic stress state is created beneath the centre of the indented surface. Immediately adjacent to the contact area there is a zone of high tensile stress in the vicinity of the surface^(170,171). In hard brittle materials, this zone is particularly susceptible to cracking⁽¹⁷⁰⁾. The maximum shear stress has been reported to occur at a depth of $0.47D$, where D is the contact diameter of the elastic flattening zone at the moment of impact^(170,171). Therefore, for PVD thin coatings, this area is within the substrate. It is important to note that the hydrostatic stress state exists in homogeneous materials; for thin hard coatings on an elastic substrate, with both materials having different elastic and plastic constants, the stress distribution differs from hydrostatic⁽¹⁷¹⁻¹⁷³⁾. High shear stresses under the indentation are expected to occur at the interface coating/substrate^(171,172).

During the impact test, a hard ball (the impact body) is set in a vertical oscillatory motion with a double-way piston driven by compressed air⁽¹⁷¹⁻¹⁷³⁾. The impact force, F , which is the main output parameter of the impact test, is affected by the impact mass, M , frequency, f , impact ball to sample distance, d , and the static air pressure, P ⁽¹⁷⁰⁻¹⁷⁵⁾. The resulting impact force is usually assessed by means of a piezoelectric force transducer. Differences in the impact force have been observed by using different ball materials⁽¹⁷¹⁾. The impact force can also be increased by adding extra weights to the piston^(171,173). The test response is the critical number of loading

cycles up to the point at which the coating surface shows no further damage. A schematic view of the impact test arrangement is shown in figure 7.1.

A model of coating degradation under repeated impact loading has been developed by Bantle and Matthews⁽¹⁷¹⁾. During the impact test, stepwise deformation takes place which leads to piling up of material. Three failure zones can often be distinguished (figure 7.2): a central zone with cohesive failure, an intermediate zone with cohesive and adhesive failure and a peripheral zone with circular (radial) cracks. In the intermediate zone, cohesive and adhesive failures are caused by bending stresses, frictional forces acting during indentation and piling up of the substrate material causing shear stresses in the interfacial region^(171,173). The cracks in the peripheral zone arise from Hertzian tensile stress, as a result of the ball/coated surface contact conditions^(170-171,173).

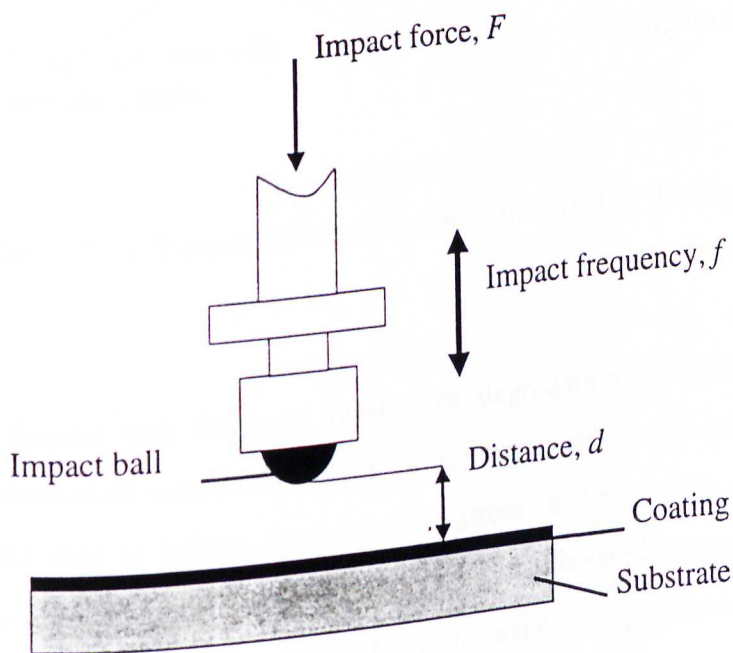


Figure 7.1 – Schematic view of the impact test arrangement.

A dependence between impact behaviour and coating microstructure has been documented⁽¹⁷⁴⁾. Coatings with more pronounced columnar structures were able to

endure more deformation than others possessing dense, less columnar structures. The deformability of the columnar structure, which is more strain-tolerant, allows coatings with such a structure to withstand a larger number of impacts without showing cohesive and adhesive failures⁽¹⁷⁴⁾.

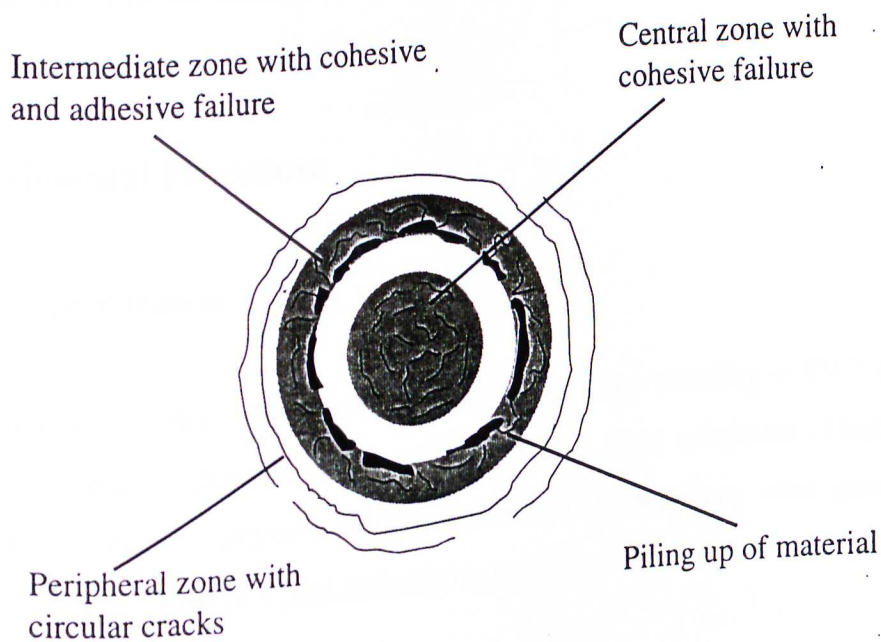


Figure 7.2 – Typical failure zones encountered after the impact test.

During the impact test, the main reason for degradation of PVD hard coatings is substrate deformation which takes place under impact, which the hard and often brittle coating is not able to follow. To reduce the stress in the coating, it starts to build a network of macrocracks inside the impact crater. Multilayered coatings, possessing high toughness, have also been reported to yield excellent performance under impact tests^(172,176).

The impact wear resistance of materials can be further optimised by either depositing coatings that are sufficiently elastic to accommodate any substrate deformation or

increasing the load support beneath the coating to reduce surface deformation. Hence, a duplex treatment is expected to provide a superior impact performance.

In this chapter the impact resistance of single-layered and duplex (Ti,Al)N, Cr-N coatings has been evaluated. Two different balls (tungsten carbide and hardened steel balls) have been used as impact bodies. Coating failure mechanisms are presented and discussed for the different coatings that have been tested.

7.2. Experimental Procedure

7.2.1. Sample preparation

Single-layered and duplex (Ti,Al)N, Cr-N coatings (plasma nitriding + PVD coating) were deposited onto hardened and tempered AISI H13 steel substrates (55 ± 2 HRC). Prior to plasma nitriding and/or coating deposition, the specimens were ground and polished to a surface finish of $R_a = (0.005 \pm 0.001) \mu\text{m}$.

7.2.2. Coating deposition and characterisation

Single-layered (Ti,Al)N, duplex (Ti,Al)N and duplex Cr-N coatings were prepared by electron beam evaporation (see chapter 5). Plasma nitriding and PVD coating were performed by means of a single operation. For all coating systems under investigation, plasma nitriding was carried out in a 60%Ar + 40%N₂ plasma for 2 hours. The nitriding temperature varied from 683 to 743K, depending on the specific duplex treatment (see table V.4). Coating deposition temperatures were in the range 669-715K (see tables V.3 and V.4).

For the duplex-treated specimens, coating deposition was initiated without carrying out any plasma etching between plasma nitriding and coating deposition. For the duplex (Ti,Al)N and Cr-N coatings, a cooling step in vacuum was performed between plasma nitriding and coating deposition to avoid deposition temperatures higher than 723K. A

0.1-0.2 μm titanium interlayer was deposited on (Ti,Al)N coatings (both single-layered and duplex).

SEM observations on fractured cross-sections were used to determine coating thickness in a Cambridge S200 scanning electron microscope. Knoop hardness measurements on polished cross-sections were carried out to estimate nitride case thickness using a Mitutoyo MVK-G1 hardness tester. Coating hardness was also determined from Knoop microhardness measurements under a load of 0.25N. The structure of the nitrided case was evaluated by SEM and XRD analyses.

7.2.3. Scratch testing

A modified commercial scratch tester (VTT-Tech, Finland) was used to assess coating adhesion. Tests were performed using a 200 μm Rockwell C stylus and a continuously increasing normal force (10Nmm^{-1}). The critical loads L_{C1} and L_{C2} (loads for cohesive and adhesive failures respectively) were determined from a set of 3 scratches on each sample. L_{C2} was taken as the load at which first exposure of the substrate took place.

7.2.4. Impact testing

The impact resistance was investigated using a cyclic loading system developed at the University of Hull. In such system the specimen surface is repetitively stressed at a defined contact point by impacts from a hard sphere. The impact force and impact frequency are controlled by a pneumatic actuation system with electronic control; a counter is used to stop the apparatus after a required number of impacts. A schematic view of the impact test arrangement was shown in figure 7.1. The impact frequency, f , and ball to sample distance, d , were set at 8Hz and 15.7mm, respectively, in all tests and the static air pressure, P , was set at $4.5 \times 10^5 \text{Pa}$. Two different balls were used as the impacting body: a tungsten carbide ball (grade 25 from SPHERIC) 6mm in diameter and a hardened AISI E52100 steel ball (grade 25 from SPHERIC) 10mm in diameter. The impact force resulting from this set of parameters was 900N for the tungsten carbide ball and 480N for the AISI E52100 steel ball. The impact force was assessed by

means of a piezoelectric force transducer and an oscilloscope. Each sample was subjected to 3 tests with 10^3 , 10^4 and 5×10^4 impacts in unlubricated conditions. The balls were always changed after carrying out a defined number of impacts and their surface, as well as the coating surface, were cleaned with acetone. After the test, samples were observed on a Cambridge S200 scanning electron microscope in order to investigate coating failure. Energy Dispersive X-Ray Analyses (EDX) were performed on the impact craters by a Link Analytical QX2000 X-Ray Analyser. The impact craters made with hardened steel balls were observed on a JEOL JSM-35C scanning electron microscope and a VOYAGER 3050 scanning electron microprobe was used for carrying out EDS analyses. These craters were also observed on a Leitz optical microscope.

7.3. Results and Discussion

7.3.1. Coating characterisation

Coating hardness and thickness are shown in table VII.1. For the duplex treatments the nitrided case structure was also included. As previously discussed, the duplex (Ti,Al)N coating has a thicker nitrided case than that of the duplex Cr-N coating. Although this work has not assessed the residual stress of the different coatings which have been produced, all PVD coatings are expected to have compressive residual stresses, as it is usually found in PVD coatings prepared by the ion plating technique. From the literature, compressive residual stresses decreases in the order (Ti,Al)N > TiN > Cr-N^(18,177). Nitrided cases are often under a state of compressive residual stress. Hence, compressive residual stresses in the subsurface region of duplex coatings are expected to lower the magnitude of an applied tensile stress on the composite surface, as in the case of impact tests.

Table VII.1 –Knoop microhardness and coating thickness of single-layered (Ti,Al)N, Cr-N and duplex (Ti,Al)N, Cr-N coatings. Nitrided case structure and thickness are also shown for the duplex coatings.

Coating	Nitrided case structure/ thickness (μm)	Coating thickness (μm)	HK _{0.025} (kgf/mm ²)	C.I. (95%)
Single-layered (Ti,Al)N	-----	2.3-2.4	3461	[3393, 3529]
Duplex (Ti,Al)N	Diffusion zone/55-60	2.6-2.7	3538	[3486, 3590]
Single-layered Cr-N	-----	2.5-2.6	2592	[2511, 2673]
Duplex Cr-N	Diffusion zone/35-40	2.0-2.1	2691	[2626, 2756]

7.3.2. Scratch testing

The benefits of the duplex treatment, in terms of improving the load support for hard PVD coatings, can be seen in terms of the highest critical loads recorded for the duplex-treated samples in comparison with their single-layered counterparts (see table V.7). The duplex (Ti,Al)N coating had the highest critical loads and its failure mechanism was characterised by tensile cracks. No external transverse cracks were observed until the substrate got exposed. Single-layered (Ti,Al)N, single-layered Cr-N and duplex Cr-N coatings exhibited flaking of the coating along the edges of the scratch, with the (Ti,Al)N showing a more severe flaking along the edges of the scratch channel. The duplex Cr-N coating also developed external transverse cracks at higher loads; however, no tensile cracks were formed inside the scratch channel.

7.3.3. Impact testing

7.3.3.1. Tests using a tungsten carbide ball ($F = 900\text{N}$)

Although the impact crater volume has not been quantified, an increase of both crater diameter and depth with increasing number of impacts was observed. After a certain

number of impacts, cohesive failures could be identified in all coatings (see figures 7.3 and 7.6). Adhesive failure leading to the exposure of the substrate material was selected as the failure criterion.

The single-layered (Ti,Al)N coating did not show any failures up to 10^3 impacts. After 10^4 impacts, cohesive failures could be observed in the central zone and cohesive + adhesive failures were present in the intermediate zone. After 5×10^4 impacts more cohesive and/or adhesive failures occurred in the central and intermediate zones.

The duplex (Ti,Al)N coating also displayed small cohesive failures in the central and intermediate zones after 10^4 impacts. A close observation of the wear craters showed a mechanism involving material transfer from the ball to the coated surface. Material transfer in the form of thin adhesive platelets occurred more dramatically after 5×10^4 impacts (figure 7.4). EDX analyses carried out on thin platelets and coating are shown in figure 7.5. Several EDX analyses were performed at different areas of the 5×10^4 impact crater and no signal from the elements constituting the substrate could be detected, indicating that the duplex (Ti,Al)N coating did not show any adhesive failures up to 5×10^4 impacts.

Single-layered Cr-N coatings did not show any cohesive and adhesive failures up to 10^4 impacts (figure 7.6). After 10^4 impacts, the piling up of material is clearly seen. Cohesive and adhesive failures could be distinguished after 5×10^4 impacts. EDX analyses on the dark areas of the 5×10^4 impact crater indicated the presence of Fe in such areas, confirming that the substrate was exposed. Compared with the single-layered (Ti,Al)N coating, the single-layered Cr-N coating was able to endure a larger number of impacts without showing any cohesive and/or adhesive failure. Moreover, single-layered Cr-N coatings demonstrated a greater ability to follow the substrate deformation, showing comparatively less cohesive and adhesive failures than a single-layered (Ti,Al)N coating.

The duplex Cr-N coating was able to withstand up to 10^4 impacts without exhibiting any cohesive failure or piling up of material (figure 7.6). After 5×10^4 impacts, only cohesive failures were observed in the central and intermediate zones. For the duplex Cr-N coating, a mechanism involving material transfer from the ball to the coated surface was not observed.

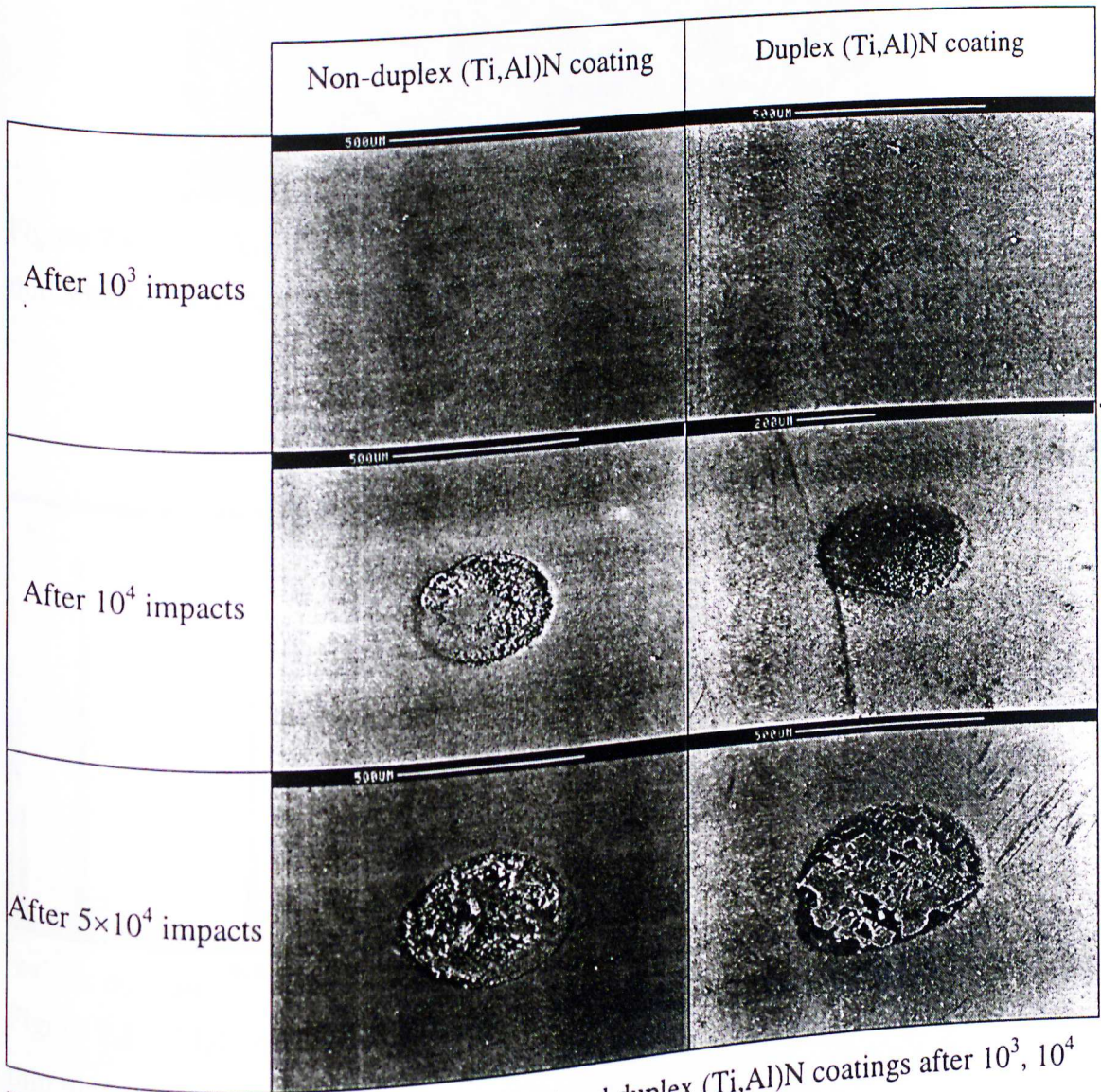
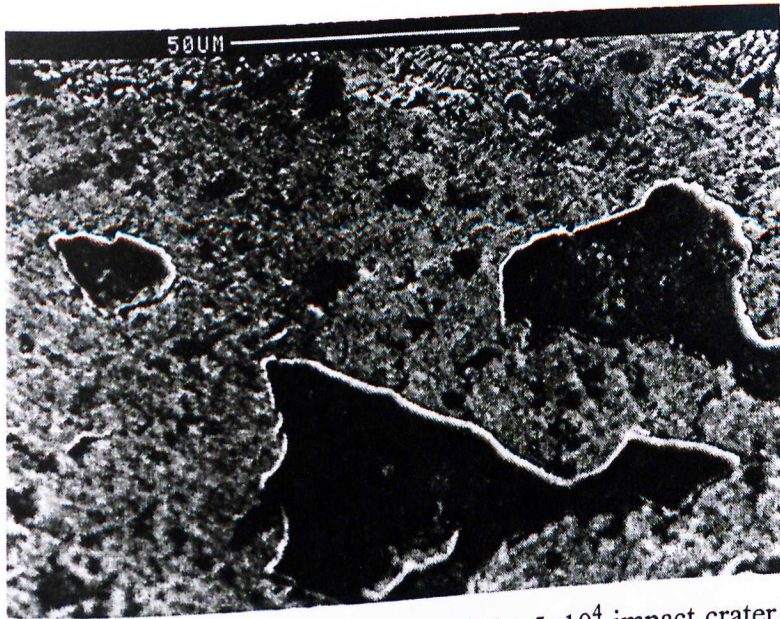


Figure 7.3 – Impact craters of single-layered and duplex (Ti,Al)N coatings after 10^3 , 10^4 and 5×10^4 impacts using a tungsten carbide ball, diameter, 6mm, $F = 900\text{N}$. SEM. The elliptical shape of some impact craters results from the tilt employed in the SEM imaging.



© DIREITO AUTORAL
 Direitos reservados e protegidos
 pela Lei 9.610/1998.
 Este trabalho não pode ser reproduzido ou
 divulgado sem a autorização expressa dos
 autores, editores, mecânicos,
 fotográficos ou quaisquer outros.

Figure 7.4 – Duplex (Ti,Al)N coating. Bottom of the 5×10^4 impact crater, showing the thin adhesive platelets transferred to the coating surface.

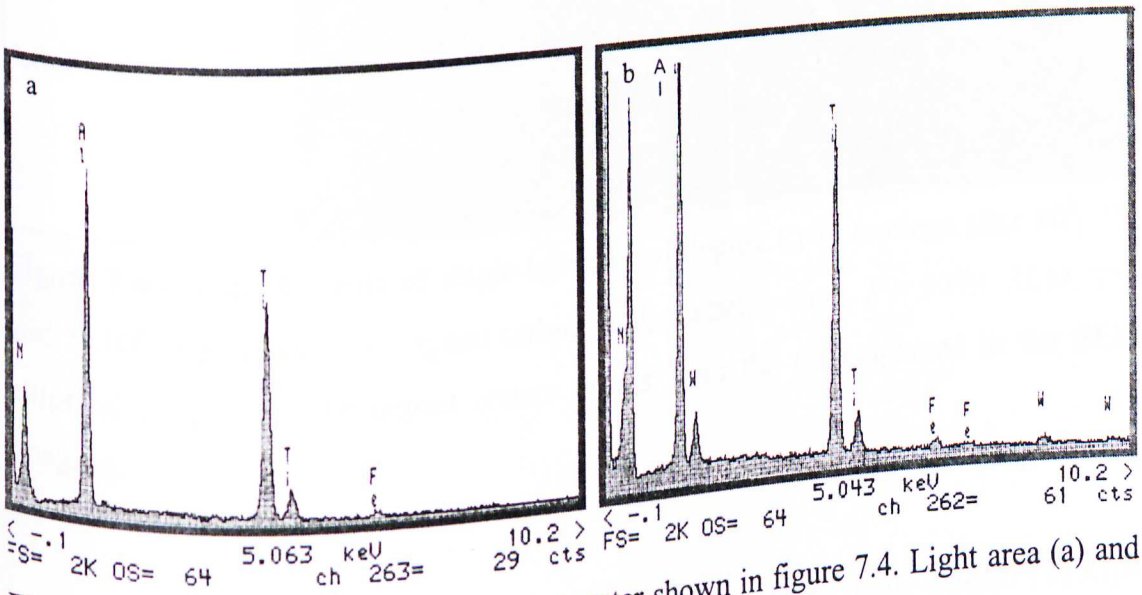


Figure 7.5 – EDX analyses of the impact crater shown in figure 7.4. Light area (a) and thin platelets (b).

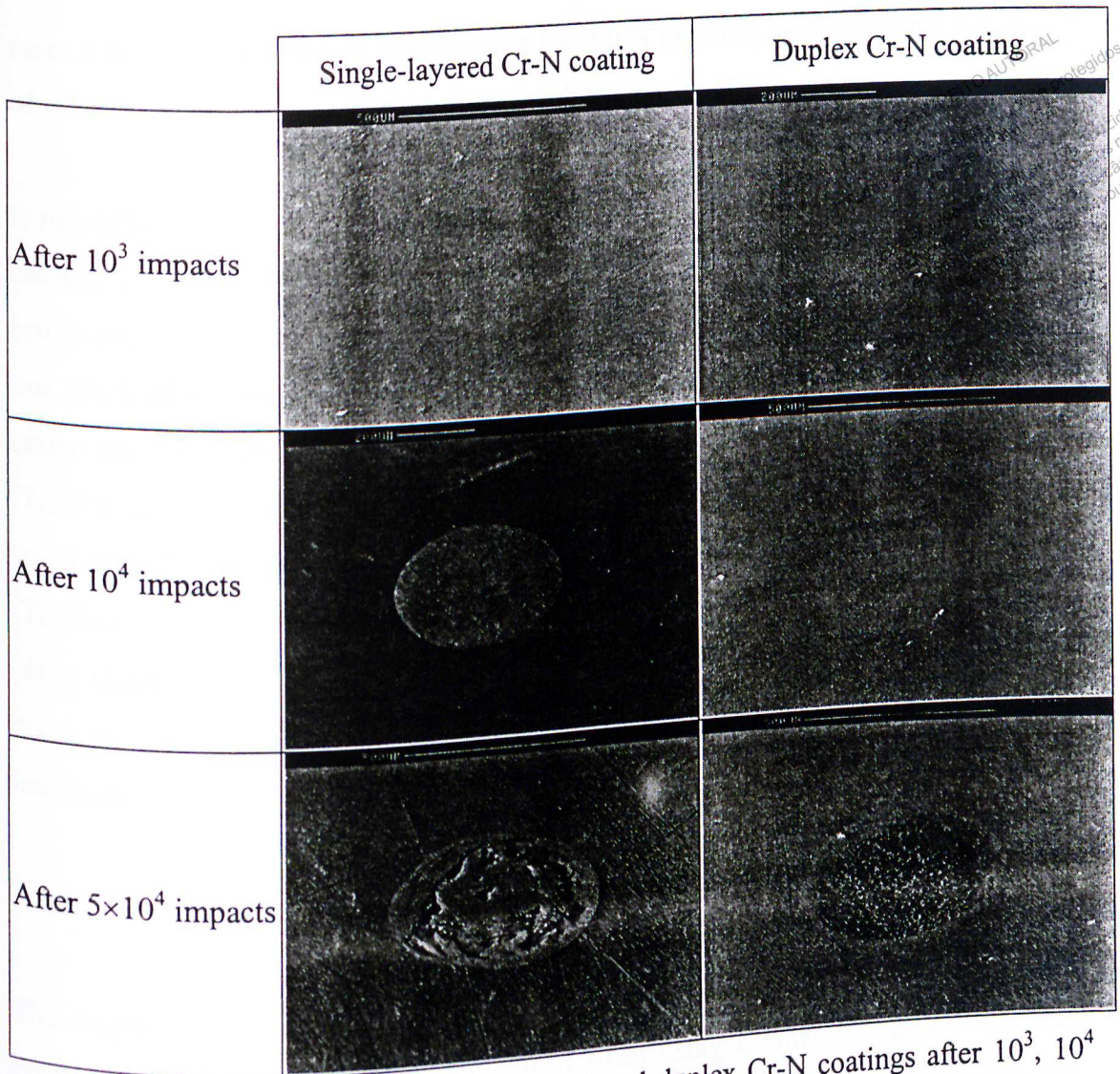


Figure 7.6 – Impact craters of single-layered and duplex Cr-N coatings after 10^3 , 10^4 and 5×10^4 impacts using a tungsten carbide ball, diameter, 6mm, $F = 900\text{N}$. SEM. The elliptical shape of some impact craters results from the tilt employed in the SEM imaging.

The duplex treatment increased the impact wear resistance of single-layered (Ti,Al)N and Cr-N coatings. The nitrided case seemed to have minimised substrate deformation under the hard PVD coating so that fewer cohesive failures occurred in the duplex coatings. Contrarily to single-layered coatings, duplex coatings did not exhibit any sort of adhesive failures. The latter coatings showed better adhesion properties than their single-layered counterparts. The improvement of the duplex treatment seemed to be more marked in the (Ti,Al)N system (also the one with the highest critical loads). In this

case, a thicker nitrided case was produced and this probably minimised the magnitude of substrate deformation when compared with the duplex Cr-N coating.

It should be noted that none of the coatings (both single-layered and duplex) displayed circular cracks in the peripheral zone. Circular cracks are expected to arise in hard brittle coatings due to the high tensile stress state in the vicinity of the impact cavity. For (Ti,Al)N coatings, the thin titanium interlayer is thought to have a positive effect under dynamic impact loading. In addition to improving the adhesion of the hard (Ti,Al)N layer to the substrate and reducing stresses at its interface with the substrate, this thin, soft and sufficient "elastic" interlayer probably increases the ability of the hard (Ti,Al)N coating to accommodate some extent of the substrate deformation which takes place under impact. Thus, the occurrence of micromechanical mechanisms, such as crack growth in the coating, was probably minimised due to the presence of this Ti interlayer.

7.3.3.2. Tests using a hardened AISI E52100 steel ball ($F = 480N$)

The impact response of single-layered (Ti,Al)N, Cr-N and duplex (Ti,Al)N, Cr-N coatings was quite similar to that obtained when using a tungsten carbide ball, with most of the coatings withstanding a larger number of impacts before showing any cohesive and adhesive failures. In these tests the resulting impact force was lower than that achieved when tungsten carbide balls were used. Besides, the hardened steel balls have a larger diameter, resulting in comparatively larger indentations. Thus, lower stresses are expected to occur under such conditions.

For the tests using hardened steel balls, it was necessary to observe the impact craters in the optical microscope. The craters were quite shallow and it was found to be very difficult to visualise them in the SEM, since this technique is based on topographic effects. For the duplex treatments, some of the craters could be barely seen in the scanning electron microscope.

The single-layered (Ti,Al)N coating (figure 7.7) did not show any adhesive failures up to 5×10^4 impacts. Cohesive failures in the central zones could be detected after 10^4 impacts and these failures increased after 5×10^4 impacts.

LEI DO DIREITO AUTORAL
 Todos os direitos reservados
 pela Lei 9.610/1998.
 Este arquivo não pode ser reproduzido ou
 transmitido sejam quais forem os meios
 empregados: eletrônicos, mecânicos,
 fotográficos ou quaisquer outros.

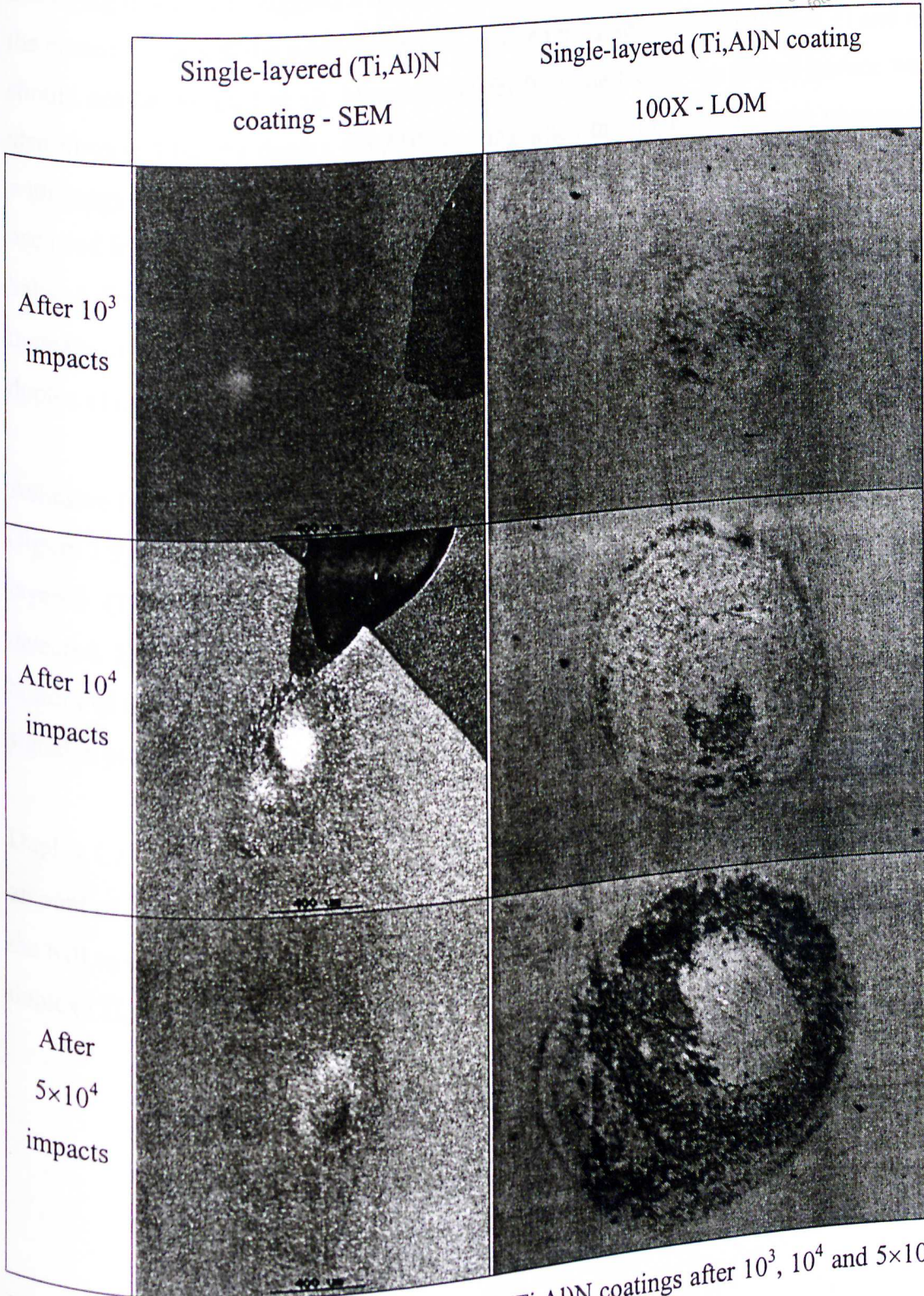


Figure 7.7 – Impact craters of single-layered (Ti,Al)N coatings after 10^3 , 10^4 and 5×10^4 impacts using a hardened AISI E52100 ball, diameter, 10mm, $F = 480\text{N}$.

The duplex (Ti,Al)N coating (figure 7.8) did not exhibit any failures up to 10^3 impacts. After 10^4 and 5×10^4 impacts, distinctive large areas could be seen in the bottom of the craters. EDS analyses that had been carried out indicated the presence of Fe in such areas; Ti and Al signals were also detected in these areas, at lower intensities than those belonging to Fe. This suggests a mechanism involving material transfer from the ball to the coated surface. If the substrate had got exposed in these areas, signal from Ti and Al should not be detected at all. Material transfer from the ball to the coated surface was also observed for the duplex (Ti,Al)N coating when the impact tests were performed with tungsten carbide balls. In the case of the hardened steel balls, material transfer occurred in a larger scale, probably owing to the lower hardness of the hardened steel balls. A Fe film was formed on the bottom of the 10^4 and 5×10^4 impact craters and an increase of transferred material was observed with increasing number of impacts. Thus, duplex (Ti,Al)N coatings did not show any adhesive failures up to 5×10^4 impacts.

Adhesive failures were not detected for single-layered Cr-N coatings up to 10^4 impacts (figure 7.9). Small cohesive failures could be distinguished in comparison to the single-layered (Ti,Al)N coating. After 5×10^4 impacts, however, adhesive failures were detected. EDS analyses that had been performed indicated the presence of Fe in the bottom of this crater and the Cr signal was particularly low, which suggests that the Cr signal is probably from Cr alloying element of the AISI H13 steel substrate.

Duplex Cr-N coatings did not show any adhesive failures up to 5×10^4 impacts. A small amount of cohesive failures seemed to occur after 5×10^4 impacts. Material transfer from the ball to the coated surface did not take place in this duplex sample, in contrast to the duplex (Ti,Al)N coating.

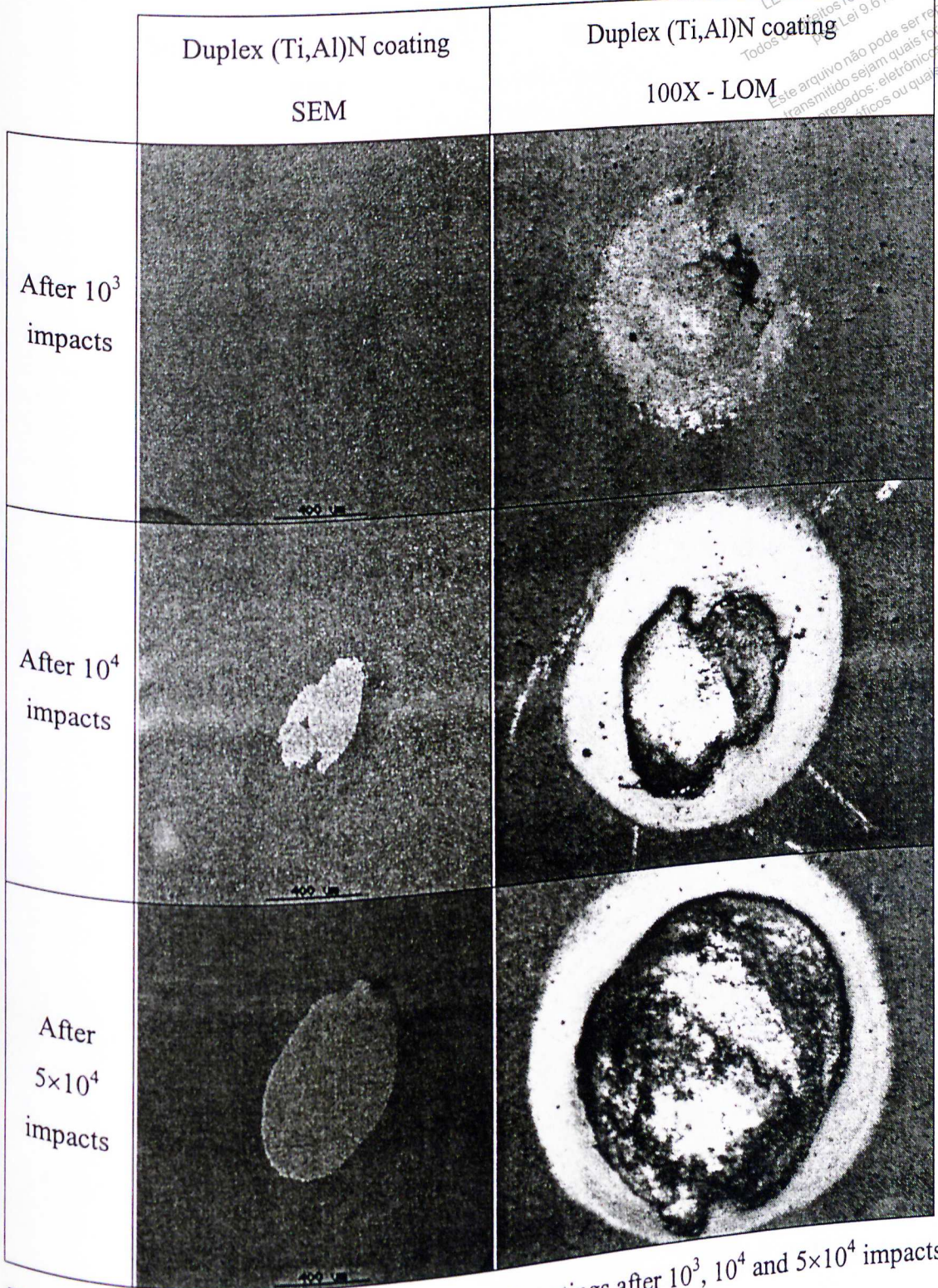


Figure 7.8 – Impact craters of duplex (Ti,Al)N coatings after 10^3 , 10^4 and 5×10^4 impacts using a hardened AISI E52100 ball, diameter, 10mm, $F = 480\text{N}$.

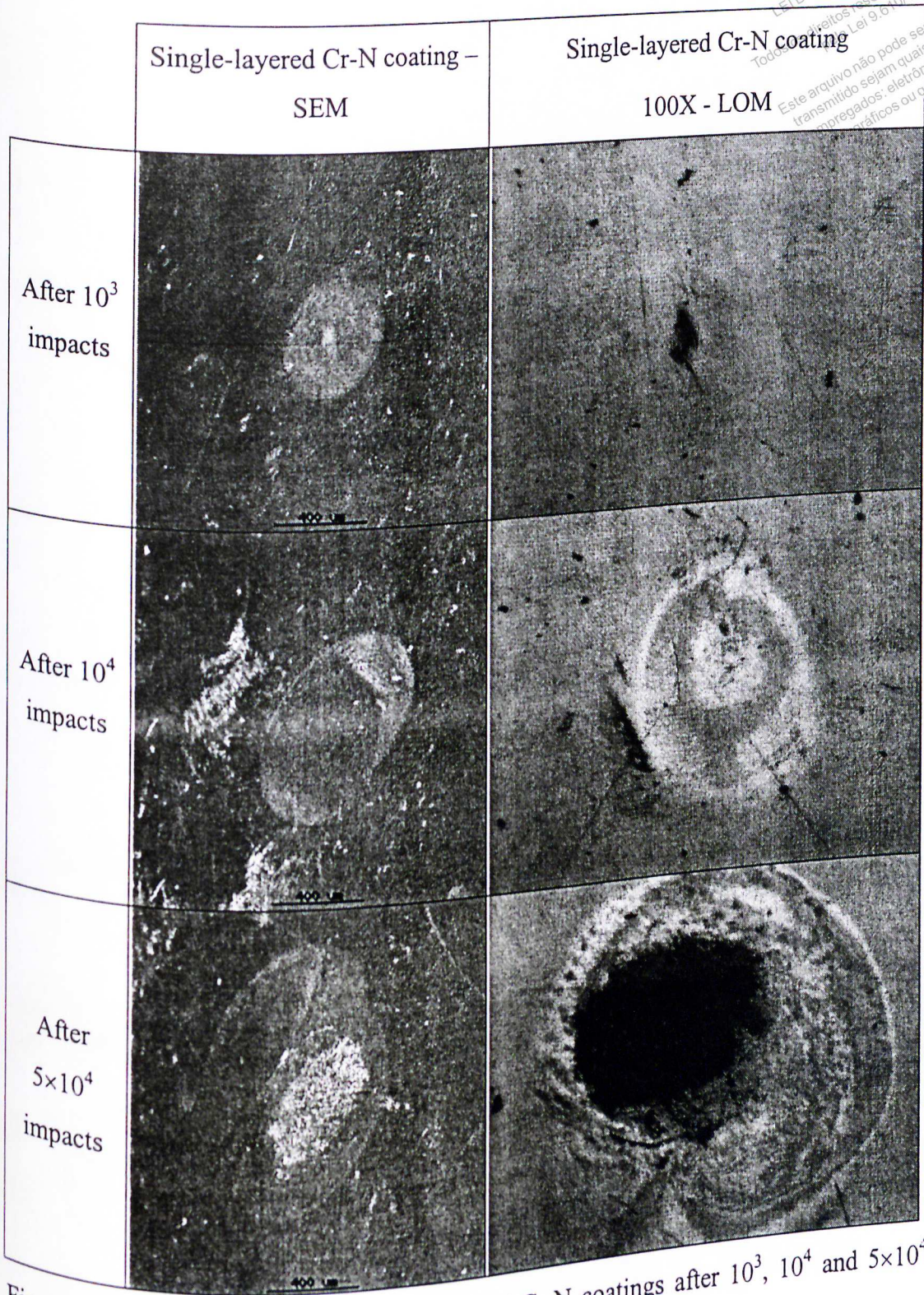


Figure 7.9 – Impact craters of single-layered Cr-N coatings after 10^3 , 10^4 and 5×10^4 impacts using a hardened AISI E52100 ball, diameter, 10mm, $F = 480N$.

EL DO DIREITO AUTORAL
 Todos os direitos reservados e protegidos
 Lei 9.610/1998.
 Este arquivo não pode ser reproduzido ou
 transmitido sejam quais forem os meios
 empregados: eletrônicos, mecânicos,
 gráficos ou quaisquer outros.

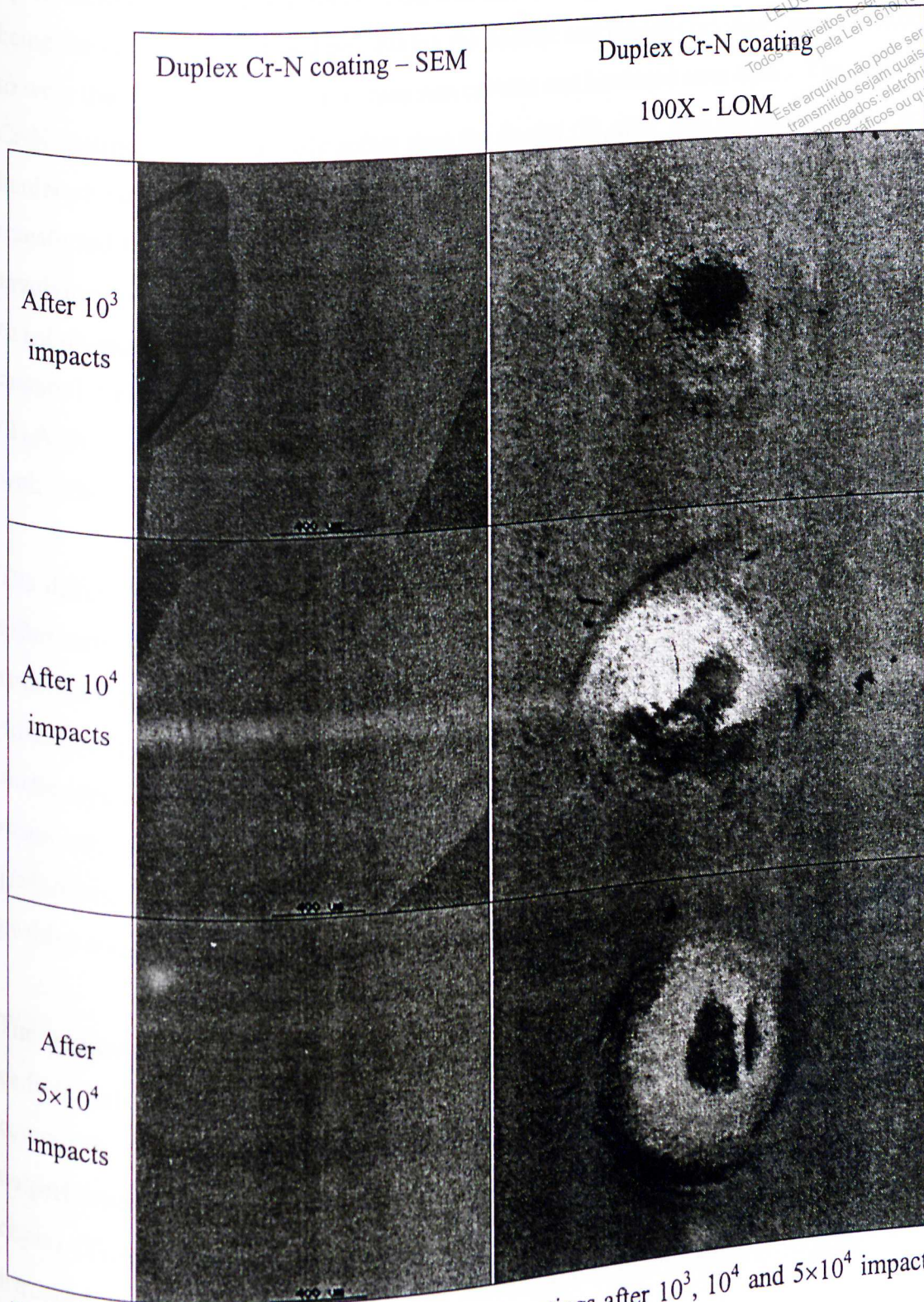


Figure 7.10 – Impact craters of duplex Cr-N coatings after 10^3 , 10^4 and 5×10^4 impacts using a hardened AISI E52100 ball, diameter, 10mm, $F = 480\text{N}$.

The transference of material from the balls to the coated surface seemed to be affected by the ratio between the hardness of the ball and coating hardness. The duplex (Ti,Al)N, being the hardest coating and possessing the hardest and thickest nitrided case, was able to wear the softer impact bodies (tungsten carbide and hardened steel balls). The duplex Cr-N coating, being relatively softer than the duplex (Ti,Al)N, was not able to wear the hardened steel and tungsten carbide balls. Hence, material from the ball was not transferred to its surface in both tests. It should be pointed out that this mechanism involving transference of the ball material to the coating surface could not be attributed to tribological compatibility between the ball and coating materials. If that was the case, material from the ball should have been observed on the surface of single-layered (Ti,Al)N coatings. Therefore, (Ti,Al)N does not form tribologically compatible pairs with either tungsten carbide or steel.

The different phase structures of single-layered and duplex Cr-N coatings could have influenced composite performance on the impact tests. Cr-N coatings with the Cr₂N structure were found to have better impact wear resistance⁽¹³⁵⁾. In this work, it is rather difficult to state that the coating phase had an influence on impact resistance, since the single-layered Cr-N coating (CrN + Cr₂N) was not submitted to a plasma nitriding treatment. Although the duplex Cr-N coating is mainly Cr₂N, its good impact performance seems to be also related to the presence of a nitride case that surely has a positive effect on impact resistance. The same holds for the (Ti,Al)N system.

The improvements yielded by the duplex treatment were more evident when tungsten carbide balls were used. In that case, higher stresses are expected to occur at the composite subsurface. Hence, single-layered coatings were more markedly outperformed by duplex coatings in the tests using tungsten carbide balls. Nevertheless, duplex (Ti,Al)N and duplex Cr-N coatings were able to withstand 5×10^4 impacts using a hardened AISI E52100 steel ball without showing any adhesive failures.

As a final comment, it should be noted that the impact test results showed a good correlation with those of the scratch tests, whereby all duplex coatings showed much better adhesion properties than their single-layered counterparts. A dependence between

coating adhesion and impact test results was also observed by Lugscheider⁽¹⁷⁴⁾ and Ollendorf⁽¹⁷⁵⁾.

LEI DO DIREITO AUTOREAL
Todos os direitos reservados e protegidos
pela Lei 9.610/1998.
Este arquivo não pode ser reproduzido ou
transmitido sejam quais forem os meios
empregados: eletrônicos, mecânicos,
fotográficos ou quaisquer outros.

7.4. Conclusions

Impact tests were carried out on single-layered and duplex (Ti,Al)N and Cr-N coatings. Two different impact balls were used: a tungsten carbide ball, diameter, 6mm and a hardened AISI E52100 steel ball, diameter, 10mm. The resulting impact force was 900N for the tungsten carbide ball and 480N for the AISI E52100 steel ball. The results indicated that:

1. The duplex treatment improved the impact resistance of single-layered (Ti,Al)N and Cr-N coatings. The nitrided case minimised substrate deformation under the hard PVD coatings so that fewer cohesive failures occurred in the duplex coatings. The improvements of the duplex treatment could be more markedly noted when tungsten carbide balls were used, since higher stresses are expected to occur for this impact body.
2. None of the duplex coatings exhibited adhesive failures up to 5×10^4 impacts when both tungsten carbide and hardened steel balls were used. A mechanism involving material transfer from the ball to the coated surface was observed to occur in the duplex (Ti,Al)N coating. A larger amount of transferred material took place for tests carried out with hardened steel balls, probably owing to their relatively lower hardness in comparison to that of the tungsten carbide balls.
3. A good correlation between impact and scratch test results was observed. This suggests that adhesion is one of the key parameters which influence the impact resistance of PAPVD coatings.

CHAPTER 8: GENERAL CONCLUSIONS

This work involved the production and characterisation of single-layered and duplex TiN, (Ti,Al)N and Cr-N coatings. Duplex TiN coatings have been used to investigate the influence of an intermediate treatment (consisting of cooling down the samples in vacuum and carrying out an Ar plasma etching step) on adhesion and impact resistance of duplex coatings. After ensuring that well-adherent duplex coatings would be produced, single-layered and duplex (Ti,Al)N, Cr-N coatings were prepared for tribological evaluation. Coating characterisation was extensively discussed in chapters 3, 4 and 5. Nevertheless, a brief summary is given in table VIII.1.

Table VIII.1 – Summary of the most relevant coating properties

Coating	Coating thickness (μm)	$\text{HK}_{0.025}$ (kgf mm^{-2})	R_a (μm)	Nitrided layer structure/thickness (μm)	Coating phase structure	Critical loads	
						L_{C1} (N) C.I. (95%)	L_{C2} (N) C.I. (95%)
Duplex (Ti,Al)N	2.6-2.7	3538 \pm 60	(0.043 \pm 0.005)	Diffusion zone/ 55-60	Ti ₃ Al ₂ N ₂ , Ti ₂ AlN*, TiN*	44.0 [40.6, 47.4]	157.3 [154.5, 160.1]
(Ti,Al)N	2.3-2.4	3461 \pm 78	(0.018 \pm 0.005)	-----	Ti ₃ Al ₂ N ₂ *, Ti ₂ AlN, TiN	31.8 [30.4, 33.2]	53.3 [51.9, 54.7]
Duplex Cr-N	2.0-2.1	2691 \pm 74	(0.039 \pm 0.006)	Diffusion zone/ 35-40	Cr, Cr ₂ N*	54.0 [50.2, 57.8]	117.2 [113.3, 121.2]
Cr-N	2.5-2.6	2592 \pm 92	(0.016 \pm 0.004)	-----	CrN*, Cr ₂ N*	29.2 [26.1, 32.4]	55.3 [52.7, 57.8]
Duplex TiN	2.2-2.3	2999 \pm 40	(0.049 \pm 0.002)	Mono-phase ϵ compound layer/1.0-1.2 + diffusion zone/35-40	Ti, TiN*	37.5 [34.6, 40.4]	152.1 [146.3, 157.9]
TiN	2.1-2.2	2935 \pm 80	(0.020 \pm 0.005)	-----	Ti, TiN*	25.7 [22.5, 29.0]	52.3 [49.4, 55.2]

* Dominant phases.

LEI DO DIREITO AUTORAL
 Todos os direitos reservados e protegidos
 Este trabalho não pode ser reproduzido ou
 transmitido em quaisquer meios
 eletrônicos, mecânicos,
 gráficos ou quaisquer outros.

Based on the experimental results that were obtained, the following major conclusions can be drawn from this work:

1. It is feasible to produce well-adherent duplex coatings which have a mono-phase compound layer. The key issue is to avoid compound layer destabilisation, which can be achieved by carefully controlling process parameters during coating deposition. The structure of the compound layer seems to affect duplex coating performance. A dual-phase compound layer is expected to be detrimental, since such structure is susceptible to fracture between the phases.
2. An intermediate treatment, which allows tailoring the nitrided case structure, has been developed. This treatment was proven to be effective in avoiding compound layer destabilisation and also producing duplex coatings which are compound-layer-free. By performing an Ar plasma etching step between nitriding and coating deposition at a bias voltage of 250V and etching times of 10 and 20 minutes, it was possible to remove a 1.0-1.2 μm thick compound layer from the substrate surface. Hence, a nitrided case consisting of a diffusion zone could be produced. Compound layer destabilisation was inhibited by cooling down the samples in vacuum in order to avoid deposition temperatures higher than 723K. This intermediate treatment elucidates a systematic approach to tailor the nitrided case structure in triode ion plating systems. Clearly the etching time will vary depending on the thickness of the compound layer produced during nitriding.
3. Scratch and impact test results indicate that a compound layer does not have any detrimental effects on adhesion and impact resistance. Although the critical loads determined for duplex coatings consisting of TiN + diffusion zones were statistically similar to those obtained for a duplex coating consisting of TiN + ϵ compound layer + diffusion zone, it was found that the duplex TiN coating with a hard, dense, mono-phase ϵ compound layer + diffusion zone can outperform a duplex coating with TiN + diffusion zone in impact tests. The duplex coatings formed by TiN + diffusion zone presented circular cracks, whilst the one with an ϵ compound layer did not show any coating failure up to 5×10^4 impacts. If process parameters are carefully

controlled in order to produce a hard, dense, mono-phase compound layer and its destabilisation is successfully avoided, then it is possible to obtain duplex coatings with adhesion strength comparable to PVD hard coatings on plasma nitrided steels with a diffusion zone only. Since compound layers can improve the corrosion resistance of duplex coatings, it would be interesting to produce duplex coatings with mono-phase compound layers when resistance to corrosion and good tribological properties are desired for a given application.

4. All films had very dense columnar structures, with single-layered coatings displaying more fine-grained structures than duplex coatings. The single-layered Cr-N coating had the finest grained structure among all coatings. GDOES results indicated that single-layered and duplex (Ti,Al)N coatings have compositions close to $Ti_{0.50}Al_{0.50}N$. The single-layered Cr-N coating had a two-layer structure, with an outer layer richer in nitrogen, probably corresponding to substoichiometric CrN and an inner layer richer in chromium, corresponding to Cr_2N . The duplex Cr-N coating was comparatively poorer in nitrogen than the single-layered Cr-N coating and its composition seemed to be closer to that of the Cr_2N phase. As indicated by XRD analyses, single-layered and duplex coatings crystallised into different phases, probably due to the lower deposition temperatures that were used for producing duplex (Ti,Al)N and Cr-N coatings in comparison to those used for producing the single-layered coatings.
5. The duplex treatment was quite effective in increasing the load support for hard PVD coatings. Consequently, single-layered coatings were outperformed by their duplex counterparts in micro-abrasive wear and impact tests. The nitrided case prevented substrate deformation under such tribological contacts, resulting in an improved micro-abrasive wear and impact resistance.
6. The micro-abrasive wear resistance was strongly influenced by surface (coating) and subsurface hardness. The duplex (Ti,Al)N coating was found to be the best coating for improving abrasive wear resistance of AISI H13 steel substrates. Although the duplex treatment improved the abrasive wear resistance of single-layered PVD

coatings in comparison with their duplex counterparts, the top hard coating seems to have a stronger influence on the micro-abrasive wear performance. A duplex TiN coating was outperformed by a single-layered (Ti,Al)N coating in the micro-abrasive wear tests, suggesting that the micro-abrasion resistance is more sensitive to the choice of the PVD coating rather than to substrate deformation, which was minimised by carrying out the duplex treatment. The micro-abrasive wear resistance was also found to be influenced by (i) the ratio between abrasive particle hardness and surface (coating)/subsurface hardness and (ii) coating thickness.

7. Duplex coatings proved to be more effective than single-layered coatings in dynamic wear applications. This can be attributed to the presence of a nitrided case, which improves the load support for the hard PVD coatings and reduces substrate deformation under impact testing. All single-layered coatings displayed some extent of cohesive and adhesive failures after a certain number of impacts whereas duplex (Ti,Al)N and duplex Cr-N coatings were able to endure up to 5×10^4 impacts without showing any adhesive failures.
8. Both duplex (Ti,Al)N and duplex Cr-N coatings seemed to be promising coatings to be applied onto AISI H13 steel shear knives that are used to cut steel ingots during the continuous ingot cast process at Gerdau S.A. Although duplex Cr-N coatings did not exhibit a high resistance to micro-abrasion, owing to their relatively low hardness in comparison with the hardness of the abrasive particles (SiC) and unsuitable thickness, they showed to be quite suitable in tribological applications that require resistance to impact. Duplex (Ti,Al)N coatings showed an excellent resistance to micro-abrasion and had a good performance in impact tests. Therefore, both coatings are expected to improve the performance of AISI H13 shear knives. Another important property in such application is resistance to oxidation. According to the literature, (Ti,Al)N and Cr-N are coatings which have an enormous potential to increase the oxidation resistance of materials. In the case of duplex Cr-N coatings, it is necessary to optimise film thickness as a function of abrasive hardness and size.

CHAPTER 9: RELEVANCE OF RESULTS AND MAJOR CONTRIBUTIONS

The experimental results obtained from this work highlight that it is feasible to produce duplex coating with compound layers that have satisfactory adhesion strength to plasma nitrided substrates. This is a great potential for such nitrided case structure, especially in applications that require corrosion resistance, where the presence of a dense compound layer is expected to have a positive effect. A mono-phase ϵ ($\text{Fe}_{2.3}\text{N}$) compound layer increased the impact wear resistance of duplex TiN coatings when compared with duplex TiN coatings which were compound-layer-free. The same adhesion strength was achieved by duplex TiN coatings with a mono-phase ϵ compound layer and compound-layer-free duplex TiN coatings. These results are in principle contradictory to those of the literature. A great number of papers suggest that it is primordial to remove compound layers in order to achieve good adhesion of duplex coatings. This work, however, shows that the major issue concerning duplex coating processing is to avoid compound layer destabilisation so that well-adherent duplex coatings with compound layers can be produced. Nevertheless, the structure of the compound layer seems to be rather important. Dual-phase compound layers should be avoided because of their weak bond between phases, which can lead to composite premature failure due to interfacial fracture between the phases.

An intermediate treatment consisting of cooling down the samples in vacuum and Ar plasma etching has been developed. This treatment allows tailoring the nitrided case structure of duplex treatments that are performed by means of a single operation in triode ion plating systems. Compound layer destabilisation can be avoided by cooling down the samples and controlling the deposition temperature whereas an Ar plasma etch step allows the removal of compound layers by means of a sputter mechanism.

By simulating tribological contacts in laboratory tests, it was possible to select coatings that are suitable for specific tribological applications. A close collaboration between academic research groups and industry is still needed to optimise the development of coating materials. In most of the cases, real operating conditions are quite different from

those simulated in laboratory tests. Hence, an optimisation of coating materials may be necessary before introducing them in practical applications, since there is always a gap between laboratory tests and real operating conditions.

The duplex treatment developed in this work has already been introduced in an English company. The first trials were made with duplex TiN coatings, which were applied onto steel hobs. The duplex treatment yielded a significant improvement in the lifetime of these tools, indicating that this treatment has a great potential to successfully improve the performance of several components that are subjected to abrasive wear and cyclical loads.

LEI DO DIREITO AUTORAL
Todos os direitos reservados e protegidos
Toda e qualquer reprodução ou
transmissão, em quaisquer meios,
sem a autorização dos autores, mecânicos,
fotógrafos ou quaisquer outros.

CHAPTER 10: RECOMMENDATIONS FOR FUTURE WORK

This work dealt with optimising a duplex treatment consisting of plasma nitriding and subsequent PAPVD hard coating deposition. Tribological duplex (Ti,Al)N and Cr-N coatings were chosen for a promising application onto AISI H13 shear knives which are used to cut steel ingots during the continuous ingot cast process at Gerdau S.A. industry. These coatings have been characterised by SEM, LOM, XRD, EDX, GDOES, scratch testing, micro-abrasive wear tests and impact tests. Laboratory tests are expected to give an insight about coating performance. Nevertheless, industrial field tests need to be carried out to ensure that these duplex coatings will have the beneficial effects that they have proven to possess in laboratory testing. Tests under real operating conditions should be performed at Gerdau's industrial plant in order to establish coating suitability for this specific application.

These shear knives are subjected to dynamic loading and an intensive abrasive wear seems to take place under service. Because of the elevated temperature of the ingots (973K) during cut operation, tribochemical wear, i.e., oxidation wear, is expected to occur. From the literature, both (Ti,Al)N and Cr-N coatings are expected to provide resistance to oxidation up to 1073K. Therefore, duplex (Ti,Al)N and Cr-N coatings are promising coatings to be used onto AISI H13 shear knives. Unfortunately this work did not take into account such an important mechanism. Wear tests at elevated temperatures, or even oxidation tests, should be carried out before introducing such coatings in industrial field testing.

The structure of the nitrided case probably has a strong influence on duplex coating performance. In this work, only a mono-phase ϵ compound layer has been produced. Although dual-phase compound layers are expected to lower the adhesion of duplex coatings, this aspect was not investigated in this work. It should be interesting to prepare duplex coatings with dual-phase compound layers (without being destabilised) and evaluate their adhesion and impact behaviour in order to check this hypothesis. Surely such tests would provide useful information about nitrided case structure influence on duplex coating performance.

Since duplex coatings are expected to improve the corrosion resistance of single-layered PAPVD coatings, it would be relevant to investigate the corrosion resistance of duplex (Ti,Al)N, duplex TiN and duplex Cr-N coatings. Potentiodynamic methods and also immersion tests would be particularly useful for evaluating the corrosion resistance of duplex coatings. It is expected that a compound layer will act as a passive layer by blocking the localised corrosive attack which takes place through pinhole-type defects of single-layered PAPVD coatings. A comparison of corrosion performance could be made by producing nitrided cases with different structures, such as compound layer + diffusion zone and diffusion zone only. Hence, the influence of nitrided layer structure on corrosion resistance could be established.

REFERENCES

- (1) B.BERGHAUS, *Ger. Patent* 668,639, July 20, 1932.
- (2) B.BERGHAUS, *Ger. Patent* 683,414, September 15, 1932.
- (3) B.BERGHAUS, *Br. Patent* 510,993, August 26, 1937.
- (4) KOHONEN, A.S., SIRVIO, E.H. A new low pressure plasma nitriding method, *Thin Solid Films*, v.96, p.103-108, 1982.
- (5) KORHONEN, A.S., SIRVIO, E.H., SULONEN, M.S. Plasma nitriding and ion plating with an intensified glow discharge, *Thin Solid Films*, v.107, p.387-394, 1983.
- (6) LEYLAND, A., FANCEY, K.S., MATTHEWS, A. Plasma nitriding in a low pressure triode discharge to provide improvements in adhesion and load support for wear resistant coatings, *Surface Engineering*, v.7, n.3, p.207-215, 1991.
- (7) WILSON, A., MATTHEWS, A., HOUSDEN, J., TURNER, R., GARSIDE, B. A Comparison of the wear and fatigue properties of plasma-assisted physical vapour deposition TiN, CrN and duplex coatings on Ti-6Al-4V, *Surface and Coatings Technology*, v.62, p.600-607, 1993.
- (8) PARK, M.J., LEYLAND, A., MATTHEWS, A. Corrosion performance of layered coatings produced by physical vapour deposition, *Surface and Coatings Technology*, v.43-44, p.481-492, 1990.
- (9) SANCHETTE, F., DAMOND, E., BUVRON, M., HENRY, L., JACQUOT, P., RANDALL, N., ALERS, P. Single cycle plasma nitriding and hard coating deposition in a cathodic arc evaporation device, *Surface and Coatings Technology*, v.94-95, p.261-267, 1997.
- (10) BUECKEN, B., LEONHARDT, G., WILBERG, R., HOECK, K., SPIES, H.J. Direct combination of plasma nitriding and PVD hardcoating by a continuous process, *Surface and Coatings Technology*, v.68-69, p.244-248, 1994.
- (11) VAN STAPPEN, M., KERKHOFS, M., QUAEYHAEGENS, C., STALS, L. Introduction in industry of a duplex treatment consisting of plasma nitriding and PVD deposition of TiN, *Surface and Coatings Technology*, v.62, p.655-661, 1993.

LEI DO DIREITO AUTORAL
Todos os direitos reservados e protegidos
pela Lei 9.610/1998.
Este arquivo não pode ser reproduzido ou
transmitido sejam quais forem os meios
empregados eletrônicos, mecânicos,
fotográficos ou quaisquer outros.

- (12) D'HAEN, J., QUAEYHAEGENS, C., STALS, L.M., VAN STAPPEN, M. Interface study of physical vapour deposition TiN coatings on plasma-nitrided steels, *Surface and Coatings Technology*, v.61, p.194-200, 1993.
- (13) DINGREMONT, N., PIANELLI, A., BERGMANN, E., MICHEL, H. Analysis of the compatibility of plasma-nitrided steels with ceramic coatings deposited by the ion plating technique, *Surface and Coatings Technology*, v.61, p.187-193, 1993.
- (14) GREDIC, T., ZLATANOVIC, M., POPOVIC, N., BOGDANOV, Z. Properties of TiN coatings deposited onto hot work steel substrates plasma nitrided at low pressure, *Surface and Coatings Technology*, v.54-55, p.502-507, 1992.
- (15) VAN STAPPEN, M., MALLIET, B., STALS, L., DE SCHEPPER, L., ROOS, J.R., CELIS, J.P. Characterization of TiN coatings deposited on plasma nitrided tool steel surfaces, *Materials Science and Engineering*, v.A140, p.554-562, 1991.
- (16) HÖCK, K., SPIES, H.-J., LARISCH, B., LEONHARDT, G., BUECKEN, B. Wear resistance of prenitrided hardcoated steels for tools and machine components, *Surface and Coatings Technology*, v.88, p.44-49, 1996.
- (17) SKORIC, B., KAKAS, D., GREDIC, T. Influence of plasma nitriding on mechanical and tribological properties of steel and subsequent PVD surface treatments, *Thin Solid Films*, v.317, p.486-489, 1998.
- (18) BJÖRK, T., WESTERGARD, R., HOGMARK, S., BERGSTRÖM, J., HEDENQVIST, P. Physical vapour deposition duplex coatings for aluminium extrusion dies, *Wear*, v.225-229, p.1123-1130, 1999.
- (19) RUDENJA, S., LEYGRAPH, C., PAN, J., KULU, P., TALIMETS, E., MIKLI, V. Duplex TiN coatings deposited by arc plating for increased corrosion resistance of stainless steel substrates, *Surface and Coatings Technology*, v.114, p.129-136, 1999.
- (20) DINGREMONT, N., BERGMAN, E., COLLIGNON, P., MICHEL, H. Optimization of duplex coatings built from nitriding and ion plating with continuous and discontinuous operation for construction and hot working steels, *Surface and Coatings Technology*, v.72, p.163-168, 1995.
- (21) DINGREMONT, N., BERGMAN, E., HANS, M., COLLIGNON, P. Comparison of the corrosion resistance of different steel grades nitrided, coated and duplex treated, *Surface and Coatings Technology*, v.76-77, p.218-224, 1995.

- (22) DINGREMONT, N., BERGMAN, E., COLLIGNON, P. Application of duplex coatings for metal injection moulding, *Surface and Coatings Technology*, v.72, p.157-162, 1995.
- (23) SUN, Y., BELL, T. Plasma surface engineering of low alloy steel, *Materials Science and Engineering*, v.A140, p.419-434, 1991.
- (24) SUN, Y., BELL, T., Combined plasma nitriding and PVD treatments, *Trans. Inst. Metal Finish.*, v.70, n.1, p.38-44, 1992.
- (25) WALKOWICZ, J., SMOLIK, J., MIERNIK, K. Investigation of the influence of ion etching parameters on the structure of nitrided case in hot working steel, *Surface and Coatings Technology*, v.116-119, p.361-366, 1999.
- (26) WALKOWICZ, J., SMOLIK, J., TACIKOWSKI, J. Optimization of nitrided case structure in composite layers created by duplex treatment on the basis of PVD coating adhesion measurement, *Surface and Coatings Technology*, v.116-119, p.370-379, 1999.
- (27) ANJING, Y., YUFEI, L., XIANG, G., PENGXING, L. Structure and properties of PVD coating on nitrided steel substrates. In: 6th International Congress on Heat Treatment of Materials, 1988, Chicago, Illinois, USA. *Heat treatment and surface engineering; new technology and practical applications*. Ohio: ASM International, 1989. p.43-48.
- (28) FANCEY, K.S., MATTHEWS, A., Some fundamental aspects of glow discharges in plasma-assisted processes, *Surface and Coatings Technology*, v.33, p.17-29, 1987.
- (29) FANCEY, K.S. An investigation into dissociative mechanisms in nitrogenous glow discharges by optical emission spectroscopy, *Vacuum*, v.46, p.695-700, 1995.
- (30) FANCEY, K.S., MATTHEWS, A. Process effects in ion plating, *Vacuum*, v.41, p.2196-2200, 1990.
- (31) HOLMBERG, K., MATTHEWS A., *Coatings tribology*. Amsterdam: Elsevier, 1994. 442 p. (Tribology Series, 28)
- (32) WIIALA, U.K., KIVIVUORI, S.O.J., MOLARIUS, J.M., SULONEN, M., Wear of ion-plated hot-working tools, *Surface and Coatings Technology*, v.33, p.213-219, 1987.

- (33) O'BRIEN, J.M. Plasma (ion) nitriding. In: *ASM handbook; Heat treating*, 2nd ed. Ohio: ASM International, 1996. Vol.4, p.420-424.
- (34) SPALVINS, T. Advances and directions of ion nitriding/carburizing. In: ASM's 2nd International Conference on Ion Nitriding/Ion Carburizing, 1989, Cincinnati, Ohio, USA. *Ion nitriding and ion carburizing, Proceedings of ASM's 2nd international conference on ion nitriding/ion carburizing*. Ohio: ASM International, 1990. 1-4.
- (35) EDENHOFER, B. Physical and metallurgical aspects of ion nitriding-part 1, *Heat Treatment of Metals*, v.1, p.23-28, 1974.
- (36) KAKAS, D., ZLATANOVIC, M. Wear resistance of plasma intruded high speed steels. In: ASM's 2nd International Conference on Ion Nitriding/Ion Carburizing, 1989, Cincinnati, Ohio, USA. *Ion nitriding and ion carburizing, Proceedings of ASM's 2nd international conference on ion nitriding/ion carburizing*. Ohio: ASM International, 1990. 141-146.
- (37) REMBGES, W., LÜHR, J. Plasma (ion) nitriding and plasma (ion) nitrocarburizing units, applications and experiences. In: ASM's 2nd International Conference on Ion Nitriding/Ion Carburizing, 1989, Cincinnati, Ohio, USA. *Ion nitriding and ion carburizing, Proceedings of ASM's 2nd international conference on ion nitriding/ion carburizing*. Ohio: ASM International, 1990. 147-156.
- (38) GRÜN, R., GÜNTHER, H.J. Plasma nitriding in industry – Problems, new solutions and limits, *Materials Science and Engineering*, v.A140, p.435-441, 1991.
- (39) DRESSLER, S. Plasma parameter control for industrial situations: the role of hot wall plasma nitriding furnaces. In: ASM's 2nd International Conference on Ion Nitriding/Ion Carburizing, 1989, Cincinnati, Ohio, USA. *Ion nitriding and ion carburizing, Proceedings of ASM's 2nd international conference on ion nitriding/ion carburizing*. Ohio: ASM International, 1990. p.183-193.
- (40) SATO, K., TAKAHASHI, Y.I., YAMAZAKI, T., NITOH, Y. Surface layers produced by ion nitriding of austenitic Fe-Mn-Al alloys and the effects on hardness and corrosion resistance, *Journal of Materials Science*, v.23, p.4445-4449, 1988.
- (41) DEVI, M.U., MOHANTY, O.N. Plasma nitriding of tool steels for combined percussive impact and rolling fatigue wear applications. *Surface and Coatings Technology*, v.107, p.55-64, 1998.

- (42) CHAPMAN, B. *Glow discharge processes*. New York: John Wiley & Sons, 1980, 406p.
- (43) RICKERBY, D.S., MATTHEWS A. *Advanced surface coatings*. New York: Blackie & Son Ltd, 1991. 368 p.
- (44) BUNSHAH, R.F. *Deposition technologies for films and coatings*. New Jersey: Noyes Publications, 1982, 585p.
- (45) KRAUSS, G. Surface modification. In: KRAUSS, G. *Steels: heat treatment and processing principles*. 2.ed. Ohio: ASM International, 1993. Chapter 11, 319-350.
- (46) EDENHOFER, B. Physical and metallurgical aspects of ion nitriding-part2, *Heat Treatment of Metals*, v.2, p.59-67, 1974.
- (47) INAL, O.T., OZBAYSAL, K., METIN, E.S., PEHLINVANTURK, N.Y. A review of plasma surface modification: process, parameters, and microstructural characterization. In: ASM's 2nd International Conference on Ion Nitriding/Ion Carburizing, 1989, Cincinnati, Ohio, USA. *Ion Nitriding and Ion Carburizing, Proceedings of ASM's 2nd International Conference on Ion Nitriding/Ion Carburizing*. Ohio: ASM International, 1990. p.57-66.
- (48) HUDIS, M. Study of ion-nitriding, *Journal of Applied Physics*, v.44, n.4, p.1489-1496, Apr. 1973.
- (49) TIBBETTS, G.G. Role of nitrogen atoms in ion-nitriding, *Journal of Applied Physics*, v.45, n.11, p.5072-5073, Nov. 1974.
- (50) BINGZHONG, X., YINGZHI, Z. Collision dissociation model in ion nitriding, *Surface Engineering*, v.3, n.3, p. 226-232, 1987.
- (51) METIN, E., INAL, O.T. Formation and growth of iron nitrides during ion-nitriding, *Journal of Materials Science*, v.22, p.2783-2788, 1987.
- (52) LEYLAND, A., FANCEY, K.S., JAMES, A.S., MATTHEWS, A. Enhanced plasma nitriding at low pressures: a comparative study of dc and rf techniques. *Surface and Coatings Technology*, v.41, p.295-304, 1990.
- (53) LEYLAND, A., LEWIS, D.B., STEVENSON, P.R., MATTHEWS, A. Low temperature plasma diffusion treatment of stainless steels for improved wear resistance. *Surface and Coatings Technology*, v.62, p.608-617, 1993.

- (54) RENEVIER, N., COLLIGNON, P., MICHEL, H., CZERWIEC, T. New trends on nitriding in low pressure arc discharges studied by optical emission spectroscopy. *Surface and Coatings Technology*, v.86-87, p.285-291, 1996.
- (55) CZERWIEC, T., MICHEL, H., BERGMANN, E. Low-pressure, high-density plasma nitriding: mechanisms, technology and results, *Surface and Coatings Technology*, v.108-109, p.182-190, 1998.
- (56) FANCEY, K.S., LEYLAND, A., EGERTON, D., TORRES, D. MATTHEWS, A. The influence of process gas characteristics on the properties of plasma nitrided steel, *Surface and Coatings Technology*, v.76-77, p.694-699, 1995.
- (57) *ASM handbook*; Surface Engineering. 2.ed. Ohio: ASM International, 1996. Vol.5. 1039p.
- (58) MATTHEWS, A. Developments in ionization assisted processes, *Journal of Vacuum Science Technology A*, v.3, i.6, p.2354-2363, Nov/Dec, 1985.
- (59) MATTHEWS, A., FANCEY, K.S., JAMES, A.S., LEYLAND, A., Ionization in plasma-assisted physical vapor deposition systems, *Surface and Coatings Technology*, v.61, p.121-126, 1993.
- (60) DESHPANDEY, C.V., O'BRIEN, B.P., DOERR, H.J., BUNSHAH, R.F., HOFMANN, D. Plasma diagnostics studies of the activated reactive evaporation process, *Surface and Coatings Technology*, v.33, p.1-16, 1987.
- (61) ROSSNAGEL, S.M. Plasma diagnostics for use in reactive magnetron sputtering. In: ASM's 2nd International Conference on Ion Nitriding/Ion Carburizing, 1989, Cincinnati, Ohio, USA. *Ion Nitriding and Ion Carburizing. Proceedings of ASM's 2nd International Conference on Ion Nitriding/Ion Carburizing*. Ohio: ASM International, 1990. 13-17.
- (62) FANCEY, K.S., MATTHEWS, A. Determination of electron temperature in ion plating discharges by optical emission spectroscopy, *Vacuum*, v.42, p.1013-1015, 1991.
- (63) NESLADEK, M., QUAEYHAEGENS, C., WOUTERS, S., STALS, L.M., BERGMANN, E., RETTINGHAUS, G. Study of the ion energy distribution during physical vapour deposition of TiN, *Surface and Coatings Technology*, v.68-69, p.339-343, 1994.

- (64) RICHTER, F., PETER, S., PINTASKE, R., HECHT, G. In situ characterization of a plasma metalorganic chemical vapor deposition process, *Surface and Coatings Technology*, v.68-69, p.719-723, 1994.
- (65) BARHOLM-HANSEN, C., BENTZON, M.D., VIGILD, M.E., FINDEISEN, E., FEIDENHANS'L, R., BINDSLEV-HANSEN, J. Process control by optical emission spectroscopy during growth of a-C:H from a CH₄ plasma-enhanced chemical vapour deposition, *Surface and Coatings Technology*, v.68-69, p.702-707, 1994.
- (66) PATEL, H., SAIF, M., MEMARIAN, H. Reactive sputter deposition of indium tin oxide films onto polymeric webs using optical emission spectroscopy and mass spectroscopy as process monitoring and control, *Surface and Coatings Technology*, v.94-95, p.583-586, 1997.
- (67) VANDEVELDE, T., NESLADEK, M., QUAEYHAEGENS, C., STALS, L. Optical emission spectroscopy of the plasma during microwave CVD of diamond thin films with nitrogen addition and relation to the thin film morphology, *Surface and Coatings Technology*, v.308-309, p.154-158, 1997.
- (68) NODING, M., BECKER, F., KASSING, R. Diagnostics of SF₆ plasmas by energy-resolved mass spectrometry: influence of the electrode material on internal plasma parameters, *Surface and Coatings Technology*, v.111, p.51-55, 1999.
- (69) RAVEH, A., WEISS, M., SHNECK, R. Optical emission spectroscopy as a tool for designing and controlling the deposition of graded (Ti,Al)N layers by ECR-assisted reactive rf sputtering, *Surface and Coatings Technology*, v.111, p.263-268, 1999.
- (70) WOUTERS, S. *Plasma diagnostics in a PVD triode ion plating installation*. Diepenbeek: Institute for Materials Research, Limburgs Universitair Centrum, 1998. 117p. (Doctoral thesis, Doctor in de Wetenschappen).
- (71) DAVIS, W.D., VANDERSLICE, T.A. Ion energies at the cathode of a glow discharge, *Physics Review*, v.131, 219-228, 1963.
- (72) RICKARDS, J. Energies of particles at the cathode of a glow discharge, *Vacuum*, v.34, 559-562, 1984.
- (73) ZLATANOVIC, M. (Ti,Al)N Coating on plasma nitrated surfaces. In: 2nd International Conference on Ion Nitriding/Ion

- (84) BAEK, W.S., KWON, S.C., LEE, S.R., RHA, J.J., NAM, K.S., LEE, J.Y. A study of the interfacial structure between the TiN film and the iron nitride layer in a duplex plasma surface treatment, *Surface and Coatings Technology*, v.114, p.94-100, 1999.
- (85) BAEK, W.S., KWON, S.C., LEE, J.Y., LEE, S.R., RHA, J.J., NAM, K.S. The effect of Ti ion bombardment on the interfacial structure between TiN and iron nitride, *Thin Solid Films*, v.323, p.146-152, 1998.
- (86) TWIGG, P.C., PAGE, T.F. Investigation of thick nitride coated systems for high load applications, *Surface and Coatings Technology*, v.68-69, p.453-458, 1994.
- (87) MUSIL, J., VLCEK, J., JEZEK, V., BENDA, M. Protection of aluminium by duplex coatings, *Surface and Coatings Technology*, v.76-77, p.341-347, 1995.
- (88) GRÜN, R. Combination of different plasma assisted processes with pulsed d.c.: cleaning, nitriding and hardcoatings, *Surface and Coatings Technology*, v.74-75, p.598-603, 1995.
- (89) RUDENJA, S., KULU, P., TALLIMETS, E., MIKLI, V., STRAEDE, C.A. Corrosion performance of duplex TiN coatings deposited by arc plating, *Surface and Coatings Technology*, v.100-101, p.247-250, 1998.
- (90) BADER, M., SPIES, H.J., HÖCK, K., BROSZEIT, E., SCHRÖDER, H.J. Properties of duplex treated (gas-nitriding and PVD-TiN, -Cr₂N) low alloy steel, *Surface and Coatings Technology*, v.98, p.891-896, 1998.
- (91) MICHALSKI, J., LUNARSKA, E., WIERZCHON, T., ALGHANEM, S. Wear and corrosion properties of TiN layers deposited on nitrided high speed steel, *Surface and Coatings Technology*, v.72, p.189-195, 1995.
- (92) SPIES, H.J., LARISCH, B., HÖCK, K., BROSZEIT, E., SCHRÖDER, H.J. Adhesion and wear resistance of nitrided and TiN coated low alloy steels, *Surface and Coatings Technology*, v.74-75, p.178-182, 1995.
- (93) SUN, Y., BELL, T. The role of oxidation in the wear of plasma nitrided and PVD TiN coated steel, *Wear*, v.166, p.119-125, 1993.
- (94) SMOLIK, J., WALKOWICZ, J., TACIKOWSKI, J. Influence of the structure of the composite: 'nitrided layer/PVD coating' on the durability of tools for hot working, *Surface and Coatings Technology*, v.125, p.134-140, 2000.

- (95) VETTER, J., MICHLER, T., STEUERNAGEL, H. Hard coatings on thermochemically pretreated soft steels: application potential for ball valves, *Surface and Coatings Technology*, v.111, p.210-219, 1999.
- (96) NICKEL, J., SHUAIB, A.N., YILBAS, B.S., NIZAM, S.M. Evaluation of the wear of plasma-nitrided and TiN-coated HSS drills using conventional and micro-PIXE techniques, *Wear*, v.239, p.155-167, 2000.
- (97) KAUFMANN, H. Industrial applications of plasma and ion surface engineering, *Surface and Coatings Technology*, v.74-75, p.23-28, 1995.
- (98) WALKOWICZ, J., SMOLIK, J., MIERNIK, K., BUJAK, J. Duplex surface treatment of moulds for pressure casting of aluminium, *Surface and Coatings Technology*, v.97, p.453-464, 1997.
- (99) KARAMIS, M.B., SERT, H. The role of PVD TiN coating in wear behaviour of aluminium extrusion die, *Wear*, v.217, p.46-55, 1998.
- (100) KRAUSS, G. Tool steels. In: KRAUSS, G. *Steels: heat treatment and processing principles*. 2.ed. Ohio: ASM International, 1993. Chapter 13, 401-430.
- (101) *Heat treater's guide*; Standard practices and procedures for steel. 2.ed. Ohio: American Society for Metals, 1982.
- (102) LESLIE, W.C. Tool steels. In: *The physical metallurgy of steels*. 1.ed. New York: McGraw-Hill, 1981. Chapter 13, 358-372.
- (103) Metallographic technique for case hardening steel. In: *Metals Handbook*; Metallography structures and phase diagrams. 8.ed. Ohio: American Society for Metals, 1973. Vol.8, p.84-85.
- (104) BULL, S.J. Microstructural characterization of coatings and thin films. In: *ASM handbook*; Surface engineering. 2 ed. Ohio: ASM International, 1996. Vol.5, p.660-668.
- (105) CHALKER, P.R., BULL, S.J., RICKERBY, D.S. A review of the methods for the evaluation of coating-substrate adhesion, *Materials Science and Engineering A*, v.140, p.583-592, 1991.
- (106) RONKAINEN, H., HOLMBERG, K., FANCEY, K., MATTHEWS, A., MATTHES, B., BROSZEIT, E. Comparative tribological and adhesion studies of some titanium-based ceramic coatings, *Surface and Coatings Technology*, v.43-44, p.888-897, 1990.

- (107) STEINMANN, P.A., TARDY, Y., HINTERMANN, H.E. Adhesion testing by the scratch test method: the influence of intrinsic and extrinsic parameters on the critical load, *Thin Solid Films*, v.154, p.333-349, 1987.
- (108) ARAI, T., FUJITA, H., WATANABE, M. Evaluation of adhesion strength of thin hard coatings, *Thin Solid Films*, v.154, p.387-401, 1987.
- (109) VALLI, J., MOLARIUS, J.M., KORHONEN, A.S. The effect of nitrogen content on the critical normal force in scratch testing of Ti-N films, *Thin Solid Films*, v.154, p.351-360, 1987.
- (110) SUBRAMANIAN, C., STRAFFORD, K.N., WILKS, T.P., WARD, L.P., MCMILLAN, W. Influence of substrate roughness on the scratch adhesion of titanium nitride coatings, *Surface and Coatings Technology*, v.62, p.529-535, 1993.
- (111) BURNETT, P.J., RICKERBY, D.S. The relationship between hardness and scratch adhesion, *Thin Solid Films*, v.154, p.403-416, 1987.
- (112) LÖFFLER, F.H.W., Systematic approach to improve the performance of PVD coatings for tool applications, *Surface and Coatings Technology*, v.68-69, p.729-740, 1994.
- (113) KÖNIG, W., KAMMERMEIER, D. New ways towards better exploitation of physical vapour deposition coatings, *Surface and Coatings Technology*, Amsterdam, v.54-55, p.470-475, 1992.
- (114) VAN STAPPEN, M., STALS, L.M., KERKHOFS, M., QUAEYHAEGENS, C. State of the art for the industrial use of ceramic PVD coatings, *Surface and Coatings Technology*, v.74-75, p.629-633, 1995.
- (115) BIENK, E.J., REITZ, H., MIKKELSEN, N.J. Wear and friction properties of hard PVD coatings, *Surface and Coatings Technology*, v.76-77, p.475-480, 1995.
- (116) HAN, J.G., YOON, J.S., KIM, H.J. SONG, K. High temperature wear resistance of (Ti,Al)N films synthesized by cathodic arc plasma deposition, *Surface and Coatings Technology*, v.86-87, p.82-87, 1996.
- (117) LIN, K.L., HWANG, M.Y., WU, C.D. The deposition and wear properties of cathodic arc plasma deposition TiAlN deposits, *Materials Chemistry and Physics*, v.43, p.77-83, 1996.

- (118) PFLÜGER, E., SCHRÖER, A., VOUMARD, P., DONOHUE, L., MÜNZ, W.D. Influence of incorporation of Cr and Y on the wear performance of TiAlN coatings at elevated temperatures, *Surface and Coatings Technology*, v.115, p.17-23, 1999.
- (119) HSIEH, J.H., LIANG, C., YU, C.H., WU, W. Deposition and characterization of (Ti,Al)N and multi-layered TiN/(Ti,Al)N coatings using unbalanced magnetron sputtering, *Surface and Coatings Technology*, v.108-109, p.132-137, 1998.
- (120) PAJAN, P., NAVINSEK, B., CEKADA, M., ZALAR, A. Oxidation behaviour of TiAlN coatings sputtered at low temperature, *Vacuum*, v.53, p.127-131, 1999.
- (121) LUGSCHEIDER, E., KNOTEK, O., LÖFFLER, F., BARIMANI, C., GUERREIRO, S., ZIMMERMANN, H. Deposition of arc TiAlN coatings with pulsed bias, *Surface and Coatings Technology*, v.76-77, p.700-705, 1995.
- (122) KERKHOFS, M., VAN STAPPEN, M., D'OLIESLAEGER, M., QUAEYHAEGENS, C., STALS, L.M. The performance of (Ti,Al)N-coated flowdrills, *Surface and Coatings Technology*, v.68-69, p.741-746, 1994.
- (123) MOLARIUS, J.M., KORHONEN, A.S., HARJU, E., LAPPALAINEN, R. Comparison of cutting performance of ion-plated NbN, ZrN, TiN and (Ti,Al)N coatings, *Surface and Coatings Technology*, v.33, p.117-132, 1987.
- (124) AROMAA, J., RONKAINEN, H., MAHIOUT, A., HANNULA, S.P., LEYLAND, A., MATTHEWS, A., MATTHES, B., BROSZEIT, E. A comparative study of the corrosion performance of TiN, Ti(B,N) and (Ti,Al)N coatings produced by physical vapour deposition methods, *Materials Science and Engineering A*, v.140, p.722-726, 1991.
- (125) LUGSCHEIDER, E., BARIMANI, C., GUERREIRO, S., BOBZIN, K. Corrosion tests of PVD coatings with die lubricant used for Al high-pressure die-casting dies, *Surface and Coatings Technology*, v.108-109, p.408-412, 1998.
- (126) CUNHA, L., ANDRITSCHKY, M., REBOUTA, L., SILVA, R. Corrosion of TiN, (Ti,Al)N and CrN hard coatings produced by magnetron sputtering, *Thin Solid Films*, v.317, p.351-355, 1998.
- (127) QUINTO, D.T., WOLFE, G.J., JINDAL, P.C. High temperature microhardness of hard coatings produced by physical and chemical vapor deposition, *Thin Solid Films*, Amsterdam, v.153, p.19-36, 1987.

- (128) NAVINSEK, B., PANJAN, P., MILOSEV, I. Industrial applications of CrN (PVD) coatings, deposited at high and low temperatures, *Surface and Coatings Technology*, v.97, p.182-191, 1997.
- (129) NAVINSEK, B., PAJAN, P. Novel applications of CrN (PVD) coatings deposited at 200°C, *Surface and Coatings Technology*, v.74-75, p.919-926, 1995.
- (130) HEINZE, M., MENNIG, G., PALLER, G. Wear resistance of PVD coatings in plastics processing, *Surface and Coatings Technology*, v.74-75, p.658-663, 1995.
- (131) DEARNLEY, P.A. Low friction surfaces for plastic injection moulding dies – an experimental case study, *Wear*, v.225-229, p.1109-1113, 1999.
- (132) DJOUADI, M.A., NOUVEAU, C., BEER, P., LAMBERTIN, M. Cr_xN_y Hard coatings deposited with PVD method on tools for wood machining, *Surface and Coatings Technology*, v.133-134, p.478-483, 2000.
- (133) NAM, K.H., JUNG, M.J., HAN, J.G. A Study on the high rate deposition of CrN_x films with controlled microstructure by magnetron sputtering, *Surface and Coatings Technology*, v.131, p.222-227, 2000.
- (134) BERG, G., FRIEDRICH, C., BROSZEIT, E., BERGER, C. Development of chromium nitride coatings substituting titanium nitride, *Surface and Coatings Technology*, v.86-87, p.184-191, 1996.
- (135) REBHOLZ, C., ZIEGELE, H., LEYLAND, A., MATTHEWS, A. Structure, mechanical and tribological properties of nitrogen-containing chromium coatings prepared by reactive magnetron sputtering, *Surface and Coatings Technology*, v.115, p.222-229, 1999.
- (136) TU, J.N., DUH, J.G., TSAI, S.Y. Morphology, mechanical properties, and oxidation behavior of reactively sputtered Cr-N films, *Surface and Coatings Technology*, v.133-134, p.181-185, 2000.
- (137) PIOT, O., GAUTIER, C., MACHET, J. Comparative study of CrN coatings deposited by ion plating and vacuum arc evaporation. Influence of the nature and the energy of the layer-forming species on the structural and the mechanical properties, *Surface and Coatings Technology*, v.94-95, p.409-415, 1997.
- (138) SANJINÉS, R., HONES, P., LÉVY, F., Hexagonal nitride coatings: electronic and mechanical properties of V₂N, Cr₂N and δ-MoN, *Thin Solid Films*, v.332, p.225-229, 1998.

- (139) DÓRFEL, I., ÓSTERLE, W., URBAN, I., BOUZY, E. Microstructural characterization of binary and ternary hard coating systems for wear protection. Part I: PVD coatings, *Surface and Coatings Technology*, v.111, p.109-209, 1999.
- (140) BERTRAND, G., MAHDJOUR, H., MEUNIER, C. A Study of the corrosion behaviour and protective quality of sputtered chromium nitride coatings, *Surface and Coatings Technology*, v.126, p.199-209, 2000.
- (141) MILOSEV, I., ABELS, J.M., STREHBLOW, H.H., NAVINSEK, B., METIKOS-HUKOVIC, M. High temperature oxidation of thin CrN coatings deposited on steel, *Journal of Vacuum Science Technology A*, v.14, i.4, p.2527-2534, Jul/Ago, 1996.
- (142) PAJAN, P., NAVINSEK, B., CVELBAR, A., ZALAR, A., MILOSEV, I. Oxidation of TiN, ZrN, TiZrN CrN, TiCrN and TiN/CrN multilayer hard coatings reactively sputtered at low temperature, *Thin Solid Films*, v.281-282, p.298-301, 1996.
- (143) MILOSEV, I., STREHBLOW, H.H., NAVINSEK, B. XPS in the study of high-temperature oxidation of CrN and TiN hard coatings, *Surface and Coatings Technology*, v.74-75, p.897-902, 1995.
- (144) ALDRICH-SMITH, G., TEER, D.G., DEARNLEY, P.A. Corrosion-wear response of sputtered CrN and S-phase coated austenitic stainless steel, *Surface and Coatings Technology*, v.116-119, p.1161-1165, 1999.
- (145) CUNHA, L., ANDRITSCHKY, M., REBOUTA, L., SILVA, R. Corrosion of TiN, (Ti,Al)N and CrN hard coatings produced by magnetron sputtering, *Thin Solid Films*, v.317, p.351-355, 1998.
- (146) CREUS, J., IDRISSE, H., MAZILLE, H., SANCHETTE, F., JACQUOT, P. Improvement of the corrosion resistance of CrN coated steel by an interlayer, *Surface and Coatings Technology*, v.107, p.183-190, 1998.
- (147) BIN-SUDIN, M., LEYLAND, A., JAMES, A.S., MATTHEWS, A., HOUSDEN, J., GARSIDE, B. Substrate surface finish effects in duplex coatings of PAPVD TiN and CrN with electroless nickel-phosphorus interlayers, *Surface and Coatings Technology*, v.81, p.215-224, 1996.

- (148) SUE, J.A., CHANG, T.P. Friction and wear behavior of titanium nitride, zirconium nitride and chromium nitride coatings at elevated temperatures, *Surface and Coatings Technology*, v.76-77, p.61-69, 1995.
- (149) SU, Y.L., YAO, S.H., WU, C.T. Comparisons of characterizations and tribological performance of TiN and CrN deposited by cathodic arc plasma deposition process, *Wear*, v.199, p.132-141, 1996.
- (150) SU, Y.L., YAO, S.H., LEU, Z.L., WEI, C.S., WU, C.T. Comparison of tribological behavior of three films – TiN, TiCN and CrN – grown by physical vapor deposition, *Wear*, v.213, p.165-174, 1997.
- (151) SU, Y.L., YAO, S.H., WEI, C.S., WU, C.T., KAO, W.H. Evaluation on the wear, tension and fatigue behavior of various PVD coated materials, *Materials Letters*, v.35, p.255-260, 1998.
- (152) ODÉN, M., ALMER, J., HAKANSSON, G., OLSSON, M. Microstructure-property relationships in arc evaporated Cr-N coatings, *Thin Solid Films*, v.377-378, p.407-412, 2000.
- (153) HE, X.M., BAKER, N., KEHLER, B.A., WALTER, K.C., NASTASI, M., NAKAMURA, Y. Structure, hardness and tribological properties of reactive magnetron sputtered chromium nitride films, *Journal of Vacuum Science Technology A*, v.18, i.1, p.30-36, Jan/Feb, 2000.
- (154) ACQUAVIVA, S., D'ANNA, E., ELIA, L., FERNÁNDEZ, M., LEGGIERI, G., LUCHES, A., MARTINO, M., MENGUCCI, P., ZOCCO, A. Characterization of TiAlN films deposited by reactive pulsed laser ablation, *Thin Solid Films*, 379, p.45-49, 2000.
- (155) WU, S.K., LIN, H.C., LIU, P.L. An investigation of unbalanced-magnetron sputtered TiAlN films on SKH51 high-speed-steel, *Surface and Coatings Technology*, v.124, p.97-103, 2000.
- (156) TAKANO, I., NAKAMURA, I., KAMIYA, M., YOSHIDA, H. Formation of Ti-Al-N thin films by the dynamic ion mixing method, *Surface and Coatings Technology*, v.84, p.409-413, 1996.
- (157) VENKATRAMAN, M., NEWMAN, J.P. In: T.B. MASSALSKI (Ed.), *Binary alloy phase diagrams*, 2.ed., Ohio: ASM International, 1990.

- (158) SUE, J.A., TROUE, H.H. Friction and wear properties of titanium nitride coating in sliding contact with AISI 01 Steel, *Surface and Coatings Technology*, v.43-44, p.709-720, 1990.
- (159) RUTHERFORD, K.L., HUTCHINGS, I.M. A micro-abrasive wear test, with particular application to coated systems, *Surface and Coatings Technology*, v.79, p.231-239, 1996.
- (160) RUTHERFORD, K.L., HUTCHINGS, I.M. Theory and application of a micro-scale abrasive wear test, *Journal of Testing and Evaluation*, v.25, i.2, p.250-260, 1997.
- (161) KASSMAN, A., JACOBSON, S., ERICKSON, L., HEDENQVIST, P., OLSSON, M. A new test method for the intrinsic abrasion resistance of thin coatings, *Surface and Coatings Technology*, v.50, p.75-84, 1991.
- (162) HEDENQVIST, P., BROMARK, M., OLSSON, M., HOGMARK, S., BERGMANN, E. Mechanical and tribological characterization of low-temperature deposited PVD TiN coatings, *Surface and Coatings Technology*, v.63, p.115-122, 1994.
- (163) ALLSOPP, D.N. *Abrasive wear of bulk materials and hard coatings*. Cambridge: St. John's College, University of Cambridge, 1999. (Doctoral thesis).
- (164) MONTGOMERY, D.C., PECK, E.A. *Introduction to linear regression analysis*. New York: John Wiley & Sons Inc., 1992, 527p.
- (165) TREZONA, R.I., ALLSOPP, D.N., HUTCHINGS, I.M. Transitions between two-body and three-body abrasive wear: influence of test conditions in the microscale abrasive wear test, *Wear*, v.225-229, p.205-214, 1999.
- (166) HUTCHINGS, I.M. *Tribology - Friction and wear of engineering materials*. London: Edward Arnold, 1992, 273 p.
- (167) RUTHERFORD, K.L., BULL, S.J., DOYLE, E.D., HUTCHINGS, I. Laboratory characterisation of the wear behaviour of PVD-coated tool steels and correlation with cutting tool performance, *Surface and Coatings Technology*, v.80, p.176-180, 1996.
- (168) LEYLAND, A., MATTHEWS, A. On the significance of the H/E ratio in wear control: a nanocomposite coating approach to optimised tribological behaviour, *Wear*, v.246, p.1-11, 2000.

- (169) ZHENG, S., SUN, Y., BLOYCE, A., BELL, T. Characterization of plasma-nitrided and PVD-TiN duplex treated Armco iron and En40B steel by nanoindentation, *Materials and Manufacturing Processes*, v.10, i.4, p.815-824, 1995.
- (170) KNOTEK, O., BOSSERHOFF, B., SCHREY, A., LEYENDECKER, T., LEMMER, O., ESSER, S. A new technique for testing the impact load of thin films: the coating impact test, *Surface and Coatings Technology*, v.54-55, p.102-107, 1992.
- (171) BANTLE, R., MATTHEWS, A. Investigation into the impact wear behaviour of ceramic coatings, *Surface and Coatings Technology*, v.74-75, p.857-868, 1995.
- (172) VOEVODIN, A.A., BANTLE, R., MATTHEWS, A. Dynamic Impact wear of TiC_xN_y and Ti-DLC composite coatings, *Wear*, v.185, p.151-157, 1995.
- (173) HEINKE, W., LEYLAND, A., MATTHEWS, A., BERG, G., FRIEDRICH, C., BROSZEIT, E. Evaluation of PVD nitride coatings, using impact, scratch and Rockwell-C adhesion tests, *Thin Solid Films*, v.270, p.431-438, 1995.
- (174) LUGSCHEIDER, E., KNOTEK, O., WOLFF, C., BÄRWULF, S. Structure and properties of PVD-coatings by means of impact tester, *Surface and Coatings Technology*, v.116-119, p.141-146, 1999.
- (175) OLLENDORF, H., SCHNEIDER, D. A comparative study of adhesion test methods for hard coatings, *Surface and Coatings Technology*, v.113, p.86-102, 1999.
- (176) MATTHEWS, A., LEYLAND, A., HOLMBERG, K., RONKAINEN, H. Design aspects for advanced tribological surface coatings, *Surface and Coatings Technology*, v.100-101, p.1-6, 1998.
- (177) BROMARK, M. *Wear resistance of PVD coatings for tool applications*. Uppsala: Department of Technology, Uppsala University, 1996. (Doctoral thesis, Doctor of Philosophy in Materials Science).